

DTIC FILE COPY

**POR-2017(EX)
(WT-2017)(EX)
EXTRACTED VERSION**

OPERATION DOMINIC, FISH BOWL SERIES

Project Officer's Report—Project 6.2

Gamma-Ray Scanning of Debris Cloud

**W. W. Berning, Project Officer
Ballistic Research Laboratories
Aberdeen Proving Ground, Maryland**

**Electro-Optical Systems, Inc.
Pasadena, California**

**DTIC
ELECTE
JUN 05 1987
S D D**

11 December 1964

NOTICE:

**This is an extracted version of POR-2017, OPERATION DOMINIC,
Fish Bowl Series, Project 6.2.**

**Approved for public release;
distribution is unlimited.**

**Extracted version prepared for
Director
DEFENSE NUCLEAR AGENCY
Washington, DC 20305-1000**

1 September 1985

AD-A995 488

Destroy this report when it is no longer needed. Do not return to sender.

PLEASE NOTIFY THE DEFENSE NUCLEAR AGENCY
ATTN: TITL, WASHINGTON, DC 20305 1000, IF YOUR
ADDRESS IS INCORRECT, IF YOU WISH IT DELETED
FROM THE DISTRIBUTION LIST, OR IF THE ADDRESSEE
IS NO LONGER EMPLOYED BY YOUR ORGANIZATION.



AD-A995-488

REPORT DOCUMENTATION PAGE

1a. REPORT SECURITY CLASSIFICATION UNCLASSIFIED		1b. RESTRICTIVE MARKINGS	
2a. SECURITY CLASSIFICATION AUTHORITY		3. DISTRIBUTION / AVAILABILITY OF REPORT Approved for public release; distribution is unlimited.	
2b. DECLASSIFICATION / DOWNGRADING SCHEDULE		5. MONITORING ORGANIZATION REPORT NUMBER(S) POR-2017 (EX) (WT-2017) (EX)	
4. PERFORMING ORGANIZATION REPORT NUMBER(S)		7a. NAME OF MONITORING ORGANIZATION Defense Atomic Support Agency	
6a. NAME OF PERFORMING ORGANIZATION 1-Ballistic Research Labs 2-Electro-Optical Systems, Inc.	6b. OFFICE SYMBOL (If applicable)	7b. ADDRESS (City, State, and ZIP Code) Washington, DC	
6c. ADDRESS (City, State, and ZIP Code) 1-Aberdeen Proving Ground, MD 2-Pasadena, CA		9. PROCUREMENT INSTRUMENT IDENTIFICATION NUMBER	
8a. NAME OF FUNDING / SPONSORING ORGANIZATION	8b. OFFICE SYMBOL (If applicable)	10. SOURCE OF FUNDING NUMBERS	
8c. ADDRESS (City, State, and ZIP Code)		PROGRAM ELEMENT NO.	PROJECT NO.
		TASK NO.	WORK UNIT ACCESSION NO.
11. TITLE (Include Security Classification) OPERATION DOMINIC, FISH BOWL SERIES, PROJECT OFFICER'S REPORT; PROJECT 6.2 - Gamma-Ray Scanning of Debris Cloud, Extracted Version			
12. PERSONAL AUTHOR(S) W. W. Berning, Project Officer			
13a. TYPE OF REPORT	13b. TIME COVERED FROM TO	14. DATE OF REPORT (Year, Month, Day) 641211	15. PAGE COUNT 338
16. SUPPLEMENTARY NOTATION This report has had sensitive military information removed in order to provide an unclassified version for unlimited distribution. The work was performed by the Defense Nuclear Agency in support of the DoD Nuclear Test Personnel Review Program.			
17. COSATI CODES		18. SUBJECT TERMS (Continue on reverse if necessary and identify by block number)	
FIELD	GROUP	Dominic Debris Clouds King Fish	
18	3	Fish Bowl Star Fish	
20	8	Gamma Radiation Blue Gill	
19. ABSTRACT (Continue on reverse if necessary and identify by block number) The objective of this project was to determine the position of the debris cloud as a function of altitude for the Star Fish, Blue Gill, and King Fish events by the use of directional gamma-ray scanning instruments. Included in the report is a description of the rocket operations, hand-reduced data, some computer-reduced data, and preliminary analyses and conclusions.			
20. DISTRIBUTION / AVAILABILITY OF ABSTRACT <input checked="" type="checkbox"/> UNCLASSIFIED/UNLIMITED <input type="checkbox"/> SAME AS RPT. <input type="checkbox"/> DTIC USERS		21. ABSTRACT SECURITY CLASSIFICATION UNCLASSIFIED	
22a. NAME OF RESPONSIBLE INDIVIDUAL MARK D. FLOHR		22b. TELEPHONE (Include Area Code) 202-325-7559	22c. OFFICE SYMBOL DNA/ISCM

OPERATION DOMINIC

FISH BOWL SERIES

PROJECT OFFICER'S REPORT - PROJECT 6.2

Gamma-Ray Scanning of Debris Cloud

W. W. Berning, Project Officer
Ballistic Research Laboratories
Aberdeen Proving Ground, Maryland

Electro-Optical Systems, Inc.
Pasadena, California

11 December 1964

APPROVED FOR PUBLIC RELEASE;
DISTRIBUTION IS UNLIMITED.



NOTICE

This is an extract of POR-2017,
OPERATION DOMINIC, Fish Bowl Series,
Project 6.2.

Extracted version prepared for
Director
DEFENSE NUCLEAR AGENCY
Washington, DC 20305-1000

1 September 1985

Accession For	
NTIS CRA&I	<input checked="" type="checkbox"/>
DTIC TAB	<input type="checkbox"/>
Unannounced	<input type="checkbox"/>
Justification	
By	
Distribution/	
Availability Codes	
Dist	Avail and/or Special
A-1	

UNANNOUNCED

FOREWORD

Classified material has been removed in order to make the information available on an unclassified, open publication basis, to any interested parties. The effort to declassify this report has been accomplished specifically to support the Department of Defense Nuclear Test Personnel Review (NTPR) Program. The objective is to facilitate studies of the low levels of radiation received by some individuals during the atmospheric nuclear test program by making as much information as possible available to all interested parties.

The material which has been deleted is either currently classified as Restricted Data or Formerly Restricted Data under the provisions of the Atomic Energy Act of 1954 (as amended), or is National Security Information, or has been determined to be critical military information which could reveal system or equipment vulnerabilities and is, therefore, not appropriate for open publication.

The Defense Nuclear Agency (DNA) believes that though all classified material has been deleted, the report accurately portrays the contents of the original. DNA also believes that the deleted material is of little or no significance to studies into the amounts, or types, of radiation received by any individuals during the atmospheric nuclear test program.

OPERATION DOMINIC

FISH BOWL SERIES

PROJECT OFFICERS REPORT—PROJECT 6.2

GAMMA RAY SCANNING OF DEBRIS CLOUD

W.W. Berning, Project Officer

**Ballistic Research Laboratories
Aberdeen Proving Ground, Maryland**

and

**Staff Members of
Electro-Optical Systems, Inc.
Pasadena, California**

ABSTRACT

The objective of Project 6.2 was to determine the position of the debris cloud as a function of altitude for the Star Fish, Blue Gill, and King Fish events by the use of directional gamma ray scanning instruments. Included in the report is a description of the rocket operations, hand-reduced data, some computer-reduced data, and preliminary analyses and conclusions.

Although several instrument and rocket problems were encountered during the three events, field operations were successful, and data were obtained from all rocket flights.

Most of the data presented in the results chapter were hand-reduced. Computer reduction was performed by another contractor, but problems in the determination of payload attitude have delayed the receipt of most of this data. Samples of reduced data for Rockets 8, 9, and 19 were received, however, and some of these results are included in Chapter 3.

Data from the gamma scanners, gamma and beta detectors, and photometers are given for the three events. Plots for the scanners are given in counts per second versus altitude and time after liftoff. The gamma and beta detector plots are given in output volts versus altitude and time after liftoff. Most plots include instrument calibration data. The photometer data are plotted in 3914 Å irradiance versus altitude and time after liftoff.

Conclusions on the three events are summarized below.

1. The Star Fish debris was widely scattered at late time (roughly 20 to 30 minutes after burst), and its approximate horizontal diameter was at least
2. The Blue Gill debris was stable with a horizontal diameter of at least and a vertical dimension of about at roughly 15 to 20 minutes after burst.
3. The debris for the King Fish event expanded rapidly in the vertical direction, and its rate of ascent was

PREFACE

Reduced data from Project 6.2 of the Fish Bowl Series was not received from the data reduction contractor as scheduled, and therefore, is not included in this report. The major cause for this delay involves problems in determining the payload attitude. However, some incomplete reduced data, primarily on the beta detectors, was received on Rockets 8, 9, and 19 and is discussed in this document.

CONTENTS

ABSTRACT-----	5
PREFACE -----	6
CHAPTER 1 INTRODUCTION-----	15
1.1 Objectives -----	15
1.2 Background-----	16
1.3 Theory-----	17
1.3.1 Theoretical Models of Debris Cloud -----	18
1.3.2 Theoretical Considerations of Instrument Design -----	19
1.3.3 Measurement of Debris Contained Along a Field Line -----	20
CHAPTER 2 PROCEDURE-----	26
2.1 Operations -----	26
2.2 Payload Instruments (Project 6.2)- -----	28
2.2.1 Payload Description-----	28
2.2.2 Calibration of Gamma Detectors in the Payload -----	29
2.2.3 Gamma Scanner -----	30
2.2.4 Omnidirectional Gamma Detector-----	35
2.2.5 Beta Detector -----	36
2.2.6 Photometer -----	38
2.2.7 VHF Telemetry Systems-----	39
2.2.8 GMD Transmitter -----	41
2.2.9 C-Band Beacon -----	42
2.2.10 Three-Frequency Beacon -----	43
2.2.11 Battery Power Supplies-----	43
2.2.12 Power and Signal Switches-----	45
2.2.13 Temperature Sensors -----	46
2.2.14 Magnetometers -----	47
2.2.15 Voltage Regulator -----	49
2.2.16 Engineering Measurements -----	50
2.2.17 Ground Support Equipment-----	50
2.3 Payload Environmental Testing -----	51
2.3.1 Vibration Tests-----	51
2.3.2 Instrument Functional Tests -----	52
2.3.3 Telemetry Functional Tests -----	52
2.4 Data Requirements-----	53
2.4.1 Data Required-----	53
2.4.2 Method of Recording Data -----	53
2.4.3 Data Reduction -----	54
2.4.4 Procurement of Data -----	55
2.4.5 Requirements from Other Projects-----	55

CHAPTER 3 RESULTS -----	92
3.1 Gamma Scanner-----	92
3.1.1 Star Fish-----	93
3.1.2 Blue Gill-----	93
3.1.3 King Fish-----	94
3.2 Omnidirectional Gamma Detector-----	95
3.2.1 Star Fish-----	95
3.2.2 Blue Gill-----	95
3.2.3 King Fish-----	96
3.3 Beta Detector-----	96
3.3.1 Star Fish-----	97
3.3.2 Blue Gill-----	97
3.3.3 King Fish-----	98
3.4 Photometer-----	99
3.4.1 Star Fish-----	99
3.4.2 Blue Gill-----	100
3.4.3 King Fish-----	100
 CHAPTER 4 DISCUSSION -----	 143
4.1 Star Fish-----	143
4.1.1 Expected Gamma Produced Count Rates and the Bremsstrahlung Contribution-----	143
4.1.2 The Beta Flux-----	146
4.1.3 Debris Contained Along Field Line-----	147
4.1.4 Photometer Data-----	148
4.2 Blue Gill-----	149
4.2.1 Gamma Ray Source-----	149
4.2.2 Beta Flux-----	150
4.2.3 Debris Contained Along Field Line-----	151
4.3 King Fish-----	151
4.3.1 Gamma Ray Source-----	151
4.3.2 Beta Flux Data-----	152
4.3.3 Debris Contained Along Field Line-----	153
4.3.4 Photometer Data-----	154
4.4 Instrument Performance-----	155
4.5 Effectiveness of Instrumentation-----	156
4.5.1 Gamma Scanner-----	156
4.5.2 Omnidirectional Gamma Detector-----	156
4.5.3 Beta Detector-----	157
4.5.4 Photometer-----	157
4.6 Data Reliability-----	157
 CHAPTER 5 CONCLUSIONS AND RECOMMENDATIONS -----	 161
5.1 Conclusions-----	161
5.1.1 Star Fish-----	161
5.1.2 Blue Gill-----	162
5.1.3 King Fish-----	162

5.2 Recommendations -----	162
5.2.1 Gamma Scanners-----	162
5.2.2 Beta Detector-----	165
5.2.3 Aspect Determining Elements -----	165
5.2.4 Airborne Telemetry System -----	166
5.2.5 Ground Telemetry System-----	166
APPENDIX A ROCKET VEHICLE OPERATIONS: PROJECT 6.2-----	168
A.1 Introduction -----	168
A.2 Vehicle Descriptions -----	168
A.2.1 Project 6.2 -----	168
A.2.2 Project 6.3 -----	168
A.2.3 Project 6.4 -----	169
A.3 Launcher Design and Location -----	169
A.4 Operational Summary-----	171
A.5 Launch Control -----	171
A.6 Vehicle Performance Summary -----	173
A.7 Vehicle Failure Discussion -----	178
APPENDIX B ROCKET VEHICLE PERFORMANCE -----	223
B.1 Introduction -----	223
B.2 Trajectory Parameters -----	224
B.3 Trajectory Solutions -----	224
B.4 Results -----	229
B.5 Discussion -----	230
APPENDIX C REPORTS AND SPECIFICATIONS -----	250
C.1 Electro-Optical Systems, Inc., Reports -----	250
C.2 Electro-Optical Systems, Inc., Specifications -----	250
C.3 Subcontractor Reports -----	251
APPENDIX D CALIBRATION DATA FOR GAMMA SCANNER IN PAYLOAD -----	252
APPENDIX E INSTRUMENT CALIBRATION DATA -----	259
APPENDIX F MAGNETOMETER RESULTS AND ASPECT DETERMINATION ---	268
F.1 Magnetometer Results -----	268
F.2 Aspect Determination-----	268
F.3 Static Magnetometer Calibration -----	271
F.4 Dynamic Magnetometer Calibration -----	272
APPENDIX G INSTRUMENT ATTITUDE DETERMINATION-----	278
APPENDIX H VHF TELEMETRY SYSTEM DATA -----	292
REFERENCES-----	335

TABLE

1.1 Theoretical Total Gamma Yield of Blue Gill Debris Cloud as a Function of Time-----	24
2.1 Summary of Star Fish, Blue Gill, and King Fish Events-----	57
2.2 Rocket Operations Summary-----	58
2.3 Vibration Schedule-----	60
2.4 Data Format on Tape and Printout Records-----	61
2.5 Sample of Computer Reduced Data, 2395081 through 2395675-----	63
2.6 Sample of Computer Reduced Data, 2390842 through 2391436-----	64
2.7 Instrumentation Package Contents-----	65
4.1 Cloud Shape and Gamma Flux-----	159
4.2 Cloud Shape and Beta Flux-----	159
4.3 Airglow Locations, King Fish-----	160
A.1 Details of Rocket Operations-----	181
A.2 Rocket Payload Composition-----	184
A.3 Fire Control Panel Operation-----	185
A.4 Velocity Increments for ARGO C-22 Rockets-----	186
A.5 Velocity Increments for ARGO D-4 Rockets-----	187
A.6 Launching Project Card, Rocket 8-----	188
A.7 Launching Project Card, Rocket 9-----	193
A.8 Launching Project Card, Rocket 15-----	198
A.9 Launching Project Card, Rocket 18-----	202
A.10 Launching Project Card, Rocket 19-----	206
A.11 Launching Project Card, Rocket 26-----	210
A.12 Launching Project Card, Rocket 29-----	214
B.1 Source of Input Data for Determining Rocket Trajectories, Projects 6.2, 6.3, 6.4-----	234
B.2 Estimated Nose-Over Altitudes for Selected Rockets of Projects 6.2, 6.3, and 6.4-----	235
E.1 Photometer Calibrations-----	260
G.1 Polar Angles of Each Detector in the Payload-Centered Coordinate System-----	288
G.2 Altitudes Where Payloads Left the Atmosphere-----	288
H.1 Telemetry Channel Summary, Rocket 1-----	293
H.2 Telemetry Channel Summary, Rocket 2-----	293
H.3 Telemetry Channel Summary, Rocket 3-----	294
H.4 Telemetry Channel Summary, Rocket 4-----	295
H.5 Telemetry Channel Summary, Rocket 5-----	296
H.6 Telemetry Channel Summary, Rocket 6-----	296
H.7 Telemetry Channel Summary, Rocket 7-----	297
H.8 Telemetry Channel Summary, Rocket 8-----	298
H.9 Telemetry Channel Summary, Rocket 9-----	299
H.10 Telemetry Channel Summary, Rocket 10-----	300
H.11 Telemetry Channel Summary, Rocket 11-----	300
H.12 Telemetry Channel Summary, Rocket 12-----	301
H.13 Telemetry Channel Summary, Rocket 13-----	301
H.14 Telemetry Channel Summary, Rocket 14-----	302
H.15 Telemetry Channel Summary, Rocket 15-----	303
H.16 Telemetry Channel Summary, Rocket 17-----	304

H.17	Telemetry Channel Summary, Rocket 18	305
H.18	Telemetry Channel Summary, Rocket 19	306
H.19	Telemetry Channel Summary, Rocket 20	307
H.20	Telemetry Channel Summary, Rocket 21	307
H.21	Telemetry Channel Summary, Rocket 22	308
H.22	Telemetry Channel Summary, Rocket 23	308
H.23	Telemetry Channel Summary, Rocket 24	309
H.24	Telemetry Channel Summary, Rocket 25	309
H.25	Telemetry Channel Summary, Rocket 26	310
H.26	Telemetry Channel Summary, Rocket 27	310
H.27	Telemetry Channel Summary, Rocket 28	311
H.28	Telemetry Channel Summary, Rocket 29	312
H.29	Telemetry Data Tape Channel Allocation	313
H.30	Recorded Data Summary, Tape Record	313
H.31	Recorded Data Summary, Brush Recorder Record	314
H.32	Recorded Data Summary, CEC Recording Galvanometer Record	316
H.33	Commutated Channel Summary, Channel 11	320
H.34	Commutated Channel Summary, Channel 12	321
H.35	Commutated Channel Summary, Channel 18	322
H.36	Commutated Channel Summary, Channels 12 and 18	323
H.37	Commutated Channel Summary, Channel 13	324
H.38	Commutated Channel Summary, Channel 14	325
H.39	Commutated Channel Summary, Channel 15	326
H.40	Commutated Channel Summary, Channel 16	327
H.41	Commutated Channel Summary, Channel 12	328
H.42	Commutated Channel Summary, Channel 14	329
H.43	Commutated Channel Summary, Channel 11	330
H.44	Commutated Channel Summary, Regarding Potential Analyzer	331
H.45	Commutated Channel Summary, Channel 16	332
H.46	Telemetry Channel Summary, Rocket 25	333
H.47	Telemetry Channel Summary, Rocket 22	334

FIGURES

1.1	Expected size and altitude of Blue Gill debris cloud for various post-detonation times	25
2.1	Instrumentation layout and rocket launcher locations on Johnston Island for Projects 6.2, 6.3, 6.4	66
2.2	Rocket trajectories for Project 6.2	67
2.3	EOS payload instrumentation package	68
2.4	Payload system block diagram	69
2.5	Test setup for calibrating gamma scanner in payload	70
2.6	EOS instrumentation package, Side 1	71
2.7	Gamma scanner shield and Geiger-Mueller tube locations	72
2.8	Gamma telescope field of view	73
2.9	Plan view of detector output versus azimuth scanning angle	73
2.10	Gamma scanner block diagram	74
2.11	Data processor and rate generator schematic	75
2.12	Geiger-Mueller tube test setup	76
2.13	EOS instrumentation package, Side 2	77

2.14	Beta detector assembly -----	78
2.15	Omnidirectional gamma and beta detector block diagram-----	79
2.16	External view of photometer assembly-----	80
2.17	Photometer block diagram-----	81
2.18	Airborne telemetry system block diagram-----	82
2.19	Typical discharge curve for Silvercel battery at a 50-minute rate-----	83
2.20	Magnetometer sensor assembly-----	84
2.21	Magnetometer block diagram-----	85
2.22	Magnetometer schematic-----	86
2.23	Voltage regulator schematic-----	87
2.24	Ground support equipment setup-----	88
2.25	Test equipment and control racks-----	89
2.26	Payload mounted to exciter (vibration) table-----	90
2.27	Payload checkout block diagram-----	91
3.1	Horizontal 20° gamma scanner data, Rocket 8, 355° and 175°, Star Fish-----	102
3.2	Horizontal 20° gamma scanner data, Rocket 8, 265° and 85°, Star Fish-----	103
3.3	Horizontal 90° gamma scanner data, Rocket 8, 85° and 265°, Star Fish-----	104
3.4	Horizontal 90° gamma scanner data, Rocket 8, 175° and 355°, Star Fish-----	105
3.5	Horizontal 20° gamma scanner data, Rocket 9, 355° and 175°, Star Fish-----	106
3.6	Horizontal 20° gamma scanner data, Rocket 9, 85° and 265°, Star Fish-----	107
3.7	Horizontal 90° gamma scanner data, Rocket 9, 175° and 355°, Star Fish-----	108
3.8	Horizontal 90° gamma scanner data, Rocket 9, 265° and 85°, Star Fish-----	109
3.9	Vertical 20° gamma scanner data, Rocket 8, 212, 237, 262, and 285 km, Star Fish-----	110
3.10	Vertical 20° gamma scanner data, Rocket 8, 285, 350, and 408 km, Star Fish-----	111
3.11	Vertical 90° gamma scanner data, Rocket 8, 212, 223, 262, and 285 km, Star Fish-----	112
3.12	Vertical 90° gamma scanner data, Rocket 8, 285, 350, and 408 km, Star Fish-----	113
3.13	Gamma scanner count rate versus azimuth angle, Rocket 15, Blue Gill-----	114
3.14	Rocket altitude versus ground range and count rate, Rocket 15, Blue Gill-----	115
3.15	Vertical 20° gamma scanner data, Rocket 19, King Fish-----	116
3.16	Vertical 90° gamma scanner data, Rocket 19, King Fish-----	117
3.17	Horizontal 20° gamma scanner data, Rocket 19, King Fish-----	118
3.18	Horizontal 90° gamma scanner data, Rocket 19, King Fish-----	119
3.19	Omnidirectional gamma detector data, Rocket 8, Star Fish-----	120
3.20	Omnidirectional gamma detector data, Rocket 15, Blue Gill-----	121
3.21	Omnidirectional gamma detector data, Rocket 19, King Fish-----	122
3.22	Omnidirectional gamma detector data, Rocket 26, King Fish-----	123
3.23	Projection of Rocket 8 trajectory onto plane of magnetic field, Star Fish-----	124
3.24	Projection of Rocket 9 trajectory onto plane of magnetic field, Blue Gill-----	125
3.25	Projection of Rocket 15 trajectory onto plane of magnetic field, Blue Gill-----	126
3.26	Projection of Rocket 19 trajectory onto plane of earth's magnetic field, King Fish-----	127

3.27	Projection of Rocket 8 trajectory onto a plane through the burst point and perpendicular to the magnetic field lines of the earth, Star Fish -----	128
3.28	Projection of Rocket 9 trajectory onto a plane through the burst point and perpendicular to the magnetic field lines of the earth, Star Fish -----	129
3.29	Projection of Rocket 15 trajectory onto a plane through the burst point and perpendicular to the magnetic field lines of the earth, Blue Gill -----	130
3.30	Projection of Rocket 19 trajectory onto a plane through the burst point and perpendicular to the magnetic field lines of the earth, King Fish -----	131
3.31	Beta detector output voltage versus its field of view, Rocket 8, Star Fish -----	132
3.32	Beta detector output versus projected altitude, Rocket 8, Star Fish ----	133
3.33	Beta detector output voltage versus its field of view, Rocket 9, Star Fish -----	134
3.34	Beta detector output voltage versus its field of view, Rocket 15, Blue Gill -----	135
3.35	Beta detector output versus altitude, Rocket 15, Blue Gill-----	136
3.36	Beta detector data, Rocket 19, King Fish-----	137
3.37	Beta detector output versus projected altitude for Rocket 19, King Fish--	138
3.38	Photometer data, Rocket 8, Star Fish -----	139
3.39	Photometer data, Rocket 9, Star Fish -----	140
3.40	Direction of maximum photometer response for Rocket 19, King Fish ---	141
3.41	Airglow location during flight of Rocket 19, King Fish -----	142
A.1	Large launcher (elevation view) -----	218
A.2	Large launcher (plan view) -----	219
A.3	Large launcher (loading diagram)-----	220
A.4	Launcher locations, Projects 6.2, 6.3, and 6.4-----	221
A.5	Payload designation and nose cone outlines -----	222
B.1	Trajectory for Rocket 8, Star Fish event-----	236
B.2	Trajectory for Rocket 9, Star Fish event-----	237
B.3	Trajectory for Rocket 15, Blue Gill event -----	238
B.4	Trajectory for Rocket 18, Blue Gill event -----	239
B.5	Trajectory for Rocket 19, King Fish event-----	240
B.6	Trajectory for Rocket 26, King Fish event-----	241
B.7	Trajectory for Rocket 29, King Fish event-----	242
B.8	Slant range versus time for Rocket 8, Star Fish event-----	243
B.9	Slant range versus time for Rocket 9, Star Fish event-----	244
B.10	Slant range versus time for Rocket 15, Blue Gill event-----	245
B.11	Slant range versus time for Rocket 18, Blue Gill event-----	246
B.12	Slant range versus time for Rocket 19, King Fish event -----	247
B.13	Slant range versus time for Rocket 26, King Fish event -----	248
B.14	Slant range versus time for Rocket 29, King Fish event -----	249
D.1	Contour plot of equal shielding for vertical 20-degree gamma scanner (in payload) calibration data -----	258
E.1	Gamma scanner D-80 detector calibration curves for Rocket 8, SN 17 and 34 -----	261

E.2	Gamma scanner D-80 detector calibration curves for Rocket 8, SN 32 and 42 -----	262
E.3	Gamma scanner D-80 detector calibration curves for Rocket 9, SN 24 and 38 -----	263
E.4	Gamma scanner D-90 detector calibration curves for Rocket 9, SN 44 and 47 -----	264
E.5	Omnidirectional gamma detector calibration curves for Rockets 8 and 9 --	265
E.6	Beta detector calibration curves for Rockets 8 and 9, absorbed energy flux -----	266
E.7	Beta detector calibration curves for Rockets 8 and 9, incident energy ---	267
F.1	Error histograms of X-, Y-, and Z-magnetometers in phenolic packages -	274
F.2	Error histograms of X-, Y-, and Z-magnetometers in payload -----	275
F.3	True azimuth and elevation look angles with respect to the Y-axis magnetometer position -----	276
F.4	Assumed configuration for calculation of dynamic effects of payload on the earth's magnetic field -----	277
G.1	Coordinate systems for determining instrument attitude -----	289
G.2	Coning motion of the payload -----	290
G.3	Geometric representation of Equation G.9 -----	290
G.4	Solution of Equation G.9 on coning circle -----	291
G.5	Vehicle coning directions -----	291

CHAPTER 1

INTRODUCTION

This report covers the Project 6.2 phase of the Fish Bowl Series of high-altitude nuclear tests. The objective of Project 6.2 was to determine the position of the debris cloud as a function of altitude for the Star Fish, Blue Gill, and King Fish events by the use of directional gamma ray scanning instruments.

1.1 OBJECTIVES

The overall objective of Project 6.2 was to map debris clouds resulting from the Star Fish Prime (Star Fish), Blue Gill Triple Prime (Blue Gill), and King Fish events by detecting the gamma radiation emanating from them. Ideally, it would have been desirable to map the spatial and temporal distribution of each debris cloud and determine its gamma energy level and spectrum. However, to perform this ideal experiment would have been difficult and costly and would have required a long leadtime for instrumentation design and fabrication.

The debris cloud was mapped by a directional gamma ray sensing instrument, which scanned the cloud in a horizontal direction by spinning with its rocket about a near-vertical axis. A vertical scan of the cloud was obtained by the instrument's motion along a rocket trajectory. Thus, a vertical and horizontal distribution of the debris cloud could be determined when the test data were reduced and analyzed. The change of debris cloud distribution as a function of time was determined by payloads fired at different times in conjunction with each event. Since there were only a limited number of rockets and a single launching site available, the overall objectives of the project were limited to mapping the debris cloud resulting from

a nuclear detonation in the vertical and horizontal dimensions at discrete intervals. The time scale was determined by the launch time of the rocket vehicles. Rocket operations for Project 6.2 are described in detail in Appendix A. Although data reduction and analysis were not required for this program, limited quick-look data were produced by Electro-Optical Systems, Inc., (EOS), following the detonations.

In addition to the primary experiment of mapping the gamma radiation emanating from the debris cloud, several secondary experiments were carried on the payload. These secondary experiments were used to aid in the interpretation of data collected from the primary experiment.

Auxiliary equipments on the Project 6.2 payload were: (1) an omnidirectional gamma detector, (2) a beta detector, (3) a photometer, and (4) three orthogonal magnetometers. The omnidirectional gamma detector provided total gamma radiation as a function of time during the flight and was used to supplement the gamma scanner data. The beta detector supplied data on the energy distribution of radiation emanating from the debris cloud, and also coarse payload aspect information with respect to the debris cloud. The photometer provided aspect data for the gamma ray scanner, which supplemented data collected by the magnetometers.

Rocket payloads on Project 6.2 carried a three-frequency continuous wave beacon to permit determination of ionospheric electron content through measurements of propagation characteristics in the vicinity of the nuclear events. The frequencies employed were phase coherent 37, 148, and 888 Mc. Dispersion Doppler and Faraday rotation measurements furnished the primary information. The propagation experiment is described in Reference 5.

1.2 BACKGROUND

Several nuclear devices were detonated in space in the past. Data from these tests were not complete and thus required additional information to provide more knowledge about the mechanics of the

detonation, the aftereffects of the debris, and the interactions of radiations from the detonation with the ionosphere. Typical radiations from the detonation include neutrons, betas, gamma rays, and X-rays. One point of substantial concern to the military is the potential blackout of electromagnetic transmission that may exist for a considerable portion of time following the nuclear detonation.

Theories have been presented which indicate that the debris and its interactions with the ionosphere will yield a highly charged layer many kilometers wide, lying parallel to the earth's surface. If this is true, a complete cessation of radar, telemetry, and communication transmissions would result. Consequently, any defense system that depends upon propagation of electromagnetic energy for detection, tracking, and communications would become useless.

1.3 THEORY

Various theories describing the behavior of a debris cloud resulting from a high-altitude nuclear detonation appear to be somewhat inadequate for accurate prediction. This is especially true for the Star Fish event, which took place at an altitude of 400 km. In addition to this, very little experimental data are available concerning debris cloud behavior. Many of the theories are based upon measurements made in conjunction with the Teak and Orange shots. The altitudes of these shots bracket that of the Blue Gill fairly closely, and allow some scaling with reasonable confidence. However, there are no previous data for debris cloud behavior resulting from a 400-km detonation. In addition, the prediction of the debris cloud behavior for the Star Fish event, as a result of various theories, appeared to be somewhat inadequate and inconclusive.

Therefore, the design of a gamma ray scanner for the Star Fish event was quite difficult due to the apparent uncertainty in the prediction of the debris cloud behavior. As a result, design of the gamma ray scanner was based on the expected geometries and gamma intensities characteristic of the Blue Gill event. It was expected that this design would also yield sufficient results concerning the Star Fish and King Fish events.

1.3.1 Theoretical Models of Debris Cloud. A number of theoretical models of high-altitude nuclear detonation have been proposed. Studies have been conducted by various agencies, notably those supported by the Defense Atomic Support Agency at General Electric, TEMPO Division, at Santa Barbara. Three models of importance follow:

Ball Model. The theory behind the ball model states that the ionizing debris, resulting from the detonation, will remain in roughly a spherical ball that will rise above the detonation point due to heating of the ionosphere. Following a cooling cycle, the ball is contained on the top by the earth's magnetic field and on the bottom by the ionosphere.

Mushroom Cloud. The theory of the mushroom cloud states that upon detonation and heating of the ionosphere the cloud will tend to rise but will be immediately trapped by the earth's magnetic field and, therefore, will assume a squashed shape on the top. As a result of ionospheric heating, the lower portion of the cloud rises and is contained by the relatively dense ionosphere. Sides of the cloud expand in a normal hydrodynamic fashion, thus yielding the mushroom or toadstool appearance. A plan view of this cloud would be expected to yield an approximate elliptical configuration due to magnetic trapping of the charged particle debris, the long axis being directed from north to south, and the short axis, from east to west.

Debris Separation at Conjugate Points. The debris separation theory states that the charged particle debris will separate into two approximately equal parts and deposit in a very short time along a geomagnetic line at conjugate points across the magnetic equator. As such, the debris becomes radiation trapped by the earth's magnetic field. The balance of the debris (that not ionized) will remain in the vicinity of the detonation point and rise, due to heating of the ionosphere.

Present theory indicates that, following a detonation, the density of the charged particles deposited in the ionosphere is such that a high probability exists for poor transmission of electromagnetic energy. Such a condition, spread horizontally over many square kilometers, would probably disrupt or disable radar and radio communications for a minimum period of a few seconds to several hours. A high-altitude detonation was required to establish or confirm the true situation.

1.3.2 Theoretical Considerations of Instrument Design. In designing a gamma scanner, certain assumptions must be made with respect to the size and shape of the debris cloud as a function of time, and the gamma ray intensity as a function of time. The latter will depend on the natural decay behavior of the cloud, and the debris density, which varies with time due to the cloud expansion. In addition, it is assumed that the cloud is isotropic in its gamma radiation and that no self-absorption exists.

From the scaling nomographs contained in Reference 1, the theoretical radial expansion rates of the Blue Gill debris may be determined. From this and from data published in Reference 2, the vertical distribution of the debris cloud also can be determined. As a result, the theoretical cloud size and shape for the Blue Gill event are shown in Figure 1.1 for various times after detonation. The total gamma yield per unit time from the debris cloud may be expressed as:

$$P = Y (6 \times 10^{13}) / 3.35 (3 + 2H^{0.6} + H^{1.2}) \quad (1.1)$$

Where: P = total gamma yield in watts
Y = total energy released in megatons
H = time in seconds after detonation

Since the Blue Gill gamma scanner payloads were being launched at H + 900 and H + 1860 seconds, the predominant term in the parenthetical expression in the denominator is $H^{1.2}$. Table 1.1 shows the theoretical total gamma yield of the debris cloud resulting from the Blue Gill event as a function of time.

1.3.3 Measurement of Debris Contained Along a Field Line. A simple method is available for measuring that fraction of the debris cloud that is contained along a magnetic field line. This method involves the use of a beta detector.

Consider the beta particles contained in the vicinity of the detector. These particles can be divided into two components for simplicity: one resulting from the direct emission of betas, and one resulting from trapped or stored betas. At the altitudes of interest (~100 to 400 km), all stored or trapped betas must exist at only very large (near 90 degrees) helix pitch angles. This occurs because the adiabatic helix angle equation is

$$\frac{\sin \alpha}{\sin \alpha_0} = \sqrt{\frac{B}{B_0}}$$

where α and α_0 are the helix pitch angles and B and B_0 the magnetic field strengths at points along the field line. Then reflection occurs at $\sin \alpha = 1$, and this must occur at a sufficiently high altitude so that the reflected electrons are not absorbed by the atmosphere. This must be higher (in general) than about 75 km, which makes $\sqrt{\frac{B}{B_0}}$ for detector altitudes of interest quite close to unity, and thus is close to 90 degrees. Consequently, if beta particles are examined only at small pitch angles (those moving most nearly parallel to the magnetic field lines), samples are obtained for these particles which have been emitted instantaneously from the debris, and which make only one traversal along the field lines and are not reflected.

To obtain the explicit relationship between the response of the detector and the debris density, the following analysis is made. Let the beta detector look along the magnetic field line (either north or south) and assume it has a half-angle α_0 acceptance cone. This detector then accepts all electrons with a pitch angle less than α_0 . Its solid angle of view is then

$$\Omega_0 = 2 \pi (1 - \cos \alpha_0)$$

The fraction of debris emission in the vicinity of the detector is then

$$\frac{\Omega_0}{4\pi} = \frac{1 - \cos \alpha_0}{2}$$

This effective solid angle transforms as one proceeds along the magnetic field line away from the detector according to the adiabatic formula,

$$\frac{\sin \alpha}{\sin \alpha_0} = \sqrt{\frac{B}{B_0}}$$

The zero subscripts refer to the position of the detector. The effective available solid angle can be transformed by:

$$\begin{aligned} \frac{\Omega}{\Omega_0} &= \frac{1 - \cos \alpha}{1 - \cos \alpha_0} \\ &= \frac{1 - \sqrt{1 - \frac{B}{B_0} \sin^2 \alpha_0}}{1 - \sqrt{1 - \sin^2 \alpha_0}} \end{aligned}$$

If f is the total emission of the debris cloud per unit volume per second, the flux falling upon the detector is given by:

$$F = \int \frac{f}{4\pi} \Omega dl$$

where dl is the increment along the field line and the integral is taken along the magnetic field line away from the detector until it intercepts the atmosphere. Thus

$$F = \int f \frac{\Omega_0}{4\pi} \frac{\Omega}{\Omega_0} dl$$

where $\frac{\Omega}{\Omega_0}$ is the expression given above, and

$$\frac{\Omega_0}{4\pi} = \frac{1 - \cos \alpha}{2}$$

A great simplification can be made in the above integral in most cases of interest, because $\frac{\Omega}{\Omega_0}$ is a function which does not deviate far from unity over the region occupied by a debris cloud. To illustrate, observe that, for a small α_0 (good resolution beta detector),

$$\frac{\Omega}{\Omega_0} = \frac{1 - \sqrt{1 - \frac{B}{B_0} \sin^2 \alpha_0}}{1 - \sqrt{1 - \sin^2 \alpha_0}} \approx \frac{B}{B_0}$$

Using the dipole approximation, note that the field strength B is given by:

$$|B| = \frac{B_0 R_0^3}{R^3} \sqrt{1 + 3 \cos^2 \theta}$$

where θ is the magnetic earth polar angle ($\theta = 0$ at the north magnetic pole), and R, R_0 are radii from the center of the earth. The field line is defined by $R = K \sin^2 \theta$, where K is a constant, so

$$\frac{B}{B_0} = \frac{\sin^6 \theta}{\sin^6 \theta_0} \sqrt{1 + 3 \cos^2 \theta}$$

then

$$\frac{d}{d\theta} \left(\frac{B}{B_0} \right) \Big|_{\theta = \theta_0} = -3 \sin \theta_0 \cos \theta_0 \left\{ \frac{\sqrt{1 - 3 \cos^2 \theta_0}}{\sin^2 \theta_0} + \frac{1}{\sqrt{1 + 3 \cos^2 \theta_0}} \right\}$$

If the Johnston Island magnetic coordinates are included

$$\theta_0 = (90 - 16.5) = 73.5 \text{ degrees and}$$

$$\left. \frac{d}{d\theta} = \left(\frac{B}{B_0} \right) \right|_{\theta = \theta_0} = 1.725$$

In a typical case, a debris cloud will cover a span of no more than 300 to 400 km, or $\Delta\theta \sim 3$ degrees. Thus

$$\left| \Delta \frac{\Omega}{\Omega_0} \right| \approx \left| \Delta \frac{B}{B_0} \right| \approx \left| \frac{d}{d\theta} \left(\frac{B}{B_0} \right) \Delta\theta \right| = [1.725][0.05 \text{ rad}] = 8.6 \text{ percent}$$

When a 10-percent error is ignored, $\frac{\Omega}{\Omega_0} = 1$. The integral referred to before then becomes:

$$F = \frac{\Omega_0}{4\pi} \int f dl$$

To simplify the above equation, the following definitions are made:

$Q = \int f dl$, and $q = \frac{Q}{E}$, where E is the total emission of the entire debris cloud. The quantity q then has a definite physical significance. It is the fraction of the debris cloud contained in a tube of unit cross section following the magnetic field lines extending from the detector to the atmosphere.

To conclude the expression, note that if:

- R = response of detector at time t
- $E(t)$ = total beta emission (in power units) from debris cloud at time t . ($E(t)$ is a function of time and includes the decay function)
- K = calibration of beta detector, or output per unit power in beta per unit area.

then

$$q = \frac{2R}{(1 - \cos \alpha)E(t)K}$$

The evaluation of this function is given in Chapter 4.

CHAPTER 2

PROCEDURE

This chapter describes rocket operations, payload instrumentation, environmental testing, and data requirements for Project 6.2. A discussion of rocket operations (Section 2.1) summarizes rocket performance and illustrates flight paths for all rockets fired during Project 6.2.

Section 2.2 describes the equipment built during the project. Topics discussed include payload calibration, gamma ray scanners (gamma scanner), beta detectors, omnidirectional gamma detectors, and photometers. The last two sections include discussions of payload vibration tests and project data requirements.

2.1 OPERATIONS

The Fish Bowl Series consisted of three events: Star Fish Prime (Star Fish), Blue Gill Triple Prime (Blue Gill), and King Fish. Test data on the debris cloud and its effects on the atmosphere were collected for Projects 6.2, 6.3, and 6.4. The Ballistic Research Laboratories (BRL) and Electro-Optical Systems, Inc. (EOS) were responsible for Project 6.2 and participated in the collection of test data during the three events. Project 6.2 was monitored by BRL, and EOS designed and constructed the instruments and payloads. EOS provided seven flight payloads, a spare payload, and rocket-launching services during the Fish Bowl Series. In addition, rockets and launch services were provided for Projects 6.3 and 6.4. These rockets were launched from Johnston Island. A summary of the characteristics of each event is given in Table 2.1, and a layout of the applicable instrumentation and rocket launchers on Johnston Island is shown in Figure 2.1.

Design of the Project 6.3 experiment was performed by the Air Force Cambridge Research Laboratories (CRL), and the payloads were constructed by Geophysics Corporation of America (GCA), Bedford, Massachusetts. CRL performed the experiment design task for Project 6.4, and the payload was constructed by Zimney Corporation of Monrovia, California. All vehicle procurement for Projects 6.2, 6.3, and 6.4 was the responsibility of EOS.

The Aerolab Development Company of Pasadena, California, and the Space Vehicles Group of Atlantic Research Corporation (ARC) of El Monte, California, manufactured vehicle hardware. All rocket launchers were constructed by ARC, with the exception of two modified by Schimmelman Engineering Company of Santa Ana, California. The firing system for launching the vehicles on the above projects was constructed by the Schimmelman Engineering Company. The launching of payloads on Projects 6.2, 6.3, and 6.4 was under the overall direction of BRL, and the firing of the vehicles was performed by EOS. A summary of the vehicles launched for Projects 6.2, 6.3, and 6.4 is shown in Table 2.2. Figure 2.2 gives an isometric presentation of Project 6.2 rocket trajectories. A complete description of rocket vehicle operations is given in Appendix A.

2.2 PAYLOAD INSTRUMENTS (PROJECT 6.2)

Seven instrumentation packages (payloads) were fired into the atmosphere by Honest John Nike-Nike, C-22, and Argo D-4 rockets. These packages contained several radiation-detecting instruments, telemetry and radar equipment, and power supplies. A sketch of a typical payload is shown in Figure 2.3. The purpose of the payload was to collect data on gamma and beta radiation for determining the size, shape, and flux intensity of the debris cloud resulting from Fish Bowl Series nuclear detonations. A block diagram of the payload is shown in Figure 2.4, and descriptions of the payload and its instruments are given below. Instrument discussions include payload installation and calibration procedures.

Table 2.7 summarizes Project 6.2 instrument package contents. Appendix C lists project reports and specifications.

2.2.1 Payload Description. Radiation flux was detected by four gamma scanners, a gamma detector, a beta detector, and a photometer. Three magnetometers provided payload aspect information for determining the orientation of these instruments with respect to the debris cloud. Instrument outputs were converted into voltages compatible with telemetry input requirements and used to modulate voltage controlled oscillators (VCO's), which produced frequency changes proportional to the data signal amplitude. All instrument output signals fed through the calibrator were automatically disconnected once every minute, and a five-level reference voltage was applied to the VCO's for in-flight calibration. The outputs from the VCO's were summed and amplified by two composite signal amplifiers. The output of one amplifier was routed to the very high frequency (VHF) telemetry transmitter, and the output from the second amplifier was routed to the GMD-1 beacon transmitter, which served as a tracking beacon for the GMD-1 and a backup telemetry transmitter. The C-band radar transponder was carried as a tracking aid, and a three-frequency beacon was employed to provide data on the electron content of the ionosphere. A commutator provided a time-sharing mechanism for transmitting engineering data,

such as payload temperature and battery output voltages, on telemetry channel (band) 16. The signal monitor Ledex switch enabled preflight checkout of payload instruments by switching output signals to ground support equipment for display. The power change-over Ledex switch transferred the payload power source from external power supplies to the payload batteries before launching.

The payload consisted of an ogive fiber glass nose cone, a ground plane, antennas, a rocket adapter, electronic equipment, and a magnesium structure. The approximate weight of these units was 167 pounds. The overall height of the payload was 49 inches, and the base diameter was 15 inches. The center of gravity was on the thrust axis, 16 inches above the base.

2.2.2 Calibration of Gamma Detectors in the Payload. The gamma scanners, installed in a spare payload, were calibrated to determine the shielding effects of the structure on their performance. Other flight payloads were not tested, because stringent schedule requirements did not permit these tests to be performed before the rockets were launched from Johnston Island. Calibration data are given in Appendix D.

The shielding effects of the payload structure on each scanner detector were determined by subjecting the detectors to a point source of gamma rays as the payload was rotated about an axis through the detector and parallel to the thrust axis of the payload. The count rate was determined at 5-degree intervals as the payload rotated 360 degrees. This procedure was repeated for 21 positions of the source along the arc of a semicircle with its center located at the detector.

The X, Y, Z coordinate system shown in Figure 2.5 is fixed to the payload with the Z-axis coincident with the thrust axis of the payload. Axis-Z' is the rotation axis of the payload. It passes through the detector and is parallel to the Z-axis. Coordinates X' and Y' are also parallel to the X and Y payload coordinates as described in the previous paragraph. Theta (θ) was the angle between

the Z'-axis and the line through the source and the detector. The source location was varied from 0 to 180 degrees in increments such that $|\cos \theta_i - \cos \theta_{i+1}| = 0.1$. Thus, the polar angle increments varied from 0 to 180 degrees and provided a constant solid angle for each setting of θ . The plane in which the source moved was used as a zero reference for the azimuth angle (ϕ). Phi (ϕ) was zero when the Y'-X' plane of the payload coincided with the plane in which the source was moved. For a given source angle, θ_i , the payload was rotated 360 degrees in the clockwise direction in increments of 5 degrees. A 170-millicurie Co^{60} source was used for the calibration. The distance between the source and detector was held constant at 125 cm, which gave an incident flux at the detector of 8×10^4 Mev/cm²-sec.

The payload and Co^{60} source were aligned so that the plane of motion of the source from 0 to 180 degrees was coincident with the Z'-Y' plane of the payload. A transit and plumbbob were used to perform the alignment before calibrating each gamma detector.

Rotation of the payload was obtained by setting the unit on a motor-driven table. A remote control box was used to start the motor for each θ setting. When the table rotated 360 degrees, the motor automatically stopped until started for a new test run.

2.2.3 Gamma Scanner. Each payload contained two gamma scanner assemblies, and each assembly consisted of 20- and 90-degree aperture telescopes. Thus, four gamma telescopes were installed on each rocket. One assembly, the vertical scanner, was mounted parallel to a plane along the thrust axis with its 90-degree telescope near the axis of spin. The second assembly, the horizontal scanner, was mounted parallel to a plane tilted 15 degrees from a plane perpendicular to the thrust axis with its 90-degree telescope near the thrust axis. The locations of these assemblies in the payload structure are shown in Figure 2.6.

Equipment Description. The gamma scanner represented a unique approach to the problem of scanning the debris cloud to determine its size, shape, and gamma emission. The scanner is referred to as a negative telescope, because the detector is shielded from the area being viewed. These instruments scanned the debris cloud in the vertical and horizontal directions, as a result of the spin and trajectory movements of the payload.

The gamma scanner assembly consisted of four Nuclear-Chicago type D-80 Geiger-Mueller (G-M) tubes, two uranium 238 (U^{238}) shields, four pulse-forming circuits, four data processors, one rate generator, and a 600-volt power supply. The scanner shields, detectors, and pulse-shaper circuits were contained in a flat, disk-shaped aluminum container approximately 1.8 inches thick and 5.3 inches in diameter. The rate generator and data processors were contained in three pie sections which combined to form one circular unit. The high-voltage power supply was in a rectangular aluminum container and mounted adjacent to the scanner assemblies. Brief descriptions of the gamma telescope, data processor, and rate generator are given below.

Gamma Telescope. Two gamma-sensitive Geiger-Mueller tubes were mounted on opposite sides of a uniquely shaped shield for each gamma scanner, as shown in Figure 2.7. A saucer-shaped shield was selected to accommodate six detectors around its circumference. However, because of physical limitations, only two detectors could be used. Since these limitations were determined late in the program, a lighter conical shield could not be fabricated in time for the experiment.

One G-M tube was mounted at the apex of the 20-degree edge of the shield; the other tube was mounted opposite the first at the apex of the 90-degree edge. The shield was fabricated of depleted U^{238} for maximum shielding effects. The scanning action was due to the spin and trajectory motion of the carrier rocket. For each revolution of the payload, the debris cloud was alternately viewed through a 20-degree negative aperture and a 90-degree negative aperture. The 20-degree aperture is shown in Figure 2.8. Gamma radiation from the debris cloud within the 20-degree aperture S was attenuated by the shield before it reached the detector. Radiation outside S was received by the detector unattenuated. Thus, as the shield and detector assembly rotated in a clockwise or counterclockwise direction, due to the rocket spin, the detector output varied from a minimum value when the shield blocked the detector's field of view to a maximum when the shield rotated away

from the cloud direction. See Figure 2.9 for a plan view of detector signal amplitude versus angle of rotation. Since the gamma radiation attenuated by the shield was the most important data required for studying the debris cloud, a calculation was performed to obtain its value. This radiation flux was approximated by the conversion equation given below:

$$F_S = F_{\max} - F_U$$

Where: F_S = flux due to debris cloud that existed in the field of view (solid angle) shielded from the counter by the uranium wedge

F_U = flux received by the detector from the unshielded region

F_{\max} = maximum flux received by the counter during a payload revolution

Therefore, the radiation within the 20-degree field of view of the scanner was obtained by subtracting F_U , the radiation flux received by the detector, from F_{\max} which approximated the flux that would have been received by an unshielded counter.

Nuclear-Chicago type D-80 G-M tubes were chosen as detectors because of their small size and short deadtime of approximately 10 μ sec, which placed the maximum count rate in the order of 10^5 counts/sec. Each output pulse represented a gamma flux of 300 Mev/cm²-sec. The pulses from the detectors were fed to the Schmitt trigger circuit (pulse shaper) which produced pulses of constant amplitude and pulse-width that were routed to the data accumulator as shown in Figure 2.10.

Incident gamma radiation stimulated the G-M detector, which produced digital output pulses that were counted and converted into analog signals by the data processor. The rate generator controlled the sequence of data processor operations. Only one rate generator was required to control the operation of the four data processors in the two scanner assemblies.

Data Processor. The data processor was an electronic subsystem for processing the outputs of the G-M tubes in the gamma scanner and conditioning them for telemetry transmission to earth. The four processors

per payload converted the detector output pulses into analog voltages which were proportional to the gamma flux detected by the telescopes.

The schematic diagram is shown in Figure 2.11. The system consisted of an 8-bit accumulator, 8-bit transfer gate, 8-bit storage register, and 8-bit digital-to-analog converter. In addition, a rate generator and 5-volt reference source were provided for each set of four payload processors.

The rate generator produced a gating pulse that allowed pulses from the scanner to enter the accumulator for a period of 10 msec. At the end of this sampling period the input gate was closed for 1.25 msec, during which time the storage register was cleared and the data in the accumulator was transferred to the storage register. After the accumulator was reset to zero, the input gate was again opened for 10 msec. The output of the storage register was converted to an analog voltage for telemetry by the digital-to-analog converter. The converter consisted of transistor switches that applied 0 to 5 volts to each resistor in the resistance adder shown in Figure 2.11. The voltages applied across each resistor were summed by the adder and transferred to telemetry equipment. The output of the converter was integrated by capacitor C1 and the converter output impedance to prevent switching transients from overmodulating the telemetry. Since the sampling period was precisely controlled by a stable clock generator, the output voltage was proportional to count rate. The maximum capacity of the system was 25,600 counts/second, which was represented by a 5-volt output.

Rate Generator. The rate generator consisted of a clock generator, a 4-stage $\frac{n}{9}$ counter, two 100- μ sec delay circuits, a 5-volt reference source, and power drivers. The clock generator was a highly stable free-running multivibrator with temperature compensation. Temperature drift stabilization was 1 cps/5 $^{\circ}$ C. The output from this generator triggered the 4-stage counter, which produced one output pulse for every nine input pulses. The output from the last stage reset the storage register, closed the data input gate, and triggered the delay circuit,

which produced a 100- μ sec delay pulse. This delay pulse transferred data from the accumulator to the storage register by opening the transfer gates, and also triggered a second delay circuit. One hundred microseconds later, the falling edge of the delay pulse triggered a second delay circuit, which reset the accumulator.

Installation. The horizontal gamma scanner assembly, consisting of two negative telescopes and a high-voltage power supply, was mounted in Quadrant A just below the gamma scanner data processor (See Figures 2.3 and 2.6). The vertical scanner was mounted below the horizontal scanner. The installation procedure included mounting the scanner assembly to payload structure with five screws and connecting the signal-power cable to its input jack. The data processor and rate generator assembly were mounted with Allen-head cap screws just below the voltage-controlled oscillators. Power and signal connections were provided by two Bendix pygmy-type connectors.

Calibration. The gamma scanners were calibrated individually, using a 64-Mc Co⁶⁰ source. This procedure involved placing the source at specified distances from the detector surface and recording the count rate of the detector. The Co⁶⁰ source was placed 30 inches from each G-M tube, and the number of output pulses were recorded as the distance between the source and tube was reduced in 5-inch increments. At 5 inches from the tube, output pulses were recorded at each 1-inch increment until the source touched the scanner assembly. A curve was plotted for each detector in counts versus energy flux. Typical curves for the scanners are given in Appendix E.

Each G-M tube was checked for operating voltage range and plateau slope. Detectors with similar characteristics were mounted on each scanner assembly to reduce differences in output voltages caused by variation in the high-voltage supply output. The procedure for obtaining these characteristics was to attach the detector to a mounting fixture and to apply 500-volt dc across its terminals. The

detector was placed in the access hole of the 64-Mc Co⁶⁰ storage container (see Figure 2.12), and its output count rate was monitored on a Nuclear-Chicago scaler and recorded. This was repeated for applied voltages of 525, 550, 575, 600, 625, and 650 volts. Plots then were prepared depicting G-M tube count rate versus applied detector voltage.

2.2.4 Omnidirectional Gamma Detector. The omnidirectional gamma detector (gamma detector) was a typical crystal photomultiplier scintillator with a 4π steradian field of view. One detector was used in each payload, and its location was in the lower portion of Quadrant C (see Figures 2.3 and 2.13). The purpose of the gamma detector was to provide supplementary gamma flux data for evaluating the data collected by the gamma scanners.

Equipment Description. The gamma detector assembly is shown in Figure 2.14. (The beta and gamma detector assemblies appear the same.) The gamma detector consisted of a 1/2-by 1/2-inch cylindrical thallium-activated cesium-iodide (CsI) scintillating crystal, a Dumont 7860 photomultiplier (PM) tube, a preamplifier, integrator, dc amplifier and 1250-volt power supply. The crystal, PM tube, and electronics were mounted in an aluminum cylinder, and a magnetic shield was placed around the PM tube to reduce the effects of the earth's magnetic field on its output. The cylinder was filled with silicone rubber to prevent equipment damage from shock, vibration, and humidity. A phenolic shield was placed over the CsI crystal to prevent beta particles from stimulating the crystal and thereby producing output pulses that did not represent gamma radiation.

The CsI crystal produced photons when it was exposed to gamma radiation. These photons stimulated the PM tube, which produced output pulses with amplitudes proportional to the energy absorbed by the crystal. These pulses were amplified by a preamplifier, integrated, amplified again, and then transferred to telemetry equipment. The block diagram for the gamma detector is shown in Figure 2.15. The time constant of the integrator was 10 msec. Thus, its output was proportional to the energy absorbed per second by the crystal when the rise and fall times of the

gamma flux were greater than 10 msec. The output voltage to the telemetry equipment varied between 0 and 5.6 volts. A Zener diode prevented the output voltage from exceeding 5.6 volts when the detector saturated from overexposure to gamma radiation. The 0.75-inch-thick beta shield prevented particles with energies below 4 Mev from reaching the CsI crystal. The gamma detection range of this instrument was between 2 and 8×10^6 Mev/cm²-sec.

Installation. The gamma detector assembly was mounted to intercostal C-D (Figure 2.3) with four Allen-head cap screws. The payload power and signal harness cable was connected to the detector assembly with a Bendix 14-pin pygmy connector.

Calibration. The gamma detector was calibrated by placing a 64-Mc Co⁶⁰ source at predetermined distances from the detector. The detector output voltage was measured and recorded as the distance between the source and detector was reduced from 100 cm to zero, in 20 steps. The energies per gamma photon disintegration for the source were 1.17 and 1.33 Mev. A typical calibration chart for gamma detector No. 1 is given in Appendix E. Since the detector was subjected to a gamma energy spectrum of U²³⁵ during the experiment, the energy coordinates (abscissas) were multiplied by 1.9. This computation was necessary because the crystal absorbed only 52.9 percent of the incident energy.

2.2.5 Beta Detector. The beta detector was a scintillator-multiplier instrument. One detector was used in each payload, and its location was in the rear of the payload in Quadrant A (see Figure 2.3). The purpose of the beta detector was to provide supplementary data on beta emission from the debris cloud for comparison with gamma flux measured by the gamma detector.

Equipment Description. The beta detector is shown in Figure 2.14 and consisted of a 1/2-inch-diameter by 0.4-inch-thick stilbene scintillating crystal, a Dumont 7860 PM tube, a preamplifier, integrator, dc amplifier, and a 1250-volt power supply. A paper window was placed over the crystal to exclude visible light waves. The aperture of the

detector was 120 degrees on Rockets 8 and 9, and 30 degrees on Rockets 15, 18, 19, and 29.

The beta and gamma detectors were identical except for their crystal scintillators. A stilbene crystal was used for the beta detector; and a cesium iodide crystal, for the gamma detector. Therefore, the operation of the beta detector is the same as that given in Section 2.2.4.

Installation. The beta detector assembly was mounted to intercostal A-D (Figure 2.3) with four Allen-head cap screws, and the payload power and signal cable was connected to the detector assembly with a Bendix 14-pin pygmy connector.

Calibration. The beta detector was calibrated by placing calibrated absorbers between the detector and a 25-Mc Sr^{90} source. This source produced a beta energy spectrum from 0 to 2.25 Mev with an average energy of 1.12 Mev. The distance between the detector and Sr^{90} source was adjusted to produce a 5-volt output voltage. This voltage represented the maximum instrument output signal. Plastic absorbers of different thicknesses were then placed in a jig accurately positioned between the source and the detector. Fifteen absorbers were used during this calibration procedure, and their absorption constants varied from 0 to 1,000 mg/cm^2 .

The incident detector flux was calibrated by using the average beta energy, distance between source and detector, density of air, detector aperture, and the absorber's attenuation factor. As a result of this computation, detector output voltages versus incident radiation energies were tabulated. These tabulated values were corrected to eliminate errors due to the gamma sensitivity of the crystal and the U^{235} energy absorbed from the debris cloud. Since the beta detector absorbed 12 percent of incident gamma radiation, a correction factor curve was plotted as described previously for the gamma detector. For a U^{235} energy spectrum, the energy absorbed by the stilbene crystal was 90 percent instead of 100 percent of the incident energy from a Sr^{90}

source. Thus the absorption energy for each curve was multiplied by 1.1. The energy absorption of the light window was neglected because the error it produced did not significantly affect the accuracy of the calibrated detector output.

2.2.6 Photometer. The photometer was a conventional aurora airglow instrument with a 5-degree field of view. The photometer was located in Quadrants C and D as shown in Figure 2.3. The purpose of the photometer was to supplement the data collected by the magnetometers for determining the altitude and orientation of the gamma scanners. A secondary purpose was to measure the N_2^+ emission band intensity and distribution of the aurora induced in the upper atmosphere by the nuclear detonation.

Equipment Description. The photometer, shown in Figure 2.16, consisted of a 2- by 2- by 1/4-inch ultraviolet interference filter, a lens system, a 6935 Dumont PM tube, a dc amplifier, and 1250-volt power supply. The 2-inch-square objective lens and a 15-mm-diameter field lens were bonded to aluminum frames, which were screwed to the 3.5-inch-diameter stainless steel cylinder. The smaller (2.5-inch) cylinder contained the PM tube, dc amplifier, and power supply. These components were sealed in the cylinder with silicone rubber as previously described for the gamma detector. The photometer aperture was shielded when the vehicle was on the launch pad to prevent damaging the detector by exposure to solar or other high-intensity light sources.

The photometer produced 0-to 5.6-volt output pulses when exposed to ultraviolet radiation at 3914 \AA . Aurora-type radiation having a bandhead at 3914 \AA was generated when beta particles, emitted from the detonation, ionized nitrogen molecules in the upper atmosphere. This radiation penetrated the ultraviolet filter element shown in Figure 2.17. The filter bandwidth was 50 to 60 \AA at 50 percent of the maximum filter transmittance (27 percent). Incident radiation was focused on the plane of the objective lens. The field stop prevented radiation beyond the desired 5-degree field of view from reaching the detector. The

field lens focused all images onto the same photocathode surface area and thereby eliminated errors caused by nonuniform cathode area sensitivities. Without the field lens, images would have been focused on different areas of the cathode, and the resulting output signal amplitudes would have varied with the sensitivity of each area. Thus, the photomultiplier output signal was a function of total power and independent of the distribution of field brightness. A test lamp also was mounted on the assembly to check the functional operation of the photometer during preflight tests.

Installation. The photometer assembly was mounted to the payload structure, intercostals A-D and C-D, with eight flathead screws, and the payload power and signal cable was connected to the assembly with a Bendix 14-pin pygmy connector.

Calibration. The photometer was calibrated with a tungsten filament light standard, calibrated by the National Bureau of Standards, Washington, D.C., as described in Reference 3. The light source and photometer were placed in a black box and accurately positioned from each other. A neutral density filter reduced the light intensity to within the detection range of the photometer, and graded neutral density filters were inserted between the photometer and light source to determine response linearity.

The calibration constants for each photometer used during the Fish Bowl Series are given in Table E.1. Different constants were obtained for each instrument, because the interference filters had different spectral qualities.

2.2.7 VHF Telemetry Systems. The very high frequency (VHF) telemetry system consisted of flight and ground equipment briefly described below. The location of airborne telemetry components on the payload is shown in Figures 2.3, 2.6, and 2.13.

Airborne Telemetry. Project 6.2 flight telemetry was a standard FM/FM system with 11 inter-range instrumentation group (IRIG) channels. Ten channels were used for continuous data, and one channel for commutated data. An in-flight calibrator was employed to reduce errors due to temperature drift in the voltage-controlled subcarrier oscillators (VCO) on Rockets 8 and 9. Every 60 seconds, the calibrator inserted a 0- to 5-volt signal of 100-msec duration to the inputs of the VCO's. The 5-volt signal consisted of five 1-volt steps. The outputs of the VCO's were fed to a composite-signal amplifier, which combined and amplified the subcarrier signals and fed them to the 2.5-watt transmitter. A similar unit was employed as a buffer amplifier for the signal input to the GMD-1 beacon transmitter. On the Argo D-4 payloads, the output of the 2.5-watt transmitter was amplified by the 10-watt radio frequency (RF) amplifier and routed to the antenna. A block diagram of the telemetry system is shown in Figure 2.18.

Power to both the transmitter and the RF amplifier was supplied by a dc-to-dc converter. Telemetry channel 16 was time-shared by a miniature electromechanical commutator, which was driven by a voltage-regulated dc motor. The unit was a single-pole 10 x 30 commutator with a standard IRIG double-width synchronization pulse. The signals monitored through the commutator provided engineering data on the payload and BRL instruments, such as temperature and battery voltages. The reference voltage for the digital-to-analog converter in the gamma scanner rate generator also was monitored through this commutated channel.

Ground Telemetry. The ground telemetry system received, demodulated, and recorded telemetry signals from the various payloads. The helical antennas were coupled through a patch panel into preamplifiers and then route through a bandpass filter to a multicoupler. The multicoupler divided the signal, sending it through separate line-matching pads to the receivers, Each of the three radio-frequency channels was provided with two receivers to increase the system reliability. The outputs of the receivers were recorded on two Mincom C100

tape recorders. Tape recorder output signals were demodulated by sub-carrier discriminators for data reduction. The operator could select any eight subcarrier channels of the received telemetry data for real-time demodulation and recording on oscillographs.

The automatic gain control signal (AGC) from each receiver modulated a subcarrier oscillator and was recorded on separate tape tracks. The launch-indication pulse from the blockhouse, denoting the launch time of each rocket, and the automatic gain control signals also were recorded on magnetic tape. A spectrum display unit was provided for monitoring a 2-Mc bandwidth centered on the received signal, and was used for analyzing interference problems.

A second subcarrier spectrum display unit was provided to monitor the number and quality of subcarrier signals modulating the received RF signals. One telemetry ground station was built, and its test site location is shown in Figure 2.1.

Installation and Calibration. The telemetry system components were screw mounted at various locations on the payload. The transmitter was mounted on intercostal C-D; the VCO's and two signal amplifiers on an aluminum block screwed to intercostals A-D and B-A; the power amplifier was screwed to intercostal C-D; and the in-flight calibrator was screwed to intercostal A-D (see Figures 2.3 and 2.6). The dc-to-dc power converter was mounted to intercostal C-B; and the commutator, to intercostal B-A.

2.2.8 GMD Transmitter. The airborne GMD transmitter and three modified AN/GMD-1 Rawin receivers provided payload azimuth and elevation tracking data during the experiment. The GMD transmitter also was used as an auxiliary data transmitter for the payload VHF telemetry system.

Equipment Description. The transmitter consisted of a transistor modulator, a vacuum tube oscillator, and a

dc-to-dc converter. An internal Ledex-type wafer switch connected the internal battery to a ground support equipment battery charger.

The transmitter operating frequencies were 1660, 1670, and 1680 Mc, and its output power was between 500 and 1,000 mw. The telemetry composite signal from the VCO's deviated the GMD transmitter output frequency several hundred kilocycles.

Installation and Calibration.

The GMD transmitter was mounted in Quadrant C above the photometer and C-band beacon. A 4-inch-diameter stainless steel strap held the unit in place, and the strap was attached to intercostals D-C and C-B with four screws.

2.2.9 C-Band Beacon. The C-band beacon allowed the rockets to be tracked by radar aboard the DAMP ship. The beacon, a high-power radar AN/LFN-73 transponder, was built by Aero Geo Astro Corporation (AGAC). The superheterodyne receiver operated in the 5,400- to 5,900-Mc frequency band. The receiver sensitivity was -65 dbm over its frequency range, and its bandwidth was 8 ± 2 Mc at its half-power points. A two-cavity preselector provided high selectivity and low drift, and a duplexer prevented receiver damage during data transmission. Pulse-code spacing for two pulse operation was 3 to 9 μ sec, depending on the payload.

The magnetron transmitter frequency drift did not exceed $0.05 \text{ Mc}/^\circ\text{C}$. Minimum output pulse power was 400 watts with a pulsewidth of 0.5 μ sec.

The C-band beacon components were housed in a rectangular box 3 by 6 by 6 inches, and its weight was 5.75 pounds. The assembly was pressurized to 15 psig.

Installation and Calibration. The C-band beacon was mounted above the photometer in Quadrant C with six socket-head cap screws. Although EOS did not calibrate the C-band beacon, it was checked for proper operation at the test site by AGAC personnel.

2.2.10 Three-Frequency Beacon. The three-frequency beacon generated three phase-coherent signals at 37, 148, and 888 Mc. It was mounted above the photometer in payload Quadrant D. This transmitter was used to determine the electron density of the ionosphere after the burst, by transmitting three signals of different frequencies to a ground station. These signals were mixed and their phase shifts observed. The phase shifts indicated the degree of signal dispersion and, consequently, were a measure of the ionosphere electron density.

Equipment Description. The three-frequency beacon cylindrical package was approximately 6 inches in diameter and 6 inches deep. The unit consisted of an oscillator, a 37-Mc amplifier, a 148-Mc doubler amplifier, and an 888-Mc multiplier amplifier. The 37, 148, and 888-Mc signals from each amplifier mentioned above were fed to their respective antennas and transmitted to earth (Reference 5).

Installation and Calibration. The three-frequency beacon was mounted to intercostal A-D with a stainless steel strap 3/4 inch wide. This strap was fastened to the payload structure with four flat-head screws. This equipment was supplied by BRL.

2.2.11 Battery Power Supplies. Two packages of Yardney Silvercel PM series silver-zinc cells provided power to all payload hardware requiring external power during flight. The battery packages were located in the base of the payload. (See Figure 2.13.) One battery package consisted of 19 PM-3 cells and provided a 28-volt output. The second package consisted of 19 PM-3, 10 PM-1, 10 PM-1, and 4 PM-1 cells and provided 28-, 12-, 6-, and -12-volt outputs.

Equipment Description. The Yardney Silvercel is a silver-zinc alkaline battery. Silver and zinc were employed as the electrodes, and the electrolyte was a strong solution of potassium hydroxide (KOH).

Manually activated primary cells (PM series) were obtained dry charged for this application, which required quick activation and a high discharge rate. The life expectancy of the PM Silvercel batteries was either 3 to 5 charging cycles or 2 months' wet life, whichever came first. The Yardney Silvercel is relatively free from the hydrogen explosion hazard, which is common among conventional batteries when used in closed, nonventilated areas. However, sufficient hydrogen to cause an explosion (if ignited) could have been generated if the Silvercel became defective or badly overcharged.

The various radiation detecting instruments, and the telemetry and beacon equipment in the payload, required a stable voltage and power source during flight. The Yardney Silvercel batteries provided a very flat discharge curve at high current rates during the major portion of the discharge cycle. Refer to Figure 2.19 for a plot of typical output voltage for a 60-minute discharge rate.

Battery pack No. 1 was a quarter circle, 3 inches deep with a 7.3-inch radius. This pack contained the 28-volt battery for the telemetry equipment and also provided input power to five high-voltage power supplies for the radiation-detecting instruments. The battery consisted of 19 PM-3 type cells connected in series. Battery pack No. 2, a quarter circle 2.5 inches deep with a 7.3-inch radius, contained the primary power source for the C-band beacon. This 28-volt power supply consisted of 19 PM -1 type cells connected in series. Other power supplies in this package included eight 12-volt PM-1 type cells connected in series with the negative terminal grounded, a 6-volt tap-off from the fourth cell of the 12-volt supply, and eight -12-volt PM-1 cells connected in series with the positive terminal grounded. The capacity over a 60-minute discharge rate was 1 ampere-hour for the PM-1 cell, and 3 ampere-hours for the PM-3 cell.

Since the battery cells were dry charged, it was only necessary to fill each cell with the prescribed amount of KOH and allow the cells

to soak for 1 hour before they were ready for use. A preliminary check of the open circuit voltage ensured that each cell was functioning properly.

Installation. The two battery packs were stacked together with a soft rubber insulator and a rubber gasket between the packs. A cover plate and the two battery packs were fastened together by three flat-head screws which were countersunk below the surface of the cover plate. The package was installed in the base of the payload (Quadrant B) and fastened to the base plate with three Allen-head cap screws.

Calibration. No battery calibration was required. However, tests were conducted to ensure that the cells were capable of delivering the required power for a period which exceeded the flight time of the payload. In all cases the ampere-hour capacity of the batteries was several times greater than instrument requirements.

2.2.12 Power and Signal Switches. Two Ledex-type switches provided power control and signal monitoring functions. These switches were located in the Quadrant B, and the signal monitor switch was mounted in the center section to provide the shortest lead length to all instruments for power distribution and signal monitoring. The power change-over and signal monitoring switch enabled the payload operation to be controlled from a remote control station. External power from the ground support equipment (GSE) power supply rack was provided for instrument prelaunch checkout. Just prior to launch, the instruments were transferred to payload battery power by closing the power change-over switch with a solenoid-type stepping motor. The instruments were reconnected to the GSE power supply rack when launching delays occurred.

Equipment Description. A prelaunch checkout of instrument operation was performed by connecting the instruments to ground support equipment. The monitoring was conducted through the umbilical cable.

The signal monitoring switch facilitated the remote selection of instrument outputs to be checked for proper operation and also routed test signals from GSE to the instrument to be monitored.

The power change-over switch, a 22-pole, 2-position, nonshorting, stepper-actuated switch, was enclosed in a hermetically sealed container. When high-current switching was required, several poles were connected in parallel to increase the contact rating. Its overall dimensions were 3 by 2 by 4.5 inches. The signal monitor switch, a 2-pole, 12-position, nonshorting, stepper-actuated switch was also enclosed in a hermetically sealed container. Its dimensions were 2 by 2.25 by 3.5 inches.

Installation. The switch assemblies were screwed to the payload structure with four Allen-head cap screws. The signal monitor switch was mounted to intercostal C-B, and the power switch, to intercostal B-A. Electrical connections to the signal monitor switch were made by soldering the umbilical cable leads to header pins mounted on one end of the sealed container. Electrical connections to the power change-over switch were made by connecting two cables from the umbilical harness to connectors on one side of the container.

. 2.2.13 Temperature Sensors. The temperature sensors provided data on payload temperature during rocket flights. These sensors consisted of a Micro-Systems MSI-111-1000 sensing element and an EOS current regulator. Four sensors were mounted on each payload for Rockets 8, 9, 15, and 18. Payloads for Rockets 19, 26, and 29 did not include sensors, because the results from ground tests and the first two events indicated that the payload temperature did not vary significantly during flight period.

Equipment Description. The temperature sensor consisted of a thermally sensitive silicon element and a current regulator. The regulator

supplied the sensor with a constant current so that the sensor resistance could be accurately converted into voltages proportional to temperature. Voltages developed across the sensing element were transmitted by the telemetry system to the ground station. The sensor was designed to measure temperatures from -24 to 150°C .

Installation and Calibration. One temperature sensor (sensing element and regulator) was bonded to each payload intercostal with epoxy. The sensing element was placed near circuits which were most sensitive to temperature changes to correlate their operation with payload temperature during flight.

The current to each sensing element was adjusted to provide a 1.3- to 5-volt output when the sensor was subjected to a temperature range from -25 to 150°C . The linearity of each detector was checked before payload installation.

2.2.14 Magnetometers. Three Schonstedt type RAM-3 magnetic aspect sensors (magnetometers) were on each rocket to provide payload aspect with respect to the earth's magnetic field vector. Each magnetometer consisted of a field sensor and a data-conditioning electronic unit. The field sensors (see Figure 2.20) and their electronic units were mounted at the top of the payload. The magnetometers provided information with respect to the direction of the earth's magnetic field. Since the payload detection instruments were directional, data on the earth's magnetic field was required for determining their orientations with respect to the debris cloud.

Equipment Description. The electronics unit was in a cylindrical package 3 inches long and 1.75 inches in diameter. Two connectors mounted on one end of the package provided electrical connections for the field sensor, external power input, and output signals. The field sensor, a cylinder 3.2 inches long and 0.75 inch in diameter, was permanently attached to a 1-foot cable, which was connected to the electronics unit. Refer to Figure 2.3. The electronics unit contained an input voltage regulator, oscillator, phase detector, and rectifier. The field sensor was a highly permeable magnetic core transformer. A block diagram of the magnetometer is given in Figure 2.21.

The presence of a magnetic field parallel to the axis of sensitivity (long axis) of the field sensor resulted in the generation of second-harmonic voltages in the split-secondary winding of the sensor. No output was generated when the field was perpendicular to the sensor axis. The second-harmonic signals were fed to the phase-sensitive rectifier where they were added to a 5-kc oscillator reference voltage. When the signal from the sensor was zero, the reference voltage produced equal dc voltages across R4 and R5 (see Figure 2.22); hence, the output voltage across C6 was zero. Any second harmonic voltage produced in the center-tapped winding of the sensor unit combined with the reference voltage in such a way that the voltages across R4 and R5 were no longer equal. The magnitude of the resulting voltage across C6 was proportional to the sensor voltage, and its polarity depended upon the phase of the sensor voltage with respect to the reference voltage. The proper operation of the circuit depended on the resistance-capacitance time constants of the circuit being sufficiently long that only the peak values of the voltages were detected by diodes D1 and D2.

The output voltage was biased to 2.4 volts by a Zener diode so that no negative output voltages appeared at the VCO input. Thus, the magnetometer output signals were compatible with telemetry input requirements.

Installation. The three sensors were mounted in a phenolic block so that they were mutually perpendicular to each other. The sensors were then bonded to the block with epoxy, and the block was attached to a mounting plate on the payload structure top with four screws. The electronic units were screwed to the underside of the mounting plate with three screws.

Calibration. Calibration of the field sensor was performed by the manufacturer before delivery to EOS. Instrument operation was checked by subjecting the sensors to the earth's magnetic field. In every check, the calibration was accurate to ± 1 percent. A procedure for calibrating the magnetometer before and after payload installation is described in Appendix F.

2.2.15 Voltage Regulator. The voltage regulator was a modified series transistor negative-feedback regulator. This unit was flown in the last three payloads and regulated the -12-volt and 12-volt power supply outputs to within ± 2 percent. The regulator package was mounted in Quadrant B (see Figure 2.3).

Equipment Description. The regulator consisted of two identical sections, except for loading resistor R11 which was connected across the -12-volt output. Circuit components included transistors, Zener diodes, diodes, and resistors. These components were mounted on an anodized aluminum chassis. The overall dimensions of the package were 4.5 by 2.5 by 1.25 inches.

The regulator circuit is shown in Figure 2.23. The diodes CR5 and CR6 provided thermal compensation for the transistor Q6 and Zener diode CR2. Transistor Q2 absorbed changes in input voltage by varying its impedance, and Q6 detected changes in output voltages by comparing the reference voltages across CR2 with the voltage across R10. Components Q3, Q4, Q5, CR1, CR3, CR4, and R8 in the second section served the same functions as Q1, Q2, Q6, CR2, CR5, CR6, and R10.

Installation. The regulator was mounted in Quadrant B just below the magnetometer mounting plate. Four Allen-head cap screws fastened the assembly to the payload structure (intercostal B-A).

Calibration. The voltage regulators were calibrated by connecting the output voltage from a power supply to the 12-volt regulator input. A 30-ohm, 10-watt resistor was connected across the output terminals, and the 12-volt trimpot was adjusted for a 12-volt output when the power supply voltage was 13 volts. The output of the power supply was then increased to 15 volts dc, and the regulator output voltage was checked. When this output voltage exceeded 12.2-volt dc, the calibration procedure given above was repeated until the voltage remained within 12 ± 0.2 volts. The -12-volt section was calibrated as described above, except that the 30-ohm load resistor was replaced with a 60-ohm resistor.

2.2.16 Engineering Measurements. Engineering measurement circuits were included in the payload for monitoring instrument operating voltages during flight. Voltage dividers were employed to measure only positive voltages, and a 15-volt battery was used to bias the -12-volt input to the instrument power supplies to a positive value. Thus, all voltages were compatible with telemetry requirements. The purpose of these measurements was to provide data on the operation of the payload power supplies during the flight.

The voltages monitored were the 28-volt dc power for the telemetry system and high-voltage power supplies used by the detecting instruments, 28-volt dc for the C-band beacon, 12-volt dc for the electronics circuit of the instruments, 6-volt dc for the magnetometers, and -12-volt dc for the electronic circuits of the detecting instruments. The divider board was near the center of the payload in Quadrant B.

Equipment Description. The engineering measurement circuits were fabricated on a Fiberglas board approximately 3 by 2 by 0.25 inches and terminals were installed on one side to accommodate the voltage divider resistors. Input and output leads were attached to a connector for ease of installation. A 15-volt battery was secured to the board by a clip, and connected in series with the -12-volt battery and the telemetry input.

Installation and Calibration. The circuit board was mounted to the structure in Quadrant B, intercostal B-A, with four Allen-head cap screws. The connector was attached to a stand-off, which was secured to the structure with two Allen-head cap screws.

Before installation of the voltage divider network into the payload, precise voltages were applied to the divider, and the voltage at each junction was measured to verify that the correct value was obtained.

2.2.17 Ground Support Equipment. Four racks of ground support equipment were used to perform preflight checkout of payload operation (see Figures 2.24 and 2.25). These racks contained standard electronic test equipment, power supplies, and battery chargers. A control panel facilitated the manual selection of instrument outputs, which were

monitored with oscilloscopes, voltmeters, and recorders. The umbilical cable from the rocket was connected to the payload power supply rack. Two other racks in the blockhouse were connected to the power supply rack with 2,000 feet of cable. These racks contained the control panel, test equipment, and power supplies. A fourth rack contained battery chargers for the payload Silvercel batteries.

2.3 PAYLOAD ENVIRONMENTAL TESTING

Seven payloads were subjected to preflight vibration tests before shipment to the Johnston Island test site. The instrumentation payloads were vibrated from 5 to 5,000 cps at 0.6 to 36 g, according to EOS Specification 2193-45. The maximum vibration amplitude was selected to simulate the fourth stage of the Argo D-4 rocket, which produced the highest vibration levels of all the rockets flown. The instruments and telemetry equipment were checked for correct functional performance before, during, and after vibration. No electronic or structural failures occurred during these tests. Although Specification 2193-45 included several other tests, such as high and low temperatures, humidity, fungus, shock, and salt-fog environments, insufficient time was available to complete them as planned.

2.3.1 Vibration Tests. The payload was mounted to the exciter as shown in Figure 2.26. The instruments were subjected to vibration along three mutually perpendicular axes; the principal axis was along the payload thrust axis. An accelerometer for monitoring and controlling the vibration levels was mounted with epoxy near the exciter-payload interface. The vibration schedule for the payload along the thrust and lateral axes is given in Table 2.3.

Equipment used for this test included a 5,000-force-lb MB C-50 exciter, and a 15-kw MB Model T-451 vibration amplifier; an Endevco Model 2213 accelerometer was used to control vibration force levels.

2.3.2 Instrument Functional Tests. The payload instruments were connected as shown in Figure 2.27, and instrument outputs were monitored through the umbilical cord, which was connected to the payload test set. External power supplies were used to operate the instruments. The output signals of each instrument were monitored on the oscilloscope cathode-ray tube by stepping the signal Ledex switch through its 12 positions (see Section 2.2). A 100-Mc Co⁶⁰ source was used to stimulate the gamma scanner detectors by placing it near the payload, and the magnetometers were checked by moving a small magnet near the phenolic block. The 28-, 15- and 15-volt payload batteries were checked with a multimeter. After checking the battery voltages, the payload was switched to internal power, and the instruments were rechecked as described above.

Test equipment for this checkout procedure included an EOS payload test box, a 535A Tektronix oscilloscope, a Triplet 630 multimeter, and a 100-Mc Co⁶⁰ gamma radiation source. The EOS test box controlled the application of internal or external power to the payload and operated the signal Ledex. Its dimensions were 14 by 11 by 8 inches.

2.3.3 Telemetry Functional Tests. Functional tests performed on the telemetry system before, during, and after vibration were performed with a receiver which was used to monitor changes in the telemetry transmitter signal strength and frequency deviation. These outputs were observed on meters mounted to the receiver panel. Each subcarrier channel was checked by applying the demodulated signal from the receiver to a bandswitching discriminator. The output of this discriminator was recorded by a direct-write oscillograph, and subcarrier frequencies were measured.

Test equipment used to check the telemetry system included a Nems-Clarke 1455A telemetry receiver, a Hallamora bandswitching discriminator, a Hewlett-Packard 410B vacuum tube voltmeter, a Tektronix 535A oscilloscope, and a Hewlett-Packard 523C electronic counter.

2.4 DATA REQUIREMENTS

The data requirements, methods of recording data, data reduction techniques, and computer-reduced data procurement are discussed in this section.

2.4.1 Data Required. To determine the position of the debris cloud, gamma rays emitted by the debris were measured by the gamma scanners which were carried aboard a spinning rocket payload. In addition to the data collected from these instruments, it was necessary to know the position and orientation of the instruments in the reference coordinate system (Figure 2.2) as a function of time. Therefore, each payload contained a set of three mutually perpendicular magnetometers to provide rocket aspect information with respect to earth's magnetic field. Trajectories were computed by BRL from Doppler data obtained from a three-frequency beacon carried on the payload. Supplementary trajectory data were obtained from the GMD beacon and the DAMP ship. The calculation of payload attitude, and hence the orientation of the instruments, requires both magnetometer and trajectory data. Appendix G describes a method for computing payload attitude.

As the payload moved along its trajectory, the gamma scanners viewed the cloud from different positions. If the dynamic behavior of the cloud during a particular payload flight was small, then a three-dimensional view of this cloud was obtained by the gamma scanners viewing the cloud from widely different points on the trajectory. However, if the debris cloud moved rapidly through space, then it would be impossible to separate space and time so far as the payload flight was concerned. Thus, when the gamma scanner viewed the cloud from widely different points on the payload's trajectory, it viewed a different cloud and obtained data sufficient for constructing only a two-dimensional model of the debris cloud.

2.4.2 Method of Recording Data.

Airborne and Ground Telemetry Systems, two Mincom C100 tape recorders were employed for the real-time storage of all Project 6.2, 6.3, and

6.4 data. These recorders employed 1-inch tape with a 14-channel recording capacity. While both units had recording capability, only one recorder contained playback amplifiers for reproducing recorded data. Composite (FM/FM) subcarrier signals were recorded directly from as many as six VHF telemetry receivers and three GMD-1 receivers. Also recorded were 100-kc reference signals for electronic tape speed compensation, 17-kc speed-lock signals, B-1 and B-5 time codes, receiver automatic gain control (AGC), liftoff signals, and the voice countdown and intercom audio. Quick-look recording was accomplished during tape playback by reproducing the outputs of IRIG subcarrier discriminators with a Brush chart recorder and/or a Consolidated Electrodynamics Corporation oscillograph.

2.4.3 Data Reduction. Although data reduction and analysis were not part of Project 6.2, considerable effort was made to provide the data reduction contractor with methods and techniques for performing the reduction task. To avoid confusion, data reduction was defined as the process which prepared raw data collected from the experiment for (final) data analysis (to be performed on another contract). The purpose of the data analysis task was to determine the location of the debris cloud. In some cases this only requires performing an analog-to-digital conversion to prepare the data for computer analysis. In other cases, calculations will be performed on the reduced data.

The following steps were necessary to reduce the data in preparation for data analysis:

1. Analog-to-digital conversion.
2. Adjust time delays caused by data processing in the payload and variable bandwidths on the telemetry channels.
3. Incorporate telemetry calibrations on payloads which contained in-flight calibrators (Rockets 8 and 18) into the data.
4. Incorporate instrument calibrations of incident radiation versus output voltage into the data.
5. Determine payload attitude from magnetometer signals and trajectory data. This process is described in Appendixes F and G.

A manual was furnished to the data reduction contractor describing the operations to be performed and suggesting methods to perform these tasks. Portions of this document appear in Appendixes F and G.

Item 5 above was not completed for this report. It is intended that, upon completion of the data reduction, a separate report will be prepared, which will include new results, discussion, and conclusions when applicable.

The output of the final data reduction process will consist of magnetic tapes and printouts of the data. The format of the tapes and printouts is given in Table 2.4. Tables 2.5 and 2.6 give a sample of the printout (values of functions on these tables are not necessarily correct).

2.4.4 Procurement of Data. Upon completion of the data reduction task, additional printouts will be available to qualified requestors directly from the data reduction contractor. Contact:

General Electric Company
Reentry Systems Department
Data Reduction Group
3198 Chestnut Street
Philadelphia, Pennsylvania

Financial arrangements should be made with the request.

2.4.5 Requirements From Other Projects. Analysis of Fish Bowl data for Project 6.2 is being performed under another contract. Two methods are currently being studied to accomplish this analysis task. One method is an iterative calculation and involves the fitting of parameters of an assumed cloud to actual debris data. The second method involves approximating an integral equation by solving a set of simultaneous equations. The successful solution of the iterative method can be aided considerably by the use of photographic data from other projects and is briefly discussed below.

The debris cloud configuration is assumed, and the received radiation from this cloud is calculated and then compared with the data actually received during the experiment. If the calculated and

actual data do not match, the assumed parameters, which define the position and shape of the cloud, are changed until the calculated signal and the actual signal are the same. The amount of computation that must be performed in a process like this depends upon how well the assumed analytical model of the cloud actually fits the data and the number of iterations required before a good fit is achieved between the assumed cloud and the actual cloud. Therefore, any information that can be obtained from external sources, such as photographic data or other methods of data evaluation, will be a great help in assuming a correct or near to correct debris model. In some cases late-time photometric data may be of value, but it must be established that the photometers are examining the debris and not some effect of the debris. It is assumed that photographic data will be of the greatest help, particularly data which was obtained at late times.

TABLE 2.1 SUMMARY OF STAR FISH, BLUE GILL, AND KING FISH EVENTS^a

Event	Date	Detonation Time (Zulu)	Yield	Detonation Coordinates (Bravo System) ^b		
				X(minus)ft	Y(minus)ft	Z(plus)ft
Star Fish Prime	9 July 1962	0900:09.0290	1.15 Mt	37,933 ± 132	102,594 ± 132	1,312,420 ± 50
Blue Gill Triple Prime	26 Oct 1962	0959:48.4753				
King Fish	1 Nov 1962	1210:06.1263				

^aReferences: TWX 2-3-8196, 25 Feb 1963
 TWX 4-3-8161, 15 Apr 1963
 TWX 4-3-8368, 1 May 1963

^bReferenced to a tangent plane through point John (Latitude 16 degrees, 44 minutes, 03.30 seconds North; Longitude 169 degrees, 31 minutes, 41.48 seconds West).
 Positive pointing directions: X Coordinate-East, Y Coordinate-True North, Z Coordinate-Vertical.

TABLE 2.2 ROCKET OPERATIONS SUMMARY

Rocket No.	Project	Vehicle Type ^e	Nominal Launch Time	Flight Time ^c		Apogee Range km	Impact Range km	Performance
				minutes	seconds			
Event: Star Fish								
1	6.4	D-4	H - 10	725 ^d	490	545	Normal operation	
2	6.3	N-C	H - 1	260	100 ^a	56 ^a	Normal operation	
3	6.3	HJ-N	H - 1.5	108	18 ^a	5 ^a	No second-stage operation	
4	6.3	HJ-N	H + 7	251	85.1	43.6	Normal operation	
5	6.4	D-4	H + 7	700 ^d	537	925	Normal operation	
6	6.3	N-C	H + 8	329	100.5 ^a	49 ^a	Normal operation	
7	6.4	D-4	H + 16	749	515	949.1	Normal operation	
8	6.2	D-4	H + 20	824	632.1	1076	Normal operation	
9	6.2	D-4	H + 40	871	685.8	787.6	Normal operation	
Event: Blue Gill								
10	6.3	N-C	H - 1	270	97.4	78.1	Normal operation	
11	6.3	HJ-N	H - 2	240	79.7	68.5	Normal operation	
12	6.3	HJ-N	H + 5	240	81.2	73.5	Normal operation	
13	6.3	N-C	H + 6	265	97.1	61.0	Normal operation	
14	6.3	HJ-N	H + 11	265	93.9	43.3	Normal operation	
15	6.2	HJ-N-N	H + 15	340	137.5	158	Excessive third-stage coning	
16	Deleted from program							
17	6.3	HJ-N	H + 22	240	81.7	82.0	Excessive third-stage coning	
18	6.2	HJ-N-N	H + 31	175	50.5	28.3 ^a	Third stage tumbled	

TABLE 2.2 ROCKET OPERATIONS SUMMARY (continued)

Rocket	Project	Vehicle Type ^e	Nominal Launch Time	Flight Time ^c		Apogee Range	Impact Performance
				minutes	seconds		
Event: King Fish						km	
19	6.2	C-22	H - 2	360	162 ^b	104.5 ^b	Normal operation
20	6.3	C-22	H - 2	370	161.8	82.4	Normal operation
21	6.3	B-1	H - 0	280	105.0	40.2	Normal operation
22	6.4	D-4	H + 1	400	142 ^b	313 ^b	No second-stage operation
23	6.3	B-1	H + 6	280	113	90	Normal operation
24	6.3	C-22	H + 6	360	153.9	157.2	Normal operation
25	6.4	D-4	H + 9	785	560.0	561.2	No nose cone ejection; flight normal
26	6.2	C-22	H + 13	370	161.6	104.1	Normal operation
27	6.3	C-22	H + 13.5	360	157.3	89.0	Normal operation
28	6.3	C-22	H + 40	360	152.0	156.6	Normal operation
29	6.2	C-22	H + 25	229	67.6	36.2	Low second-stage thrust

^a Estimated

^b Post-flight computer simulation

^c Based on duration of VHF telemetry reception except as noted

^d Three-frequency beacon reception

^e Vehicle legend:

- D-4 = Argo D-4 (Aerolab)
- HJ-N = Honest John-Nike (ARC)
- N-C = Nike-Cajun (ARC)
- HJ-N-N = Honest John-Nike-Nike (ARC)
- C-22 = Honest John-Nike-Nike (Aerolab)
- B-1 = Nike-Cajun (Aerolab)

TABLE 2.3 VIBRATION SCHEDULE

Axis	Frequency	Duration	Displacement Peak-to-Peak	Acceleration Zero-to-Peak
	cycle/sec	seconds	inches	g
Thrust	5.0 - 7.6	3	0.5	
	7.6 - 50	45		1.5
	50 - 500	48		7.1
	500 - 2000	30		14
	2000 - 3000	7.8		36
	3000 - 5000	10.2	14	
Lateral	5.0 - 50	48		0.6
	50 - 500	48		1.4
	500 - 2000	30		2.8
	2000 - 5000	18		11.3

TABLE 2.4 DATA FORMAT ON TAPE AND PRINTOUT RECORDS

T1	Time from H = 0 in milliseconds
F1	X-position of payload (from Johnston Island) in meters
F2	Y-position of payload (from Johnston Island) in meters
F3	Z-position of payload (from Johnston Island) in meters
F4	Range (burst to payload) in meters
F5	Azimuth of line between burst point and payload in degrees
F6	Elevation of line between burst point and payload in degrees
F7	Azimuth of vertical gamma scanner (20°) in degrees
F8	Elevation of vertical gamma scanner (20°) in degrees
F9	Gamma scanner vertical (20°) in counts per 10 milliseconds
F10	Gamma scanner vertical (90°) in counts per 10 milliseconds
F11	Azimuth of horizontal gamma scanner (20°) in degrees
F12	Elevation of horizontal gamma scanner (20°) in degrees
F13	Gamma scanner horizontal (20°) in counts per 10 milliseconds
F14	Gamma scanner horizontal (90°) in counts per 10 milliseconds
F15	Azimuth of Z'-axis (vehicle) in degrees
F16	Elevation of Z'-axis (vehicle) in degrees
F17	Azimuth of beta detector and photometer in degrees
F18	Elevation of beta detector and photometer in degrees
F19	Beta detector in Mev/cm^2 -second
F20	Beta detector in volts
F21	Photometer in watts/cm^2 /steradians
F22	Photometer in volts
F23	Total gamma detector in Mev/cm^2 -sec
F24	Total gamma detector in volts
F25	AGC in microvolts or DBM

TABLE 2.4 DATA FORMAT ON TAPE AND PRINTOUT RECORDS (CON'T)

F26	X-magnetometer in gauss
F27	Y-magnetometer in gauss
F28	Constructed Z-magnetometer in gauss
F29	$\sqrt{X^2 + Y^2 + Z^2}$ in gauss
F30	Theoretical value of F (total magnetic field) in gauss
F31	Theoretical value of declination of F in degrees
F32	Theoretical value of inclination of F in degrees
F33	Altitude of payload from earth's surface in meters

TABLE 2.8. SAMPLE OF COMPUTER REDUCED DATA

Tabulated function values are not necessarily correct.

TIME	F1	F2	F3	F4	F5	F6	F7	F8	F9	F10	F11	F12	F13	F14	F15	F16	F17	F18
2395081.	-88575.	-88717.	-250472.	2303660.	95.	-4.	40.	57.	39.	0.	110.	25.	0.	0.	23.	73.	143.	9.
2395092.	-88570.	-88705.	-250450.	2303661.	95.	-4.	40.	57.	83.	32.	110.	25.	9.	26.	23.	73.	143.	9.
2395103.	-88565.	-88693.	-250408.	2303662.	95.	-4.	40.	57.	42.	0.	110.	25.	0.	26.	23.	73.	143.	9.
2395113.	-88560.	-88681.	-250367.	2303663.	95.	-4.	40.	57.	63.	0.	110.	25.	3.	50.	23.	73.	143.	9.
2395126.	-88553.	-88667.	-250310.	2303664.	95.	-4.	40.	57.	48.	0.	117.	25.	0.	130.	23.	73.	143.	9.
2395137.	-88548.	-88655.	-250276.	2303665.	95.	-4.	40.	57.	33.	0.	110.	25.	0.	0.	23.	73.	143.	9.
2395147.	-88543.	-88642.	-250235.	2303667.	95.	-4.	40.	57.	48.	5.	110.	25.	0.	0.	23.	73.	143.	9.
2395159.	-88537.	-88629.	-250189.	2303668.	95.	-4.	40.	57.	121.	8.	110.	25.	36.	0.	23.	73.	143.	9.
2395170.	-88532.	-88617.	-250148.	2303669.	95.	-4.	40.	57.	39.	5.	110.	25.	0.	26.	23.	73.	143.	9.
2395181.	-88527.	-88605.	-250106.	2303670.	95.	-4.	40.	57.	40.	5.	110.	25.	36.	5.	23.	73.	143.	9.
2395192.	-88521.	-88592.	-250061.	2303671.	95.	-4.	40.	57.	45.	32.	110.	25.	36.	26.	23.	73.	143.	9.
2395204.	-88515.	-88579.	-250015.	2303672.	95.	-4.	40.	57.	60.	20.	110.	25.	16.	5.	23.	73.	143.	9.
2395215.	-88510.	-88567.	-249974.	2303673.	95.	-4.	40.	57.	37.	20.	110.	25.	19.	38.	23.	73.	143.	9.
2395226.	-88505.	-88555.	-249932.	2303674.	95.	-4.	40.	57.	60.	14.	110.	25.	22.	17.	23.	73.	143.	9.
2395237.	-88499.	-88542.	-249887.	2303676.	95.	-4.	40.	57.	42.	0.	110.	25.	0.	26.	23.	73.	143.	9.
2395249.	-88493.	-88528.	-249842.	2303677.	95.	-4.	40.	57.	84.	6.	110.	25.	36.	26.	23.	73.	143.	9.
2395260.	-88488.	-88516.	-249800.	2303678.	95.	-4.	40.	57.	60.	32.	110.	25.	36.	26.	23.	73.	143.	9.
2395271.	-88483.	-88505.	-249759.	2303679.	95.	-4.	40.	57.	23.	0.	120.	25.	0.	0.	23.	73.	143.	9.
2395281.	-88478.	-88492.	-249717.	2303680.	95.	-4.	40.	57.	78.	0.	110.	25.	3.	26.	23.	73.	143.	9.
2395293.	-88472.	-88479.	-249672.	2303681.	95.	-4.	40.	57.	48.	0.	119.	25.	0.	0.	23.	73.	143.	9.
2395305.	-88466.	-88466.	-249626.	2303683.	95.	-4.	40.	57.	48.	0.	119.	25.	0.	0.	23.	73.	143.	9.
2395315.	-88461.	-88454.	-249589.	2303684.	95.	-4.	40.	57.	97.	0.	110.	25.	9.	0.	23.	73.	143.	9.
2395327.	-88455.	-88441.	-249540.	2303685.	95.	-4.	40.	57.	33.	20.	110.	25.	0.	0.	23.	73.	143.	9.
2395338.	-88450.	-88429.	-249498.	2303686.	95.	-4.	40.	57.	60.	0.	110.	25.	0.	38.	23.	73.	143.	9.
2395350.	-88444.	-88416.	-249453.	2303687.	95.	-4.	40.	57.	72.	0.	110.	25.	58.	2.	23.	73.	143.	9.
2395360.	-88439.	-88406.	-249411.	2303688.	95.	-4.	40.	57.	48.	23.	110.	25.	77.	26.	23.	73.	143.	9.
2395372.	-88431.	-88390.	-249366.	2303689.	95.	-4.	40.	57.	14.	32.	110.	25.	0.	0.	23.	73.	143.	9.
2395383.	-88428.	-88378.	-249324.	2303691.	95.	-4.	40.	57.	84.	0.	110.	25.	0.	26.	23.	73.	143.	9.
2395395.	-88422.	-88365.	-249279.	2303692.	95.	-4.	40.	57.	109.	0.	119.	25.	22.	26.	23.	73.	143.	9.
2395405.	-88417.	-88353.	-249237.	2303693.	95.	-4.	40.	57.	2.	0.	110.	25.	36.	5.	23.	73.	143.	9.
2395417.	-88411.	-88340.	-249192.	2303694.	95.	-4.	40.	57.	48.	0.	110.	25.	0.	26.	23.	73.	143.	9.
2395428.	-88406.	-88328.	-249151.	2303695.	95.	-4.	40.	57.	48.	5.	119.	25.	31.	0.	23.	73.	143.	9.
2395438.	-88401.	-88316.	-249109.	2303696.	95.	-4.	40.	57.	8.	2.	110.	25.	0.	14.	23.	73.	143.	9.
2395450.	-88395.	-88303.	-249064.	2303698.	95.	-4.	40.	57.	91.	0.	110.	25.	0.	2.	23.	73.	143.	9.
2395462.	-88389.	-88290.	-249018.	2303699.	95.	-4.	40.	57.	75.	0.	110.	25.	34.	26.	23.	73.	143.	9.
2395473.	-88384.	-88278.	-248977.	2303700.	95.	-4.	40.	57.	97.	0.	119.	25.	39.	26.	23.	73.	143.	9.
2395483.	-88377.	-88266.	-248935.	2303701.	95.	-4.	40.	57.	36.	0.	110.	25.	0.	0.	23.	73.	143.	9.
2395495.	-88373.	-88252.	-248890.	2303702.	95.	-4.	40.	57.	60.	0.	119.	25.	19.	0.	23.	73.	143.	9.
2395507.	-88368.	-88239.	-248845.	2303703.	95.	-4.	40.	57.	45.	5.	110.	25.	3.	0.	23.	73.	143.	9.
2395518.	-88362.	-88227.	-248803.	2303704.	95.	-4.	40.	57.	146.	32.	110.	25.	9.	38.	23.	73.	143.	9.
2395528.	-88357.	-88215.	-248762.	2303706.	95.	-4.	40.	57.	107.	32.	110.	25.	36.	0.	23.	73.	143.	9.
2395540.	-88351.	-88202.	-248716.	2303707.	95.	-4.	40.	57.	133.	81.	110.	25.	0.	0.	23.	73.	143.	9.
2395552.	-88346.	-88159.	-248671.	2303708.	95.	-4.	40.	57.	48.	29.	110.	25.	0.	0.	23.	73.	143.	9.
2395563.	-88340.	-88177.	-248630.	2303709.	95.	-4.	40.	57.	60.	32.	117.	25.	3.	14.	23.	73.	143.	9.
2395573.	-88335.	-88165.	-248588.	2303710.	95.	-4.	40.	57.	26.	0.	110.	25.	0.	26.	23.	73.	143.	9.
2395585.	-88329.	-88152.	-248543.	2303711.	95.	-4.	40.	57.	33.	0.	117.	25.	3.	0.	23.	73.	143.	9.
2395597.	-88324.	-88138.	-248497.	2303713.	95.	-4.	40.	57.	72.	0.	110.	25.	0.	0.	23.	73.	143.	9.
2395607.	-88318.	-88126.	-248456.	2303714.	95.	-4.	40.	57.	48.	0.	110.	25.	0.	0.	23.	73.	143.	9.
2395619.	-88313.	-88113.	-248411.	2303715.	95.	-4.	40.	57.	60.	93.	110.	25.	0.	26.	23.	73.	143.	9.
2395630.	-88307.	-88101.	-248369.	2303716.	95.	-4.	40.	57.	48.	0.	110.	25.	34.	0.	23.	73.	143.	9.
2395641.	-88302.	-88089.	-248328.	2303717.	95.	-4.	40.	57.	60.	35.	110.	25.	0.	14.	23.	73.	143.	9.
2395651.	-88297.	-88077.	-248286.	2303718.	95.	-4.	40.	57.	54.	0.	110.	25.	0.	0.	23.	73.	143.	9.
2395664.	-88291.	-88063.	-248247.	2303720.	95.	-4.	40.	57.	45.	45.	113.	25.	34.	0.	23.	73.	143.	9.
2395675.	-88286.	-88051.	-248195.	2303721.	95.	-4.	40.	57.	95.	32.	110.	25.	0.	0.	23.	73.	143.	9.

TABLE 2.6 SAMPLE OF COMPUTER BENCHMARK DATA

Tabulated function values are not necessarily correct.

TIME	F1	F2	F3	F4	F5	F6	F19	F20	F21	F22	F23	F24	F25	F26	F27	F28	F29	F30	F31	F32
2390842.	-40645.	-93478.	-266968.	2303303.	95.	-5.	0.16E 05	0.0-0.23E-08-0.0	0.13E 06-0.0	0.13E 06-0.0	0.13E 06-0.0	0.13E 06-0.0	1072.-0.3	0.1	0.	0.4	0.39	349.	29.	
2390853.	-40440.	-93465.	-266926.	2303303.	95.	-5.	0.16E 05	0.0-0.11E-08-0.0	0.13E 06-0.0	0.13E 06-0.0	0.13E 06-0.0	0.13E 06-0.0	1163.-0.3	0.1	0.	0.4	0.39	349.	29.	
2390864.	-40634.	-93452.	-266881.	2303306.	95.	-5.	0.16E 05	0.0-0.39E-07-0.0	0.13E 06-0.0	0.13E 06-0.0	0.13E 06-0.0	0.13E 06-0.0	1104.-0.3	0.1	0.	0.4	0.39	349.	29.	
2390876.	-40628.	-93434.	-266835.	2303306.	95.	-5.	0.16E 05	0.0-0.15E-08-0.0	0.13E 06-0.0	0.13E 06-0.0	0.13E 06-0.0	0.13E 06-0.0	1146.-0.3	0.1	0.	0.4	0.39	349.	29.	
2390887.	-40623.	-93427.	-266793.	2303306.	95.	-5.	0.16E 05	0.0-0.21E-08-0.0	0.13E 06-0.0	0.13E 06-0.0	0.13E 06-0.0	0.13E 06-0.0	1094.-0.3	0.1	0.	0.4	0.39	349.	29.	
2390897.	-40418.	-93415.	-266751.	2303306.	95.	-5.	0.16E 05	0.0-0.63E-07-0.0	0.13E 06-0.0	0.13E 06-0.0	0.13E 06-0.0	0.13E 06-0.0	1171.-0.3	0.1	0.	0.4	0.39	349.	29.	
2390910.	-40612.	-93401.	-266702.	2303307.	95.	-5.	0.16E 05	0.0-0.10E-08-0.0	0.13E 06-0.0	0.13E 06-0.0	0.13E 06-0.0	0.13E 06-0.0	1187.-0.3	0.1	0.	0.4	0.39	349.	29.	
2390921.	-40607.	-93389.	-266660.	2303308.	95.	-5.	0.16E 05	0.0-0.35E-08-0.0	0.13E 06-0.0	0.13E 06-0.0	0.13E 06-0.0	0.13E 06-0.0	1174.-0.3	0.1	0.	0.4	0.39	349.	29.	
2390932.	-40601.	-93377.	-266618.	2303309.	95.	-5.	0.16E 05	0.0-0.22E-09-0.0	0.13E 06-0.0	0.13E 06-0.0	0.13E 06-0.0	0.13E 06-0.0	1247.-0.3	0.1	0.	0.4	0.39	349.	29.	
2390942.	-40596.	-93364.	-266576.	2303310.	95.	-5.	0.16E 05	0.0-0.88E-09-0.0	0.13E 06-0.0	0.13E 06-0.0	0.13E 06-0.0	0.13E 06-0.0	1177.-0.3	0.1	0.	0.4	0.39	349.	29.	
2390955.	-40590.	-93350.	-266532.	2303310.	95.	-5.	0.16E 05	0.0-0.26E-09-0.0	0.13E 06-0.0	0.13E 06-0.0	0.13E 06-0.0	0.13E 06-0.0	1225.-0.3	0.1	0.	0.4	0.39	349.	29.	
2390968.	-40585.	-93338.	-266484.	2303311.	95.	-5.	0.16E 05	0.0-0.13E-09-0.0	0.13E 06-0.0	0.13E 06-0.0	0.13E 06-0.0	0.13E 06-0.0	1247.-0.3	0.1	0.	0.4	0.39	349.	29.	
2390977.	-40574.	-93326.	-266442.	2303312.	95.	-5.	0.16E 05	0.0-0.11E-09-0.0	0.13E 06-0.0	0.13E 06-0.0	0.13E 06-0.0	0.13E 06-0.0	1175.-0.3	0.1	0.	0.4	0.39	349.	29.	
2390987.	-40574.	-93314.	-266400.	2303313.	95.	-5.	0.16E 05	0.0-0.24E-08-0.0	0.13E 06-0.0	0.13E 06-0.0	0.13E 06-0.0	0.13E 06-0.0	1225.-0.3	0.1	0.	0.4	0.39	349.	29.	
2390999.	-40568.	-93301.	-266355.	2303313.	95.	-5.	0.16E 05	0.0-0.38E-08-0.0	0.13E 06-0.0	0.13E 06-0.0	0.13E 06-0.0	0.13E 06-0.0	1247.-0.3	0.1	0.	0.4	0.39	349.	29.	
2391010.	-40563.	-93289.	-266313.	2303314.	95.	-5.	0.16E 05	0.0-0.14E-08-0.0	0.13E 06-0.0	0.13E 06-0.0	0.13E 06-0.0	0.13E 06-0.0	1247.-0.3	0.1	0.	0.4	0.39	349.	29.	
2391021.	-40557.	-93276.	-266267.	2303315.	95.	-5.	0.16E 05	0.0-0.22E-08-0.0	0.13E 06-0.0	0.13E 06-0.0	0.13E 06-0.0	0.13E 06-0.0	1242.-0.3	0.1	0.	0.4	0.39	349.	29.	
2391033.	-40552.	-93262.	-266221.	2303316.	95.	-5.	0.16E 05	0.0-0.39E-08-0.0	0.13E 06-0.0	0.13E 06-0.0	0.13E 06-0.0	0.13E 06-0.0	1220.-0.3	0.1	0.	0.4	0.39	349.	29.	
2391044.	-40546.	-93250.	-266179.	2303317.	95.	-5.	0.16E 05	0.0-0.65E-08-0.0	0.13E 06-0.0	0.13E 06-0.0	0.13E 06-0.0	0.13E 06-0.0	1245.-0.3	0.1	0.	0.4	0.39	349.	29.	
2391055.	-40541.	-93238.	-266137.	2303317.	95.	-5.	0.16E 05	0.0-0.64E-09-0.0	0.13E 06-0.0	0.13E 06-0.0	0.13E 06-0.0	0.13E 06-0.0	1234.-0.3	0.1	0.	0.4	0.39	349.	29.	
2391066.	-40535.	-93225.	-266092.	2303318.	95.	-5.	0.16E 05	0.0-0.36E-08-0.0	0.13E 06-0.0	0.13E 06-0.0	0.13E 06-0.0	0.13E 06-0.0	1246.-0.3	0.1	0.	0.4	0.39	349.	29.	
2391078.	-40530.	-93212.	-266046.	2303318.	95.	-5.	0.16E 05	0.0-0.99E-09-0.0	0.13E 06-0.0	0.13E 06-0.0	0.13E 06-0.0	0.13E 06-0.0	1242.-0.3	0.1	0.	0.4	0.39	349.	29.	
2391089.	-40524.	-93200.	-266004.	2303320.	95.	-5.	0.16E 05	0.0-0.41E-09-0.0	0.13E 06-0.0	0.13E 06-0.0	0.13E 06-0.0	0.13E 06-0.0	1217.-0.3	0.1	0.	0.4	0.39	349.	29.	
2391100.	-40519.	-93188.	-265962.	2303320.	95.	-5.	0.16E 05	0.0-0.21E-08-0.0	0.13E 06-0.0	0.13E 06-0.0	0.13E 06-0.0	0.13E 06-0.0	1260.-0.3	0.1	0.	0.4	0.39	349.	29.	
2391111.	-40513.	-93175.	-265916.	2303321.	95.	-5.	0.16E 05	0.0-0.34E-08-0.0	0.13E 06-0.0	0.13E 06-0.0	0.13E 06-0.0	0.13E 06-0.0	1142.-0.3	0.1	0.	0.4	0.39	349.	29.	
2391123.	-40508.	-93161.	-265871.	2303322.	95.	-5.	0.16E 05	0.0-0.24E-08-0.0	0.13E 06-0.0	0.13E 06-0.0	0.13E 06-0.0	0.13E 06-0.0	1138.-0.3	0.1	0.	0.4	0.39	349.	29.	
2391134.	-40503.	-93149.	-265829.	2303322.	95.	-5.	0.16E 05	0.0-0.17E-08-0.0	0.13E 06-0.0	0.13E 06-0.0	0.13E 06-0.0	0.13E 06-0.0	1068.-0.3	0.1	0.	0.4	0.39	349.	29.	
2391145.	-40497.	-93137.	-265787.	2303324.	95.	-5.	0.16E 05	0.0-0.42E-10-0.0	0.13E 06-0.0	0.13E 06-0.0	0.13E 06-0.0	0.13E 06-0.0	1045.-0.3	0.1	0.	0.4	0.39	349.	29.	
2391155.	-40492.	-93125.	-265745.	2303324.	95.	-5.	0.16E 05	0.0-0.33E-08-0.0	0.13E 06-0.0	0.13E 06-0.0	0.13E 06-0.0	0.13E 06-0.0	1031.-0.3	0.1	0.	0.4	0.39	349.	29.	
2391167.	-40486.	-93112.	-265709.	2303325.	95.	-5.	0.16E 05	0.0-0.36E-08-0.0	0.13E 06-0.0	0.13E 06-0.0	0.13E 06-0.0	0.13E 06-0.0	969.-0.3	0.1	0.	0.4	0.39	349.	29.	
2391177.	-40481.	-93099.	-265654.	2303326.	95.	-5.	0.16E 05	0.0-0.85E-09-0.0	0.13E 06-0.0	0.13E 06-0.0	0.13E 06-0.0	0.13E 06-0.0	954.-0.3	0.1	0.	0.4	0.39	349.	29.	
2391189.	-40475.	-93087.	-265612.	2303327.	95.	-5.	0.16E 05	0.0-0.62E-09-0.0	0.13E 06-0.0	0.13E 06-0.0	0.13E 06-0.0	0.13E 06-0.0	923.-0.3	0.1	0.	0.4	0.39	349.	29.	
2391201.	-40470.	-93074.	-265566.	2303328.	95.	-5.	0.16E 05	0.0-0.21E-08-0.0	0.13E 06-0.0	0.13E 06-0.0	0.13E 06-0.0	0.13E 06-0.0	910.-0.3	0.1	0.	0.4	0.39	349.	29.	
2391212.	-40464.	-93062.	-265524.	2303328.	95.	-5.	0.16E 05	0.0-0.34E-08-0.0	0.13E 06-0.0	0.13E 06-0.0	0.13E 06-0.0	0.13E 06-0.0	916.-0.3	0.1	0.	0.4	0.39	349.	29.	
2391224.	-40459.	-93048.	-265478.	2303329.	95.	-5.	0.16E 05	0.0-0.15E-08-0.0	0.13E 06-0.0	0.13E 06-0.0	0.13E 06-0.0	0.13E 06-0.0	870.-0.3	0.1	0.	0.4	0.39	349.	29.	
2391234.	-40453.	-93036.	-265436.	2303330.	95.	-5.	0.16E 05	0.0-0.37E-08-0.0	0.13E 06-0.0	0.13E 06-0.0	0.13E 06-0.0	0.13E 06-0.0	852.-0.3	0.1	0.	0.4	0.39	349.	29.	
2391246.	-40448.	-93023.	-265391.	2303331.	95.	-5.	0.16E 05	0.0-0.80E-09-0.0	0.13E 06-0.0	0.13E 06-0.0	0.13E 06-0.0	0.13E 06-0.0	833.-0.3	0.1	0.	0.4	0.39	349.	29.	
2391257.	-40442.	-93011.	-265349.	2303332.	95.	-5.	0.16E 05	0.0-0.18E-08-0.0	0.13E 06-0.0	0.13E 06-0.0	0.13E 06-0.0	0.13E 06-0.0	875.-0.3	0.1	0.	0.4	0.39	349.	29.	
2391268.	-40437.	-92999.	-265307.	2303332.	95.	-5.	0.16E 05	0.0-0.17E-08-0.0	0.13E 06-0.0	0.13E 06-0.0	0.13E 06-0.0	0.13E 06-0.0	912.-0.3	0.1	0.	0.4	0.39	349.	29.	
2391279.	-40432.	-92987.	-265265.	2303333.	95.	-5.	0.16E 05	0.0-0.24E-08-0.0	0.13E 06-0.0	0.13E 06-0.0	0.13E 06-0.0	0.13E 06-0.0	902.-0.3	0.1	0.	0.4	0.39	349.	29.	
2391291.	-40426.	-92973.	-265215.	2303334.	95.	-5.	0.16E 05	0.0-0.29E-08-0.0	0.13E 06-0.0	0.13E 06-0.0	0.13E 06-0.0	0.13E 06-0.0	974.-0.3	0.1	0.	0.4	0.39	349.	29.	
2391302.	-40420.	-92960.	-265174.	2303335.	95.	-5.	0.16E 05	0.0-0.35E-09-0.0	0.13E 06-0.0	0.13E 06-0.0	0.13E 06-0.0	0.13E 06-0.0	851.-0.3	0.1	0.	0.4	0.39	349.	29.	
2391313.	-40415.	-92949.	-265132.	2303335.	95.	-5.	0.16E 05	0.0-0.93E-09-0.0	0.13E 06-0.0	0.13E 06-0.0	0.13E 06-0.0	0.13E 06-0.0	914.-0.3	0.1	0.	0.4	0.39	349.	29.	
2391323.	-40410.	-92936.	-265090.	2303336.	95.	-5.	0.16E 05	0.0-0.27E-09-0.0	0.13E 06-0.0	0.13E 06-0.0	0.13E 06-0.0	0.13E 06-0.0	935.-0.3	0.1	0.	0.4	0.39	349.	29.	
2391336.	-40404.	-92922.	-265048.	2303337.	95.	-5.	0.16E 05	0.0-0.17E-08-0.0	0.13E 06-0.0	0.13E 06-0.0	0.13E 06-0.0	0.13E 06-0.0	899.-0.3	0.1	0.	0.4	0.39	349.	29.	
2391347.	-40398.	-92910.	-264998.	2303338.	95.	-5.	0.16E 05	0.0-0.29E-08-0.0	0.13E 06-0.0	0.13E 06-0.0	0.13E 06-0.0	0.13E 06-0.0	873.-0.3	0.1	0.	0.4	0.39	349.	29.	
2391357.	-40393.	-92898.	-264957.	2303339.	95.	-5.	0.16E 05	0.0-0.96E-09-0.0	0.13E 06-0.0	0.13E 06-0.0	0.13E 06-0.0	0.13E 06-0.0	907.-0.3	0.1	0.	0.4	0.39	349.	29.	
2391369.	-40388.	-92885.	-264911.	2303340.	95.	-5.	0.16E 05	0.0-0.63E-09-0.0	0.13E 06-0.0	0.13E 06-0.0	0.13E 06-0.0	0.13E 06-0.0	914.-0.3	0.1	0.	0.4	0.39	349.	29.	
2391381.	-40382.	-92872.	-264865.	2303340.	95.	-4.	0.16E 05	0.0-0.23E-08-0.0	0.13E 06-0.0	0.13E 06-0.0	0.13E 06-0.0	0.13E 06-0.0	946.-0.3	0.1	0.	0.4	0.39	349.	29.	
2391392.	-40377.	-92860.	-264823.	2303341.	95.	-4.	0.16E 05	0.0-0.18E-08-0.0	0.13E 06-0.0	0.13E 06-0.0	0.13E 06-0.0	0.13E 06-0.0	940.-0.3	0.1	0.	0.4	0.39	349.	29.	
2391402.	-40371.	-92848.	-264781.	2303342.	95.	-4.	0.16E 05	0.0-0.91E-09-0.0	0.13E 06-0.0	0.13E 06-0.0	0.13E 06-0.0	0.13E 06-0.0	983.-0.3	0.1	0.	0.4	0.39	349.	29.	
2391414.	-40366.	-92834.	-264736.	2303343.	95.	-4.	0.16E 05	0.0-0.56E-09-0.0	0.13E 06-0.0	0.13E 06-0.0	0.13E 06-0.0	0.13E 06								

TABLE 2.7 INSTRUMENTATION PACKAGE CONTENTS

Instrument	Rocket Number						
	8	9	15	18	19	26	29
Instrument	Serial Number						
X-Aspect sensor (magnetometer)	637	639	631	596	790	788	787
Y-Aspect sensor (magnetometer)	638	642	633	597	784	791	786
Z-Aspect sensor (magnetometer)	634	636	634	598	--	789	785
Telemetry power converter	500	503	500	504	506	508	505
Commutator	10881	10882	10879	10878	10934	10928	10922
Gamma scanner power supply	112	117	114	120	124	134	139
Horizontal gamma scanner D-80	34	24	29	22	36	1005	40
	32	44	41	37	133	130	27
Vertical gamma scanner D-80	17	38	13	15	136	132	38
	42	47	39	16	30	29	31
Telemetry transmitter	1588	1557	1554	1559	1556	1588	1587
GMD transmitter	13	20	13	12	--	--	--
Temperature sensor A	19	--	38	50	*	*	*
Temperature sensor B	11	20	133	54	*	*	*
Temperature sensor C	56	--	57	35	*	*	*
Temperature sensor D	24	41	55	48	*	*	*
Gamma detector	4	3	1	2	6	7	8
Beta detector	4	5	1	2	6	7	8
Signal Ledex	5	3	1	2	4	6	8
Power Ledex	5	3	1	4	7	6	8
Voltage controlled oscillator package	3	4	2	1	6	7	8
C-Band beacon	23	5	9	2	25	28	29
In-flight calibrator	10935	*	*	*	10940	*	*
Photometer	4	5	1	2	7	6	8
Three-frequency beacon (BRL)	--	--	--	--	--	*	--
Power amplifier	885	884	*	*	891	806	808

* Not flown
 -- No number

LEGEND.

- ① - BRL Ionospheric Instrumentation Vane
- ② - Bldg. Nr. 200 Project 6.2, 6.3 & 6.4 Rocket Control Center
- ③ - Bldg. No. 236 Project 6.2, 6.3 & 6.4 Offices
- ④ - BRL Antenne Field
- ⑤ - BRL GMD Instrumentation Van
- ⑥ - E O S Telemetry Van
- ⑦ - Payload Assembly Building
- ⊙ - Indicates Rocket Launcher Location
- ▽ - Indicates GMD Antenna Location

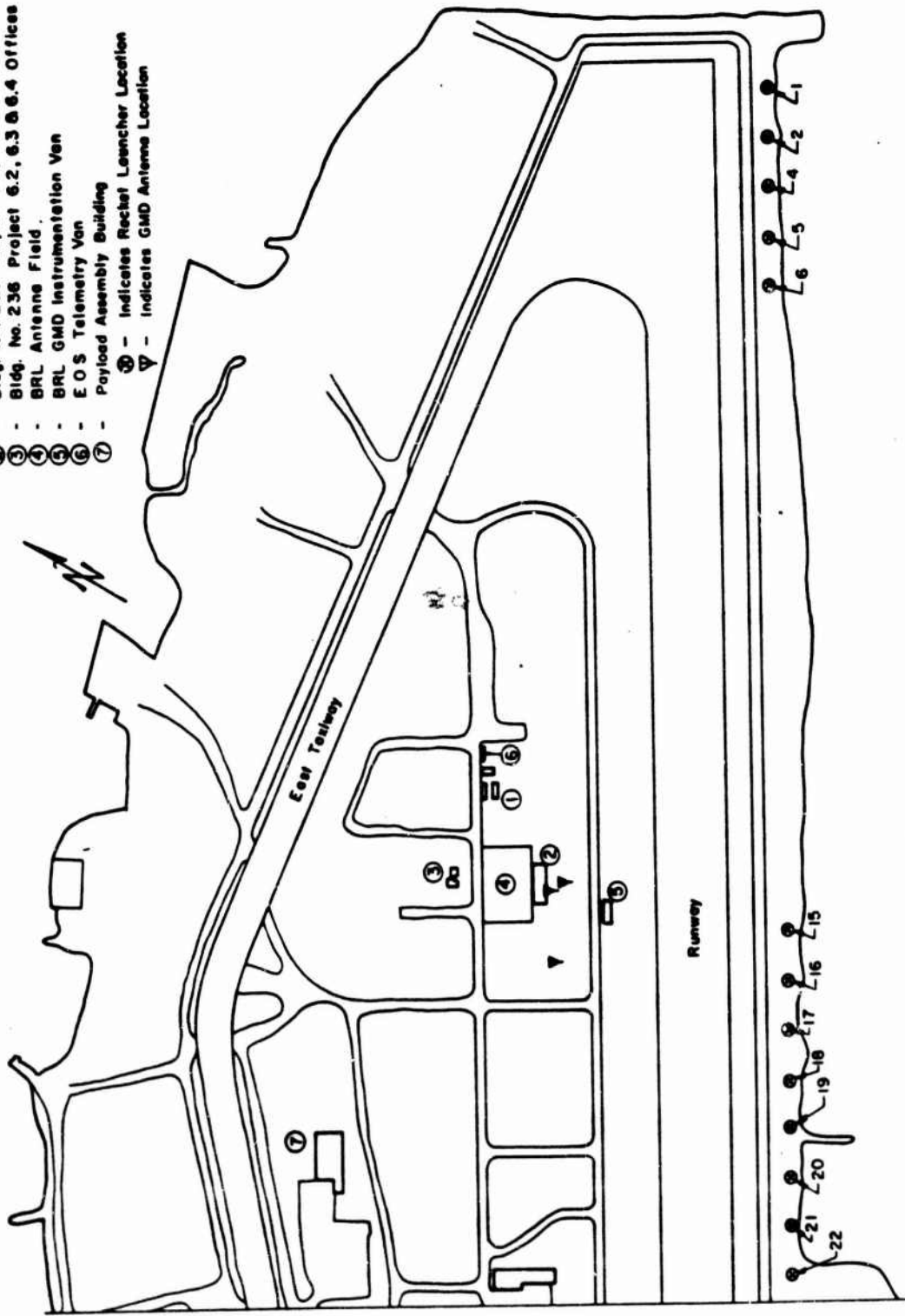


Figure 2.1 Instrumentation layout and rocket launcher locations on Johnston Island for Projects 6.2, 6.3, 6.4.

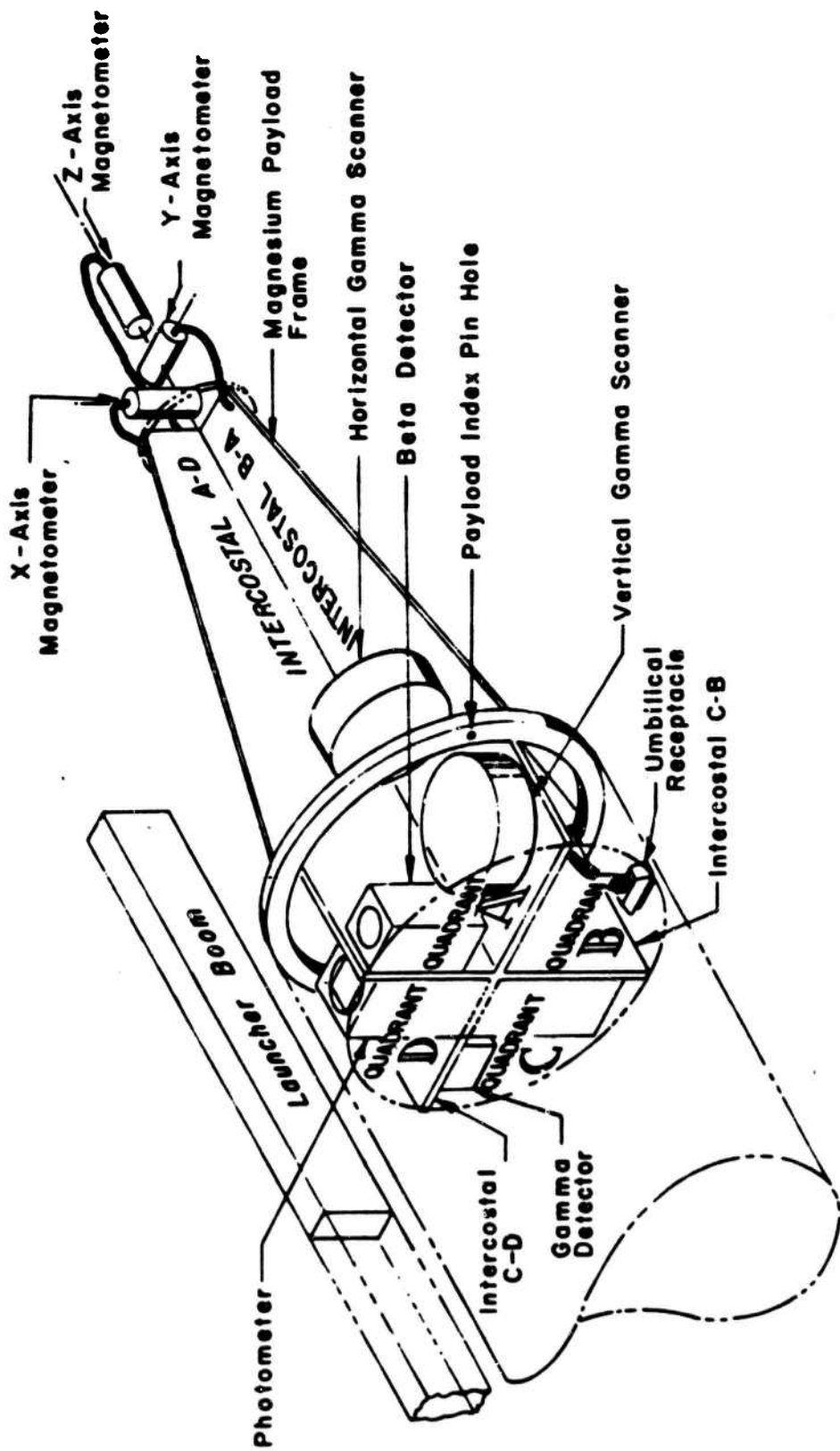


Figure 2.3 EOS payload instrumentation package.

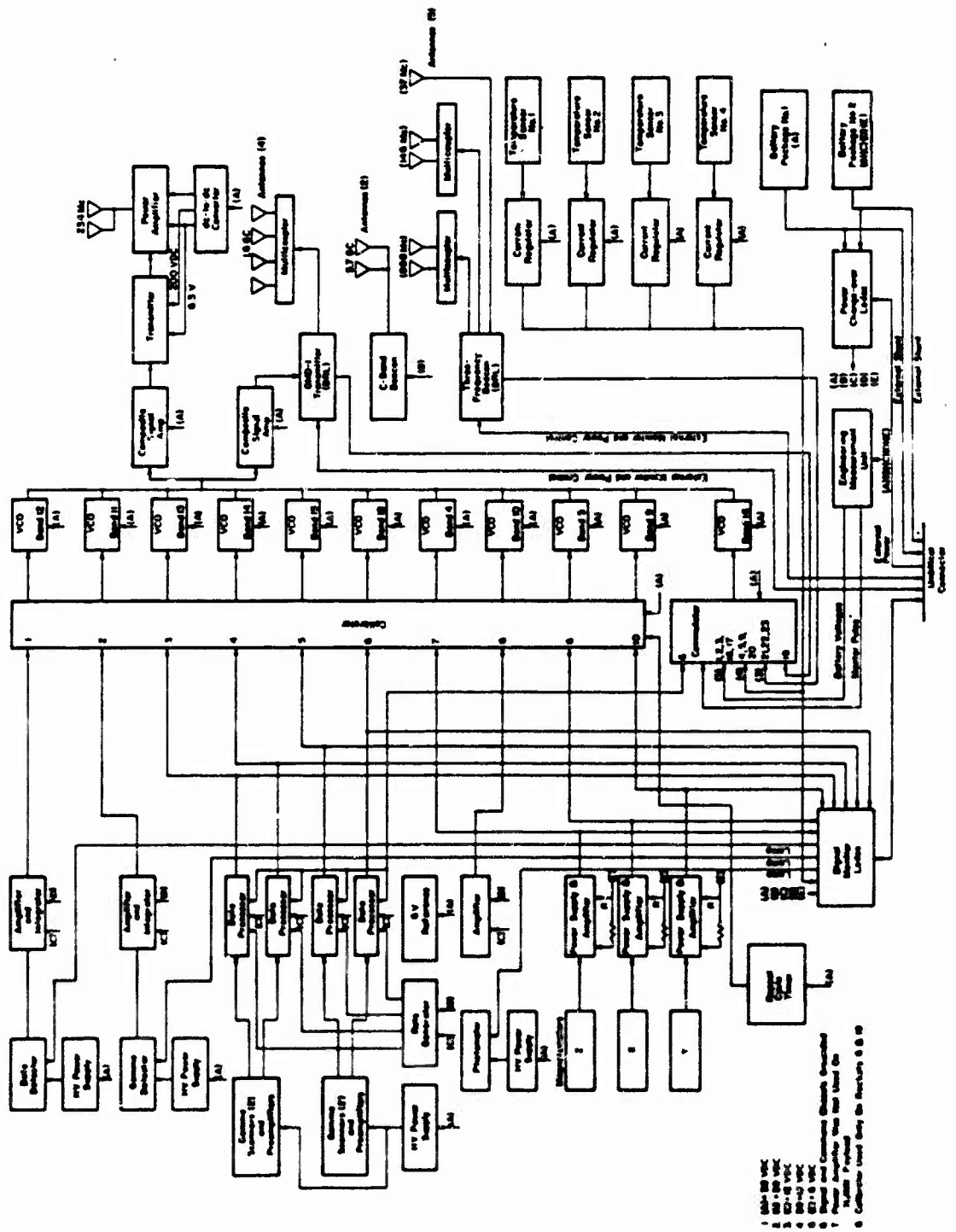


Figure 2.4 Payload system block diagram.

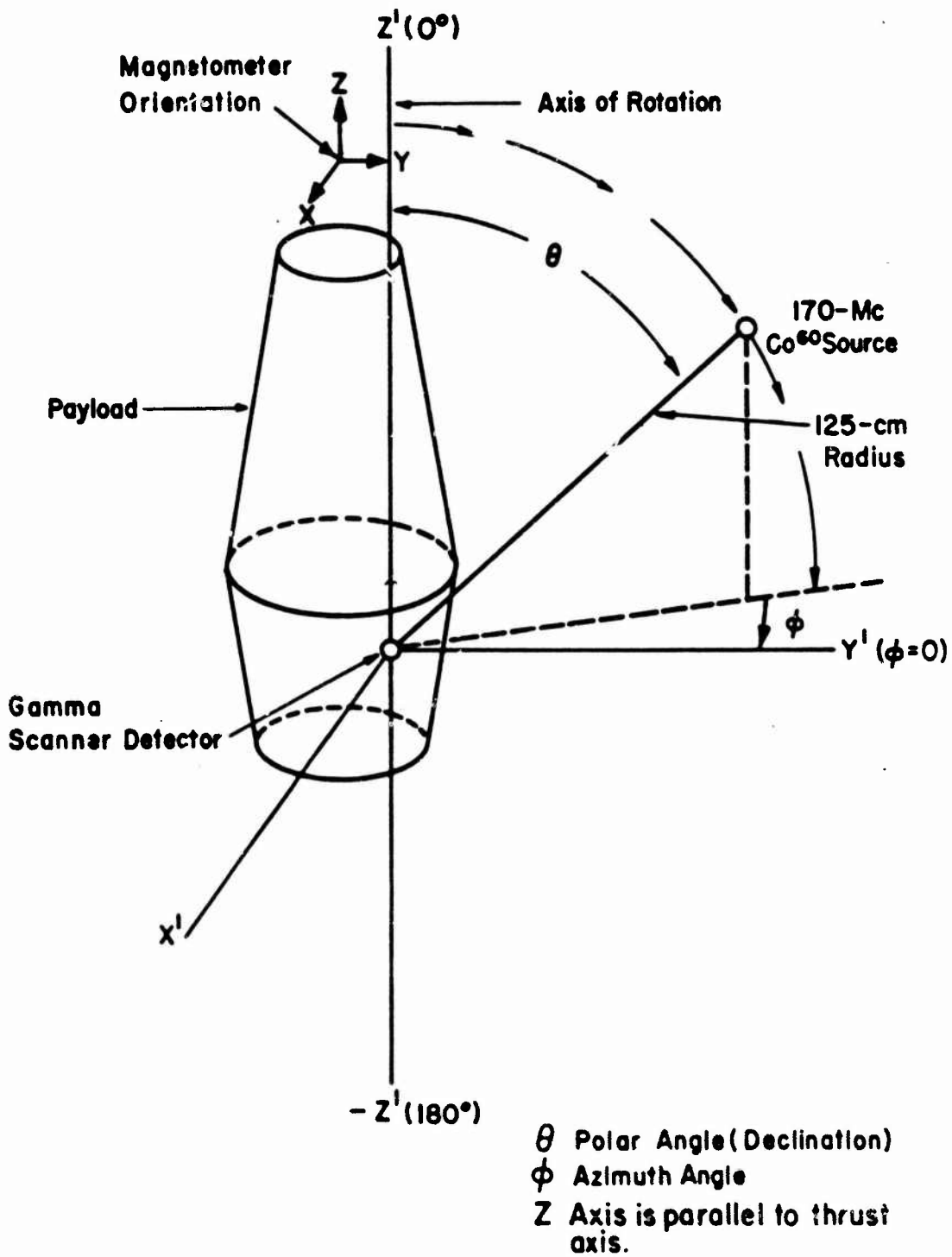


Figure 2.5 Test setup for calibrating gamma scanner in payload.

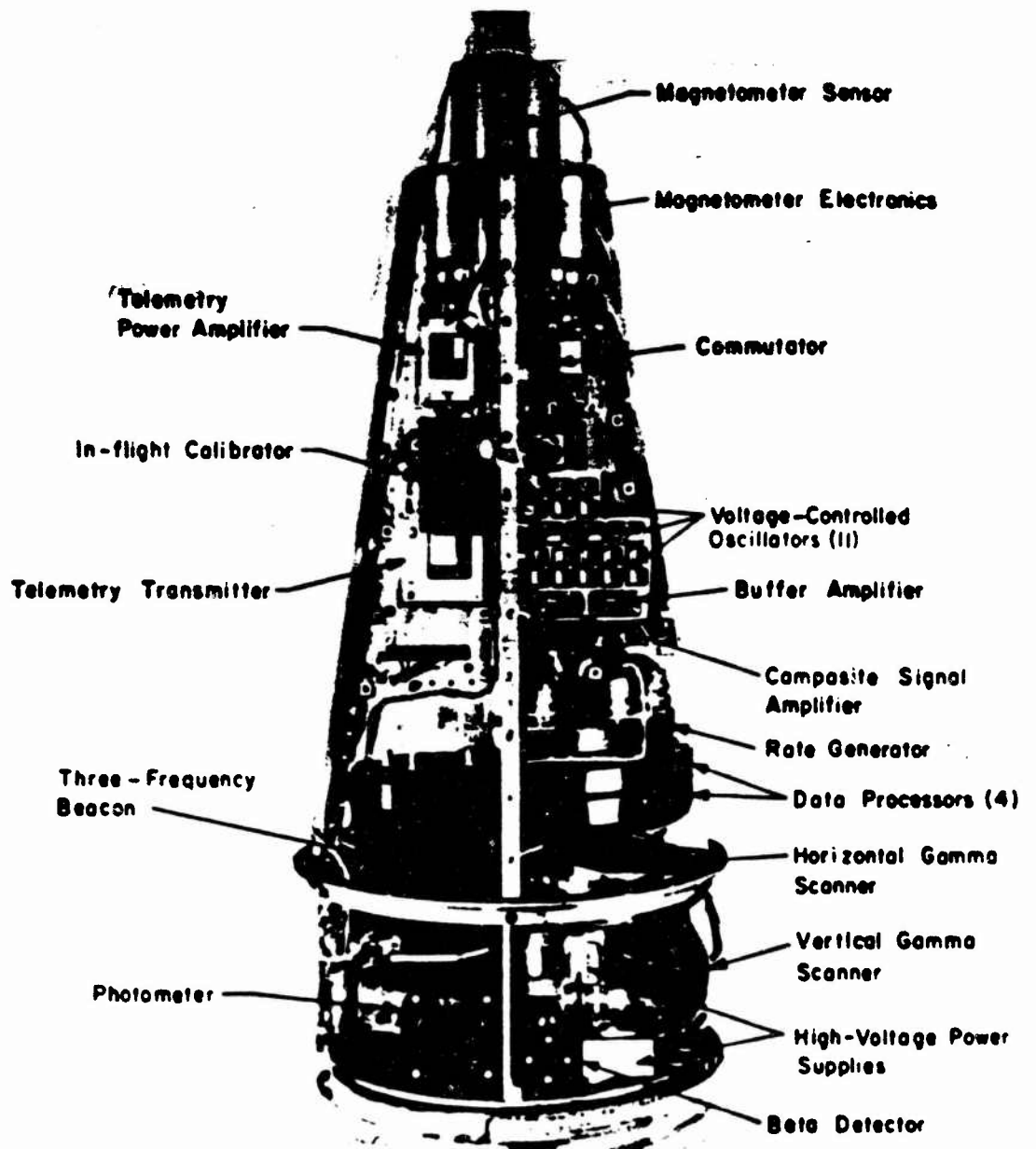


Figure 2.6 EOS instrumentation package, Side 1. (EOS photo)

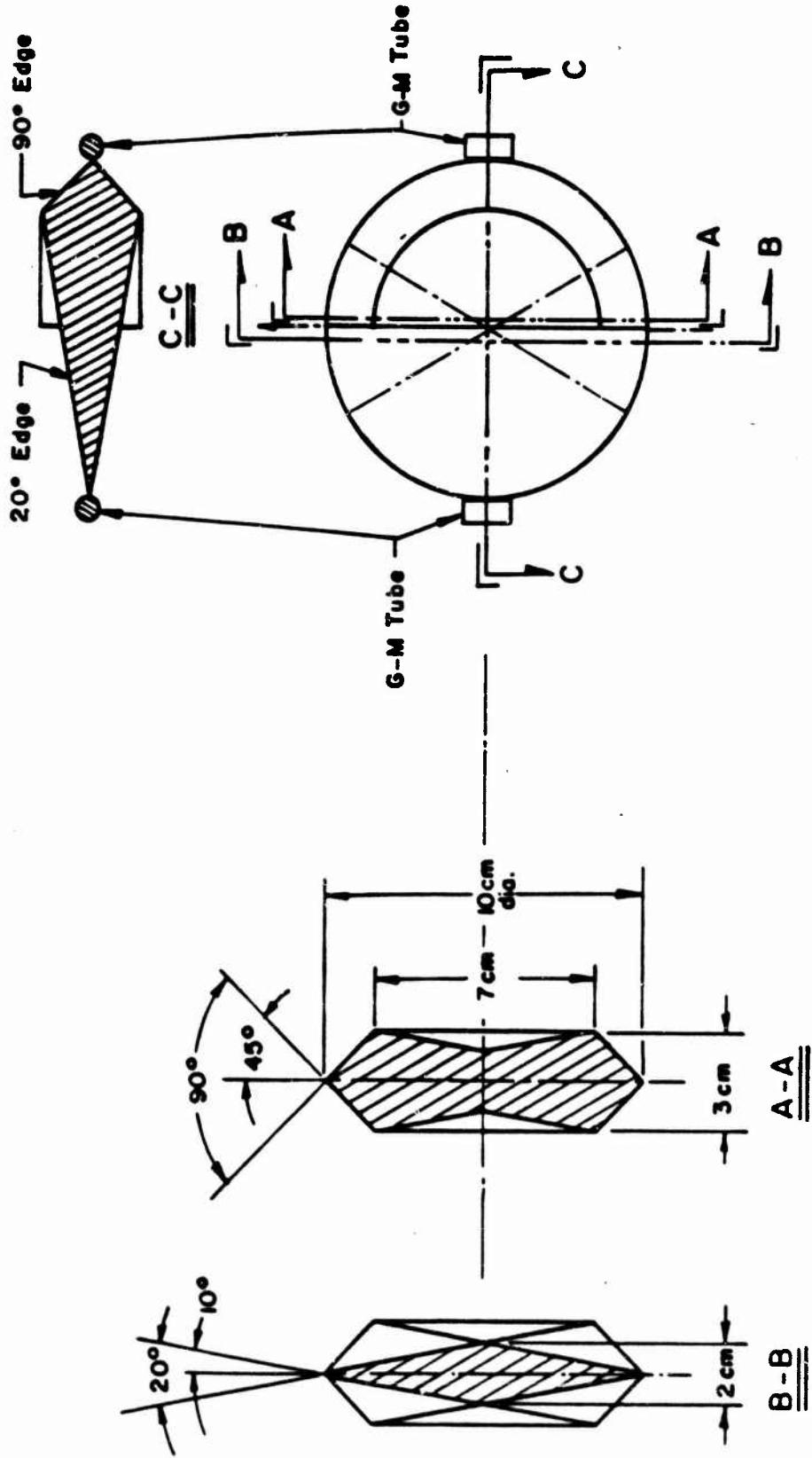


Figure 2.7 Gamma scanner shield and Geiger-Mueller tube locations.

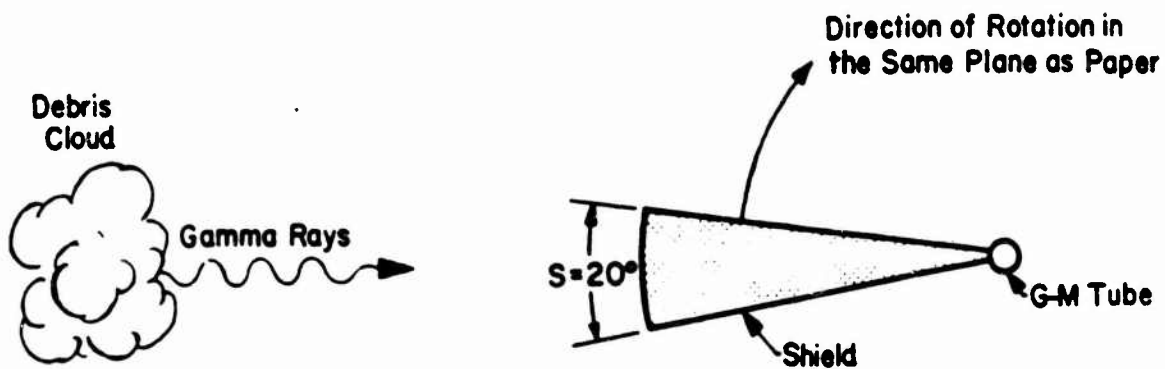


Figure 2.8 Gamma telescope field of view.

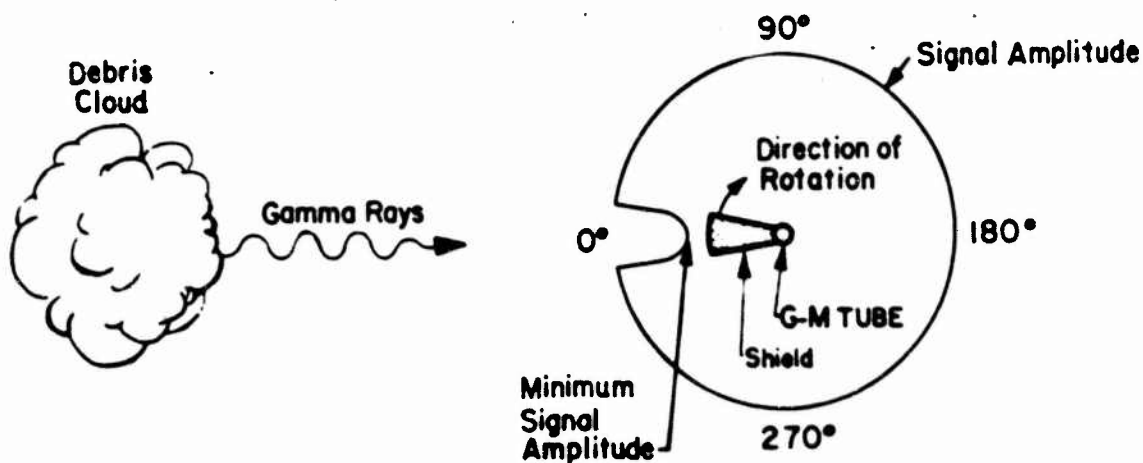


Figure 2.9 Plan view of detector output versus azimuth scanning angle.

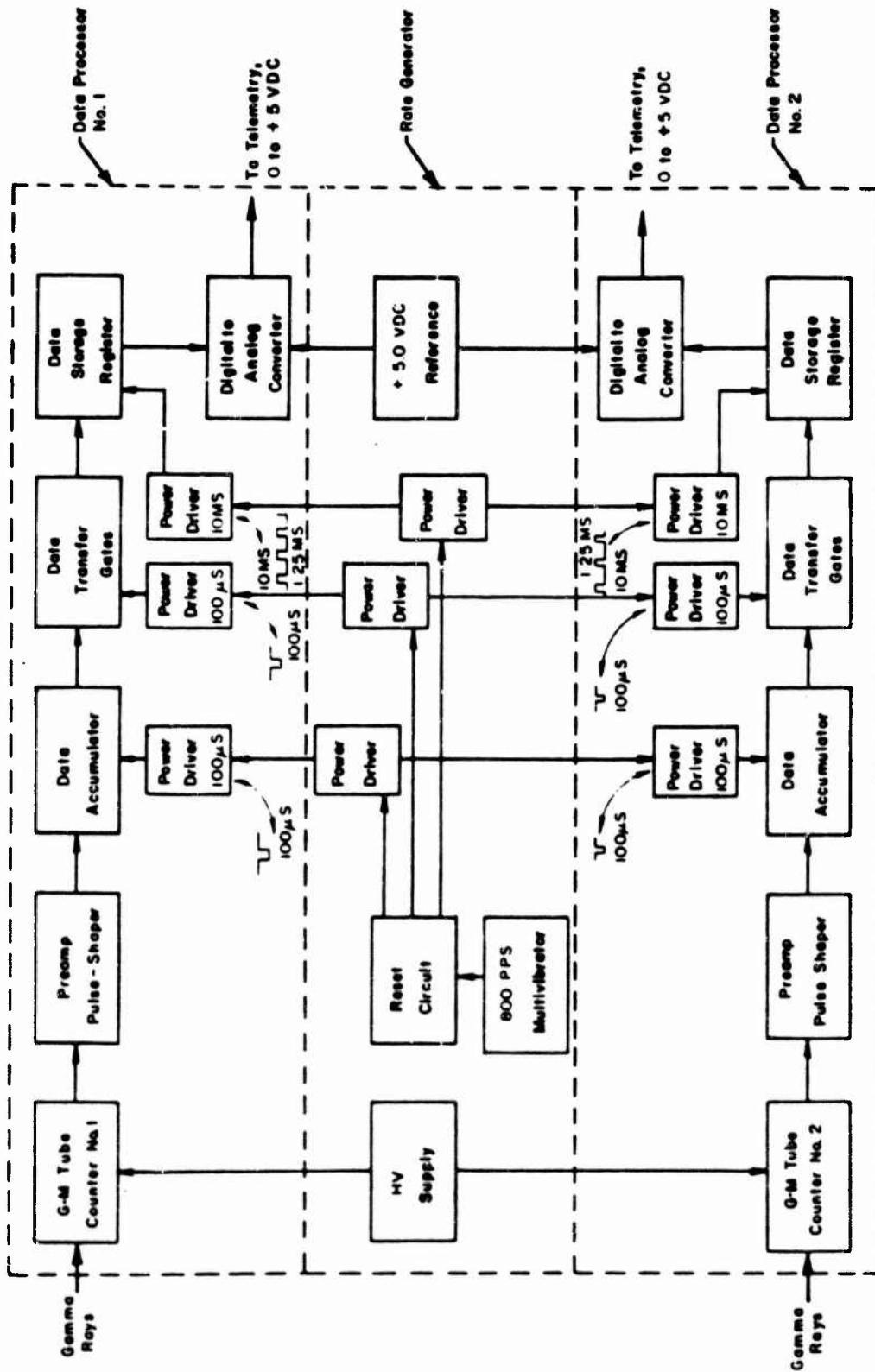


Figure 2.10 Gamma scanner block diagram.

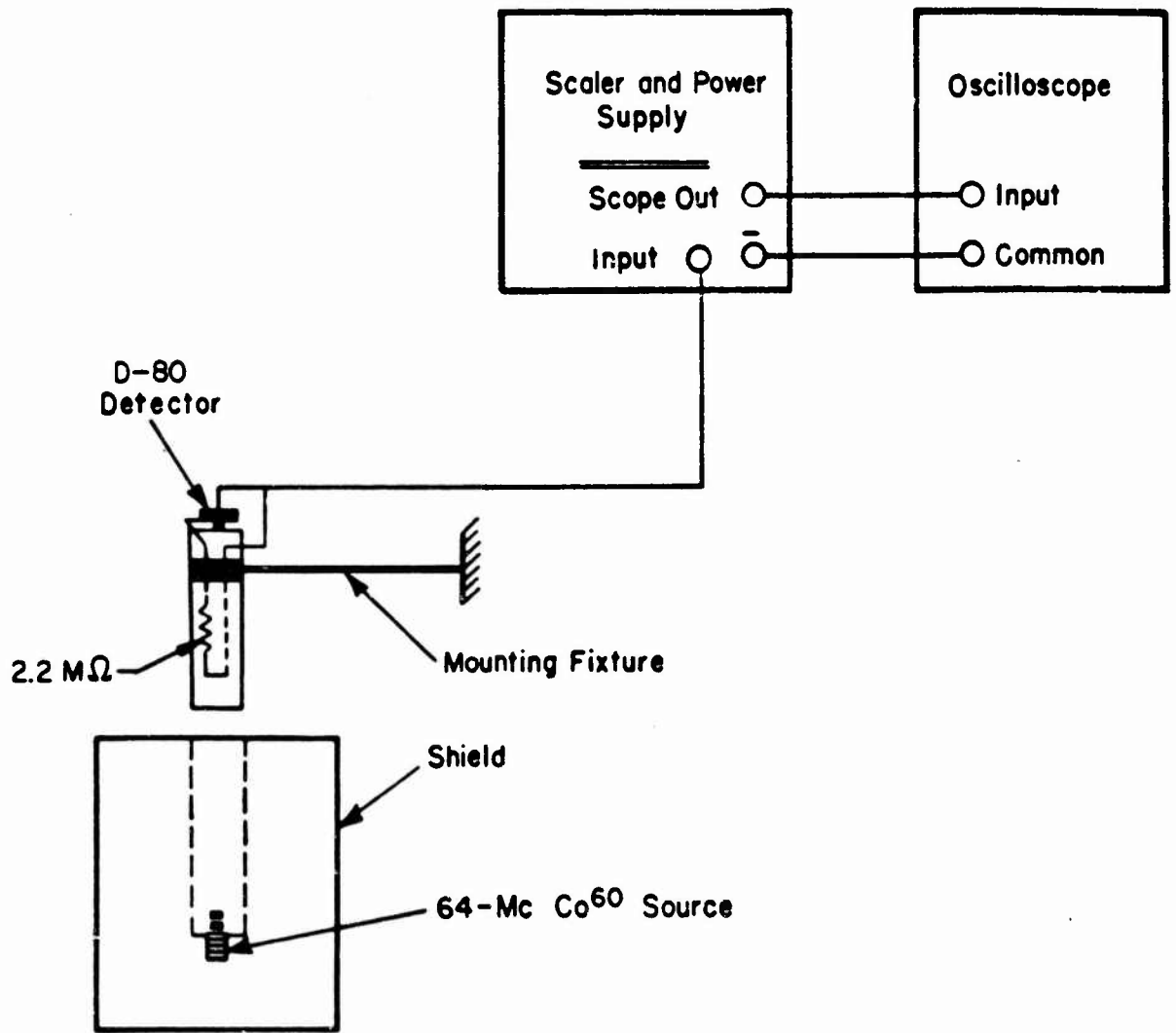


Figure 2.12 Geiger-Mueller tube test setup.

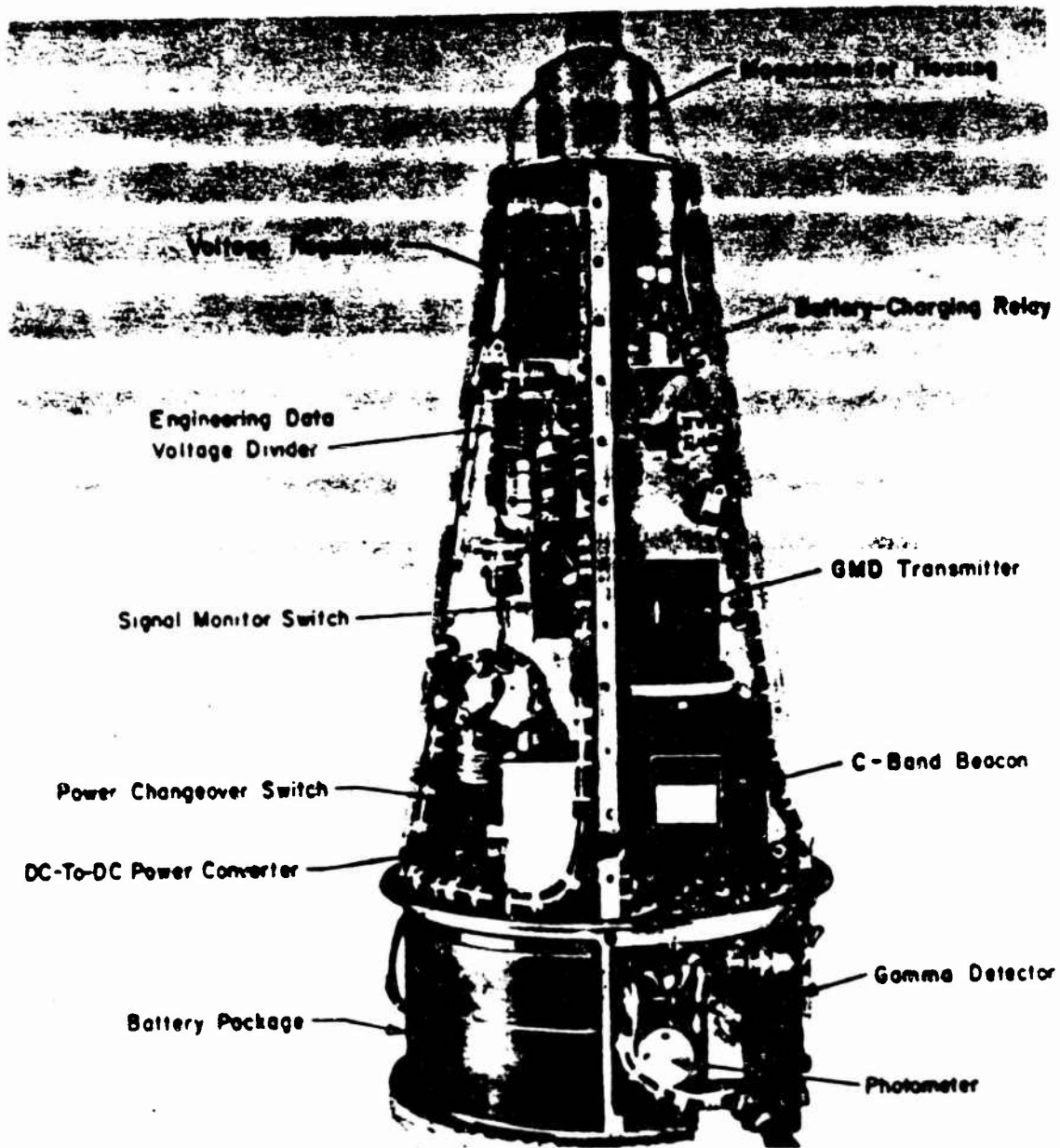


Figure 2.13 EOS instrumentation package, Side 2. (EOS photo)



Figure 2.14 Beta detector assembly. (EOS photo)

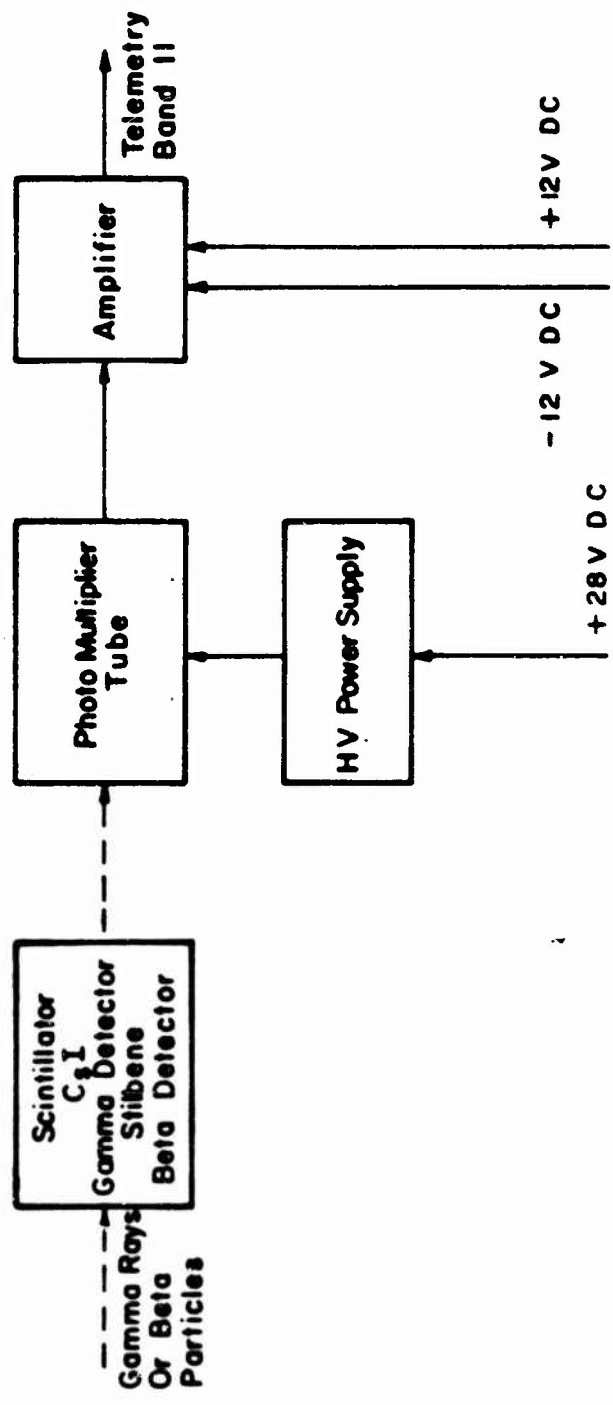


Figure 2.15 Omnidirectional gamma and beta detector block diagram.



Figure 2.16 External view of photometer assembly. (EOS photo)

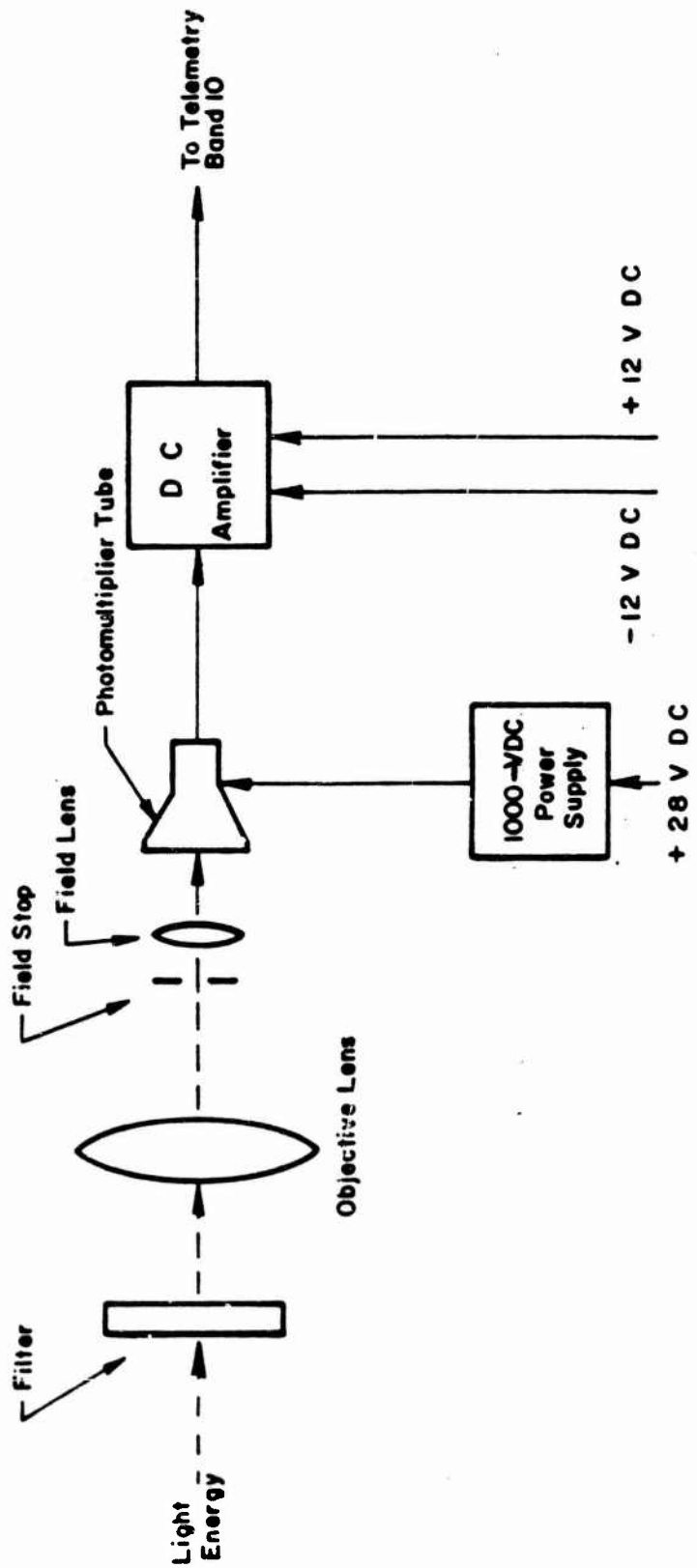


Figure 2.17 Photometer block diagram.

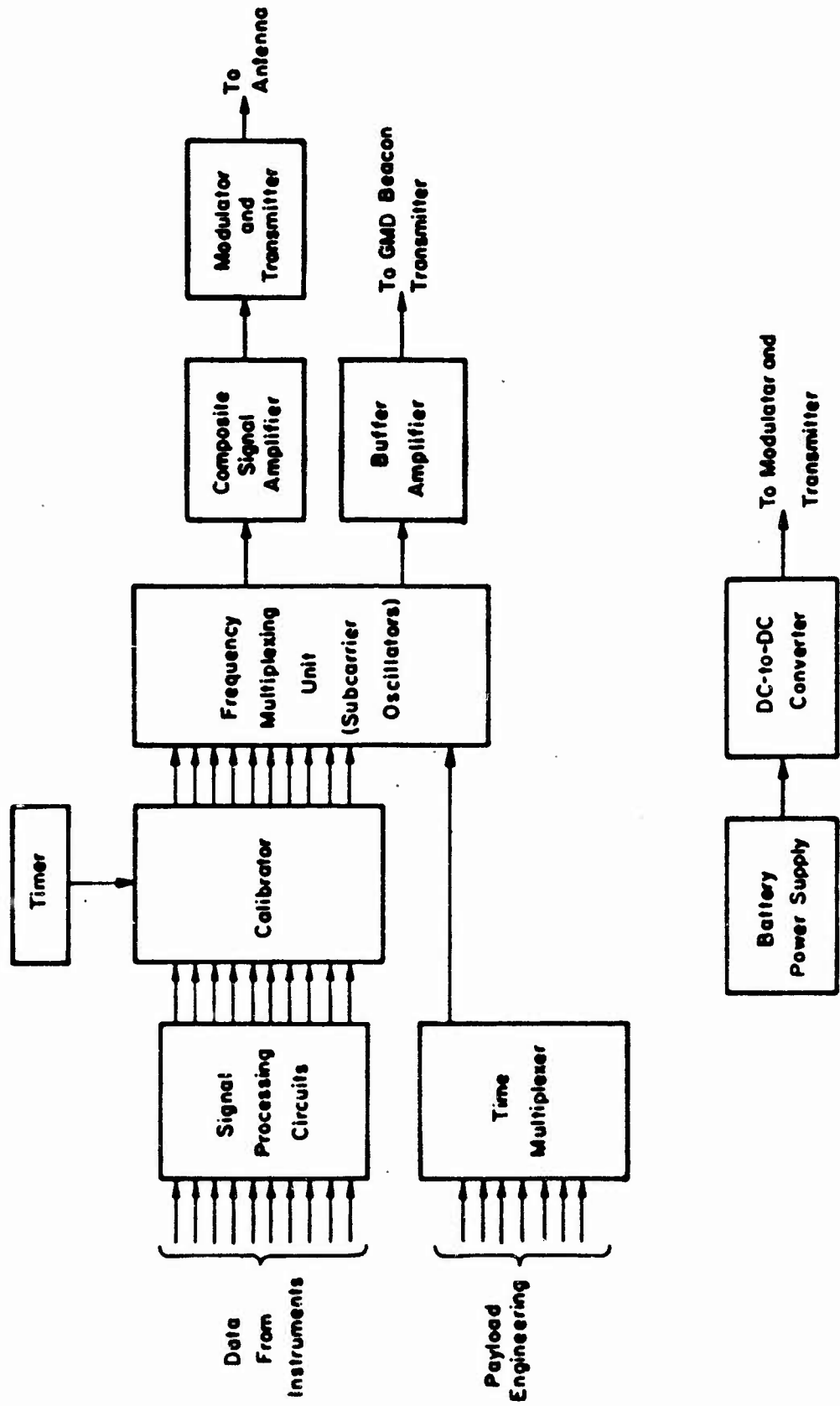


Figure 2.18 Airborne telemetry system block diagram.

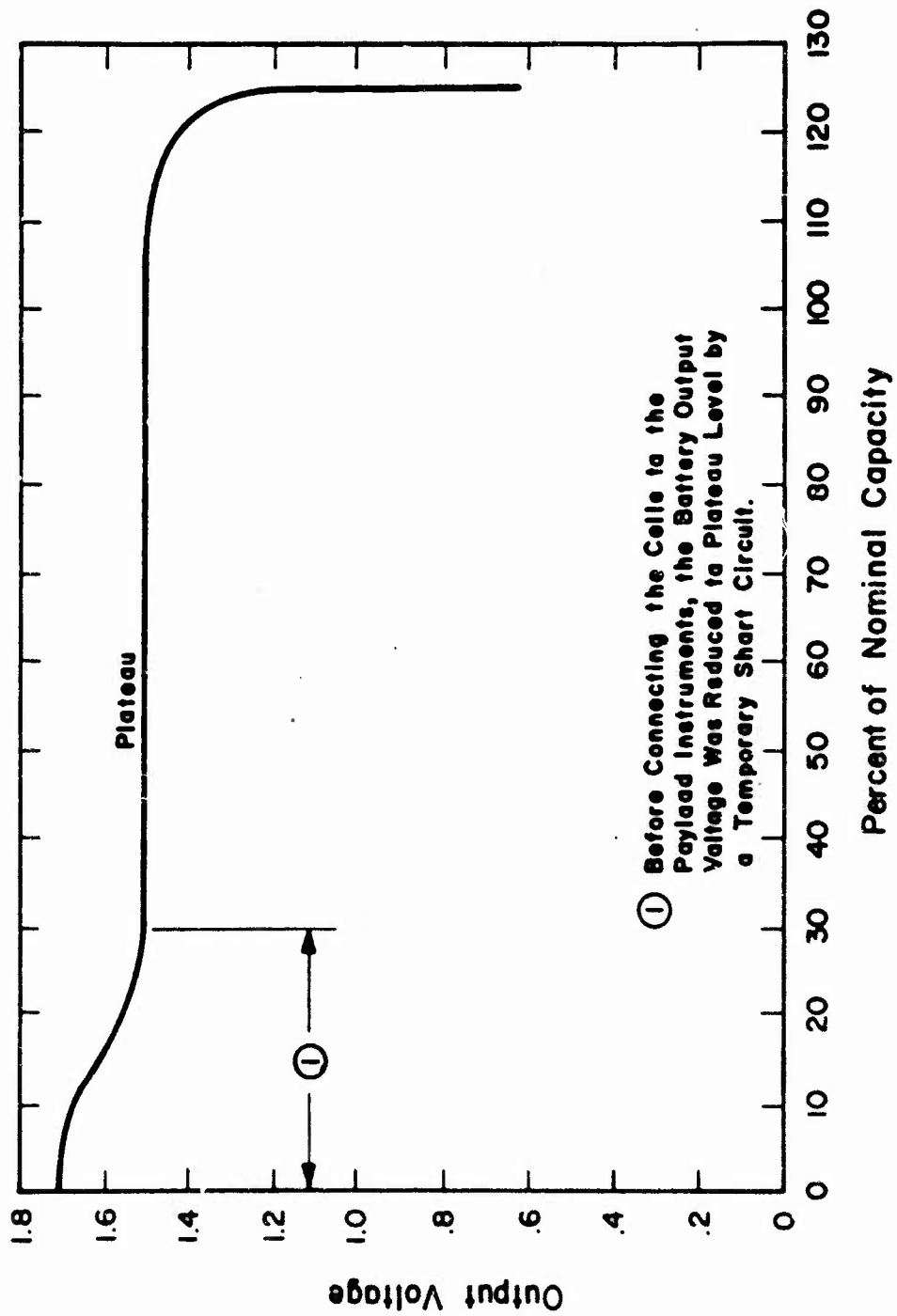


Figure 2.19 Typical discharge curve for Silvercel battery at a 60-minute rate.

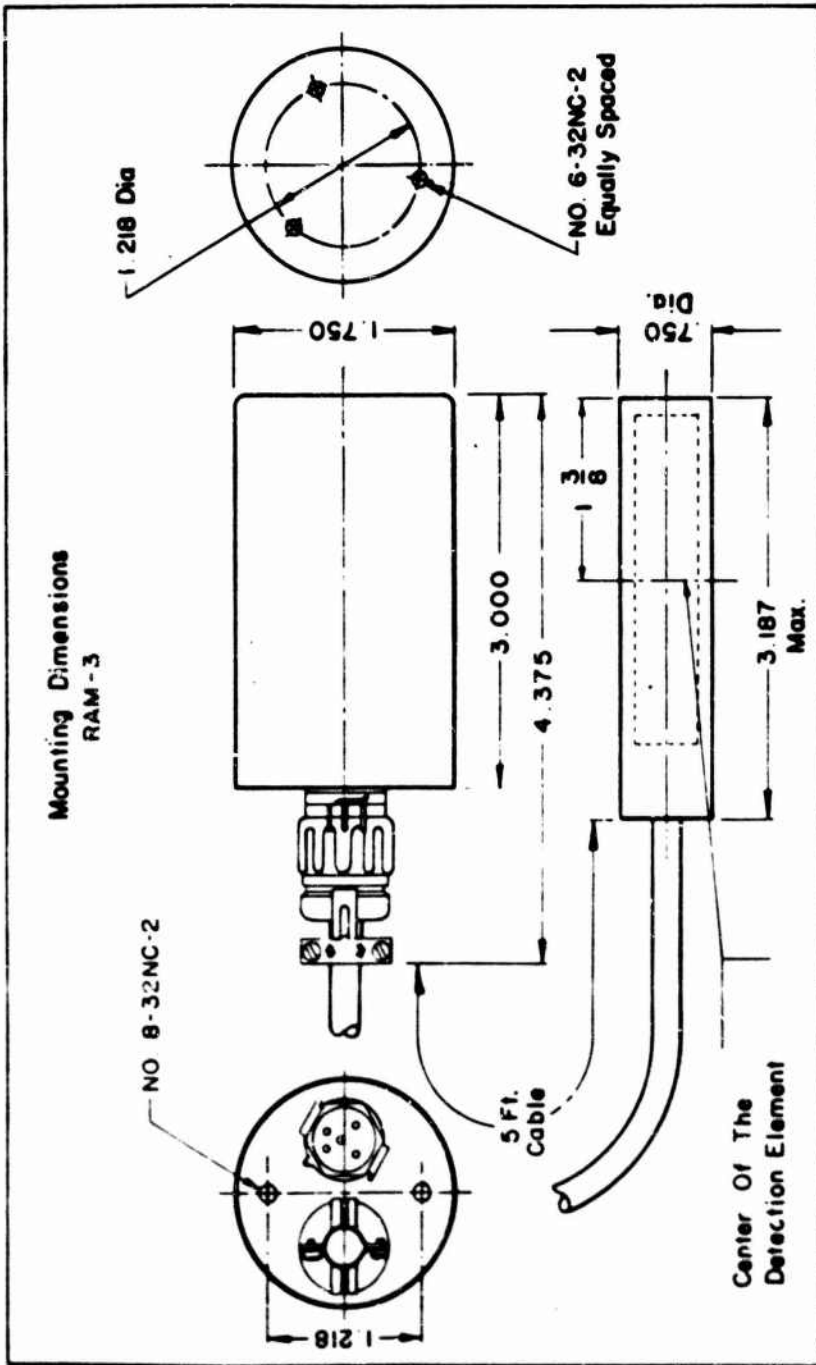


Figure 2.20 Magnetometer sensor assembly.

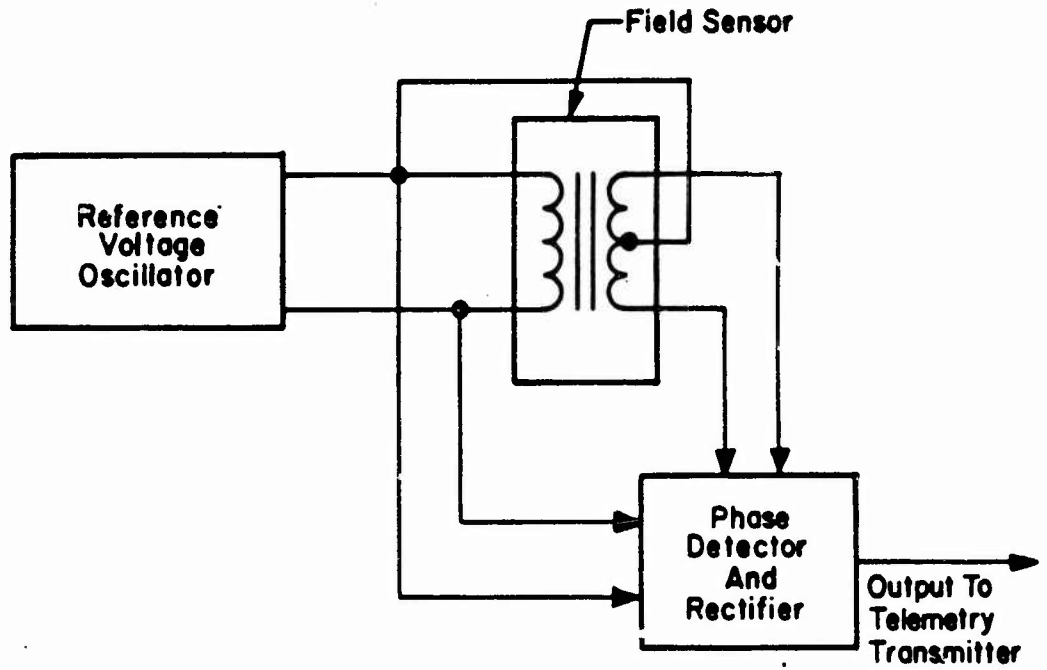


Figure 2.21 Magnetometer block diagram.

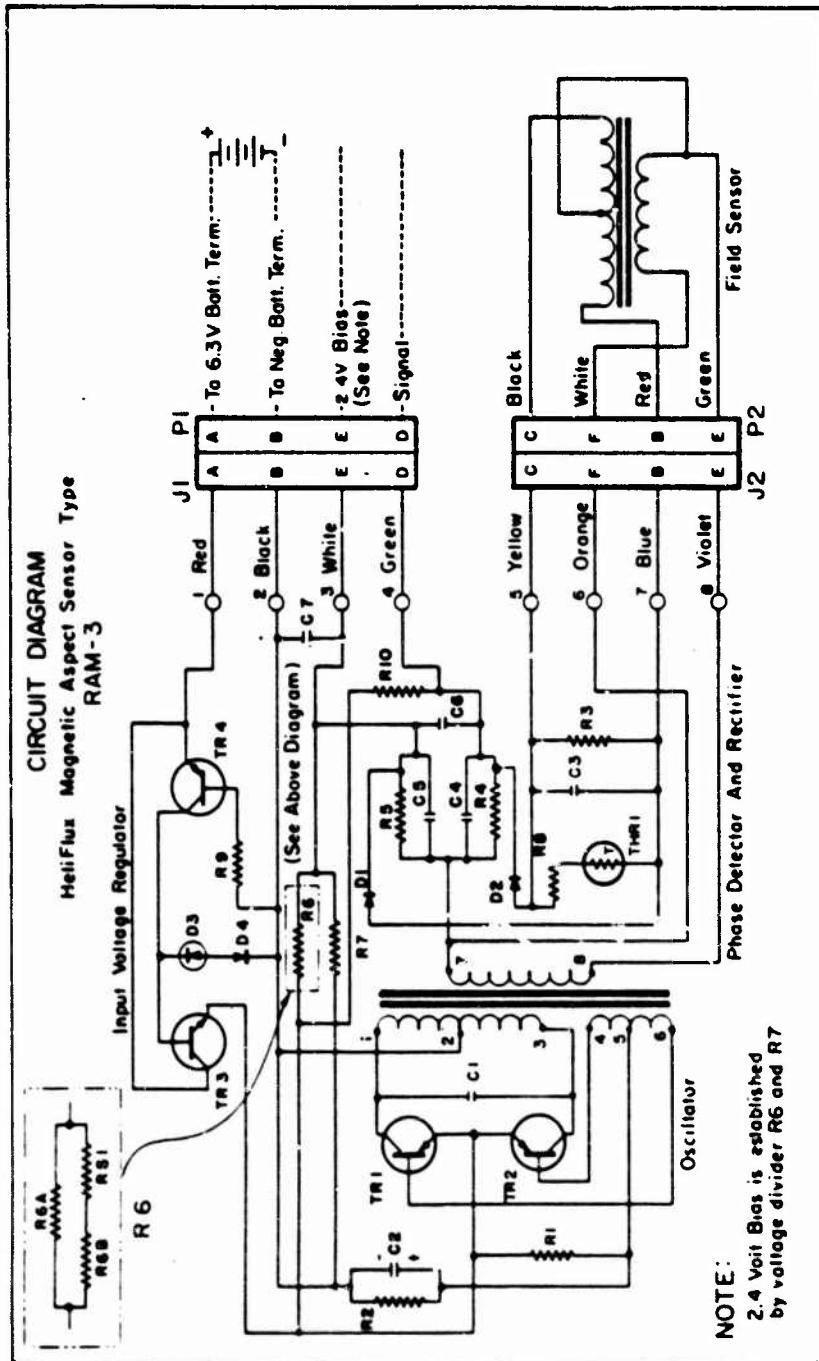


Figure 2.22 Magnetometer schematic.

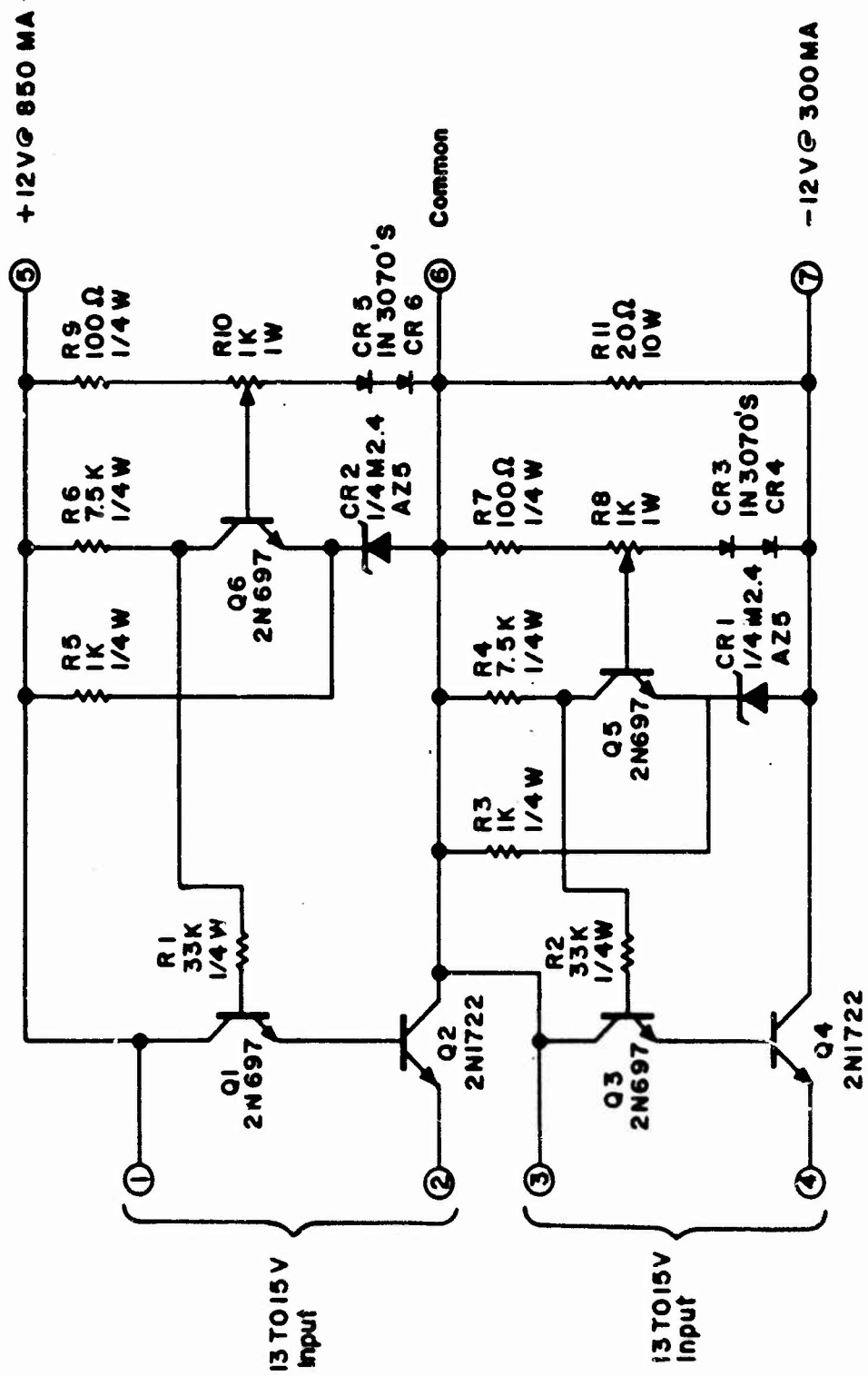


Figure 2.23 Voltage regulator schematic.

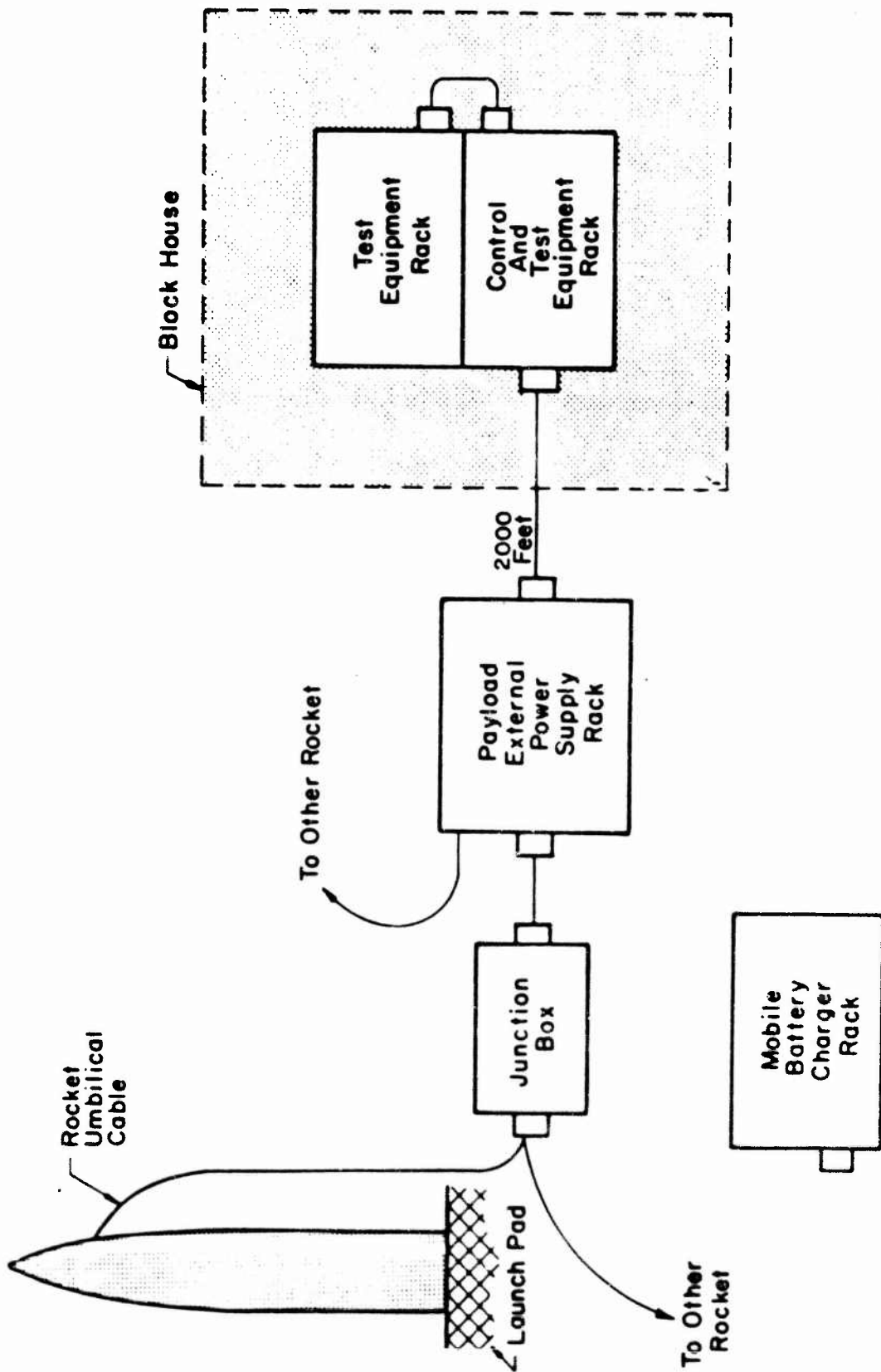


Figure 2.24 Ground support equipment setup.

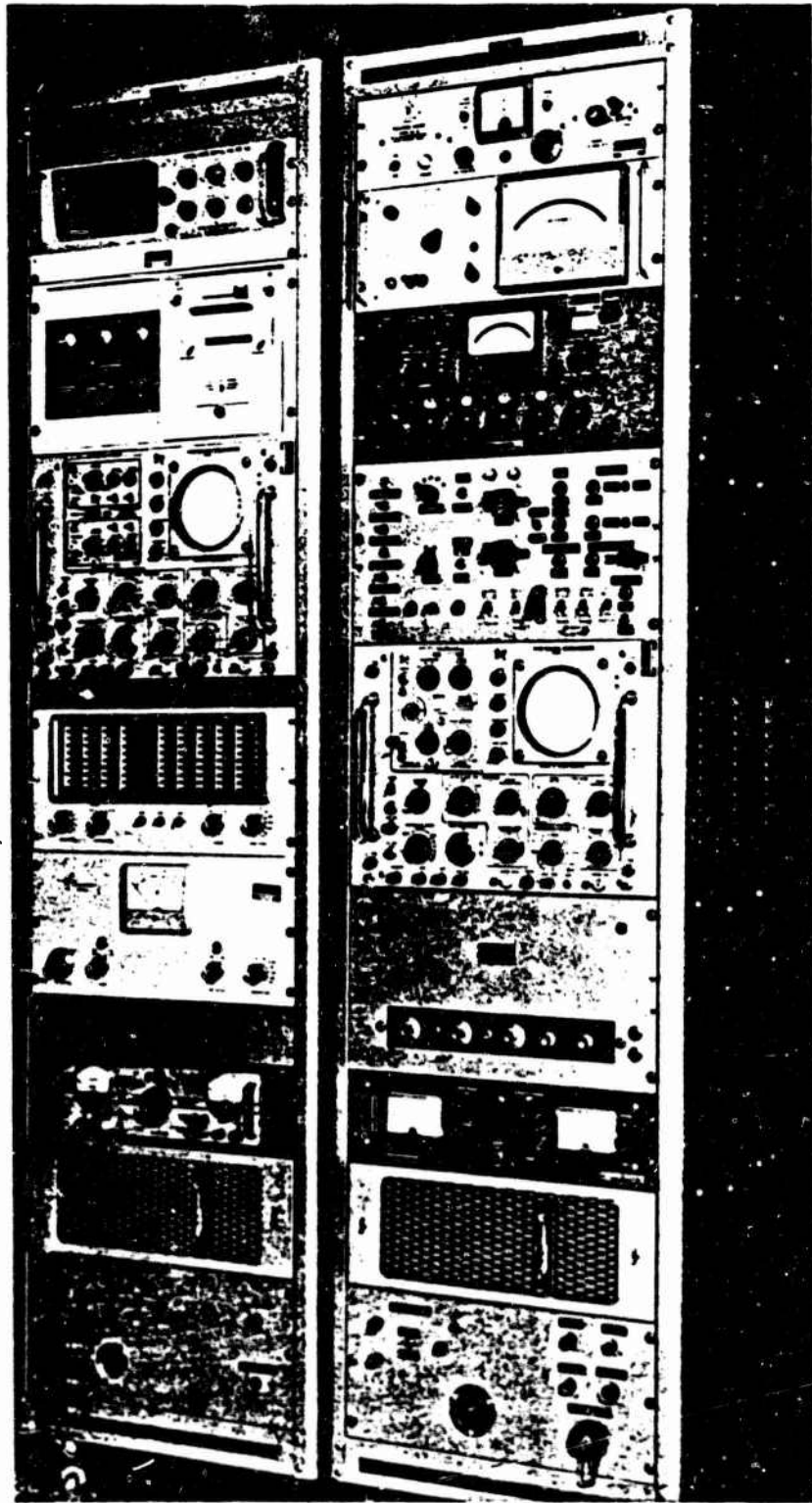


Figure 2.25 Test equipment and control racks. (EOS photo)

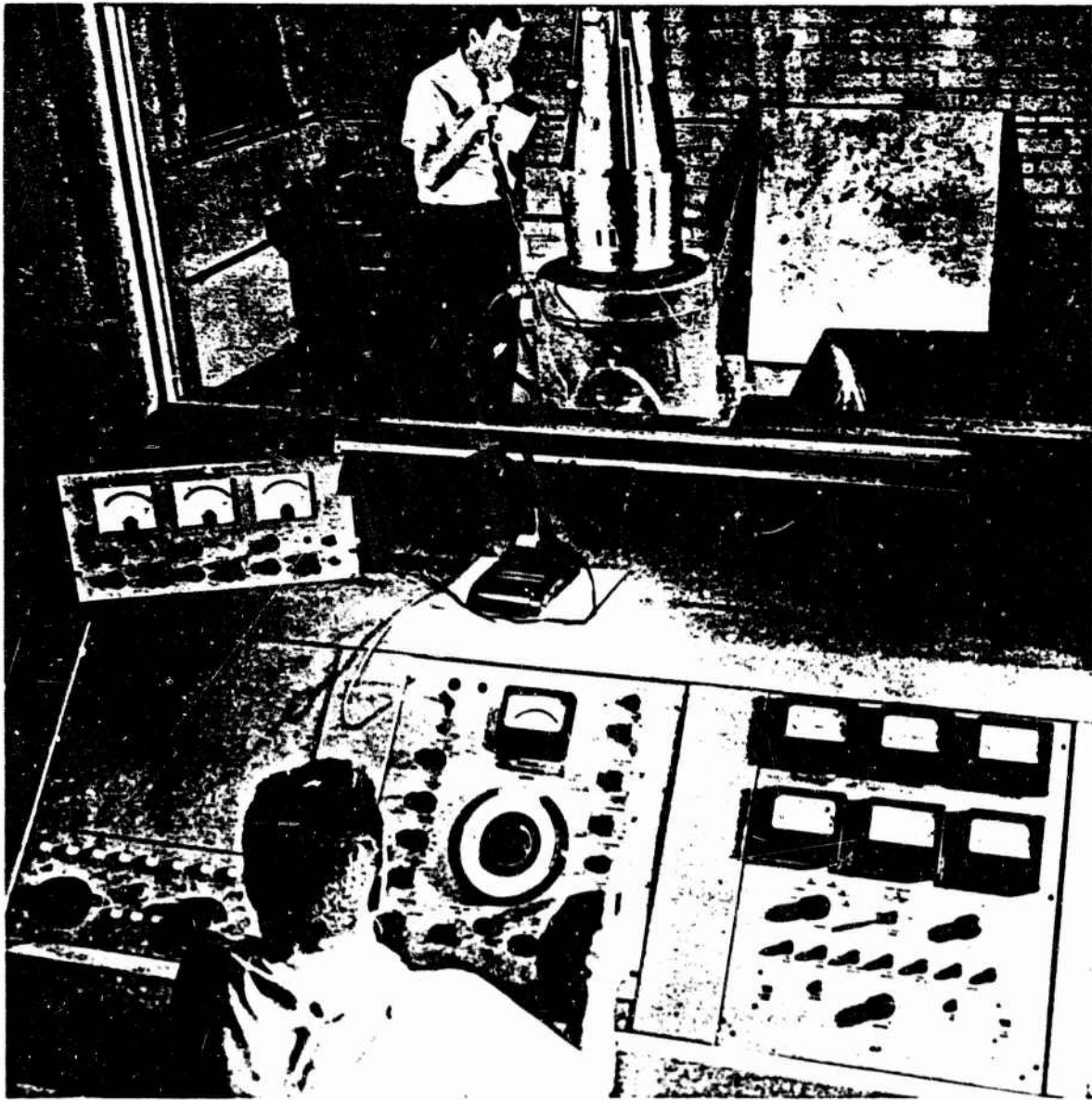


Figure 2.26 Payload mounted to exciter (vibration) table. (EOS photo)

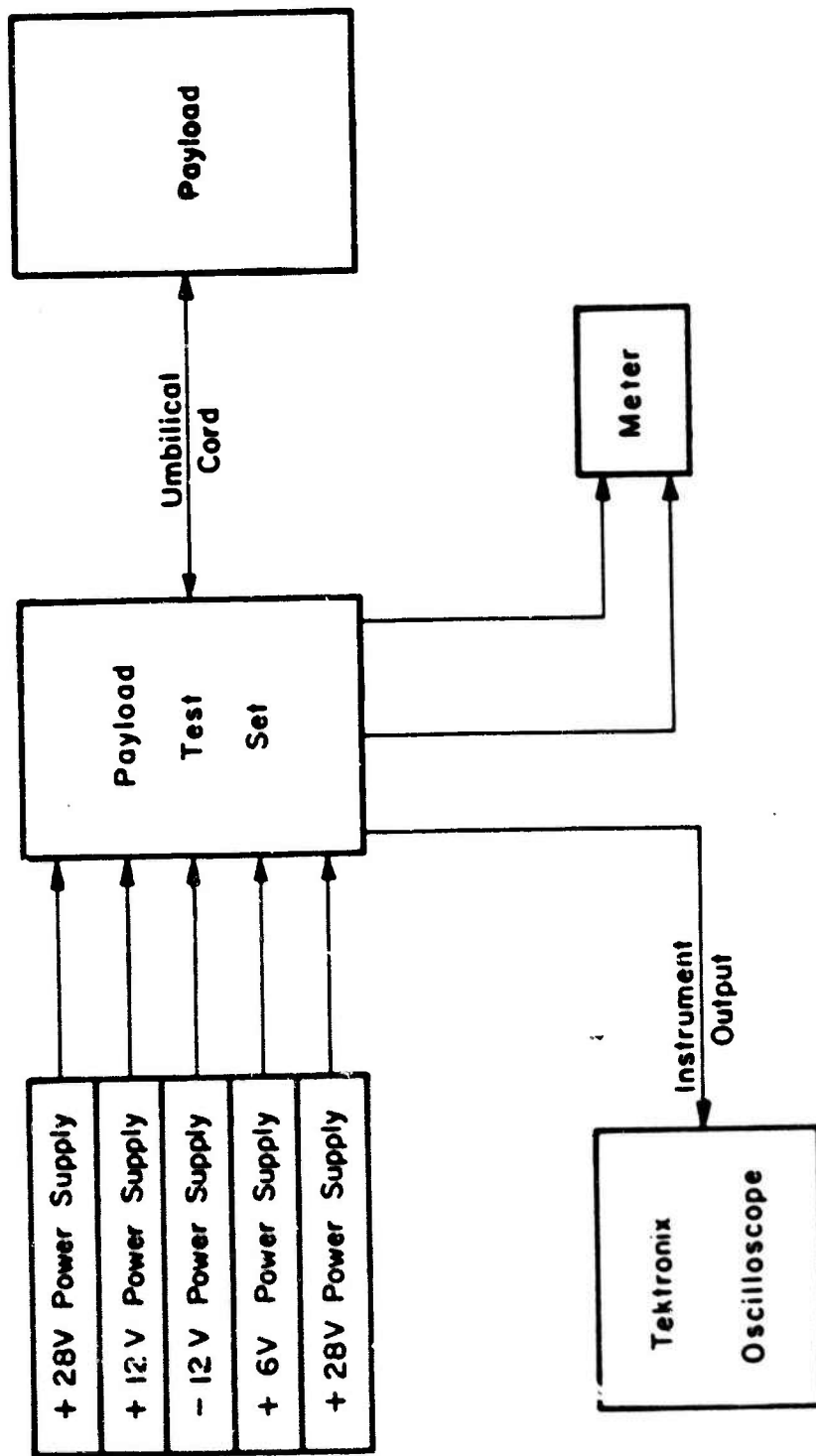


Figure 2.27 Payload checkout block diagram.

CHAPTER 3

RESULTS

The results of Fish Bowl Series Project 6.2 are summarized in this chapter. Samples of reduced data for the gamma scanners, omnidirectional gamma detectors, beta detectors, and photometers are presented for Rockets 8, 9, 15, 18, 19, 26, and 29. The launch times of these rockets to the nearest second with respect to burst time are given below. Rockets discussed in the text are identified by their liftoff times (seconds) in parentheses.

ROCKET	LAUNCH TIME (Seconds)
8	H + 1203
9	H + 2400
15	H + 901
18	H + 1861
19	H - 120
26	H + 780
29	H + 1500

Rockets 8, 9, 15, and 18 were fired from Johnston Island to the north, and Rockets 19, 26, and 29 were fired in a southeasterly direction from the island as shown in Figure 2.2. Additional trajectory information is given in Appendix B.

Test data for each instrument includes information collected from the Star Fish, Blue Gill, and King Fish events. Whenever possible, causes for loss of data also are identified.

3.1 GAMMA SCANNER

The number of output pulses F_U from the scanners was due to gamma radiation (from the debris) which existed in the unshielded field of view of the instrument as illustrated in Figure 2.8. However,

the shielded field of view S was the region of interest. To obtain the count rate F_S due to debris in region S , F_U was subtracted from F_{\max} where F_{\max} approximated the count rate of an unshielded detector.

Two types of plots for the gamma scanner are given below to illustrate the data obtained: (1) F_S versus azimuth angle, and (2) F_S versus altitude for a given azimuth angle. For Rockets 8 (H + 1203) and 9 (H + 2400), F_U instead of F_S is plotted, because F_S could not be easily calculated for the Star Fish event. Calculation of F_S by the previous procedure was difficult, because the widely spread debris invalidated the assumption that $F_{\max} \approx F_0$.

3.1.1 Star Fish. Gamma scanner data plotted for the horizontal 20-degree (H - 20) and horizontal 90-degree (H - 90) scanners were taken approximately every 5 seconds for Rocket 8 (H + 1203) and every 15 seconds for Rocket 9 (H + 2400). F_U versus altitude was plotted when the unshielded region of the H - 20 and H - 90 scanners were pointing 85 degrees, 175 degrees, 265 degrees, and 355 degrees ± 10 degrees from true north. These plots are shown in Figures 3.1 through 3.8. For Rocket 8 (H + 1203) a maximum count rate corresponding to 1.41×10^7 Mev/cm²sec occurred at an altitude of 305 km, and for Rocket 9 (H + 2400) a maximum count rate corresponding to 1.47 Mev/cm²-sec occurred at an altitude of 325 km. The azimuth dependence of the data from the vertical V - 20 and the V - 90 scanners from Rocket 8 (H + 1203) are shown in Figures 3.9 through 3.12. These plots show F_U versus azimuth angle, ϕ , at various altitudes as indicated on the plots.

3.1.2 Blue Gill. For both the vertical 20 degree (V - 20) and horizontal 90 degree (H - 90) scanners, F_S versus azimuth angle, ϕ , was calculated for five consecutive cycles at various flight times. Phi, ϕ , was the direction of the shielded region of the scanners with respect to true north. The average of the five values of F_S versus ϕ was plotted, and a family of curves corresponding to different altitudes was obtained. Examples of these plots are shown in Figure 3.13 for the V - 20 and the H - 90 scanners. Using the family of

curves from the H - 90 scanner, another family of curves of F_S versus payload altitude was obtained, where each curve represents a different azimuth angle. (See Figure 3.14.)

All the scanners on Rocket 18 (H + 1861), with the exception of the V - 90, which stopped counting shortly after H + 1932 seconds, seemed to have worked satisfactorily throughout the flight. However, the randomness of the count rates from one sampling period to the next indicates that the data are not reliable.

3.1.3 King Fish. A series of F_S versus azimuth angle plots at different times are shown for all four scanners of Rocket 19 (H - 120) in Figures 3.15, 3.16, 3.17, and 3.18. This series of scans is presented to depict the characteristics of the rapidly moving cloud. The high count rates obtained during this flight provided good counting statistics and thus did not require averaging over a number of cycles to smooth the random fluctuations in data as required for Rocket 15.

Scanners on Rocket 26 (H + 780) indicated a low count rate of less than 2000 counts per second starting at H + 810 seconds and lasting until H + 822 seconds. Although some signal modulation was noticed on all channels, there was no correlation with the spin frequency of the payload. Starting at H + 822 seconds, and lasting for about 20 seconds, the scanner output signal randomly alternated between less than 0.5 volt and 5 volts. The signal variations on all four scanner channels were identical. Noise was also observed on other telemetry channels during this time. After this period, a system malfunction affected the normal operation of the scanners. This malfunction was indicated by the absence of the normally present 10-millisecond sampling periods in the output signals.

On Rocket 29 (H + 1500) both the horizontal and vertical scanners operated normally, but their output signals indicated a low radiation level. Therefore, reduced data was not included below. Count rates were less than 1000 cps which corresponded to a radiation flux of $< 3 \times 10^6$ Mev/cm²-sec. However, a slight amount of signal modulation due to the spinning payload indicated that debris was probably above

the rocket. At H + 1673 seconds all four scanners ceased to operate. The cause for this malfunction was not determined.

3.2 OMNIDIRECTIONAL GAMMA DETECTOR

The output of the omnidirectional gamma detector (gamma detector) was a function of the energy absorbed by the scintillator. To determine the incident energy flux, a gamma energy spectrum for U^{235} was assumed.

Although this instrument was designed to be omnidirectional, the output was modulated at the payload spin frequency due to the shielding characteristics of payload components. The maximum output in volts per revolution versus altitude was plotted to illustrate the data obtained during the Star Fish, King Fish, and Blue Gill events.

3.2.1 Star Fish. The output from the gamma detector on Rocket 8 (H + 1203) was modulated at the same frequency as the payload spin frequency between H + 1251 and H + 1338 seconds. A minimum output level occurred when the X-magnetometer was oriented 40 degrees from true north. From H + 1338 to H + 1448 seconds, two minimums per revolution occurred when the X-magnetometer pointed 40 degrees and 220 degrees from true north. The gamma detector signal intensity in the 220-degree position was lower than in the 40-degree position. Maximum radiation energy flux corresponding to 1.4×10^6 Mev/cm²-sec occurred at H + 1380 seconds (305 km). The maximum detector output (volts) per revolution versus payload altitude for Rocket 8 is shown in Figure 3.19. The gamma detector did not produce any noticeable output signal on Rocket 9.

3.2.2 Blue Gill. The detector on Rocket 15 indicated a response to gamma radiation starting at H + 933 seconds. It was partially saturated for 7 seconds between H + 972 and H + 979 seconds. The output oscillated at the spin frequency of the payload, with the minimum occurring whenever the X-magnetometer was pointing 50 degrees from true north. A plot of maximum output (volts) per revolution versus payload altitude is shown in Figure 3.20.

The detector on Rocket 18 (H + 1861) did not provide an output signal until H + 2021 seconds when the output suddenly jumped to 1.1 volts. The abruptness of this change from 0 to 1.1 volts indicated that the instrument was not functioning properly before this time. A maximum output corresponding to 3.2×10^6 Mev/cm²-sec occurred at H + 2024 seconds (34 km).

3.2.3 King Fish. Telemetry blackout was observed from H = 0 to H + 3 seconds for Rocket 19 (H - 120). However, after blackout, the gamma detector provided an output signal until H + 215 seconds. The detector was saturated for 9 seconds after blackout. After this period, a modulated output signal was observed during every revolution of the payload. The minimum of the modulated signal occurred when the X-magnetometer was pointed 265 degrees from north. A plot of maximum signal output (volts) per revolution versus payload altitude and range from Johnston Island is shown in Figure 3.21.

The gamma detector on Rocket 26 (H + 780) started to respond to radiation at H + 30.5 seconds and reached a maximum of approximately 5.12×10^5 Mev/cm²-sec at H + 177.5 seconds. A plot of maximum output (volts) versus payload altitude and range from Johnston Island is shown in Figure 3.22. A small amount of signal modulation corresponding to the payload spin frequency was present until the payload lost its stability during re-entry.

On Rocket 29 (H + 1500) the gamma detector output signal indicated a low level of radiation throughout the flight. However, a small amount of signal modulation was noticed which indicated that debris was still present at H + 1500 seconds.

3.3 BETA DETECTOR

In order to determine the beta source distribution of the debris cloud, it was decided to project the payload trajectory along the magnetic field lines to the vicinity of the burst. The first step in accomplishing this was to plot the magnetic field lines in the vicinity of Johnston Island using the data from Reference 4. The actual trajectory was then projected on a plane parallel to the field

lines and containing the burst point as shown in Figures 3.23, 3.24, 3.25 and 3.26 for Rockets 8, 9, 15, and 19, respectively. This new trajectory was then projected along the field lines to obtain the projected altitude in the plane perpendicular to the field lines and containing the burst point. The cross range, measured from a vertical line through the burst point, was obtained by a simple geometric projection of the actual trajectory onto this plane. Cross range versus projected altitude in this plane (perpendicular to the field and containing the burst point) is shown in Figures 3.27, 3.28, 3.29, and 3.30.

On Rockets 8 (H + 1203) and 9 (H + 2400) the beta detector had a conical field of view with a half angle of 60 degrees which is equal to a solid angle of π steradians. The beta detectors on Rockets 15 (H + 901), 18 (H + 1861), 19 (H - 120), 26 (H + 780), and 29 (H + 1500) had a half angle of 15 degrees, which is equal to 0.2 steradian. The output of the beta detector represented the energy flux which was absorbed by the stilbene crystal.

3.3.1 Star Fish. On Rocket 8 (H + 1203) the first indication of an output signal occurred at approximately H + 1274 seconds with two maximums per payload revolution occurring at 100 to 280 ± 10 degrees from true north (see Figure 3.31). The amplitude of the signal increased until the detector saturated at approximately H + 1309 seconds. By H + 1323 seconds the instrument was completely saturated and remained in this condition for the rest of the flight. (Also see Figure 3.32.)

On Rocket 9 (H + 2400), the instrument saturated abruptly at H + 2400 seconds (10 km) and remained saturated until H + 3000 seconds (640 km). Thereafter, two minimums per revolution were observed at 0 and 190 ± 10 degrees from north (see Figure 3.33). The output was completely saturated again at H + 3180 seconds (420 km). The initial apparent saturation was probably caused by an instrument malfunction.

3.3.2 Blue Gill. The detector on Rocket 15 (H + 901) produced an output signal at H + 935 seconds (23 km). A large maximum signal was generated whenever the instrument was pointed toward the magnetic south.

At H + 961 seconds (58.3 km) the output was partially saturated indicating an energy flux of greater than 2×10^6 Mev/cm²-sec. Immediately after, two maximums per payload revolution were observed in the magnetic east and west directions. The two maximums were of equal amplitude and lasted until H + 987 seconds (86.7 km), after which there was only one maximum per payload revolution. A typical scan at H + 960 seconds (56.5 km) is shown in Figure 3.34. Another plot of output voltage versus altitude for azimuth orientation of magnetic north, south, east, and west is shown in Figure 3.35.

The beta detector on Rocket 18 (H + 1861) did not operate properly during the flight; therefore, test data is not included below. The cause of failure was not determined.

3.3.3 King Fish. Telemetry blackout on Rocket 19 (H - 120) was observed for 3 seconds following the burst. After blackout, the beta detector was saturated whenever it scanned between 90 and 330 degrees from north. This lasted for about 3.5 seconds after which a maximum was indicated between 120 and 300 degrees from north. From H + 165 seconds (166 km) to H + 180 seconds (178 km) two maximums were observed during each revolution of the payload. These two maximums occurred at 110 and 290 degrees from north. The maximum and minimum values versus time and payload altitude are shown in Figure 3.36. Energy flux, (normalized to remove decay) versus the projected altitude for azimuth angles of 10 degrees and 190 degrees are shown in Figure 3.37. No beta detector data was obtained on Rocket 26 (H + 780). The cause for this lack of data was not determined.

On Rocket 29 (H + 1500) the beta detector started to respond at H + 1560 seconds and continued to indicate the presence of radiation until H + 1680 seconds. A maximum modulated output was observed for each revolution of the payload whenever the detector was facing south. The maximum level of radiation was 2.6×10^5 Mev/cm²-sec.

3.4 PHOTOMETER

The output of the photometer was a function of the irradiance of 3914 Å incident radiation at the objective lens of the instrument. Plots of irradiance versus payload altitude are included below to describe the magnitude and distribution of the emitting region.

3.4.1 Star Fish. The photometer output signal on Rocket 8 (H + 1203) indicated a sharp maximum at about 40 degrees from north starting at H + 1277 seconds (75 km). The sharp peak then broadened and shifted toward the west until the peak value had shifted to 295 degrees from north. By H + 1290 (95 km) the output had decreased to background level. The output signal remained low until H + 1293 seconds (98 km) and then gradually increased without any azimuth dependence to a maximum at H + 1295 seconds (100 km). This maximum gradually decreased with a second smaller maximum at 1303 seconds (111 km) to background level at H + 1308 seconds (120 km). After H + 1308 seconds the signal remained at a low value throughout the remainder of the flight. A plot of irradiance versus altitude for Rocket 8 (H + 1203) is shown in Figure 3.38.

The photometer on Rocket 9 (H + 2400) produced an output signal starting at H + 2479 seconds (85 km). At H + 2489 seconds (100 km) the output signal started to increase and reached a maximum at H + 2493 seconds (103 km). The signal decreased until H + 2497 seconds (110 km) when it again increased to a second maximum and then gradually decreased until H + 2505 seconds (129 km). Throughout the remainder of the flight, the output signal remained at background level. The only azimuth dependence was noticed between H + 2489 seconds (100 km) and H + 2495 seconds (108 km). This signal indication occurred between north and northwest. A plot of irradiance versus altitude for Rocket 9 (H + 2400) is shown in Figure 3.39.

3.4.2 Blue Gill. The photometer on Rocket 15 (H + 901) started to generate a low output signal, just above background level, at H + 948 seconds (41 km) when the photometer was pointing in the northern and southern directions. The signal level continued at about the same amplitude until H + 958.5 seconds (55 km). After this time the output signal returned to background level.

Although inspection of operational voltage telemetry data indicated that the photometer on Rocket 18 (H + 1861) was operating properly, the output signal had insufficient amplitude to provide any useful information.

3.4.3 King Fish. A telemetry blackout occurred during the flight of Rocket 19 (H - 120) at H = 0 and lasted until H + 3 seconds (141 km). Immediately after this 3-second blackout, the photometer output signal saturated until H + 5 seconds (143 km). As the photometer output decreased, minimums in output signal levels occurred at 120 and 300 degrees from north. At H + 7 seconds (144 km), the output decreased from saturation, and maximum signal output levels occurred at 60 and 160 degrees from north. At about H + 15 seconds (150 km), a very intense peak, superimposed on the original signal, appeared at 220 degrees from north. Initially, the width of this peak was about 10 degrees, but it gradually increased in amplitude and width. At H + 20 seconds (154 km), the amplitude was maximum with a signal width of about 50 degrees. After this the amplitude decreased without any noticeable change in width until H + 77 seconds (176 km) when this peak was no longer distinguishable from the other data. Sharp peaks were noticed at zero degrees from north between H + 120 seconds (174 km) and H + 127 seconds (172 km), H + 140 seconds (166 km) and H + 149 seconds (162 km), H + 163 seconds (153 km) and H + 177 seconds (143 km), and between H + 184 seconds (137 km) and H + 195 seconds (127 km). Loss of + 12-volt dc from the battery, probably due to regulator failure, at H + 225.5 seconds terminated the generation of any further output signals. The direction of maximum photometer response is shown in Figure 3.40. Airglows, observed at later times in the northern direction, are shown in Figure 3.41. Airglow configurations are approximated by patterns shown in Figure 3.41.

The photometer on Rocket 26 (H + 780) produced an output signal of about 10 degrees in width at 0 degrees from north between H + 807 seconds (19 km) and H + 831 seconds (53.8 km) and between H + 1116 seconds (79 km) and H + 1122 seconds (71.5 km). Erratic payload attitude occurred at H + 1117 seconds (78 km) and became quite violent at H + 1122 seconds (71 km). Some directional indications were observed after the erratic motion began; however, due to the erratic motion of the payload, these results will require further analysis.

Although inspection of operation voltage telemetry data indicated that the photometer on Rocket 29 (H + 1500) was operating properly, the output signal was too low to obtain any useful information.

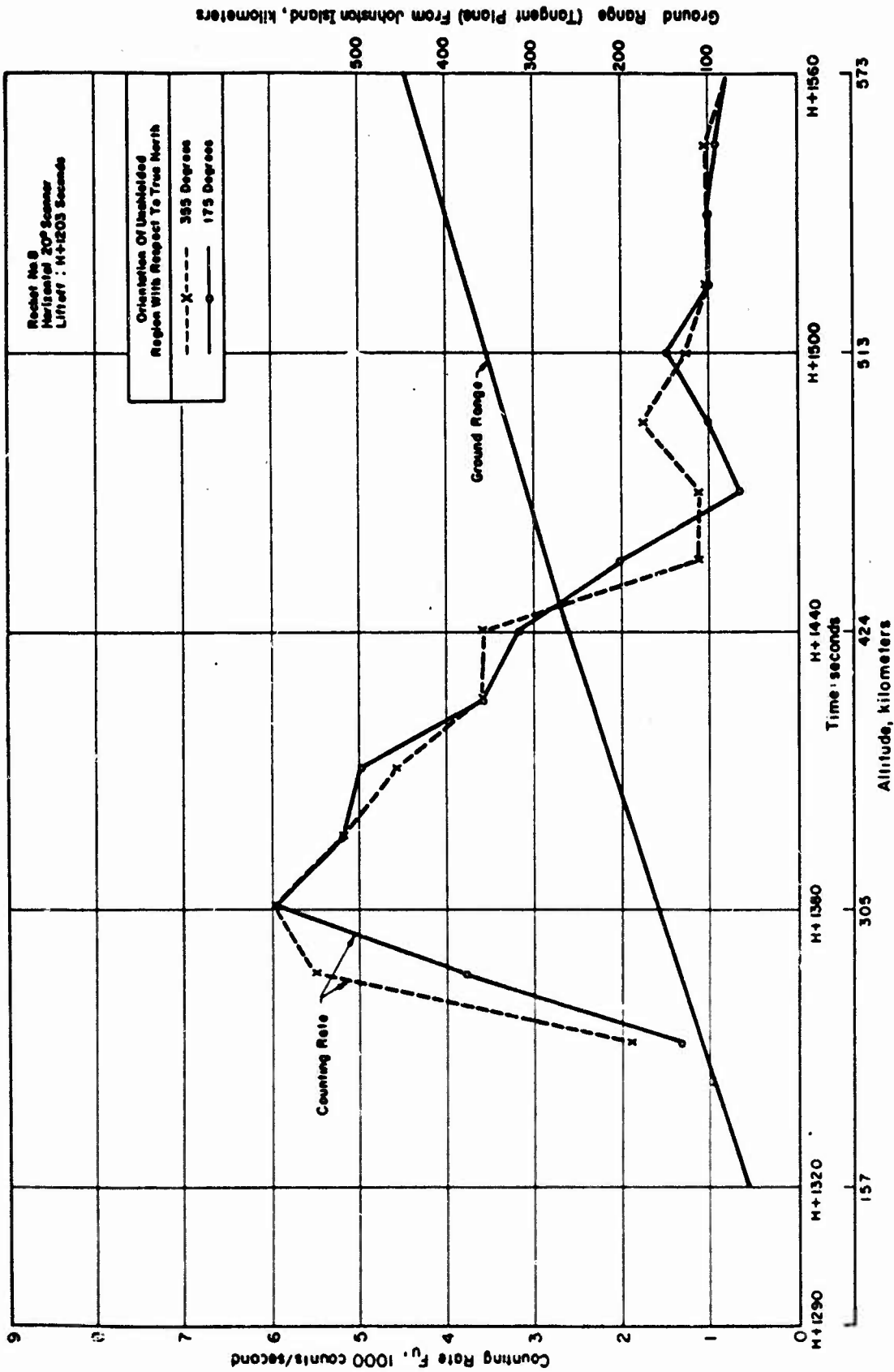


Figure 3.1 Horizontal 20° gamma scanner data, Rocket 8, 355° and 175°, Star Plan.

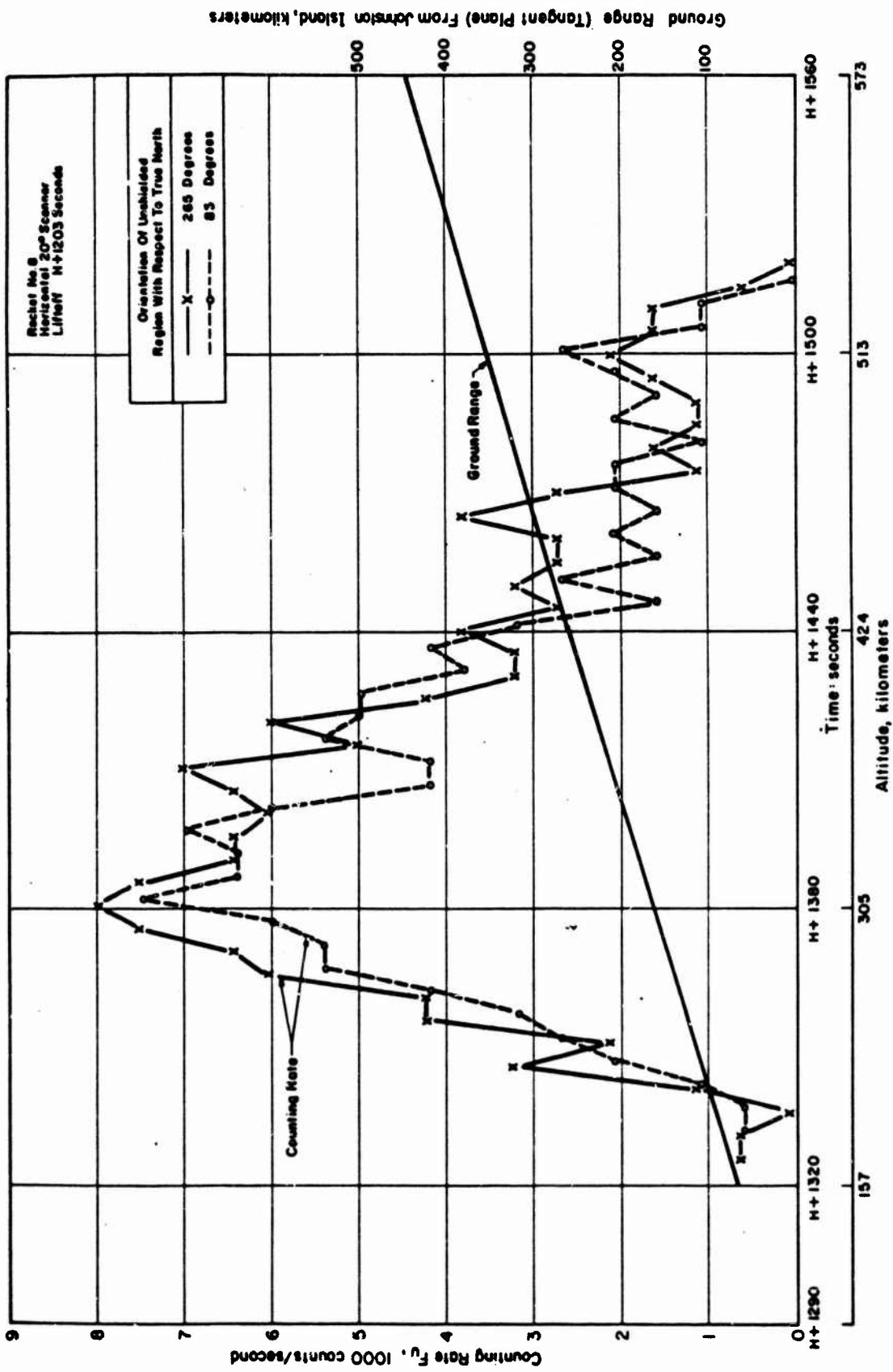


Figure 3.2 Horizontal 20° gamma scanner data, Rocket 8, 265° and 85°, Star Fish.

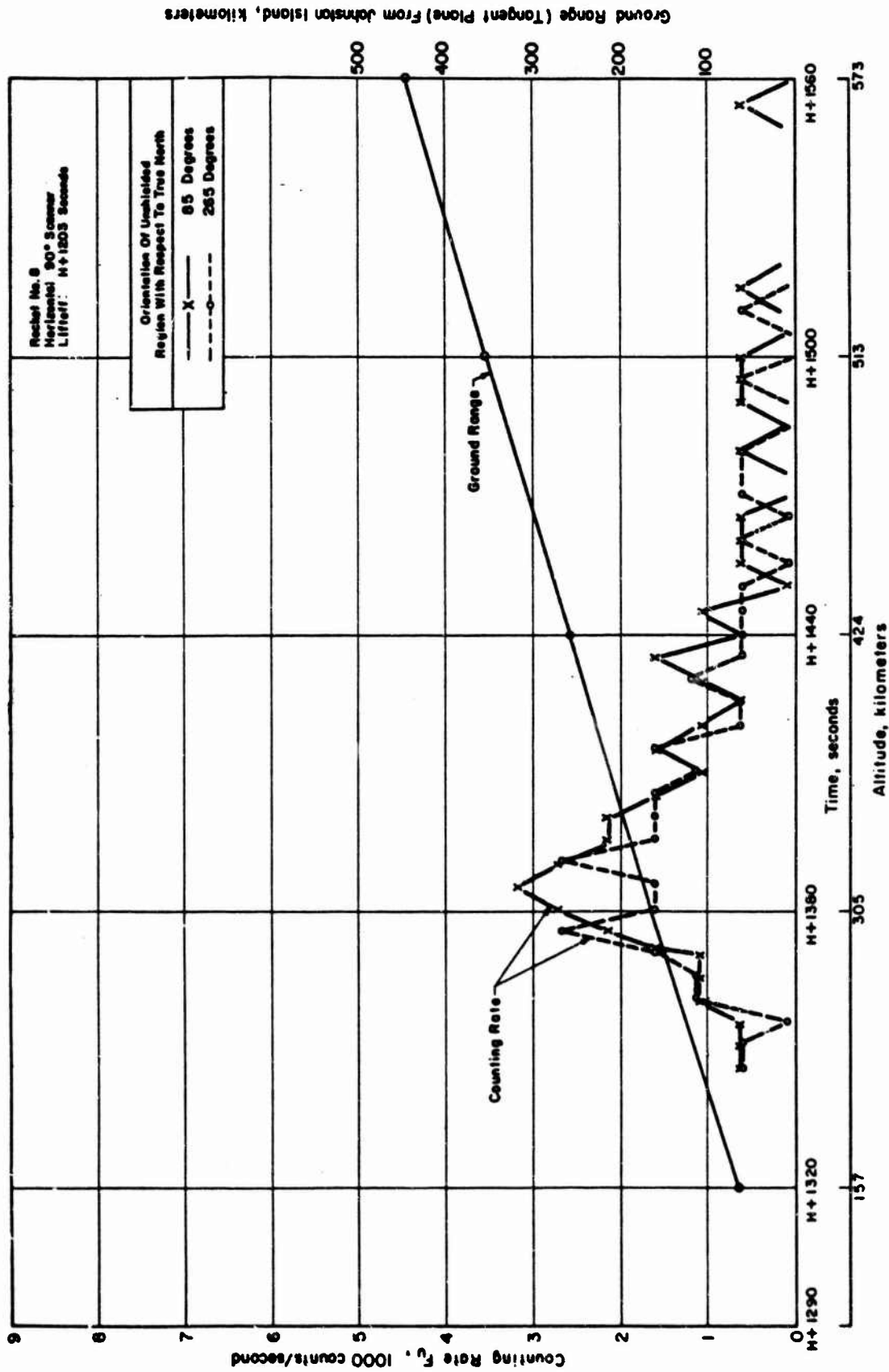


Figure 3.3 Horizontal 90° gamma scanner data, Rocket 8, 85° and 265°, Star Fish.

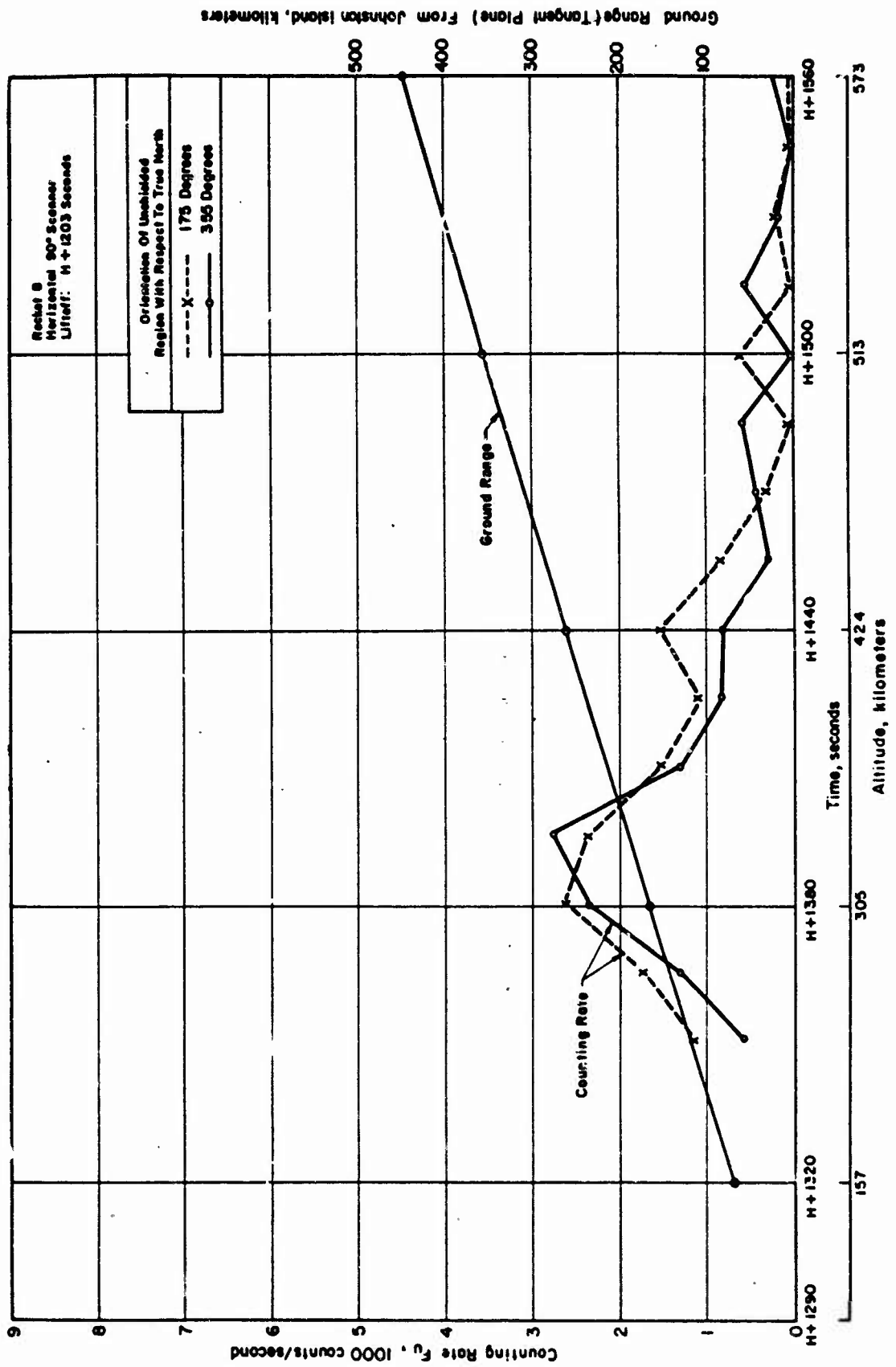


Figure 3.4 Horizontal 90° gamma scanner data, Rocket 8, 175° and 355°, Star Fish.

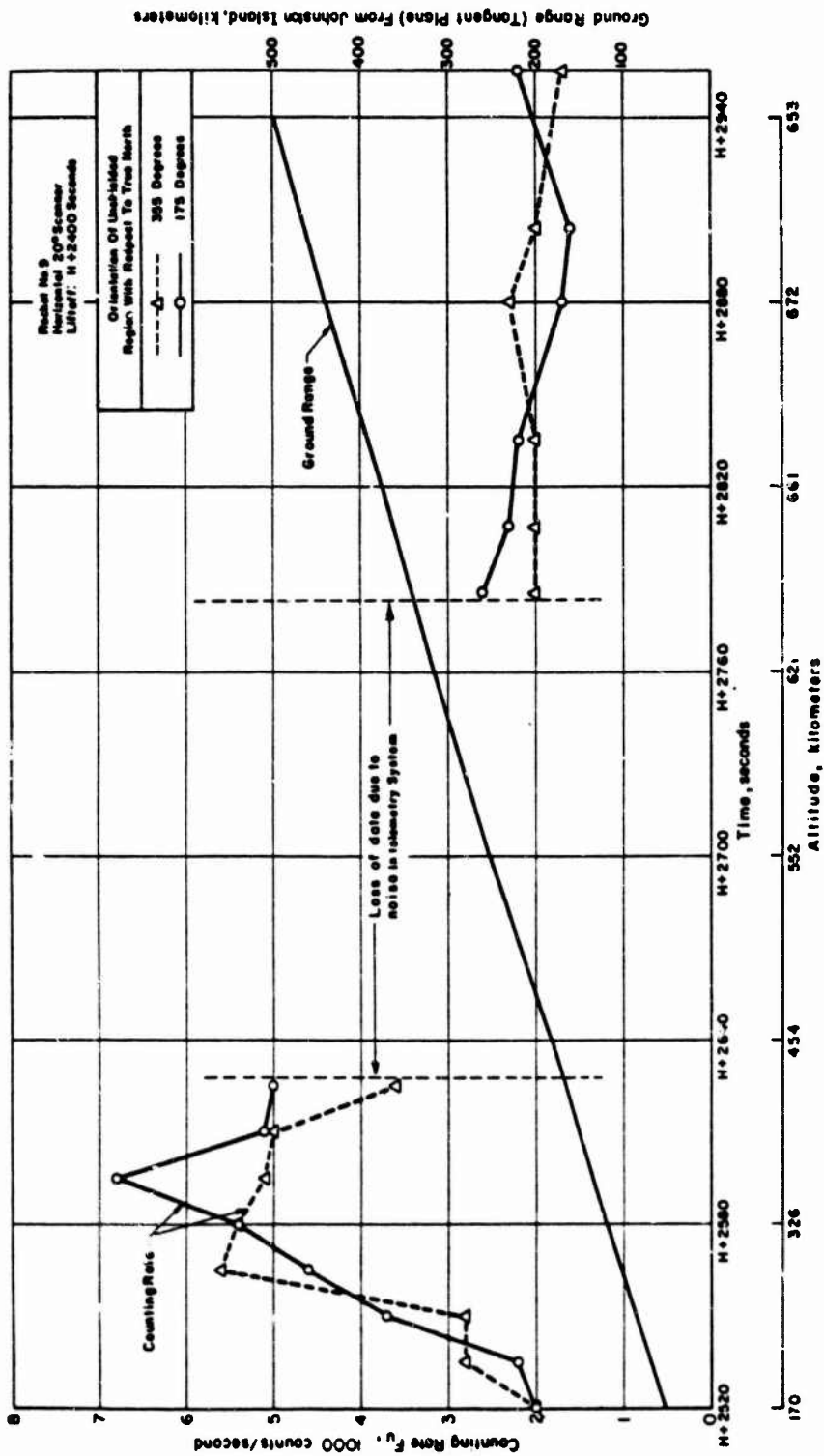


Figure 3.5. Horizon at 20° gamma scanner data, Rocket 9, 355° and 175°, Star Fish.

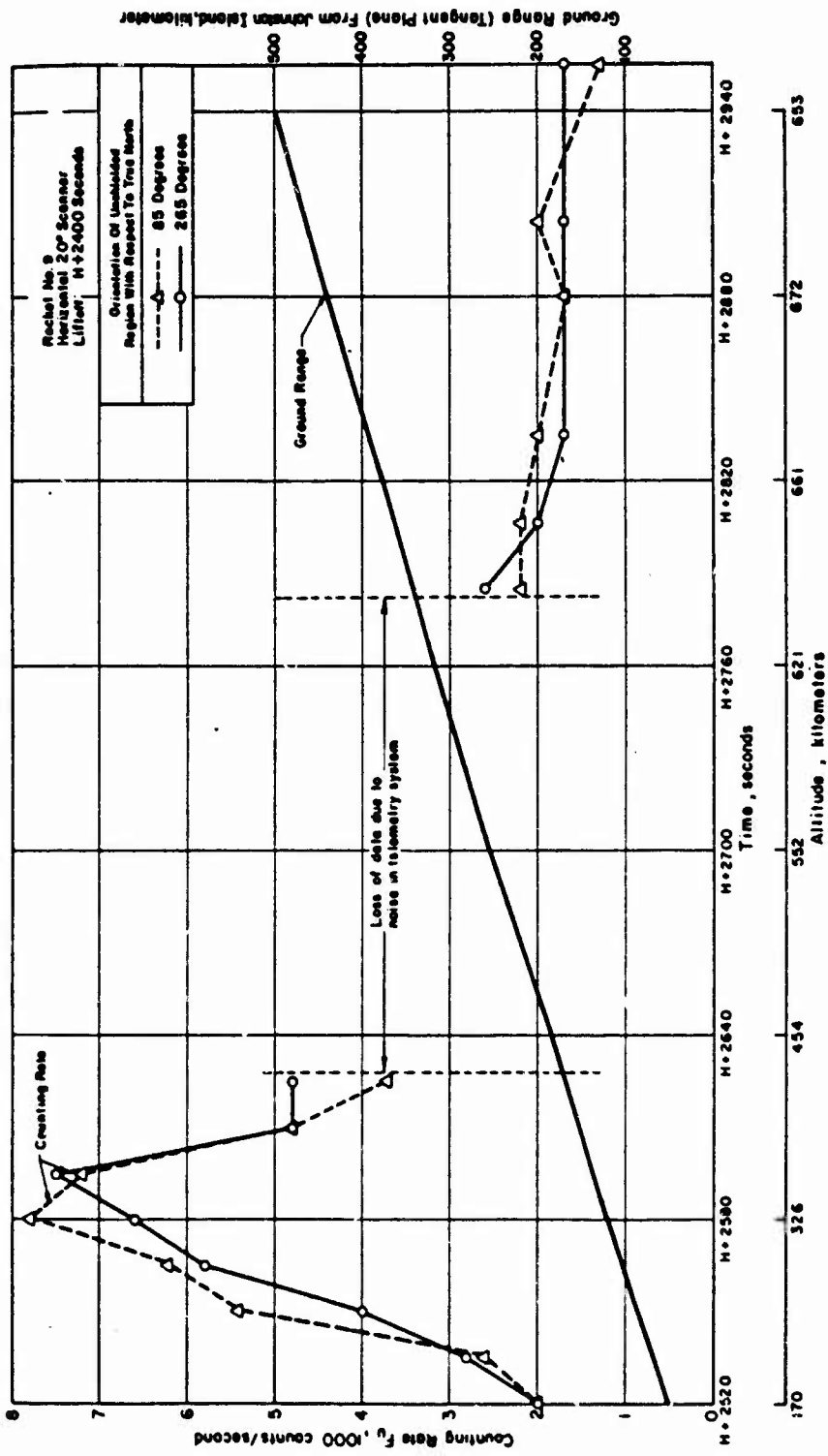


Figure 3.6 Horizontal 20° gamma scanner data, Rocket 9, 85° and 265°, Star Fish.

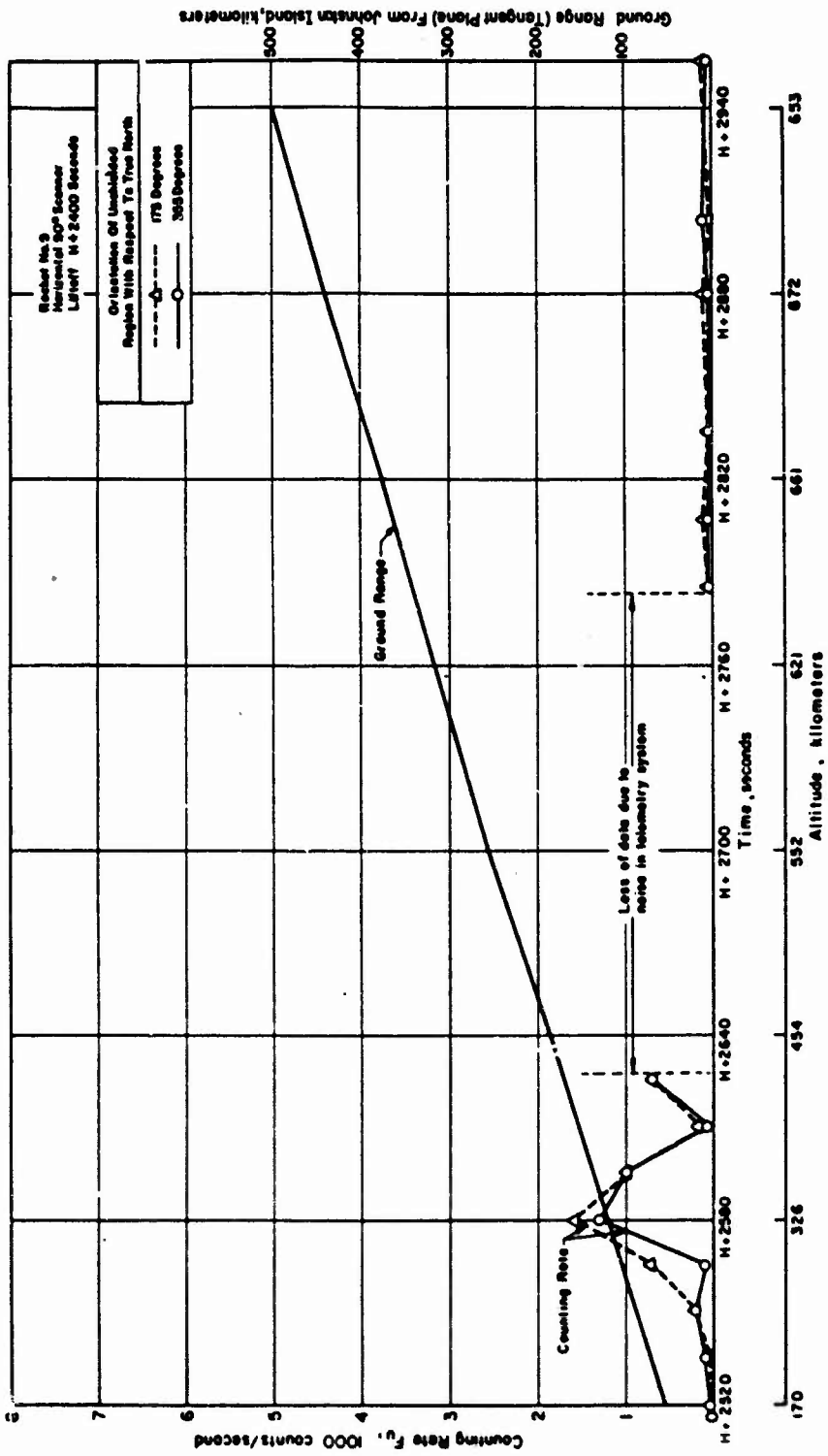


Figure 3.7 Horizontal 90° gamma scanner data, Rocket 9, 175° and 355°, Star Flab.

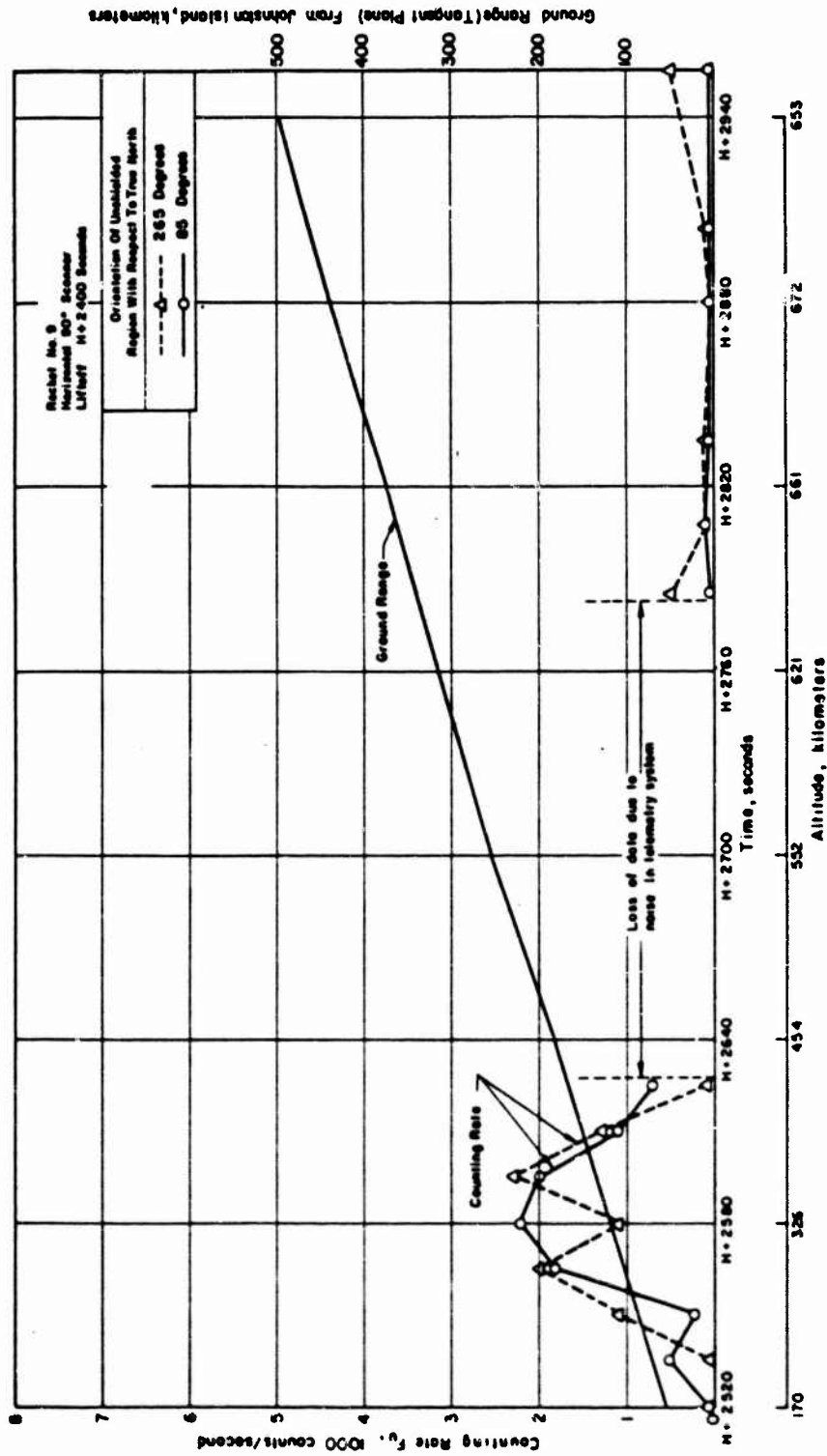


Figure 3.8 Horizontal 90° gamma scanner data, Rocket 9, 265° and 85°, Star Fish.

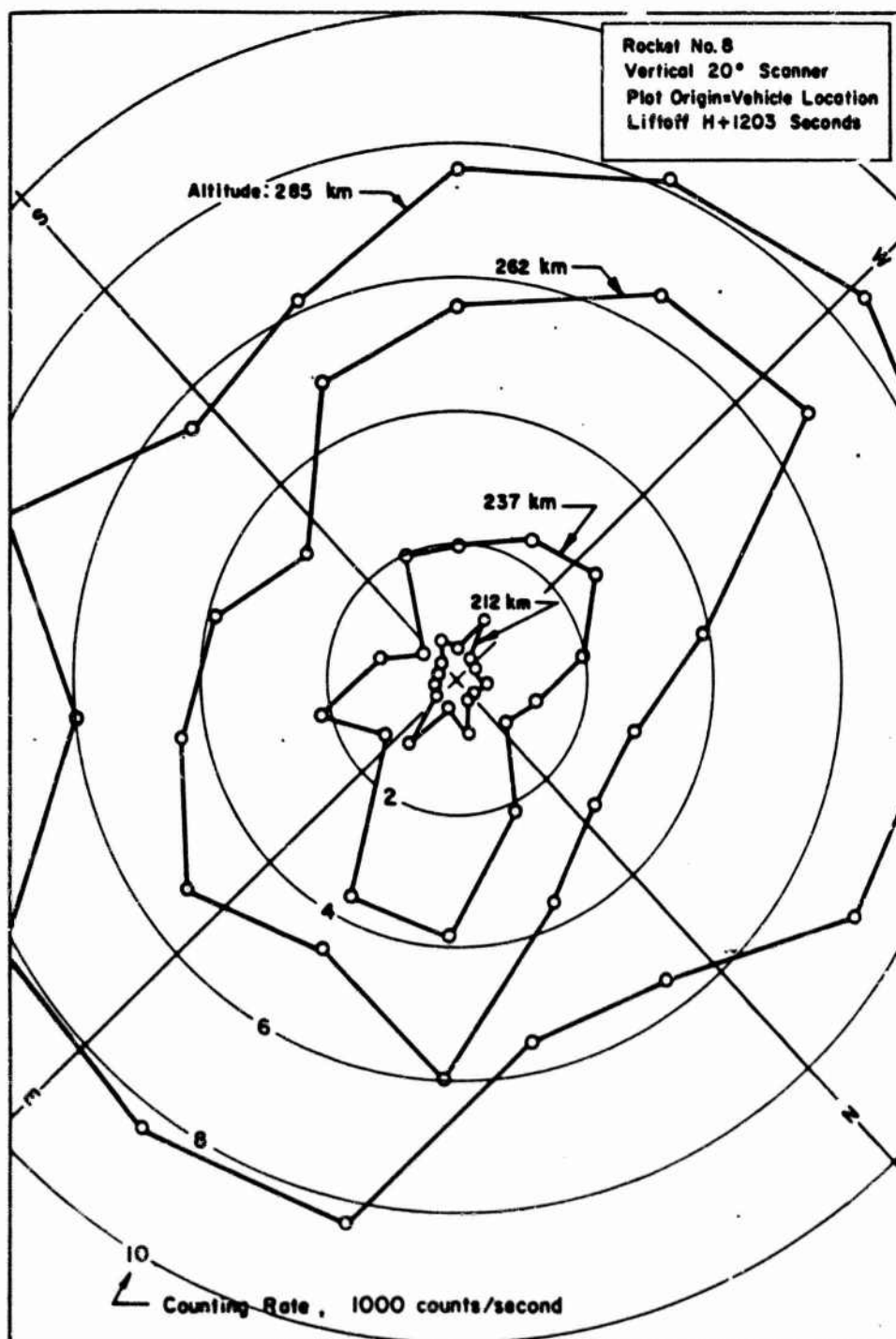


Figure 3.9 Vertical 20° gamma scanner data, Rocket 8, 212, 237, 262 and 285 km, Star Fish.

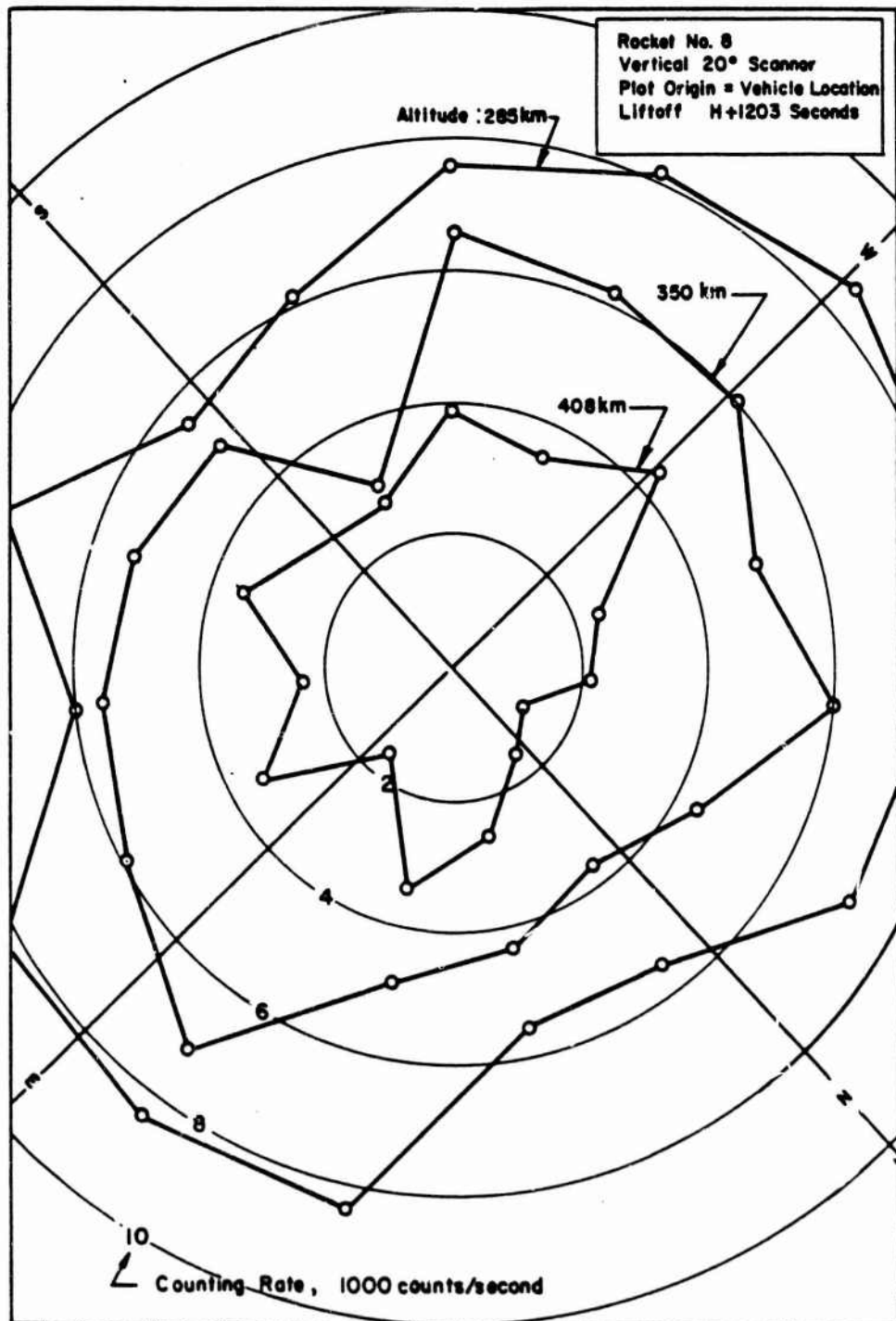


Figure 3.10 Vertical 20° gamma scanner data, Rocket Rocket 8, 285, 350, and 408 km, Star Fish.

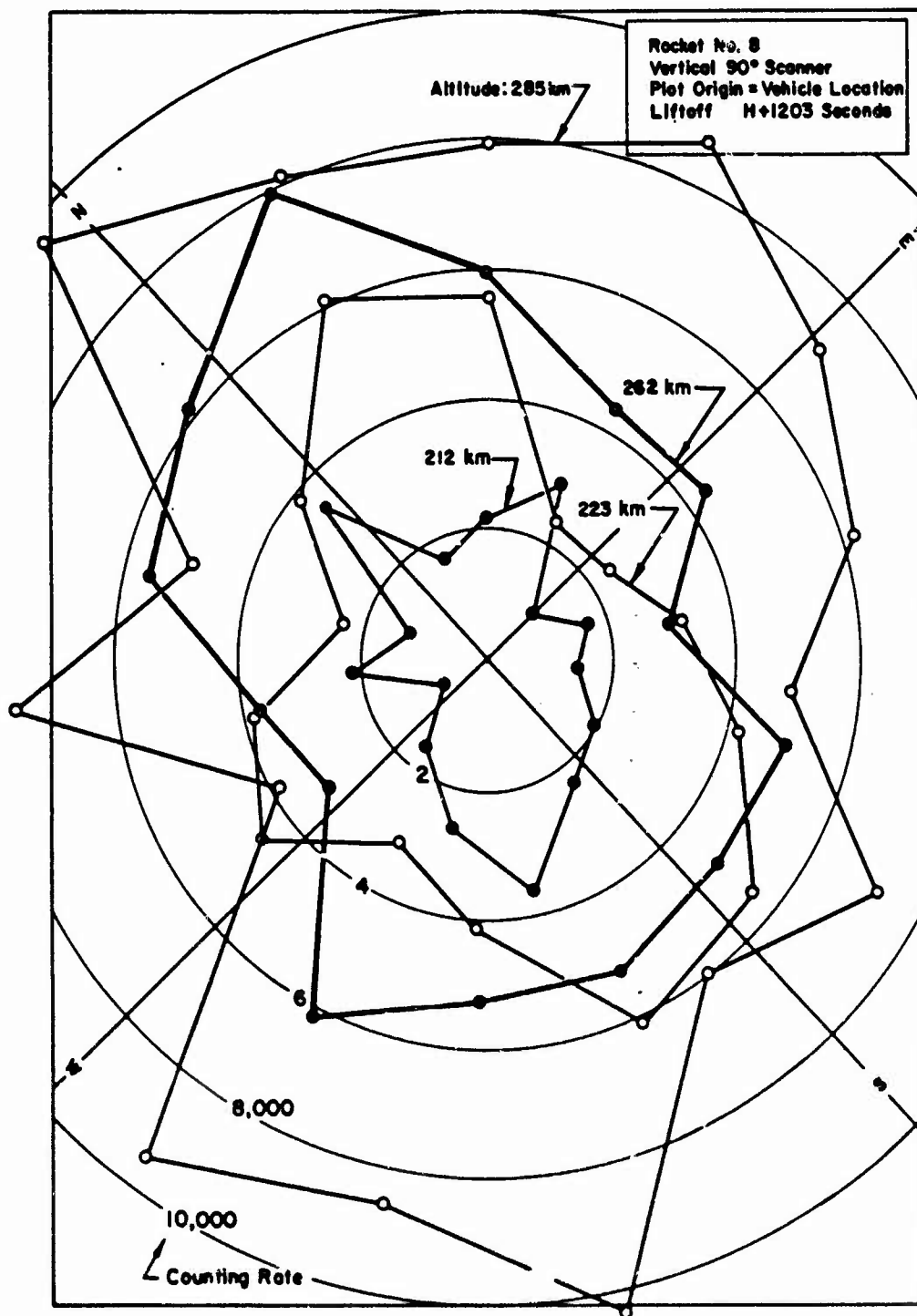


Figure 3.11 Vertical 90° gamma scanner data, Rocket 8, 212, 223, 262, and 285 km, Star Fish.

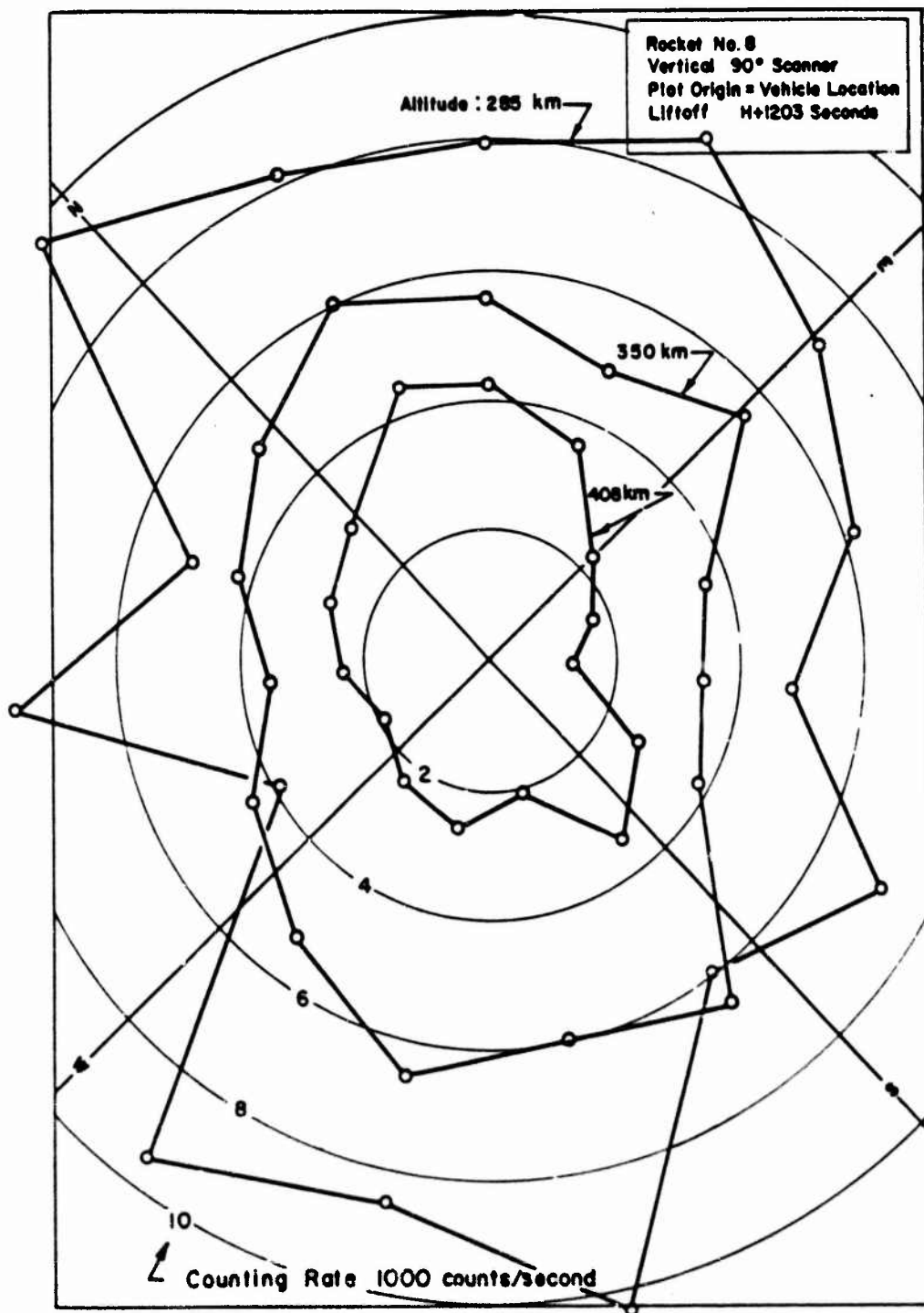


Figure 3.12 Vertical 90° gamma scanner data, Rocket 8, 285, 350, and 408 km, Star Fish.

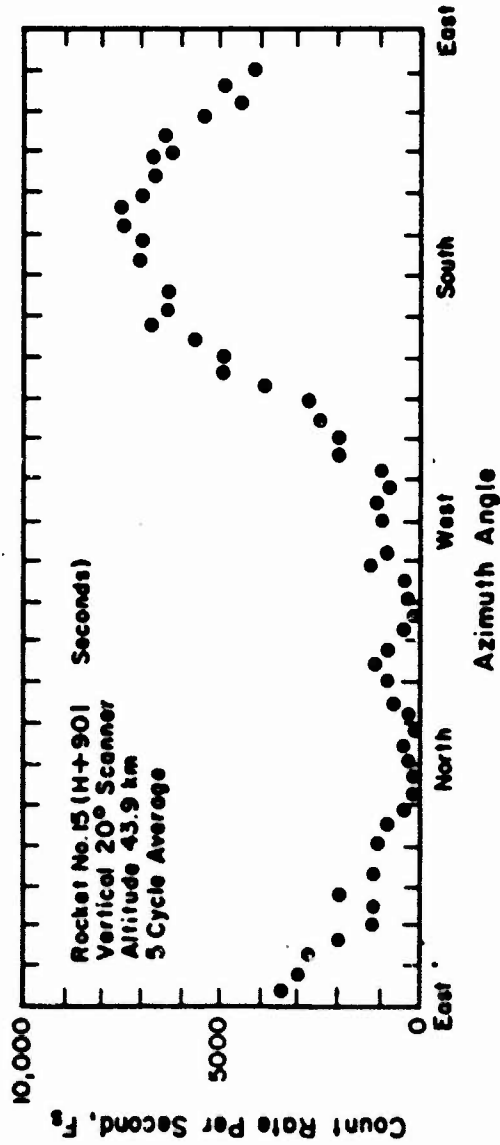
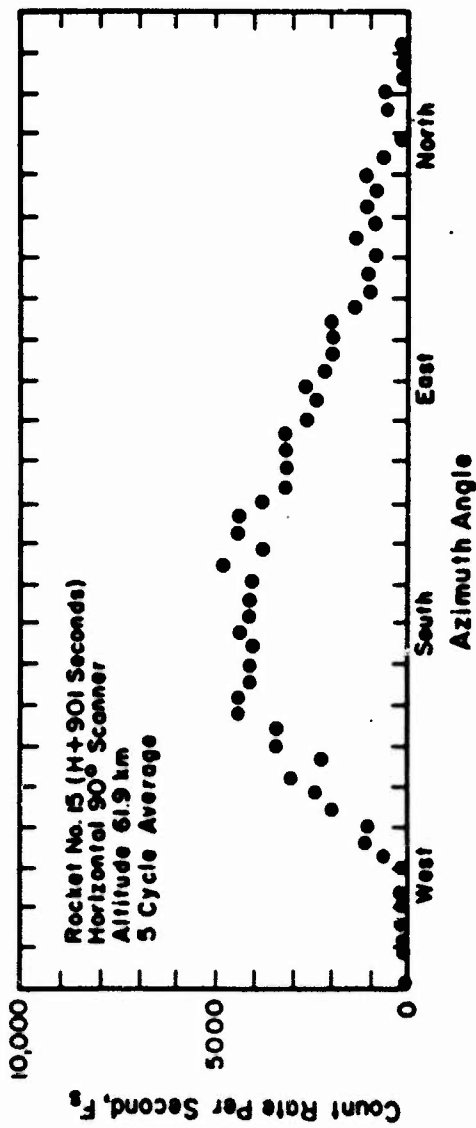


Figure 3.13 Gamma scanner count rate versus azimuth angle, Rocket 15, Blue Gill.

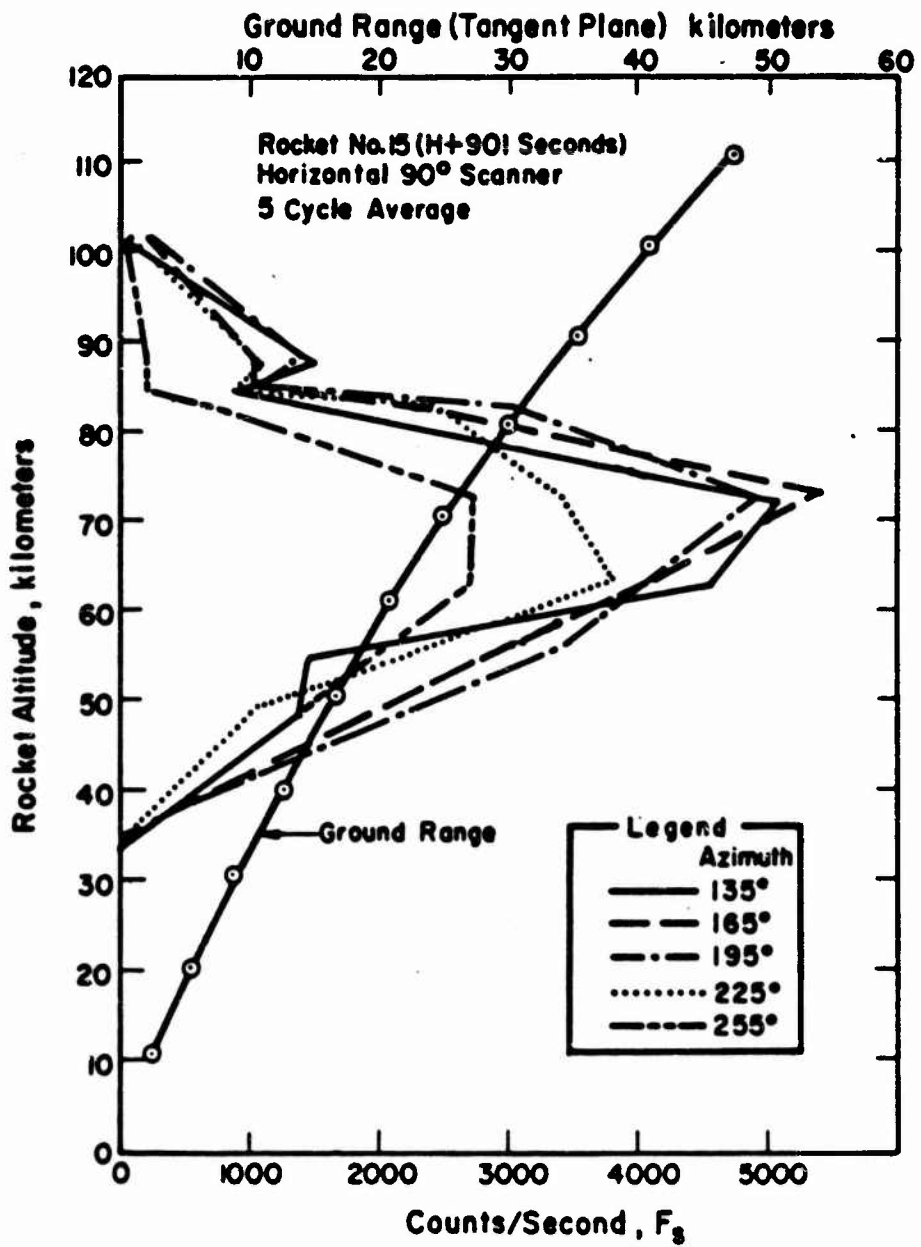
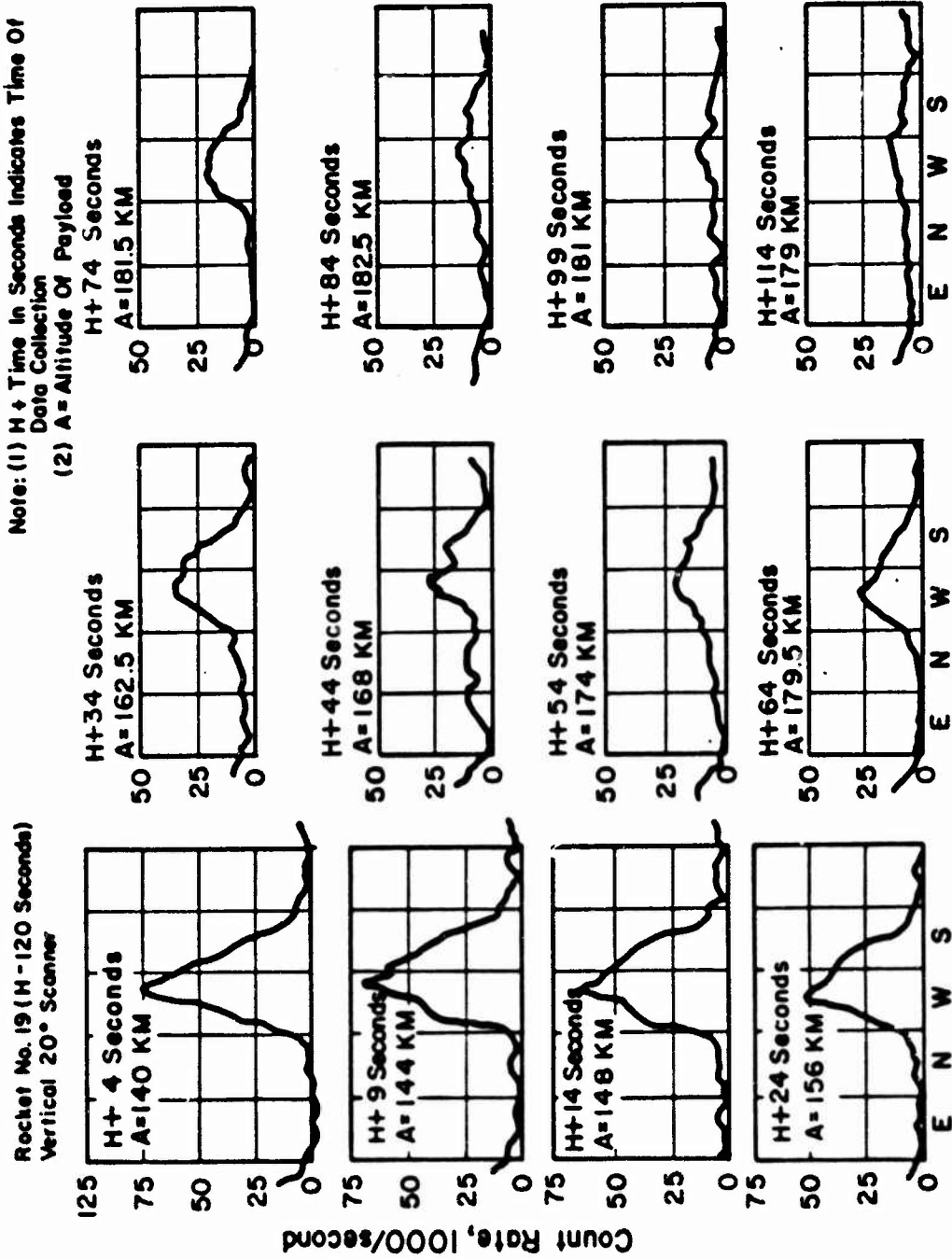


Figure 3.14 Rocket altitude versus ground range and count rate, Rocket 15, Blue Gill.



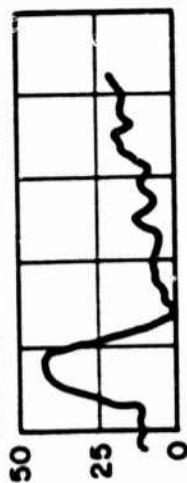
Note: See Figure B.5 for correct altitude and ground range.

Figure 3.15 Vertical 20° gamma scanner data, Rocket 19, King Fish.

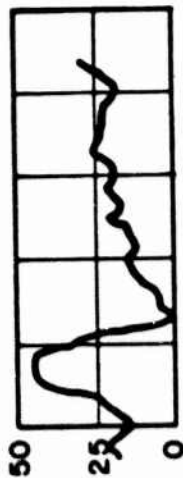
Note: (1) H+ Time in Seconds indicates Time Of Data Collection
 (2) A = Altitude Of Payload

Rocket No. 19 (H-120 Seconds)
 Vertical 90° Scanner

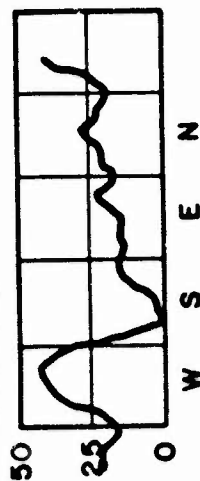
H+ 4 Seconds
 A=140 KM



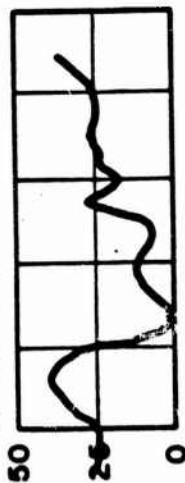
H+ 9 Seconds
 A=144 KM



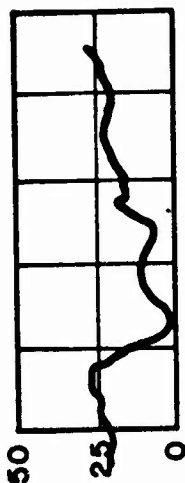
H+ 14 Seconds
 A=148 KM



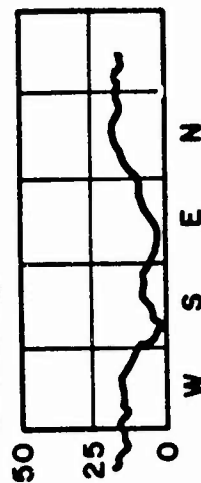
H+ 24 Seconds
 A=156 KM



H+ 34 Seconds
 A=162.5 KM



H+ 44 Seconds
 A=168 KM



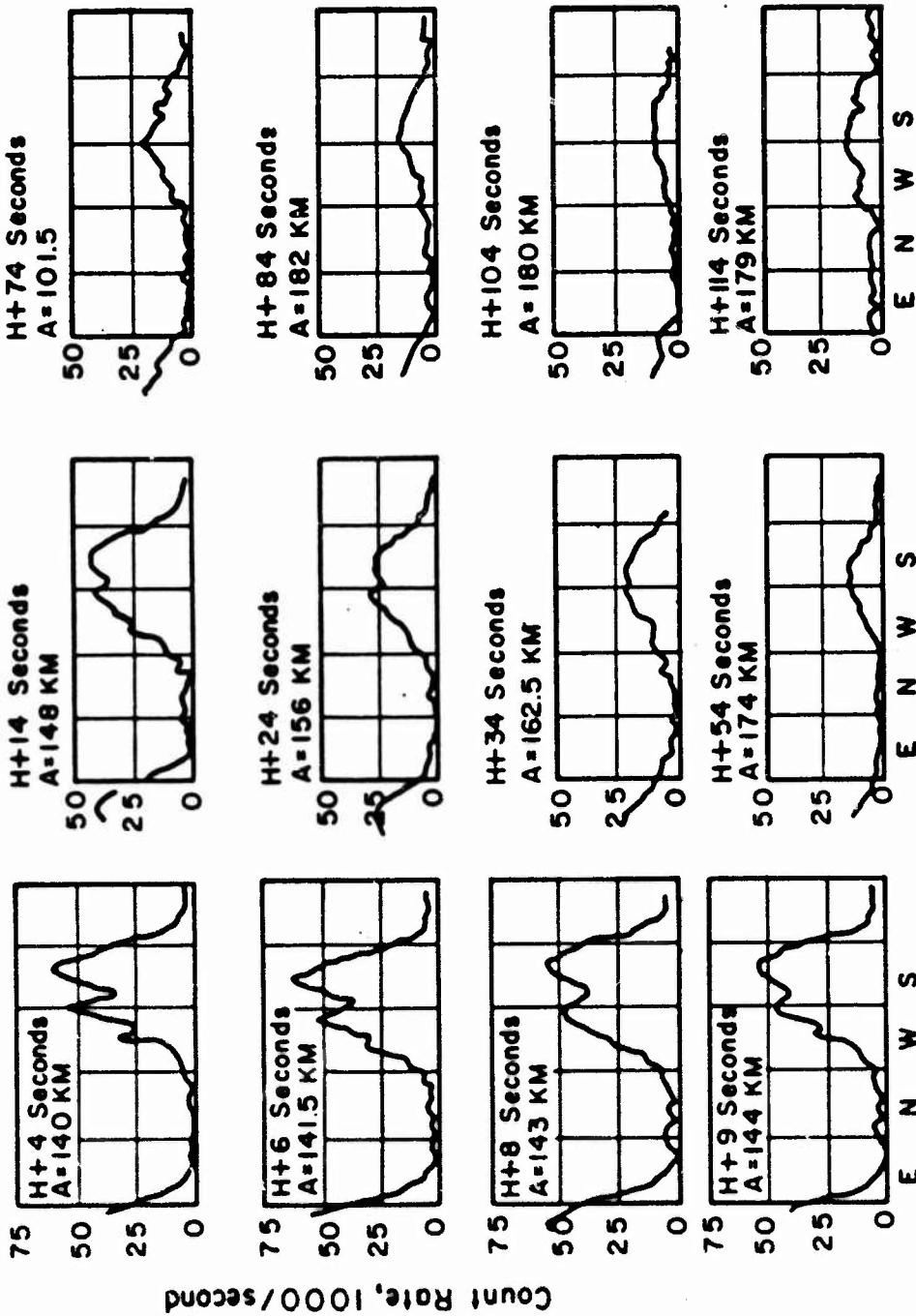
Count Rate, 1000/second

Note: See Figure B.5 for correct altitude and ground range.

Figure 3.16 Vertical 90° gamma scanner data, Rocket 19, King Fish.

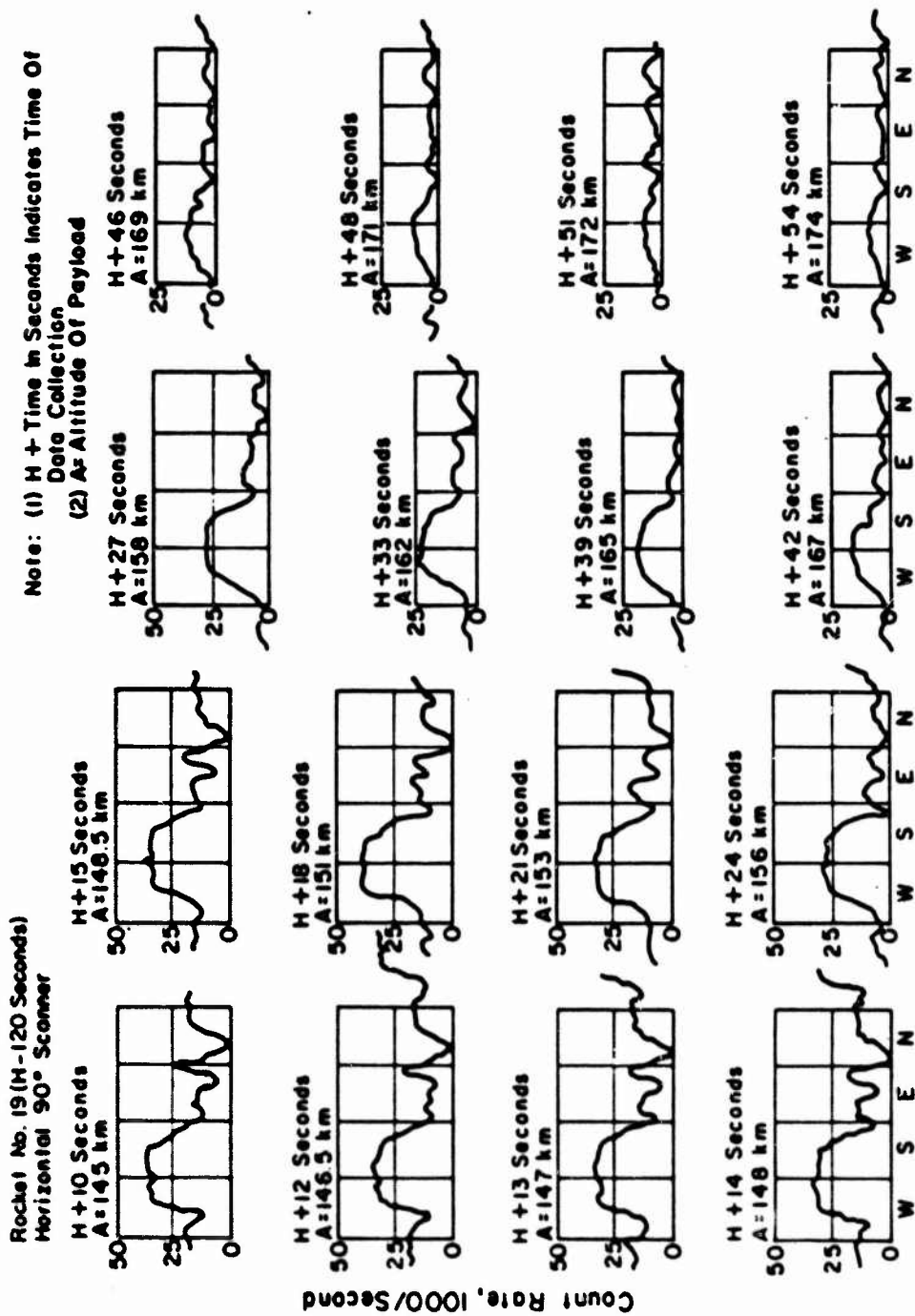
Rocket No. 19 (H-120 Seconds)
Horizontal 20° Scanner

Note: (1) H+Time in Seconds Indicates Time Of
Data Collection
(2) A = Altitude Of Payload



Note: See Figure B.5 for correct altitude and ground range.

Figure 3.17 Horizontal 20° gamma scanner data, Rocket 19, King Fish.



Note: See Figure B.5 for correct altitude and ground range.

Figure 3.18 Horizontal 90° gamma scanner data, Rocket 19, King Fish.

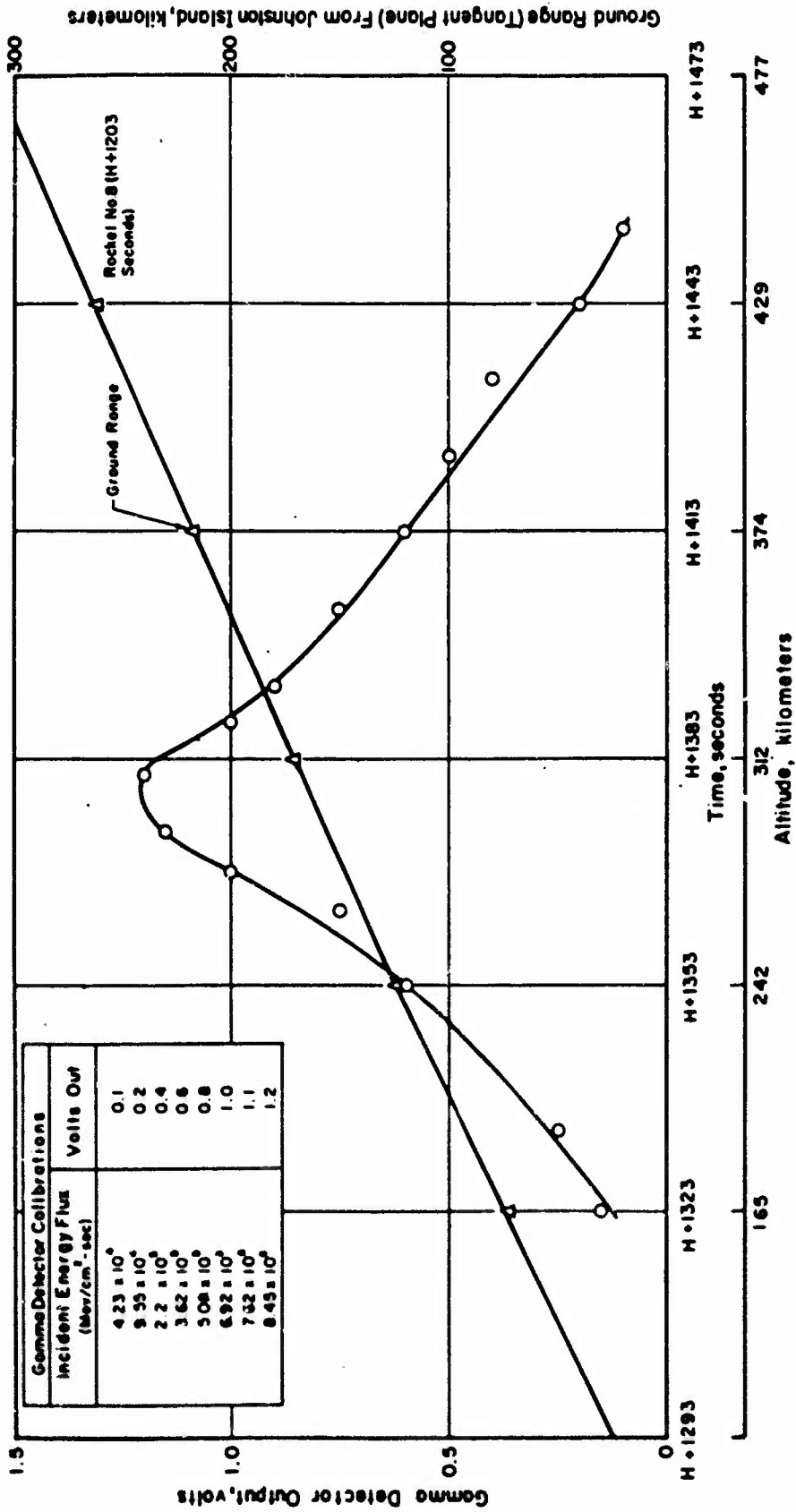
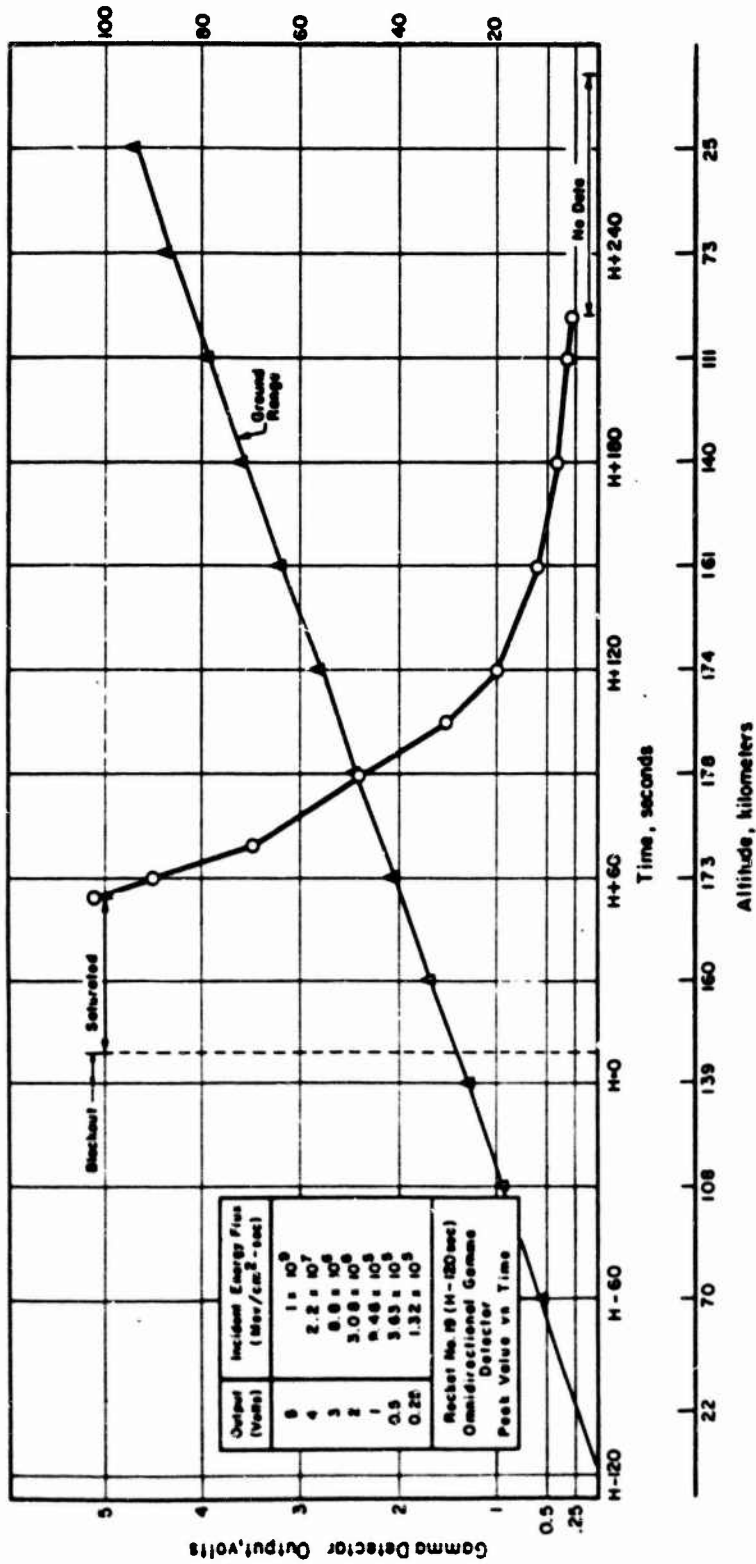


Figure 3.19 Omnidirectional gamma detector data, Rocket 8, Star Fish.

Ground Range (Tangent Plane) From Johnston Island, kilometers



Note: See Figure B.5 for correct altitude and ground range.

Figure 3.21 Omnidirectional gamma detector data, Rocket 19, King Fish.

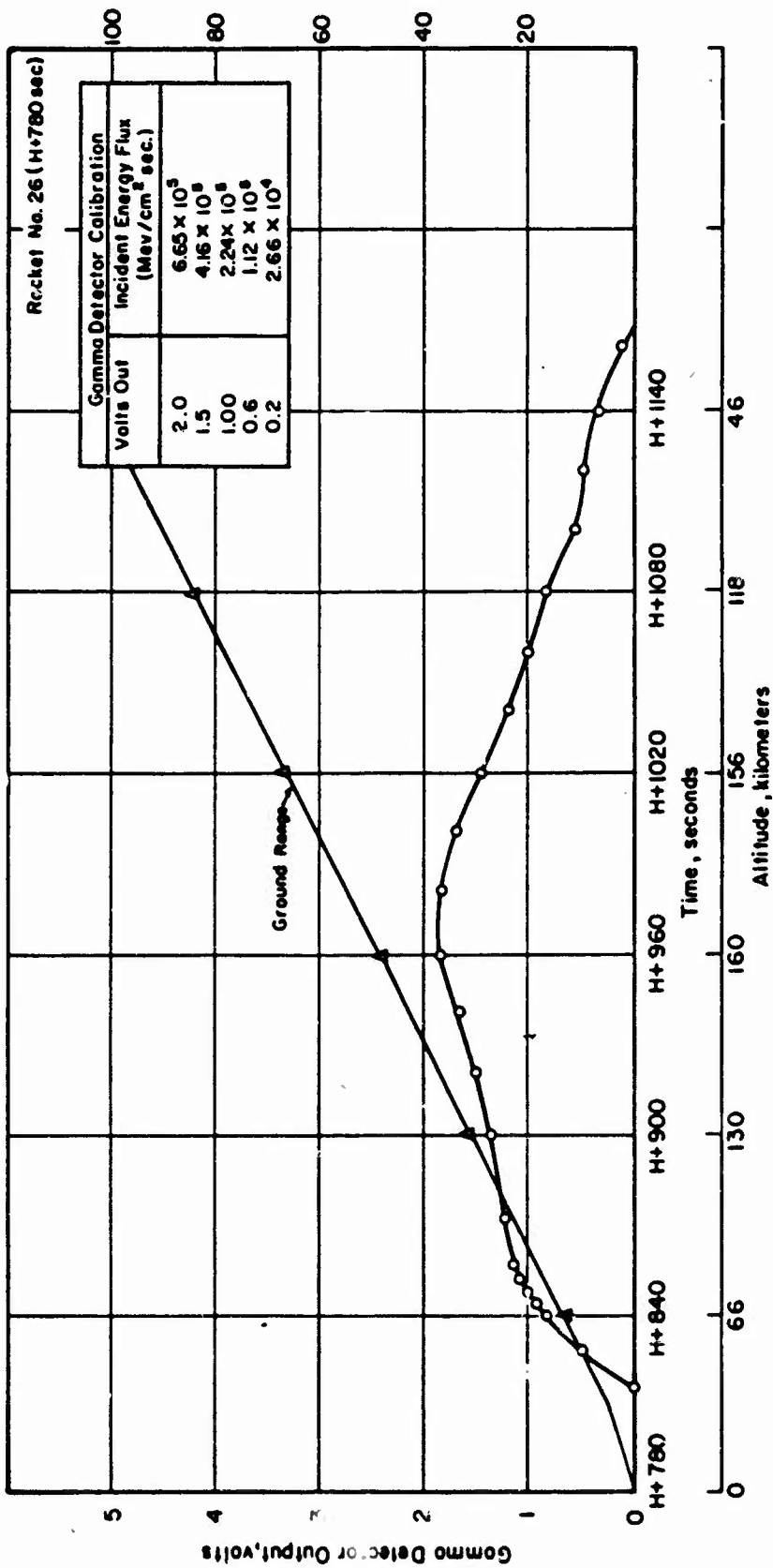


Figure 3.22 Omnidirectional gamma detector data, Rocket 26, King Fish.

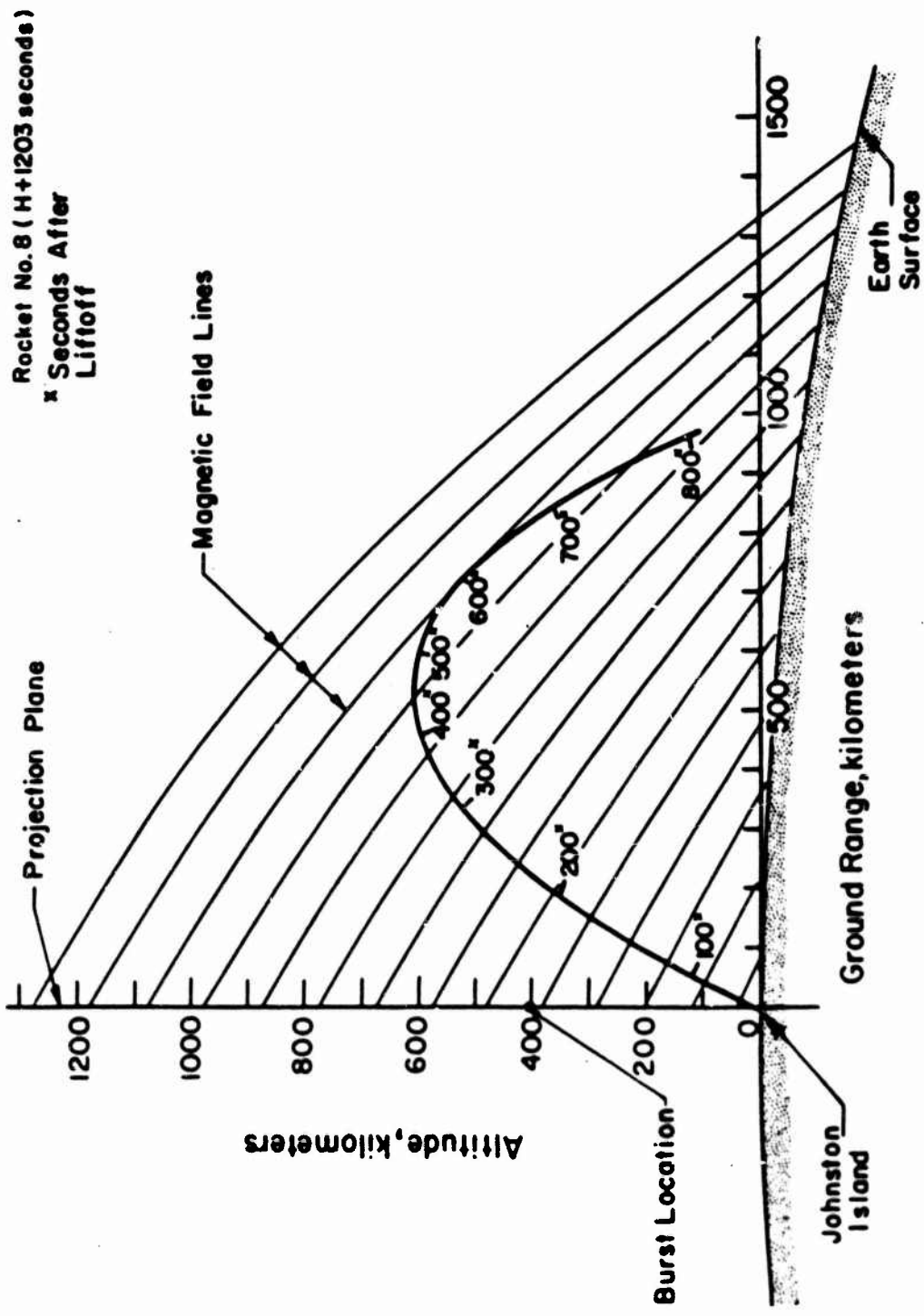


Figure 3.23 Projection of Rocket 8 trajectory onto plane of magnetic field, Star Fish.

Note: Projected Altitude is Measured From a Plane Tangent to Earth Through Johnston Island.

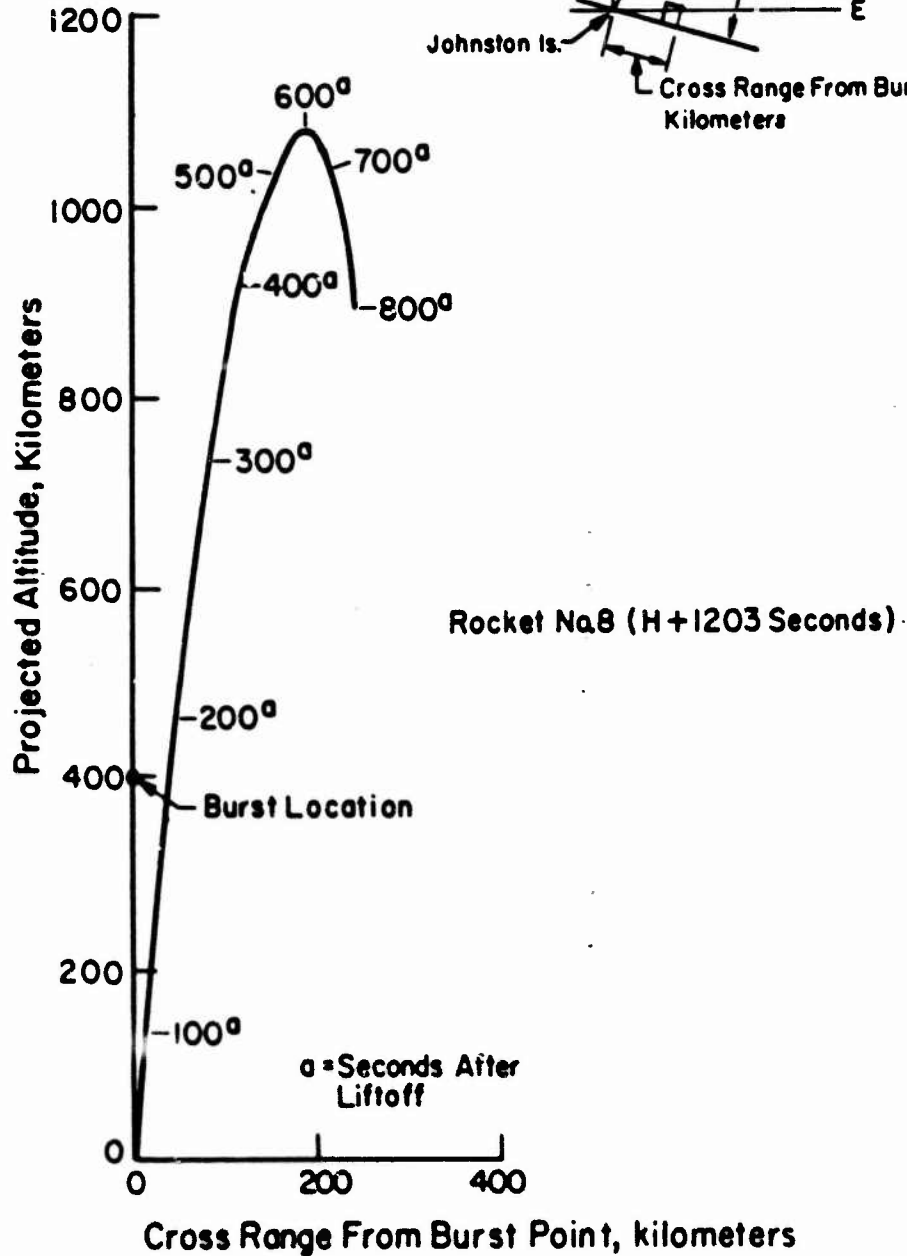
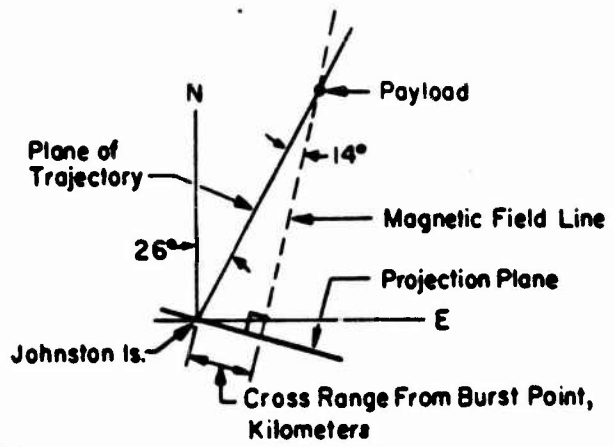


Figure 3.27 Projection of Rocket 8 trajectory onto a plane through the burst point and perpendicular to the magnetic field lines of the earth, Star Fish.

Note: Projected Altitude is Measured From a Plane Tangent to Earth Through Johnston Island.

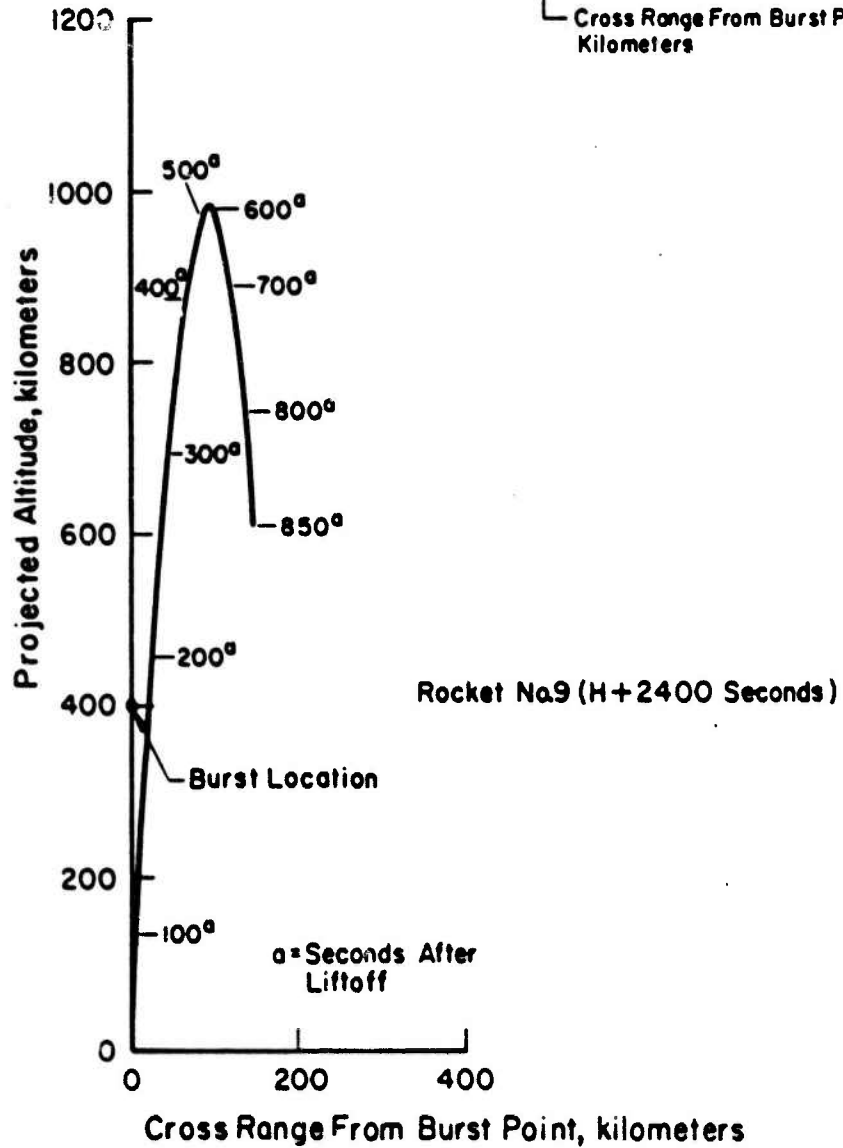
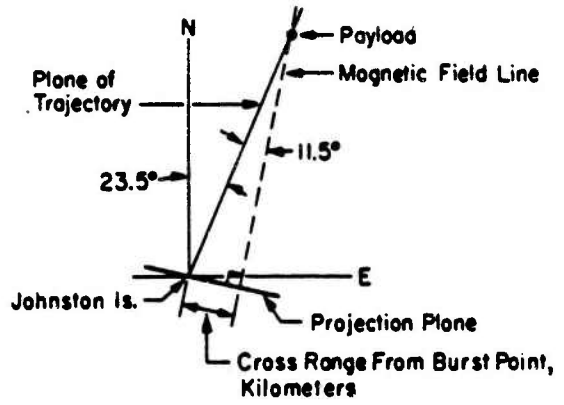


Figure 3.28 Projection of Rocket 9 trajectory onto a plane through the burst point and perpendicular to the magnetic field lines of the earth, Star Fish.

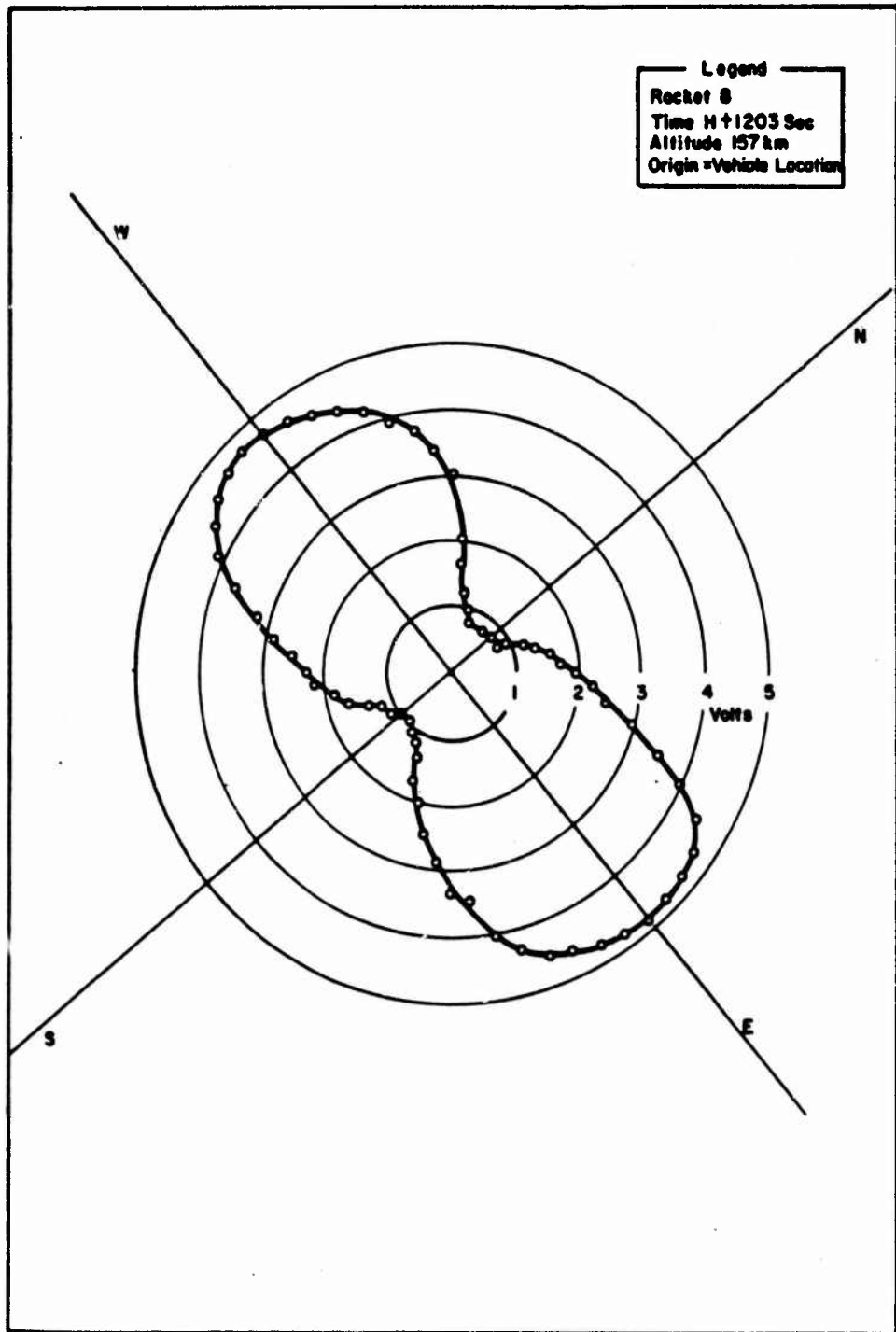


Figure 3.31 Beta detector output voltage versus its field of view, Rocket 8, Star Fish.

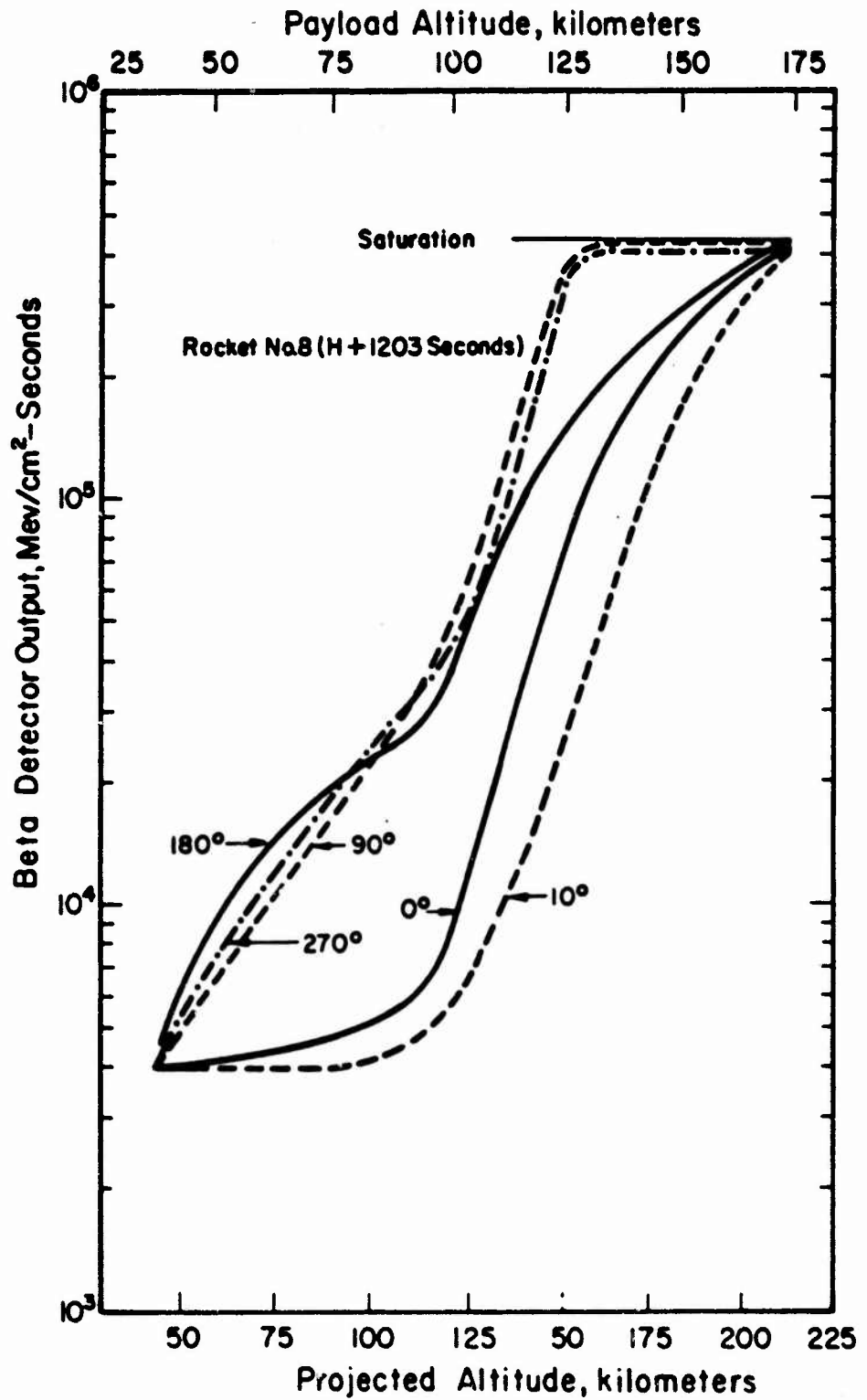


Figure 3.32 Beta detector output versus projected altitude, Rocket 8, Star Fish.

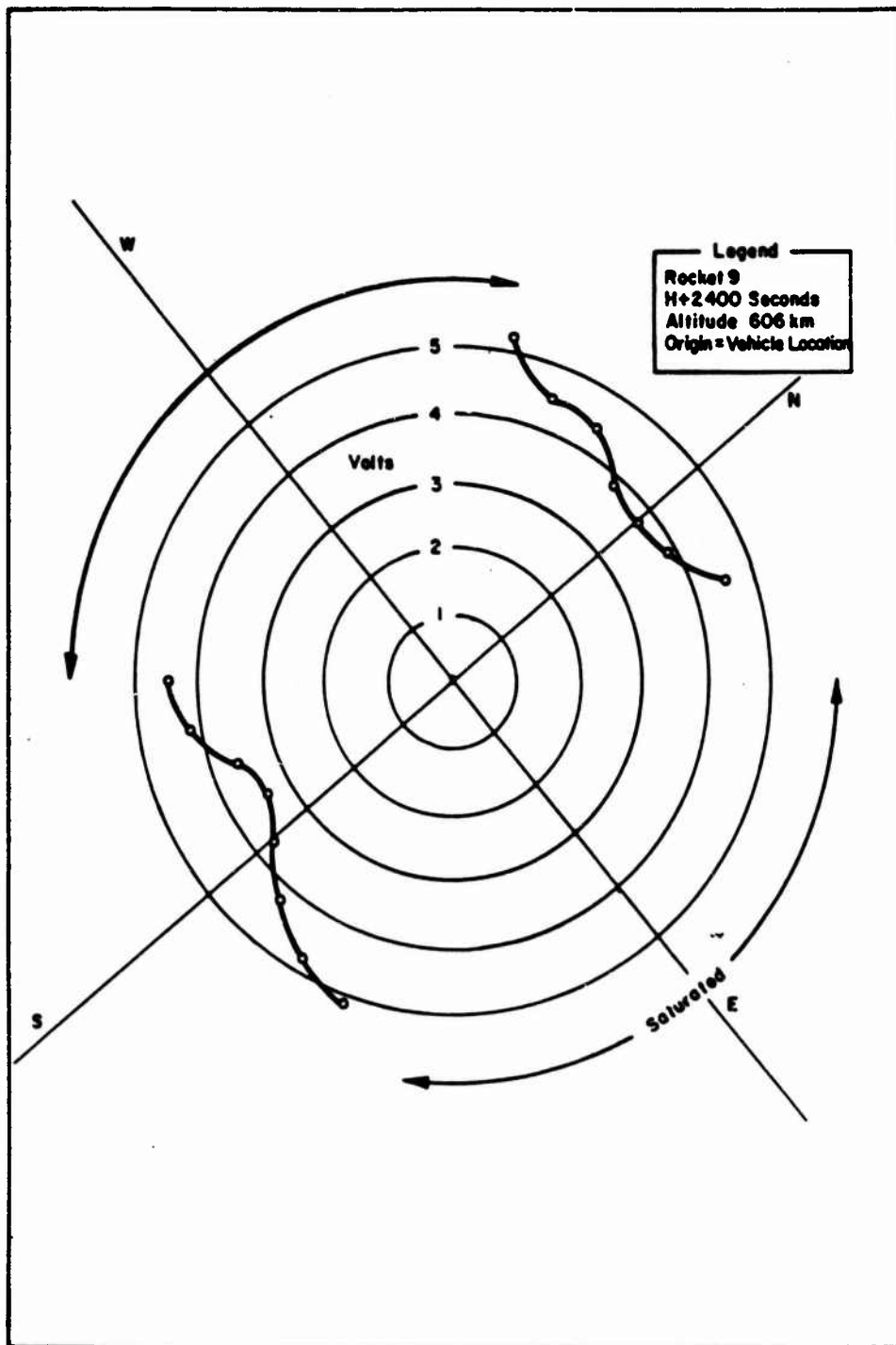


Figure 3.33 Beta detector output voltage versus its field of view, Rocket 9, Star Fish.

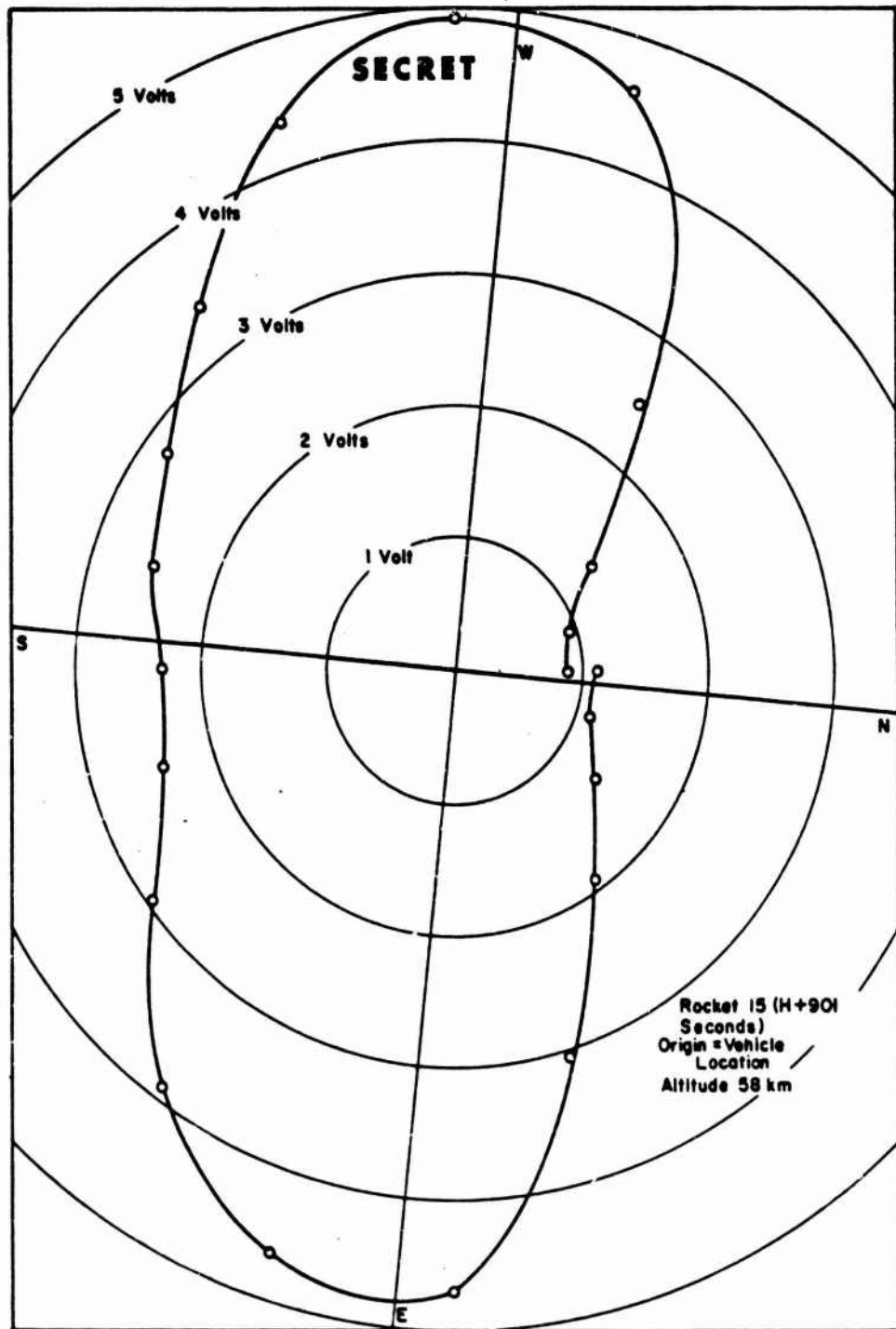


Figure 3.34 Beta detector output voltage versus its field of view, Rocket 15, Blue Gill.

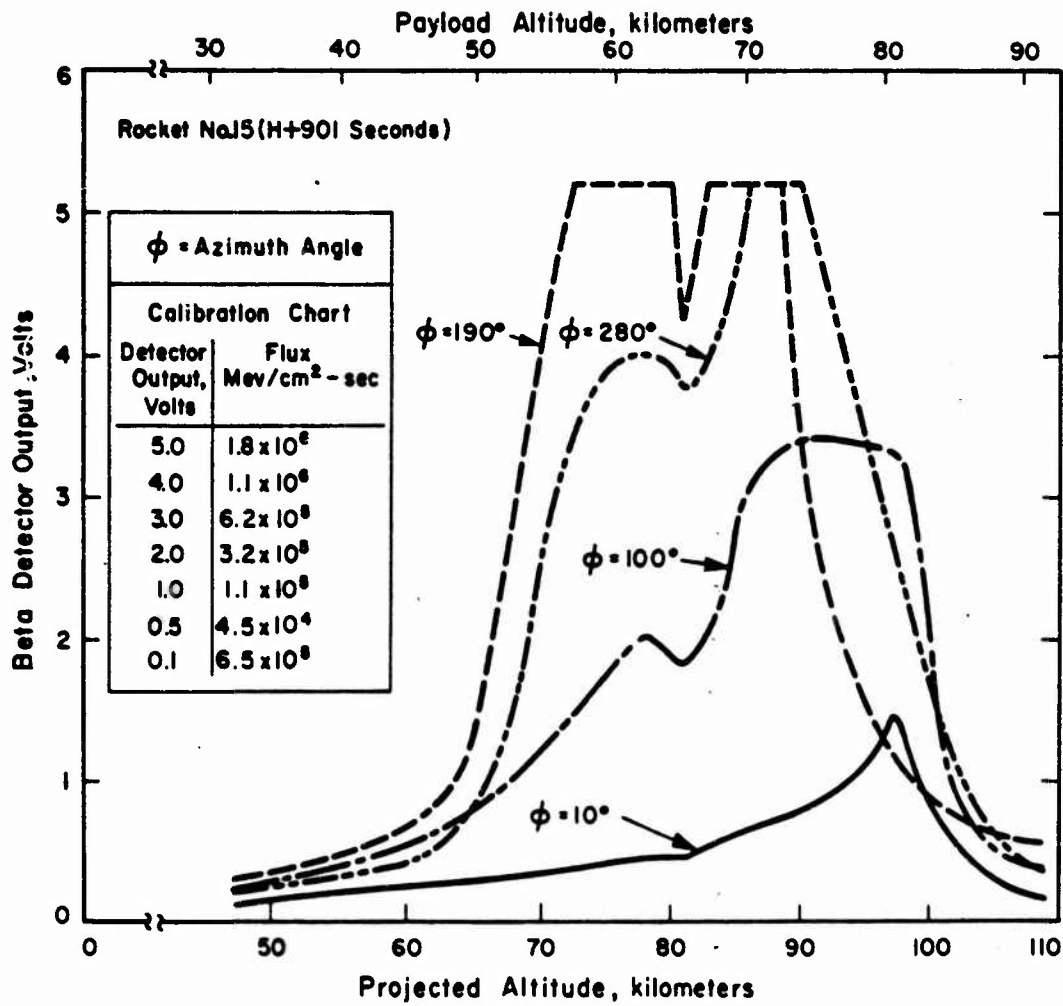
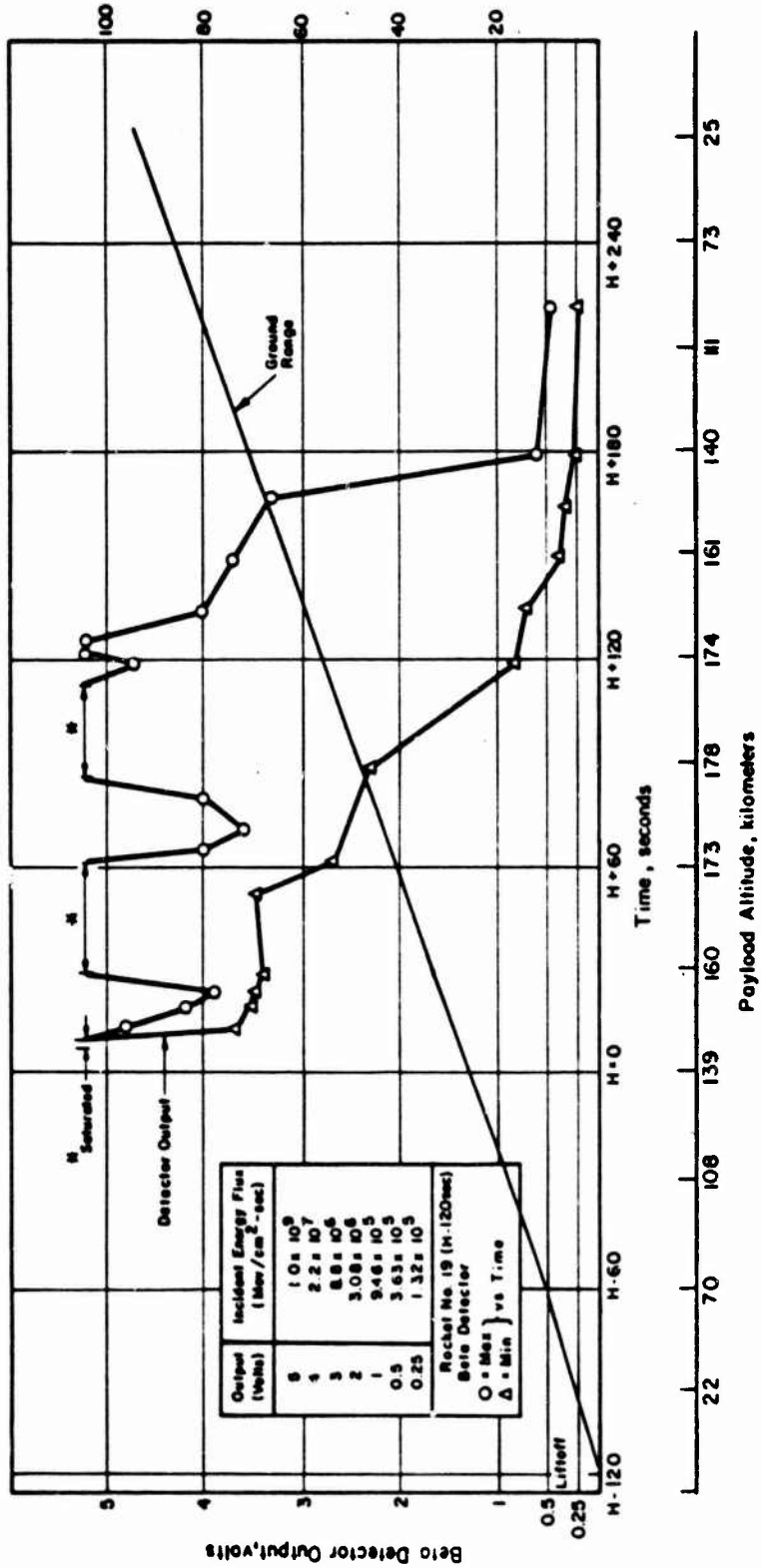


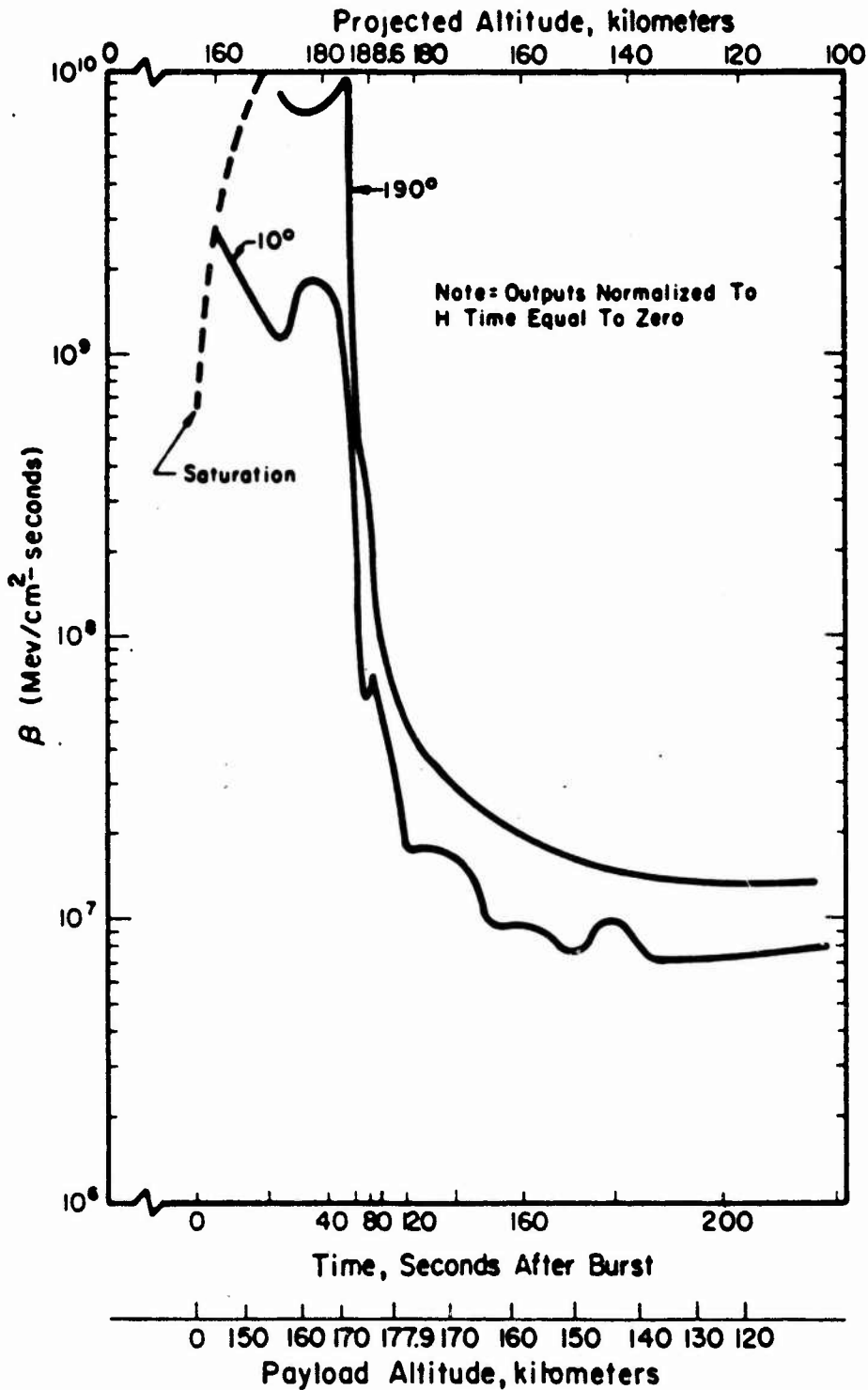
Figure 3.35 Beta detector output versus altitude, Rocket 15, Blue Gill.

Ground Range (Tangent Plane) From Johnston Island, kilometers



Note: See Figure B.5 for correct altitude and ground range.

Figure 3.36 Beta detector data, Rocket 19, King Fish.



Note: See Figure B.5 for correct altitude and ground range.

Figure 3.37 Beta detector output versus projected altitude for Rocket 19, King Fish.

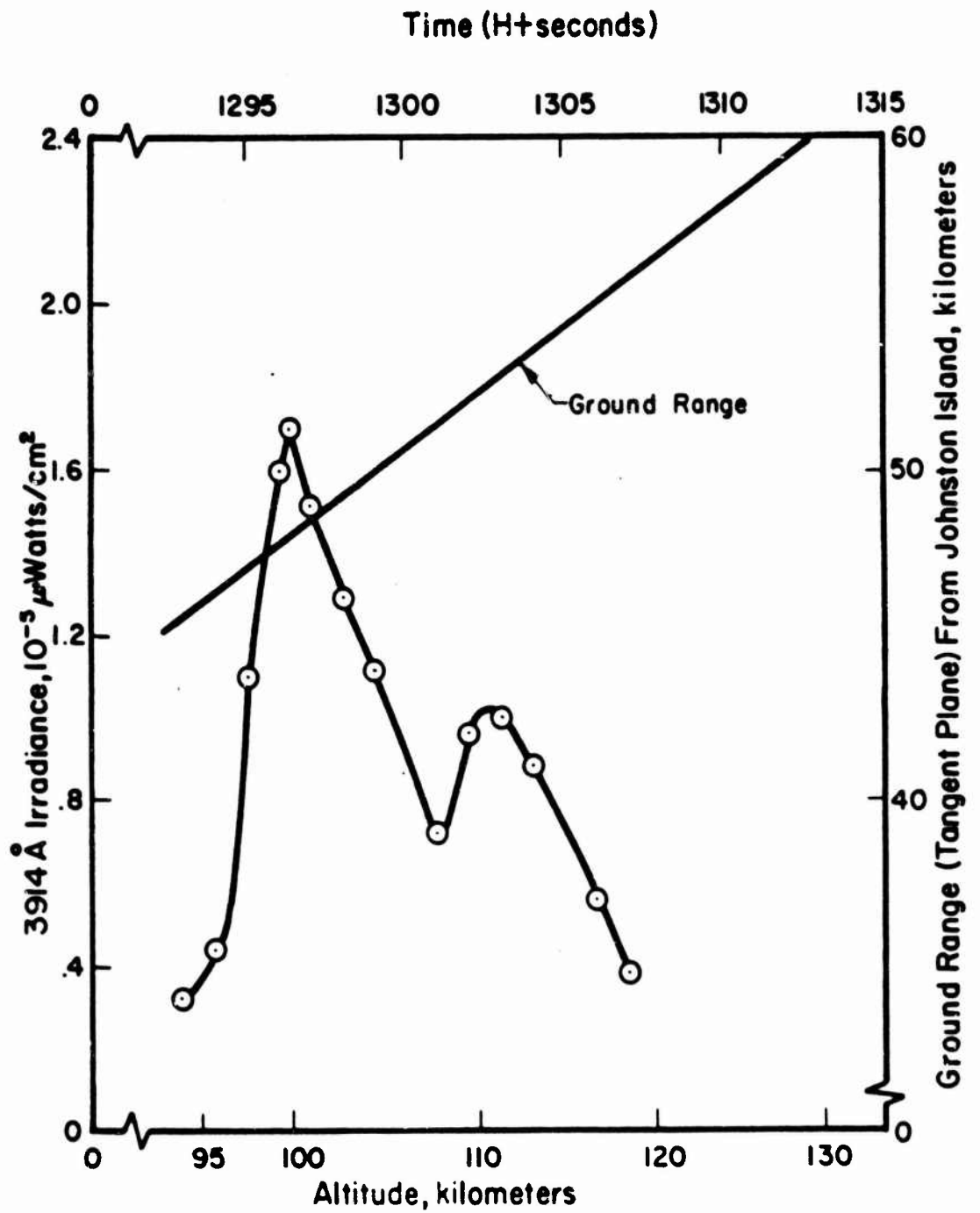


Figure 3.38 Photometer data, Rocket 8, Star Fish.

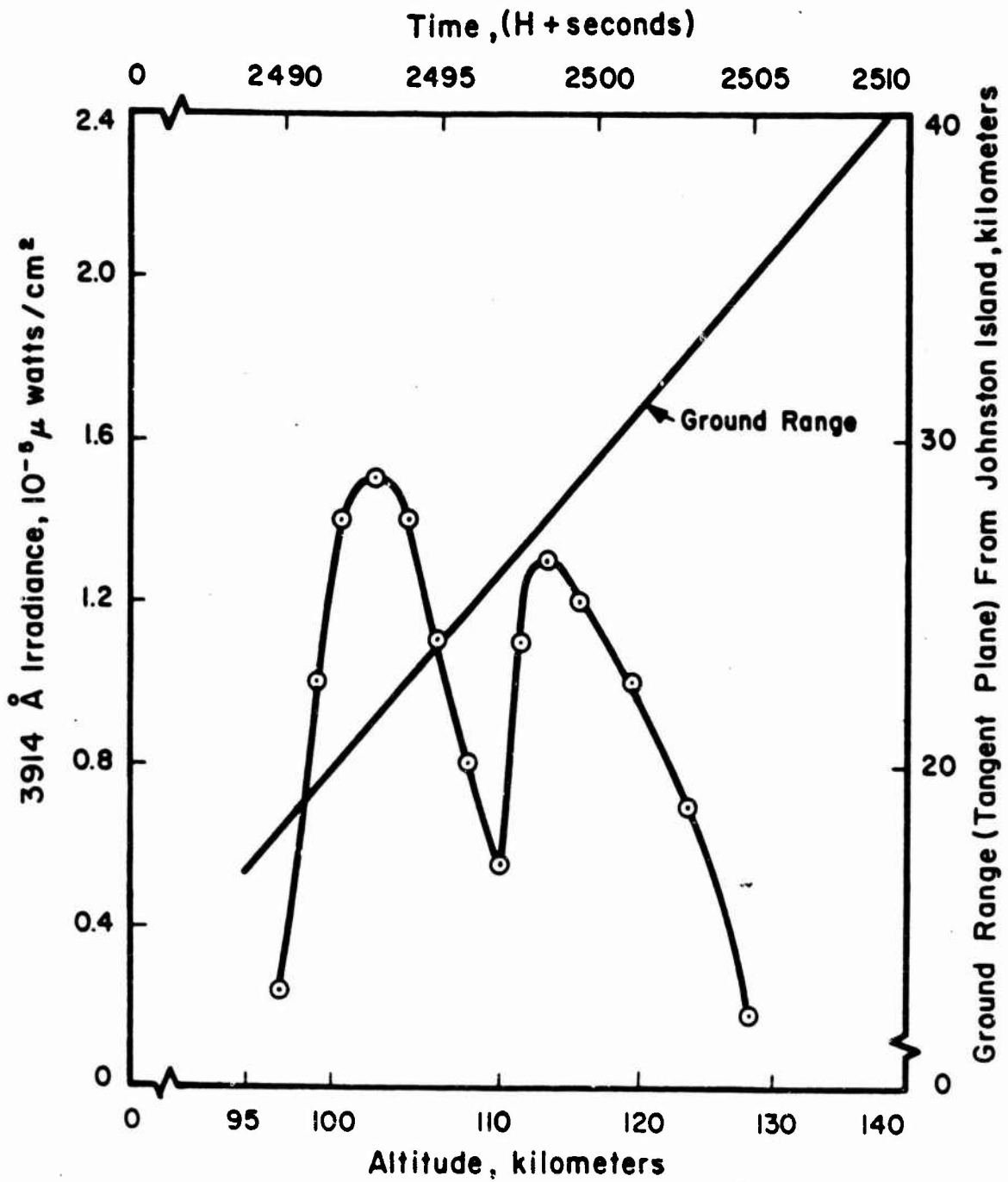


Figure 3.39 Photometer data, Rocket 9, Star Fish.

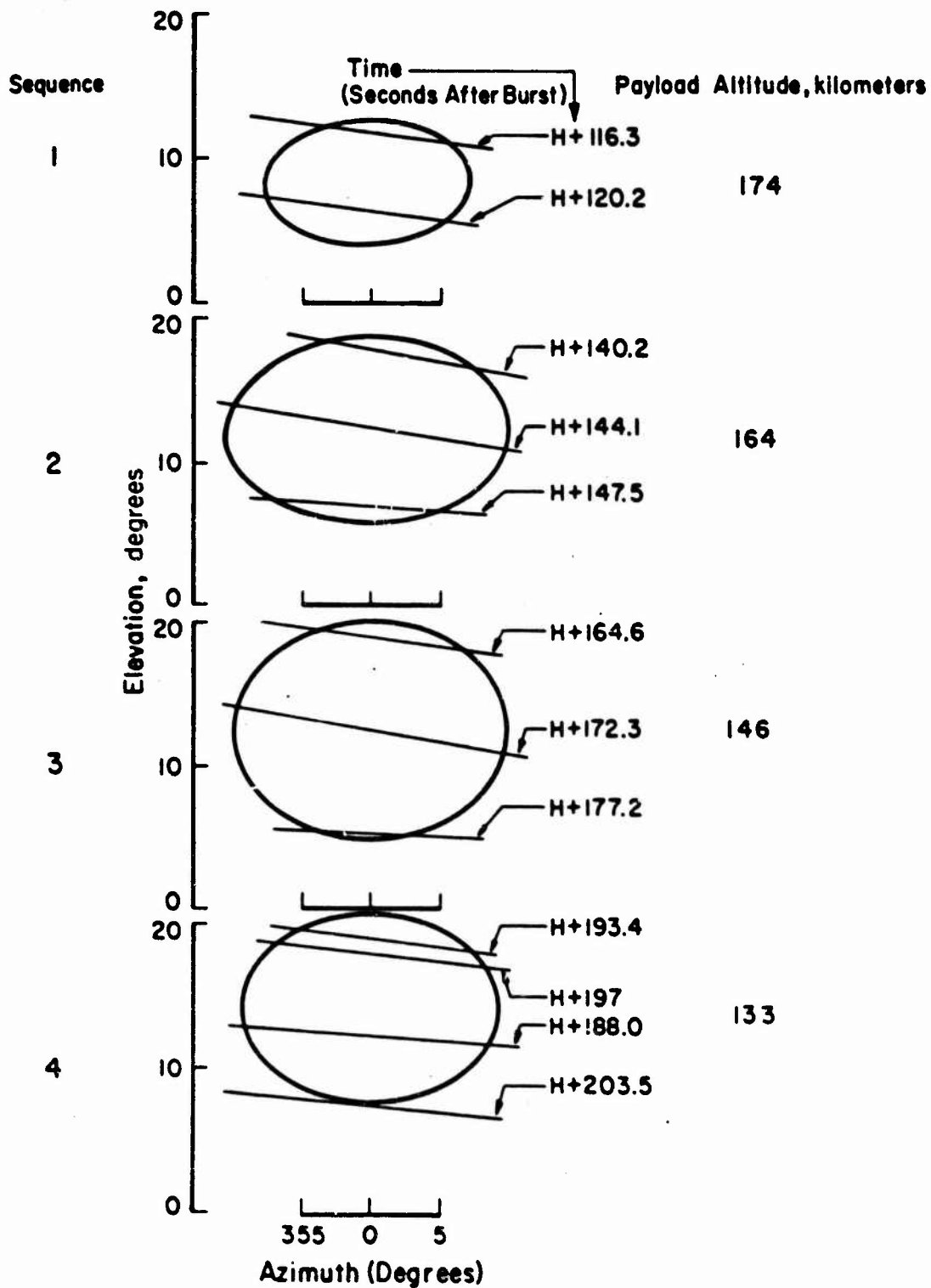


Figure 3.41 Airglow location during flight of Rocket 19, King Fish.

CHAPTER 4

DISCUSSION

The following discussion of results is based mostly on hand-reduced data obtained from the Star Fish, Blue Gill, and King Fish events. Computer-reduced data for Rockets 8, 9, and 19 were received from the data reduction contractor, but most of the attitude information was either wrong or unreliable. When possible, reduced attitude data has been used and is given in Chapter 3. Unfortunately, this discussion is incomplete, due to the lack of attitude information and the short period of time available after the decision was made to publish this report without the use of computer-reduced data.

In the following discussions of the Star Fish, Blue Gill, and King Fish events, the data from the various instruments are discussed separately, but corroborating evidence of the effects measured by other instruments is included in the text.

4.1 STAR FISH

Both Rockets 8 (H + 1203) and 9 (H + 2400) encountered a high intensity of trapped and possibly untrapped beta radiation starting near the upper fringes of the atmosphere (90 km). The high intensity of the beta radiation produced bremsstrahlung in the payload components which in turn was read as gamma radiation on the Geiger-Mueller tubes of the gamma scanners. This indicated that the debris was scattered over an extremely wide area.

4.1.1 Expected Gamma Produced Count Rates and the Bremsstrahlung Contribution. To make meaningful interpretations of the data, it was useful to illustrate what count rates would be expected on the basis of some simple models of the behavior of the burst and its byproducts. In keeping with the preliminary state of the experimental data, the following pictures are simple and very approximate. As more refined techniques are used to reduce the data, more sophisticated models will have to be used for fitting the burst to theoretical models.

However, the following discussion is intended as a guide to point up gross features of the data and should not be interpreted as final.

To begin with, the expected energy release in gamma radiation is given by:

$$P = Y (1.5 \times 10^{-2}) / 3.35 (3 + 2t^{0.6} + t^{1.2})$$

where P is the energy released in gamma radiation per second, Y is the total yield of the burst, and t is in seconds, where t = 0 is the time of burst. Where it is required in the models, it was assumed that the beta energy release was the same as that of the gamma. To determine the following estimates, the yield was taken as 1.2 megatons and the time as 23 minutes (1380 seconds), which coincided with the time at which Rocket 8 recorded its peak gamma flux. Using the above numbers, the gamma release rate from the total debris cloud at 23 minutes was

$$3.54 \times 10^9 \text{ watts} = 2.21 \times 10^{22} \text{ Mev/sec}$$

If a rather widespread debris cloud is assumed, which seems to be an inescapable conclusion, then some estimates of the gamma flux at the vehicle can be obtained by assuming that it was near the center of the cloud. The following numbers are illustrative. Table 4.1 gives the total gamma flux seen by an unshielded detector at the center of a cloud of uniform density, of the proportions described.

The actual peak counting rate observed by the gamma scanners in Rocket 3, corrected approximately for the shielding effect of the uranium shields, was about 10,000 counts per second. According to the preflight instrument calibrations, this corresponded to an incident gamma flux of about

$$1.1 \times 10^7 \text{ Mev/cm}^2\text{-sec}$$

In the absence of other data, this is not an unreasonable flux, and it corresponds to the flux in the center of a debris cloud with a lateral and vertical dimension of about 250 km by around 1200 km long.

However, examination of the beta detector energy flux indicated that bremsstrahlung was the main contributor to the gamma scanner output signal rather than gamma radiation. Thus, the above dimensions represented the minimum extent of the debris. In fact, examination of Table 4.1 indicated that movement of a large portion of the debris into the conjugate areas may have occurred.

Unfortunately, the beta detector was saturated during most of the period during which the gamma scanners recorded a large flux. However, the data are meaningful at the beginning of beta detector saturation. At this time (about 140-km altitude), the outputs from the gamma scanners were beginning their sharp rise and yielded a corrected count rate of about 700 counts per second, implying a gamma flux of about:

$$0.83 \times 10^6 \text{ Mev/cm}^2\text{-sec}$$

The beta detector, on the other hand, recorded a total beta flux of about

$$1.1 \times 10^7 \text{ Mev/cm}^2\text{-sec}$$

where the angular distribution of beta particles as shown by the beta detector output signals was taken into account. The measured gamma flux, from the numbers quoted above, was approximately 7-1/2 percent of the beta flux. A rough bremsstrahlung efficiency calculation was made for aluminum which has an efficiency of 1 percent; however, there were a number of objects of high atomic number such as depleted uranium, which could have contributed considerably more to the bremsstrahlung. Thus, a 7-percent bremsstrahlung efficiency would not be too surprising, and the results are consistent with the assumption that essentially all of the gamma flux was bremsstrahlung above 140-km altitude. A further confirming fact is that peaks of the gamma count in both Rockets 8 and 9 occurred near the point of closest approach to the magnetic field line through the burst. The peak counts occurred

at about 305-km altitude and 140 km north northeast of Johnston Island in Rocket 8 and about 325-km altitude and 100 km north northeast of Johnston Island for Rocket 9. Something of this kind would be expected if the radiation had its source in bremsstrahlung.

4.1.2 The Beta Flux. If the assumption is made that the total gamma flux measured in the high-count region was due to bremsstrahlung, then the gamma counter can be used as a measure of the beta flux at higher altitudes. The following numbers are based upon preliminary data reduction, and more careful analysis may change the results by as much as a factor of two. However, they suffice to give a general picture of the beta flux.

The magnitude of the peak beta flux, under the above assumption, can be obtained by calibrating the gamma counter against the beta counter at its initial saturation point. Then the peak beta flux (at 280 km) is given by the gamma instruments on Rocket 8 as

$$1.5 \times 10^8 \text{ Mev/cm}^2\text{-sec}$$

This clearly implies a rather extensive trapped electron component. For illustration, the expected beta flux, with no trapping, can be computed from the previous models of extensive debris cloud, approximately as given in Table 4.2. The flux refers to the center of the cloud.

In no case, of course, do the fluxes equal the levels recorded by the instruments, particularly for those very widespread clouds indicated by other measurements. Undoubtedly, the incident flux attributable to trapped electrons completely overwhelms that ascribable to the instantaneous emission from debris.

Also, the angular distribution of the beta flux leaves little doubt about the large trapped components. As can be seen from Figure 3.31 the incident beta radiation for Rocket 8 had a very marked azimuth asymmetry. In fact, compared to the peak rate occurring at magnetic east and west, the minimum almost vanished. Since the full opening angle of the beta scanner was about 120 degrees, the above fact implies

that very few electrons were contained in the 120-degree segments on either side of the long axis of symmetry of the azimuth plot. Thus, nearly all electrons were contained in the two remaining 60-degree segments. This is to be expected of a trapped electron component. During the portion of the flight of Rocket 8 just after apogee, the spin axis was almost normal to the magnetic field lines, so that the beta detector looked successively parallel to and normal to the field lines. If we assume the minimum allowable altitude for reflection of trapped electrons to be even as low as 50 km, then the minimum angle between the trapped electron trajectory and the earth field line at the 300-km altitude of the rocket was around 65 degrees. Thus, it was expected that all trapped electrons had orbits described by helices with pitch angles greater than 65 degrees. This expectation was in complete accord with the data.

Figure 3.31 shows the record of the beta detector just before saturation. The first modulation seen as the vehicle rose has the fundamental frequency of the rotating rocket. The minima occurred when the beta counter was pointing north. As the rocket rose higher, the broad maxima centered about the south suddenly developed minima also, which rapidly evolved until they were almost the size of the north minima. Just before saturation, the east-west maxima were typified by those shown in the azimuth plot. The region of trapped electrons was well marked and began at an altitude of about 90 km.

4.1.3 Debris Contained Along Field Line. The fraction of total debris q contained along a field line of unit cross sectional area (described in Section 1.3.3) can be evaluated only approximately for Rockets 8 and 9, since the half-angle of the cone of acceptance (field of view) for the beta detectors was not small. Thus Ω/Ω_0 is not approximately equal to unity. Bearing this in mind, q can be evaluated by multiplying the sum of the north and south beta energy values in Figure 3.31 by the following constant,

$$2/(1 - \cos \alpha)(ET) \approx 9.0 \times 10^{-24} \text{ cm}^2 \text{-sec/Mev}$$

where,

α = half angle of beta detector viewing cone = 60 degrees

E = total emission of debris at time equal to zero =
 7.5×10^{24} Mev/sec

T = decay function of debris normalized to unity at time
equal to zero.

Thus, the value of q increased from 9×10^{-20} to 7×10^{-18} between
projected altitudes of 50 km and 215 km.

4.1.4 Photometer Data. The photometers on Rockets 8 (H + 1203) and 9 (H + 2400) observed ionized nitrogen emission ($\lambda = 3914 \text{ \AA}$) at approximately the same spatial position, 75- to 130-km altitude and north northeast of Johnston Island. The lower of these two altitudes was reached shortly after Rocket 8 encountered beta radiation that was undoubtedly causing the airglow.

Some azimuth dependence was noted at about 75 km on Rocket 8 and at 100 km on Rocket 9. The orientation of both payloads was such that the photometer was looking in a horizontal plane when a response was recorded at azimuth angles of roughly 60 degrees west of north. As the payload rotated toward the north, the photometer field of view depressed below the horizontal. It appears, therefore, that the photometer viewed a patch of ionized air generally located north of Johnston Island at an altitude of roughly 75 km. The payload then passed through an extension of, or possibly another patch of ionized air from 100-km to 130-km altitude, with an area of decreased intensity at 115 km. Figure 3.23 shows a cross section of the trajectory reflected onto the earth's magnetic field lines. Field lines that intersect the trajectory at altitudes of 100 to 130 km intersect a plane through the burst point at altitudes of 120 to 150 km. These field lines pass through an altitude of 400 km roughly 500 km south of Johnston Island.

Approximately the same phenomenon was observed 20 minutes later when Rocket 9 passed through the same region. At that time the lower edge of the ionized air patch had moved up to approximately 85 km and there was sufficient change in the shape of the patch so that photometer

output was recorded only in the north to northwest direction up to an altitude of 108 km. Above this altitude and up to about 140 km (again with an area of decreased intensity at 115 km) the rocket was again apparently inside the ionized air patch.

4.2 BLUE GILL

4.2.1 Gamma Ray Source. To make a preliminary interpretation of the hand-reduced data the following assumptions were made:

1. The debris cloud was stationary during the flight of the payload.
2. The debris cloud was uniform in density.
3. The burst point lay in the plane of the trajectory.

As the vertical scanner rotated, it sampled vertical slices of the cloud so that an angular distribution of the debris about the thrust axis of the payload was determined. Figure 3.13 shows an angular distribution obtained from the vertical 20-degree scanner on Rocket 15 (H + 901) at an altitude of 44 km and horizontal range of 60 km from the vertical line through burst point. Due to payload attitude, the pointing direction of the scanner was tilted up at an elevation angle of roughly 18 degrees from horizontal so that its direction of maximum shielding intersected the vertical line through burst point at an altitude of 68 km. The range distance to this intersection point was about 63 km. The half-amplitude width of the cloud was approximately 125 degrees. If a spherical cloud whose center coincides with the intersection of the field of view and the vertical line through burst point is assumed, then its minimum radius can be determined from the angular debris distribution obtained from the vertical scanner. For example, if the scanner was located on the edge of the assumed debris sphere, then the half-amplitude width would be 90 degrees. Since the half-amplitude width was about 125 degrees, the radius of an assumed spherical cloud must therefore have been greater than 63 km.

Count rate versus altitude for various azimuth angles in the general direction of the burst is shown in Figure 3.14. The count rate was a function of the amount of debris contained in the 120-degree

by 90-degree field of view of the horizontal 90 degree scanner. It is reasonable to assume that 120 degrees included most of the cloud when the scanner was directed at the most intense part of the debris cloud, so that the count rate was a good measure of cloud intensity in the horizontal slice scanned. From Figure 3.14 the maximum cloud intensity is seen to occur at a rocket altitude of 75 km.

4.2.2 Beta Flux. Beta rays were detected at 23-km altitude on Rocket 15 (H + 901) coming from the direction of magnetic south. This radiation was received directly from the cloud and represented electrons which were injected from the debris in a direction along the magnetic field lines. Electrons injected at large angles to the field lines were attenuated by the atmosphere at this altitude. Beta flux received from the south at 23 km originated from the vicinity of burst at approximately 40-km altitude.

As the payload rose, beta flux was received from both magnetic east and west. This flux represented electrons traveling helical paths down the field lines from the burst area and may have included some trapped betas. The beta flux observed from magnetic east did not equal that observed from magnetic west on Figure 3.35. This is most likely due to an error in the assumed instrument pointing direction. If the beta flux recorded as being received from an azimuth angle $\phi \cong 10$ degrees (magnetic north) is correct, then even allowing for the fact that the beta detector did not view directly along a field line when $\phi \cong 10$ degrees it is likely that the relatively large beta response at and near the 80-km payload altitude (98-km projected altitude) indicates that the payload was slightly inside the cloud near these altitudes. The sharp decrease in readings from magnetic east, west, and south at roughly 65 km (80-km projected altitude) could have been due to a separation in the debris cloud. The two maximums occurring at projected altitudes of 75 and 85 km for an azimuth angle of $\phi = 190$ degrees correlates with the vertical distribution indicated by the H - 90 scanner in Figure 3.14.

4.2.3 Debris Contained Along Field Line. The fraction of total debris q contained within a tube along a magnetic field line of unit cross sectional area as defined in Section 1.3.3, can be determined by multiplying the sum of the beta flux received from magnetic north and south as shown in Figure 3.35 by the following constant,

$$2/(1 - \cos \alpha)(ET) \approx 7 \times 10^{-22} \text{ cm}^2\text{-sec/Mev}$$

where

α = half angle of beta detector viewing cone = 15 degrees

E = total emission of debris at time equal to zero in
Mev/sec = 7.5×10^{24} Mev/sec

T = decay function of debris normalized to unity at time
equal to zero

q varied between 1.4×10^{-15} and 4×10^{-17} between projected altitudes of 55 km and 107 km.

4.3 KING FISH

4.3.1 Gamma Ray Source. Motion of the debris was observed by Rocket 19 which was at an altitude of 138 km and approximately 34 degrees from north with respect to the burst point at the time of detonation. The changing pattern between each scan shown in Figures 3.15 to 3.18 illustrates the dynamic nature of the cloud.

The hump that occurred between northwest and west at $H + 9$ seconds for the V - 20 scanner (Figure 3.15) was caused by shielding from the horizontal scanner located above the vertical scanner. Figure D.1 shows this interference pattern of the horizontal scanner between declination angles of 10 to 60 degrees and between azimuth angles of 140 to 170 degrees.

The three peaks that appeared during the scan of the horizontal 20-degree scanner at $H + 4$ seconds were due to payload shielding. The component which produced the first peak from the left was unaccounted for. The other two peaks were caused by a balance weight and the vertical scanner. The sharpness of these peaks indicated a well-

confined debris. The first peak disappeared for a while and reappeared at H + 9 seconds, indicating payload axis or cloud motion.

The expansion of the debris was indicated on all the scanners by the disappearance of the fine cloud structure. As the payload descended, the structure of the debris cloud became increasingly difficult to discern.

The determination of attitude as a function of time for Rocket 19 was not completed. Therefore, the altitudes and directions of the King Fish debris are not dependable for obtaining quantitative conclusions.

4.3.2 Beta Flux Data. Figure 3.37 shows the north and south components of the beta detector outputs versus the magnetic altitude (projected altitude along the magnetic field line to vertical plane through the burst positions). This output was normalized to remove the decay factor, since Rocket 19 collected data shortly after burst when the debris was decaying rapidly.

The first peak in both the south and north components was probably due to the main body of debris rising up past the rocket. This corresponds to a rise velocity, averaged over the first 50 seconds, of 1.75 km/sec which correlates reasonably well with optical data which indicated a rise velocity of 3 km/sec for the center of the fireball and 1.5 km/sec for the lower limb. Another indication of a rising rather than a stationary debris is the delayed occurrence of the southern peak with respect to the northern peak. The reason for this is easily explainable if the rocket is moving through the debris. From optical data, "Fourth Report of the Fish Bowl Rapid Interpretation Group, King Fish", page 59, Figure 36, the diameter of the fireball at _____ was _____ making the above assumption valid, since Rocket 19 was approximately 50 km from the burst area. As the debris rises, the field line going north from the rocket will intersect the debris first, while the field line going south will be mostly above the debris. As the debris rises above the rocket, the field line going south will intersect the debris, whereas the field line going north will be below it.

The smooth decay of the south component after the first peak indicated a homogeneous distribution which was continuously expanding. The continuous expansion is inferred from the lack of any resemblance to a symmetrical function about apogee. Toward the north, concentration of debris at magnetic altitudes of 144, 160, and 178 km, and above apogee was noticed. A relative profile is seen in Figure 3.37. The second peak is symmetrical about apogee, indicating that at this point the debris was not expanding, except possibly along the field lines.

4.3.3 Debris Contained Along Field Line. To determine the fraction of total debris q which was contained in a tube of unit cross sectional area along the magnetic field line which is identified by its altitude along a vertical line through the burst point, the sum of the north and south beta flux at a given projected altitude in Figure 3.37 is multiplied by

$$2/(1 - \cos \alpha)E \approx 7.9 \times 10^{-24} \text{ cm}^2\text{-sec/Mev}$$

where,

$$\alpha = 15 \text{ degrees}$$

$$E = 7.5 \times 10^{24} \text{ Mev/sec}$$

The decay function T is not used, since the data is already normalized. At $H + 40$ seconds, $q \approx 7 \times 10^{-14}/\text{cm}^2$. From optical data, "Fourth Report of the Fish Bowl Rapid Interpretation Group, King Fish", page 58, Figure 35, the diameter of the fireball was determined to be about: which corresponds to a cross sectional area of

This is a reasonable correlation between optical data and the beta detector. One would expect the beta detector results to be higher than the reciprocal of the cross sectional area, since at $H + 40$ seconds the detectors were probably looking at the most intense portion of the debris, judging from the peak observed at this time.

At all times the south component was much larger than the north component. As time increased, the ratio of the south component to the north component decreased from about ten to two.

4.3.4 Photometer Data. The output of the photometer after saturation ($H + 7$ seconds) was probably due to airglow. The intense peak observed starting at $H + 15$ seconds was not believed to be the fireball, since its width was estimated to be expanding from 1.7 km to 8 km between $H + 15$ seconds and $H + 20$ seconds, after which it remained constant. This did not agree with optical data as published in the "Fourth Report of the Fish Bowl Rapid Interpretation Group, King Fish", which indicated that the fireball diameter was expanding from at about $H + 13$ seconds to at $H + 70$ seconds. It is likely that this was aurora. After the response in the vicinity of the burst disappeared, an airglow appeared in the direction of true north from the payload position. Actually, this may more properly be called airglows since it seems to have appeared and disappeared a number of times. Rocket 19 observed this airglow four times. This is shown in Figure 3.40. The presumed shape and location of this airglow as observed from the payload is displayed in Figure 3.41. The same position in space viewed at times between those shown in Figure 3.41 produced no photometer output. If it is assumed that these airglow patches were caused by debris traveling along the field lines from a position over the burst point, then their positions can be estimated by finding the intersection of these field lines with a line along the viewing angle from the payload. After establishing the airglow location, an extrapolation along the field lines was performed to determine the location of the beta source above the burst point. These values are given in Table 4.3. The numbers indicate the sequence shown in Figure 3.41. It should be emphasized that the attitude data shown in Figure 3.41 and used to compute the values in Table 4.3 is not considered reliable. This may even account for the apparent disappearance and reappearance of the airglow patch.

4.4 INSTRUMENT PERFORMANCE

Ninety-five percent of the instruments carried on Project 6.2 payloads operated reliably during all flights and provided useful debris data on the three events. Instrument failures and their causes, when known, are discussed below.

Gamma scanner malfunctions occurred on Rockets 15, 18, 19, 26, and 29. On Rocket 15, the 20-degree horizontal scanner did not operate until 174 seconds after liftoff, and the vertical 90-degree scanner on Rocket 18 stopped counting after $H + 1932$ seconds. All scanners on Rocket 19 stopped operating just before reentry. However, this failure did not affect the success of the experiment, because the signal level had already dropped below a usable level, and thus, no data was lost from the instrument failure. An inoperative voltage regulator was the probable cause for scanner failure on Rocket 19. All scanners on Rocket 26 operated erratically from $H + 822$ to $H + 842$ seconds, and all scanners on Rocket 29 stopped counting 173 seconds after liftoff. The cause for failure on Rocket 29 was not determined.

Beta detectors developed malfunctions on Rocket 9, 18, and 19. The detector on Rocket 9 did not generate an output signal for 600 seconds during its flight, and the detector on Rocket 18 was inoperative during the entire flight. Instrument failure on Rocket 19 was caused by a malfunctioning voltage regulator. The cause for failure of the Rocket 18 beta detector was not determined.

The gamma detectors and photometers provided data on all flights except during failure of the voltage regulator on Rocket 19.

No major telemetry failures occurred during the three events. However, some data from Rocket 9 was lost during two intervals after launch. These intervals were 220 to 365 seconds and 400 to 420 seconds. This was also true of Rocket 8 during the interval of 340 to 380 seconds after launch.

4.5 EFFECTIVENESS OF INSTRUMENTATION

In general, the payload instrumentation achieved its design objectives satisfactorily. The effectiveness of the gamma scanner, omnidirectional gamma detector, beta detector, and photometer are discussed in the following paragraphs.

4.5.1 Gamma Scanner. The scanners obtained good debris data. However, it is difficult to estimate how effective the scanners were in achieving their design objective until further analysis of the data is completed. The analysis is confronted with several difficulties. First, the orientation of the payload must be determined from the 3-axis magnetometer and other trajectory information. Second, the effects of payload shielding must be taken into account. Finally, the analysis requires a computer to perform the desired mathematical computations. Although the data has not been fully analyzed, a quick look indicated that at least the minimum design objectives were achieved for Blue Gill and King Fish; however, for Star Fish the scanners were measuring bremsstrahlung rather than gamma radiation. Crude estimates of the location of the debris can be inferred in two dimensions for the Blue Gill and King Fish events.

Although the effects of payload shielding made it more difficult to provide a quick interpretation of the data, the shielding also provided a lot more information about the debris. After analysis of this data, it is anticipated that resolutions of $\sim 10/360 \text{ } 4\pi$ steradian can be obtained due to payload shielding.

4.5.2 Omnidirectional Gamma Detector. In general, the omnidirectional gamma detector obtained good data. In some cases the detectors were not as sensitive as desired, and in other cases the detectors were saturated. The reasons for this were due to the uncertainty of the expected energy flux of gamma rays and to the fact that the 100-millicurie Co^{60} source used for calibration supplied by U. S. Nuclear was only 65 millicuries. The detector did not really measure total energy fluxes due to shielding from the payload. However, the total energy flux can be inferred from the maximum value of the output during a complete revolution of the payload. The shielding effects

also provided information as to the location and size of the debris cloud.

4.5.3 Beta Detector. The effectiveness of the beta detectors was increased considerably by decreasing its field of view from 120 degrees for Star Fish to 30 degrees for Blue Gill and King Fish. As a result, vertical distributions of beta-emitting debris were obtained. Pitch angle distribution was also obtained. Insufficient dynamic range on Rockets 8 and 9 and low sensitivity on Rockets 18, 26, and 29 reduced the detector's effectiveness.

4.5.4 Photometer. In general, the photometers did not have sufficient sensitivity except on Rockets 8, 9, and 19. Final interpretation of the data requires payload attitude data. Photometer usefulness as an aspect sensor will depend on successful correlation with optical data from other Fish Bowl projects.

4.6 DATA RELIABILITY

The accuracy of the collected data was determined mostly by the telemetry system. Errors of 3 to 5 percent can be expected for data from those rockets which did not have in-flight calibrators and an error of 2 to 3 percent on Rockets 8 and 18 which did have in-flight calibrators. Instrument errors are added to the telemetry errors.

The gamma scanner, omnidirectional gamma detector, and beta detector calibration data are accurate to within 15 percent. The accuracy of the gamma and beta detector output on Rocket 19 above 3 volts may be in error by a factor of two, because the calibration data above 3 volts was obtained by extrapolation.

Gamma scanner data accuracy was determined by statistical fluctuations which depended on the number of counts accumulated during the 10-millisecond sampling periods. The standard deviation varied from 32 percent for an output rate of 1000 counts per second to 3 percent for a rate of 100,000 counts per second.

The azimuth angles shown in the results chapter were accurate to within ± 10 degrees, but the accuracy of the photometer elevation angles was not determined, because computer data reduction was not completed.

Payload coning introduced significant elevation errors on all rockets but 8 and 9. A study to resolve the problem of coning is currently in progress.

The liftoff and flight times shown in the results were rounded off to the nearest second. Altitudes were accurate to within ± 5 km.

TABLE 4.1 CLOUD SHAPE AND GAMMA FLUX

Cloud Shape	Dimensions, km	γ Flux, Mev/cm ² -sec
Spherical	100 (radius)	5.3×10^7
Spherical	300 (radius)	5.9×10^6
Spherical	1000 (radius)	5.3×10^5
Prolate spheroid	100 x 500 (semiaxes)	2.5×10^7
Prolate spheroid	200 x 500 (semiaxes)	9.0×10^6
Prolate spheroid	200 x 1000 (semiaxes)	6.16×10^6
Prolate spheroid	400 x 1000 (semiaxes)	2.3×10^6
Half of debris at each conjugate point	---	4.6×10^5
All debris at north conjugate point	---	9×10^5
All debris at south conjugate point	---	10^4

TABLE 4.2 CLOUD SHAPE AND BETA FLUX

Cloud Shape	Dimensions, km	β Flux, Mev/cm ² -sec
Spherical	100 (radius)	5.3×10^7
Spherical	300 (radius)	5.9×10^6
Spherical	1000 (radius)	5.3×10^5
Prolate spheroid	100 x 500 (semiaxes)	5.3×10^7
Prolate spheroid	200 x 500 (semiaxes)	1.3×10^7
Prolate spheroid	200 x 1000 (semiaxes)	1.3×10^7
Prolate spheroid	400 x 1000 (semiaxes)	3.3×10^6

CONCLUSIONS AND RECOMMENDATIONS

Conclusions on the distribution of the debris for the Star Fish, Blue Gill, and King Fish events are given below. These conclusions were based on data obtained from the gamma scanners and other radiation detection instruments flown on seven Project 6.2 payloads during the Fish Bowl Series. Section 5.2 includes recommendations for improving the payload instruments to provide more accurate data during future nuclear events.

5.1 CONCLUSIONS

Preliminary analysis of Fish Bowl Series data indicated that the debris distribution for the King Fish and Blue Gill events can be determined during the final analysis program. Unfortunately, the distribution and altitude of the debris for the Star Fish event probably cannot be ascertained, because it was too widely scattered, and the gamma signal, if it existed, was lost in the bremsstrahlung.

Project 6.2 data is currently being computer-reduced at the facilities of another contractor, and final data analysis will be completed by EOS in 1964 under another contract. Preliminary conclusions on the debris location and distribution, derived from the hand-reduced data given in Chapter 3, are summarized below for the three events.

5.1.1 Star Fish. Analysis of gamma scanner data indicated that the debris was widely scattered (diameter was at least 1200 km), and a description of the cloud distribution cannot be attempted until computer-reduced data is available for further analysis. However, even with this information, mapping of the Star Fish debris is not anticipated, because it may not be possible to separate the large component of bremsstrahlung from the gamma radiation. The bremsstrahlung radiation was generated by the interaction of trapped beta particles with the payload structure and equipment.

5.1.2 Blue Gill. Most of the debris generated during the Blue Gill event was contained within the test area. The horizontal distribution of the debris was at least wide, and the distribution in the vertical direction was contained between at roughly 15 minutes after burst. The instruments observed maximum gamma radiation when the payload was at an altitude of 75 km.

5.1.3 King Fish. Data obtained from the gamma scanner, beta detectors, and gamma detector indicated that the debris was moving rapidly in the vertical direction. Based on beta detector data, the rate of debris ascent was The horizontal distribution of debris could not be determined during the initial gamma scanner data analysis performed for this program.

5.2 RECOMMENDATIONS

Recommendations are given below for improving the methods of data reduction and the quality of data collected during high-altitude nuclear detonations. These recommendations include techniques for improving the results obtained with the gamma scanner, beta detector, gamma detector, photometers, magnetometers, and telemetry systems. These recommendations are based on the analysis of hand-reduced data discussed in Chapters 3 and 4. However, results obtained from the final analysis of Project 6.2 data (scheduled for completion in 1964) may modify these recommendations.

5.2.1 Gamma Scanners. Two major problems arose from the use of the negative gamma scanner employed on Project 6.2. These problems included difficulties in hand-analyzing the data obtained from these instruments, and the measurement of bremsstrahlung (generated within the payload) instead of gamma rays from the debris. Recommendations for solving these problems are discussed below.

Data Analysis. The data obtained from the negative gamma scanners was very difficult to manually analyze. An accurate representation of the debris cloud was virtually unobtainable by hand, and a computer analysis was required. Although a simpler method of data analysis

was desirable, the light weight of the negative gamma scanner made its choice necessary, and simplification of manual analysis can be obtained by improving the radiation acceptance pattern. This pattern can be improved by careful placement of the scanner within the payload and by employing simple geometrical shapes for the shields. Careful placement of the scanners was not performed on Project 6.2, because tight schedule requirements did not provide sufficient time to complete the work as planned.

Bremsstrahlung Interference. Very little can be done to overcome the interference caused by bremsstrahlung in the operation of negative gamma scanners. Solutions to this problem can only be found in narrow acceptance angle telescopes. There are three gamma ray telescopes that can replace the negative telescopes (gamma scanners) employed during the Fish Bowl Series of tests. These are: (1) a mosaic filter scanner, (2) a positive telescope, and (3) a Compton telescope.

The mosaic filter scanner has some similarity to the negative telescope in that the detection element (Geiger tube or substitute) is partially or totally exposed directly to the gamma ray source over some solid angle. The celestial sphere is divided into a number of equal solid angles and each solid angle has a different depth of shielding from that of all other solid angles. The detector resolution (the number of solid angles discernible under the above arrangement) depends upon its ability to distinguish between different depths of shielding, which are dependent upon the counting statistics and total depth available, the latter being a function of the allowable total weight. This detector will have somewhat more trouble with the wide radiation spectrum received from a nuclear burst, because the different lengths of shield will represent different cutoffs for higher energy particles. However, this problem should not cause great difficulties, since the spectrum of nuclear bursts is known. The mosaic telescope has the same two problems as the negative telescope: it responds to bremsstrahlung, particularly in those solid angles that are only slightly shielded, and it is difficult to hand-analyze its data.

Actually, if properly constructed, e.g., with high resolution, it will be almost impossible to hand-analyze data from this telescope. Other disadvantages include a much lower maximum flux rate than the positive telescope and a smaller dynamic range for a given angular velocity. The advantage of this telescope is its ability to look at all angles simultaneously, e.g., during each revolution of the payload the detector will collect data from all directions in space.

The positive telescope consists of a conventional spherical shield with a detector placed at its center. A conical solid angle is cut out of the shield to expose the detector to incident gamma rays from only one direction. Data from this type of telescope is very easy to analyze, and if trajectory and attitude data are available, it can be displayed on a real-time basis. An extension to this type of telescope is to rotate the sphere around an axis perpendicular to both the spin axis and the field of view of the detector, such that the instrument then scans the celestial sphere in azimuth by the rotation of the payload and in elevation by motion of the telescope around its axis of rotation. Its real-time output data can be displayed as a raster or a television scan. The primary disadvantage of this type of detector is its weight and the difficulty it causes in payload mechanical design. The latter is due to the motion of the large mass which requires that the telescope be located very close to the center of gravity of the payload. This, of course, then requires the whole payload to be carefully designed around only this detector.

The Compton telescope is a lightweight narrow-angle telescope that detects gamma rays by coincidence detection of the Compton scattered electron produced by the incident gamma ray, and the reflected gamma ray. Unfortunately this detector is insensitive to gamma rays below approximately 2 Mev, which makes it useful as an auxiliary device for measuring gamma radiation from high-altitude debris, but not as a primary gamma detector.

The information-gathering ability of these instruments is, of course, dependent on the bandwidth available in the telemetry systems. It has been assumed in the above discussion that the systems are not bandwidth limited. The mosaic filter scanner may become bandwidth limited when a large number of elements are employed and the payload spin frequency is high. The same statement applies to a narrow beam positive or Compton telescope.

5.2.2 Beta Detector. The beta detector carried on Rockets 8 and 9 for the Star Fish event had a wider field of view than those used on the later flights. This field of view proved to be so wide that it was difficult to discern the minimum reading of the beta detector as the instrument looked along the earth's magnetic field lines. Additional shielding material was added to the detector for the Blue Gill and King Fish events, and it provided an adequate field of view. However, some difficulty was encountered in detector saturation. To avoid detector saturation in future tests, it may also be advantageous to place two separate detectors opposite each other around the vehicle spin axis, so that their fields of view can be simultaneously aligned along the magnetic field line when the vehicle is properly oriented. This latter technique will depend upon the payload weight limitations established for such experiments.

5.2.3 Aspect Determining Elements. The magnetometer package was carried on the Project 6.2 payloads to determine magnetic aspect for the purpose of determining payload attitude. As stated in Appendix G, the magnetometer data was not sufficient to accomplish this task. Instrument packages for the measurement of nuclear events that occurred during the day could carry both a magnetometer and a solar aspect sensor to determine attitude more easily. Instrumentation for night bursts is restricted to sensing the magnetic field vector; sensing the earth's horizon, which is useful only above an altitude of approximately 50 to 75 km; and sensing the position of a light or some other radiating source on the ground. Inertial packages that are gyro-oriented offer another solution, but their greater cost, complexity, and weight limit their application on solid-propellant sounding rockets.

Improvements on Project 6.2 magnetometer packages should include:

(1) the isolation of the magnetometers from the payload by mounting them above the end of the antenna ground plane, or (2) slotting this ground plane so that no current paths exist in the vicinity of the magnetometers.

5.2.4 Airborne Telemetry System. It is very desirable to have in-flight calibration, because it provides rapid and efficient periodic maximum and minimum signal check points. Three-point calibration (zero, half scale, and full scale) is adequate, since significant linearity changes are not expected. Care should be taken to ensure that the duration of each calibration level is sufficiently long to remain within the frequency response of the lowest frequency channel. Also it is desirable to have an S-band backup RF link during Fish Bowl Series-type tests. This will minimize the duration of RF blackout and will frequently allow continuous reception of telemetered data. In-flight tape recording is advisable to collect data at early times during RF blackout at the telemetry frequency.

An improvement in the transmission of data collected digitally, such as from Geiger-Mueller tubes, can be made with very little extra cost or airborne equipment. Small tone generators, which are keyed on or off by a one or zero stored in the various stages of the digital counter, can be used in place of the digital-to-analog converter and subcarrier oscillators employed on Project 6.2. This technique will preserve the digital character and accuracy of these signals, but will not affect the analog transmission of data obtained from the other instruments.

5.2.5 Ground Telemetry System. Remote azimuth and elevation control of the ground antennas would be a great asset for maintaining contact with the payloads. Even without the refinement of automatic tracking antennas, a good azimuth elevation manual control system would allow the antennas to be periodically set to predetermined pointing directions. An automatic five- or ten-point calibrator for the ground recording system also would be very desirable. Manual calibration is slow

and laborious, and three calibration points before and after a run are not sufficient to prevent errors of several percent due to tape speed changes and discriminator drift. To further reduce playback errors, an electronic tape speed compensator would be very valuable. The compensator would reduce errors from tape wow and flutter to a fraction of a percent. Increases in playback capability would provide more rapid data reduction. At least two tape machines should be equipped for independent playback into two sets of oscillograph and pen recorders.

APPENDIX A
ROCKET VEHICLE OPERATIONS,
PROJECT 6.2

A.1 INTRODUCTION

Rocket vehicle operations for Project 6.2 are described in this appendix, along with related information from Projects 6.3 and 6.4. Projects 6.2 and 6.3 launched rockets during the Star Fish, Blue Gill, and King Fish events, and Project 6.4 launched rockets during the Star Fish and King Fish events.

A.2 VEHICLE DESCRIPTIONS

A.2.1 Project 6.2.

Project 6.2 launched two Argo D-4 (Javelin) vehicles during the Star Fish event. The D-4 consisted of a first-stage Honest John, a second- and third-stage Nike, and a fourth-stage X-248 motor. The second-stage Nike was fired by a delay squib, and the third-stage Nike and fourth-stage X-248 were fired by on-board timers. Project 6.2 launched two Honest John-Nike-Nike vehicles during the Blue Gill event. The second-stage Nike was fired by a delay squib, and the third-stage Nike was fired by an on-board timer. Both Nikes had wedge-shaped (cross section) fins for increased aerodynamic stability.

Three Honest John-Nike-Nike vehicles were fired during the King Fish event.

A.2.2 Project 6.3.

In conjunction with the Star Fish event, Project 6.3 launched two Nike Cajuns and two Honest John-Nikes. All vehicles were standard, and the second stages were fired by delay squibs. Project 6.3 launched two Nike Cajuns and four Honest John-Nike vehicles during the Blue Gill event.

During the King Fish event four Honest John-Nike-Nike, one D-4 and one Nike Cajun (B-1) were fired.

A:2.3 Project 6.4.

Project 6.4 launched three Argo D-4's during the Star Fish event and two D-4's during the King Fish event. The second-stage Nike was fired by a delay squib, and the third-stage Nike and fourth-stage X-248 were fired by on-board timers. No vehicles were fired during the Blue Gill event.

A.3 LAUNCHER DESIGN AND LOCATION

There were two basic types of vehicle launchers for Projects 6.2, 6.3, and 6.4. The two different types of launchers were designated as large and small. The large launcher was capable of firing the D-4, Honest John-Nike-Nike, or Honest John-Nike vehicles. The small launcher was capable of launching only the Nike-Cajun vehicle. The primary difference between the large and small launchers was the length of the launcher boom and the existence of a third launch fitting at the end of the longer boom.

The launcher consisted of a vertical mast supported by two rigid stays with a pivoted boom supported by a pulley and cable arrangement (see Figures A.1 and A.2). The launcher mast was a reinforced I-beam. The reinforcement consisted of steel plates welded along each side to form a box-like structure. At the base of the mast was a large pin to locate the mast in the azimuth bearing. A graduated scale enabled the launcher to be set to the correct azimuth position. At the top of the mast a pin accommodated the two launcher supports. These supports were made of heavy tubular construction and fastened to anchors that were bolted to the deadman portion of the launcher pad. In this manner the launcher azimuth could be adjusted without disturbing the mast supports. Fastened to the mast was a trunnion that supported the launcher boom. This trunnion had a calibrated elevation dial. Also fastened to the boom were three sheaves which, in conjunction with

the cable, supported and elevated the launcher boom. The cable was connected to a power-driven winch, which was located on the mast directly behind the boom trunnion. This winch had a 5-hp motor with a brake and clutch. This arrangement was capable of setting the launch angle of elevation to within 1/2 degree. The elevation of the boom could also be adjusted manually. On the under side of the boom were the standard launch fittings (zero length) for the Honest John and Nike vehicles. The small launcher had two of these fittings, and the larger launcher had three fittings. The third launch fitting located at the end of the boom was retractable by spring action so as not to interfere with the vehicle as it was launched. The azimuth setting of the launcher was achieved by the azimuth boom that extended from the mast and opposite to the boom. This azimuth arm was hinged at the mast so that its back end rested upon the launcher pad. The back end of the launcher boom was connected to one of the mast support bases (anchors) by two telescoping tubular ties. These telescoping ties had holes at 3-inch intervals, and the total length of the ties could be adjusted by dropping a pin into the appropriate holes. The fine adjustment was accomplished by an ordinary turnbuckle.

The launcher azimuth was capable of almost 270-degree rotation, although it was desirable to keep the azimuth setting to within ± 45 degrees of the bisector of the angle between the two mast supports. The launcher elevation angle range was from -5 degrees to +85 degrees. The lateral acceleration of a vehicle due to starting or stopping while raising or lowering the launcher did not exceed 0.015 g. The launcher hoisting motor was remotely operated at about fifty feet from the launcher. A loading diagram of the large launcher is shown in Figure A.3.

The locations of the launchers for Projects 6.2, 6.3, and 6.4 on Johnston Island are shown in Figure A.4. Each launcher location was designated by a letter that will aid in identifying the launcher project and vehicle given in Table A.1. The locations of the launcher

deadman are also shown on this drawing. A large launcher is designated by L and a small launcher is designated by S.

A.4 OPERATIONAL SUMMARY

In order to understand the rocket vehicle operations for Projects 6.2, 6.3, and 6.4, it was necessary to summarize information concerning each of the above projects and their associated vehicles, the trajectories of these vehicles, the launchers from which the vehicles were fired, and the time of launching. Tables A.1 and A.2 list all the pertinent information concerning the rocket vehicle operations on the above three projects. Rocket cards for Project 6.2 are given in Tables A.6 through A.12. Abbreviations for each type of rocket discussed in Table A.1 are given below:

ROCKET VEHICLE NOMENCLATURE

ABBREVIATION	PROPULSION SYSTEM
Atlantic Research Corporation	
N-C	M5-Cajun
HJ-N	M6-M5
HJ-N-N	M6-M5-M5
Aerolab Development Company	
B-1	M5-Cajun
C-22	M6-M5-M5
D-4	M6-M5-M5-X248

NOTE: M5-Nike
M6-Honest John

A.5 LAUNCH CONTROL

Before each launching, several ground operations were performed. Some of these operations were verbal or visual indications of readiness, and others took an active part in the firing control circuits. The verbal and visual functions consisted of informing the project

director of the state of readiness of the payload and ground telemetry systems. The condition of the payload and ground telemetry was indicated by a voice confirmation or a visual confirmation in the form of ready lights. This information was displayed or transmitted to the project officer who evaluated the overall readiness of the vehicle.

There were four active control operations in the firing circuit for Project 6.2, 6.3, and 6.4 vehicles. The first was performed by a pad or section control switch that was activated by a key. This key was in the possession of the pad leader during the process of elevating the launcher and vehicle, arming the vehicle, performing pad checkouts, and final wind weighing corrections. When the pad leader had performed these functions, cleared the pad, and returned to the blockhouse, he then inserted his key in the ready switch, thus indicating that the vehicle was ready to be launched. The second control operation was performed by the master firing switch, which was under the control of the launch director. The closure of this switch was determined by the presence of the vehicle pad keys and the overall readiness of the firing circuits. There was only one master switch for all vehicles on Projects 6.2, 6.3, and 6.4. A third control switch was operated by the project officer when all payload, ground telemetry, and general range safety requirements were satisfied. A fourth control switch, operated by a relay, was actuated by a preprogrammed timer. Because of the large number of vehicles being launched during both events, it was necessary to have a single source for the overall control of the operation to insure range safety. The switch closure occurred at a predetermined time after detonation and lasted for 15 seconds. If the vehicle in question was not ready to be launched as determined by the above three control switches (pad switch, master switch, and project officer's switch), then the vehicle was not launched by the Edgerton, Germeshausen and Grier (EG&G) closure. If the vehicle was ready for launching as determined by the above three control switches, but the 15-second time limit had expired, the vehicle was not fired, because the signal from the EG&G control timer was no longer available.

Once all four control operations had been completed, the vehicle was launched. The launching of the vehicle was accomplished by the contact closure of the EG&G relay which simultaneously fired the vehicle umbilical and initiated a delay timer. This delay timer closed the final firing relay at about five seconds after the firing of the umbilical. Once this had been accomplished the vehicle was launched.

The firing control panel had a series of visual displays (lights) indicating the status of the launch operation. The first was a light indicating that there was power to the launch control console. The ready lights indicated the closure of the pad (section) and master control switches, and another light indicated the presence of the EG&G firing signal. An umbilical release light indicated the status of this operation. Finally, a first-motion switch actuated a firing light indicator when the vehicle left the pad.

The sequence of launch operations for the fire control panel are given in Table A.3.

A.6 VEHICLE PERFORMANCE SUMMARY

Within the three phases of field operations, EOS was responsible for preparing, assembling, and firing 28 sounding rockets involved in three high-altitude nuclear events. These rockets included 79 stages and nine configurations with ten types of payloads. The rocket configurations were as follows:

<u>Designation</u>	<u>Propulsion System</u>	<u>Manufacturer^a</u>
ARGO D-4	M6-M5-M5-X248	ADC
ARGO D-4 w/blunt nose	M6-M5-M5-X248	ADC
ARGO C-22	M6-M5-M5	ADC
HJ-N-N	M6-M5-M5	ARC
HJ-N	M6-M5	ARC
ARGO B-1	M5-Cajun	ADC

<u>Designation</u>	<u>Propulsion System</u>	<u>Manufacturer^a</u>
N-C	M5-Cajun	ARC
N-C	M5-Cajun	ADC/ARC
N-C	M5-Cajun	ADC/AGC/PSL

^aADC Aerolab Development Co.

ARC Space Vehicle Group, Atlantic Research Corp.

AGC Aerojet-General Corp.

PSL Physical Science Laboratory, New Mexico
State University

A 96-percent-successful operation was realized from all stages. Eight failures occurred on five vehicles yielding an 82-percent vehicle success. A discussion of these failures is given in Section A.7.

A summary of the rocket firings describing significant performance information is presented below. The launchings are listed by event and described in detail in Table A.1 in accordance with the following index:

<u>Event Designation</u>	<u>Event Date</u>
Star Fish	9 July 1962
Blue Gill	26 October 1962
King Fish	1 November 1962

Some discrepancies between actual and predicted flight azimuth of the vehicles are noted. Such errors were predominately a function of wind measurements. Since each vehicle was very wind sensitive, small changes in surface wind had a significant effect on the final azimuth. For example, an ARGO D-4 launched at a nominal 83 degrees quadrant elevation and 120 degrees true north azimuth in a steady wind from 90 degrees true north and blowing 20 knots from the surface to 20,000 feet would require a launcher setting of 169 degrees azimuth and 85.2 degrees quadrant elevation. If this wind reduces to 15 knots for 15 seconds, the launcher

setting should be 85.6 degrees quadrant elevation and 154 degrees azimuth. Obviously, wind readings and corresponding launcher settings should be made as close to launch time as possible to minimize these errors.

Review of the postflight information clearly indicates that over-aged motors were one problem that was beyond control in vehicle design and assembly preparation. Many of the vehicles did not perform as predicted. This deficiency can often be caused in the first flight of a new vehicle or payload configuration by an underestimate of the aerodynamic drag. Such a conclusion might be applicable in this situation except for the following facts:

1. The Nike rocket motors (GFE) used in each vehicle were over 6 years old.
 2. Storage decreased the performance capability of the propellant utilized in the Nike motors.
 3. One second-stage Nike motor (Rocket 29) operated, but apparently produced very little, if any, thrust.
 4. Rockets 8, 9, and 25 (ARGO D-4); and Rockets 20, 24, 27, and 28 (ARGO C-22) produced nominal predicted flights.
 5. The measured velocity increment of the 3rd stage of Rocket No. 19 was 10 percent low.
 6. Large quantities of Nike propellant were found on several launch sites after vehicle liftoff.
 7. Each Honest John, Nike, and Cajun motor was visually inspected by one Aerolab staff to locate gross defects such as cracks and moisture.
- It is concluded, therefore, that those vehicles yielding lower performance and improper motor operation were the direct result of using out-of-date rocket motors. For example, it is estimated that a 10 percent loss of second- and third-stage motor impulse on the ARGO C-22 would reduce the nominal apogee by over 30 km.

In addition to the three basic payloads employed on the Nike-Cajun type vehicles, Figure A.5 is presented to distinguish between the various payloads used with the other rockets. This form of designation has been applied to the performance data contained below.

Vehicle Summary

The vehicle performance can be summarized by type as follows:

ARGO B-1 (Nike-Cajun) (Aerolab)

Two ARGO B-1 vehicles were launched with satisfactory flights. Available performance data indicated that these rockets produced nominal flights. ARGO B-1 vehicles were prepared for a 3-cps spin during first stage and no spin requirement on the second stage. It is interesting to note that 30 seconds after launch, the spin rate on Rockets 21 and 23 had decayed approximately one cycle to about 1.5 cps. This indicated a very low fin damping force.

Nike-Cajun (ARC)

There were 4 Nike-Cajun rockets launched. All of these rockets produced successful flights.

Honest John-Nike

Four of these vehicles were successfully fired, and nominal predicted performance was measured for each rocket.

Honest John-Nike-Nike

As with the Honest John-Nike vehicles, these Rockets, 15 and 18, had been assembled twice previously. The rockets carried payloads nearly identical to Rockets 19, 26, and 29, except that ballast weight was not added to the nose cone for stability. The flight of Rocket 15 was satisfactory with performance close to predicted values, extrapolated from the 83-degree quadrant elevation launch angle. Significant coning was measured during third-stage operation, which was apparently due to insufficient stability. The coning condition could have been the major contributing factor in reducing the final spin rate achieved by the vehicle.

Rocket 18 tumbled during third-stage operation. This condition significantly reduced the trajectory performance.

ARGO C-22

Seven of ARGO C-22 vehicles were launched, and six produced successful flights. A second-stage motor malfunction on Rocket 29 prevented the vehicle from achieving full altitude.

Inspection of tracking data revealed that the rocket performance for vehicles carrying payload "B" (Rockets 20, 24, 27, and 28) was generally lower than predicted. An investigation revealed that the estimated third-stage drag was low by approximately 15 percent. It should be noted that the drag estimate had been prepared on the given smooth payload shape without knowledge of surface roughness (antennas, etc.).

The velocity increments given in Table A.4, compare the performance of each stage to predicted values. Inspection of Table A.4 reveals that the required velocity was achieved in most flights. However, the velocity increment for the third stage of Rocket 19 was considerably lower than the predicted value. This condition was probably caused by propellant deterioration.

The third-stage fins on these vehicles were equipped with a special leading edge design. This installation was employed to obtain qualitative data and field experience on the design. An extensive analysis was conducted by the Aerolab Engineering Staff before the fins were incorporated on the vehicle, to determine their effect on vehicle adequacy if a failure of the edge design occurred during flight. This investigation revealed that a failure would not be serious, and the worst condition would be a slight increase in drag. At least six leading edge strips were found on the site after launches. Inspection of these strips revealed that four had been struck by a hard object causing failure in the installation. This evidence indicated that failure may have been initiated by contact from the ejected payload umbilical block and cable.

ARGO D-4

Seven ARGO D-4 vehicles were launched during two major events. Six of these rockets produced satisfactory flights, and one rocket failed. The second stage of Rocket 22 failed to operate causing low performance. The cause of the failure was unknown. An equipment malfunction on Rocket 25 prevented nose cone ejection. This failure initiated a design study at Aerolab to prevent this condition on future flights.

The velocity increments given in Table A.5 compare the performance of each stage to predicted values. Within measurement and reduction tolerances, all stages attained the predicted velocity except as noted on Rocket 22.

The payload telemetry systems for Rockets 8, 9, 22, and 25 performed satisfactorily and yielded considerable data on vehicle behavior. Unfortunately, payload failures in Rockets 1, 5, and 7 prevented obtaining complete information.

A.7 VEHICLE FAILURE DISCUSSION

Twenty-three out of 28 vehicles performed satisfactorily during the Star Fish, King Fish, and Blue Gill events. This section presents information and opinions on the failures or malfunctions which occurred on the remaining five vehicles.

The causes of these vehicle failures can be attributed to one or more of two major sources; rocket hardware and/or design and rocket motors. In general, insufficient data was available on each flight to adequately make conclusions as to the cause of failure. However, the failures are listed below:

Rocket 3 (HJ-N, no S/N). Second stage did not ignite, and cause for this failure was not determined. Possible causes of malfunction were a bad motor, bad igniter, thrust blocks permitted the propellant to slip forward and damage igniter, or the firing cable was severed. First-motion actuation was displayed on the fire control panel.

Rocket 18 (HJ-N-N, S/N ARC C-1). Recorded data, verified by ground observation, indicated that the vehicle tumbled during third-stage operation. Tumbling was probably due to aerodynamic instability.

Analysis by Aerolab on a similar vehicle (ARGO C-22) using the same payload indicated an unsatisfactory relationship between the vehicle aerodynamic center of pressure and the center of gravity during third stage operation. This problem was avoided on the ARGO C-22 by using special fins and adding ballast to the nose cone. Rocket 15 precessed badly, but apparently did not tumble, which indicated that the stability of this vehicle configuration is marginal.

Rocket 25 (ARGO D-4, S/N ADC 36). Telemetered data indicated that the nose cone was not ejected as required. Prelaunch checkout of the nose cone and actuation system was satisfactory. The probable cause for failure was either a malfunction in the pin puller operation or in the nose cone release ring mechanism. Aerolab is presently developing a new nose cone and release mechanism which should improve the reliability of this component.

Rocket 29 (ARGO C-22, S/N C-3). A very low thrust was produced by the second stage. Ground observation indicated that the stage ignited at the proper time and operated for the nominal period. As a result, it is concluded that the rocket motor ejected a large quantity of its propellant at ignition. Such a failure is to be expected from motors over 5 years old. In addition to this type of failure, over-age motors generally exhibit low performance.

Rocket 22 (ARGO D-4, S/N 35). Recorded data indicates the second stage failed to operate. Although the failure caused a low apogee and shortened flight, the remaining functions of the vehicle were performed successfully, and therefore, the failure was not catastrophic. There are several causes of this type of failure; propellant deterioration, premature break in igniter firing cable, or ground firing circuit malfunction. Since the checkout records on this particular stage indicated a satisfactory igniter circuit continuity and stage checkout, it

can be concluded that the failure originated either externally or resulted from propellant deterioration.

It was unfortunate that these failures occurred. One contributing factor to these malfunctions may have been the extremely short time available to prepare for the launchings. This was particularly true in the latter portion of this program when insufficient time did not permit the normal procedure for rechecking and inspection of the vehicles to be performed.

TABLE A.1 DETAILS OF ROCKET OPERATIONS

STAR FISH EVENT

Rocket No.	1	2	3	4	5	6	7	8	9
Project No.	6.4	6.3	6.3	6.3	6.4	6.3	6.4	6.2	6.2
Vehicle type ^a	D-4	N-C	HJ-N	HJ-N	D-4	N-C	D-4	D-4	D-4
Vehicle Ser. No.	32	None	None	None	33	None	31	29	30
Launcher No.	19	16	6	18	22	15	17	5	4
Launch time (second from H-0)	-600.0	-59.7	-88.7	+420.3	+420.3	+480.3	+960.3	+1203	+2400.3
Launcher elevation (degree)	85.5	87.3	87.3	88	83.2	87.3	85.5	81.5	82.7
Launcher azimuth (degree true)	145	76	151	89	153	76	145	8	0
Flight elevation (degree) ^b	82	83	82.5	83	80	88	82	79.5	82
Flight azimuth (degree true)	127	117	114	112	137.5	103	121.5	26	22
Predicted ^b apogee (km)	463	119	86	87	440	119	520	640	672
Predicted impact ^b range (km)	779	52	41	44	1055	52	805	1160	950
Predicted flight ^b time (second)	800	360 ^f	300 ^f	300 ^f	786	360 ^f	834	877	905
Actual apogee (km)	496	100 ^g	18 ^g	85.1	537	100.5 ^g	515	632.1	685.8
Actual impact range (km)	545	56 ^g	5 ^g	43.6	925	49 ^g	949.1	1076	787.6
Actual flight time (second) ^d	725 ^e	260	108	251	700 ^e	329	749	824 ^e	871 ^e
Payload type	IV	II	III-B	III	V	II	V	I	I
Payload configuration ^h	D				E		E	A	A
Contractor	Zimney	GCA	GCA	GCA	Zimney	GCA	Zimney	EOS	EOS
AME/DME frequency (RCVR/XMTR-Mc)	310/338	None	310/285	310/270	310/273	None	310/335	None	None
C-band frequency (RCVR/XMTR-Mc)	None	None	None	None	None	None	None	5700/5775	5700/5775
GMC beacon frequency (Mc)	1660	1670	1680	1660	1670	1680	1660	1670	1680
Three-frequency beacon (Mc)	36.94 147.76 886.56	None	None	36.94 147.76 886.56	36.44 145.76 874.56	None	36.94 147.76 886.56	36.44 145.76 874.56	36.94 147.76 886.56
VHF telemetry frequency (Mc)	253.8	234.0	245.3	234.0	245.3	253.8	253.8	234.0	234.0

^a Legend:

D-4: Argo D-4 (Aerolab)

N-C: Nike-Cajun (ARC)

HJ-N: Honest John-Nike (ARC)

^b Postflight prediction based upon best wind data at launch and other pertinent data^c Postflight computer simulation^d Based upon duration of VHF telemetry reception (except as noted)^e Three-frequency beacon reception^f Nominal^g Estimated^h See Figure A.5

TABLE A.1 (continued)

BLUE GILL EVENT								
Rocket No.	10	11	12	13	14	15	17	18
Project No.	6.3	6.3	6.3	6.3	6.3	6.2	6.3	6.2
Vehicle type ^a	N-C	HJ-N	HJ-N	N-C	HJ-N	HJ-N-N	HJ-N	HJ-N-N
Vehicle Ser. No.	A-11	B-1	B-6	A-12	B-5	C-1	B-3	C-2
Launcher No.	16	19	6	15	18	5	17	4
Launch time (second from H-0)	-59.3	-119.2	+301.0	+360.9	+670.4	+900.8	+1320.8	+1861.2
Launcher elevation (degrees)	84.0	84.0	83.0	84.0	87.0	83.0	82.5	83.0
Launcher azimuth (degrees true)	112	106	0	112	143	0	143	0
Flight elevation (degrees)	80.5	80	82.5	84	84.5	82.5	80	82.5
Flight azimuth (degrees true)	102	86	20	88	100.5	21	117.5	35.5
Predicted ^b apogee (km)	113	82	83	115	88	129	82	129
Predicted impact ^b range (km)	104	88	71	62	46.5	100	88	100
Predicted flight ^d time (second)	340	278	290	350	300	345	278	345
Actual apogee (km)	97.4	79.7	81.2	97.1	93.9	137.5	81.7	50.5
Actual impact range (km)	78.1	68.5	73.5	61.0	43.3	158	82	283 ^c
Actual flight time (second)	270	240	240	265	265	340	240	175
Payload type	II	III-A	III-A	JI	III	I	III	I
Payload configuration ^c		B	B		B	A	B	A
Contractor	GCA	GCA	GCA	GCA	GCA	EOS	GCA	EOS
AME/DME frequency (RCVR/XMTR-Mc)	None	310/285	310/270	None	310/279	None	310/273	None
C-band frequency (RCVR/XMTR-Mc)	None	None	None	None	None	5700/5775	None	5700/5775
GMD beacon frequency (Mc)	1660	1670	1680	1660	1670	1680	1660	1670
Three-frequency beacon (Mc)	None	36.94 147.76 886.56	36.44 145.76 874.56	None	36.44 145.76 874.56	36.94 147.76 886.56	36.44 145.76 874.56	36.94 147.76 886.56
VHF telemetry frequency	253.8	245.3	234.0	253.8	245.3	234.0	245.3	234.0

^a Legend:

N-C: Nike-Cajun (ARC)

HJ-N: Honest John-Nike (ARC)

HJ-N-N: Honest John-Nike-Nike (ARC)

^b Postflight prediction based upon best wind data at launch and other pertinent data^c Estimated^d See Figure A.5

TABLE A.1 (continued)

KING FISH EVENT											
Rocket No.	19	20	21	22	23	24	25	26	27	28	29
Project No.	6.2	6.3	6.3	6.4	6.3	6.3	6.4	6.2	6.3	6.3	6.2
Vehicle type ^a	C-22	C-22	B-1	D-4	B-1	C-22	D-4	C-22	C-22	C-22	C-22
Vehicle Ser. No.	C-7	C-6	106	35	105	C-2	36	C-1	C-5	C-4	C-3
Launcher No.	1	17	15	19	16	5	22	2	18	6	4
Launch time (second from H-0)	-119.7	-119.7	-0.3	+59.6	+359.6	+360.2	+542.3	+780.4	+810.1	+2400.4	+1500
Launcher elevation (degree)	86.1	86.5	87.0	85.5	82.0	83.0	83.2	86.1	86.5	83.0	86.1
Launcher azimuth (degree true)	155	135	112	131	109	0	177	155	135	0	155
Flight elevation (degree)	85	85	85	82.5	80	82	83	85	85	82	85
Flight azimuth (degree true)	123 ^b	109	79	100 ^b	100.5	19.5	130	115.5	109	18	92.5
Predicted ^b apogee (km)	194	180	115	500	113	170	490	194	180	170	194
Predicted impact ^b range (km)	100	91	62	770	104	130	790	109	93	130	100
Predicted flight ^b time (second)	430	413	350	818	350	413	807	430	413	413	430
Actual apogee (km)	162 ^c	161.8	105	142 ^c	113	153.9	560	162.6	157.3	152	67.6
Actual impact range (km)	104.5 ^c	82.4	40.2	313 ^c	90	157.2	561.2	104.1	89	156.6	36.2
Actual flight ^d time (second)	360	370	280	400	280	360	785	370	360	360	224
Payload type	I	III-B	II	IV-A	II	III-C	V	I-A	III	III	I
Payload configuration ^a	A	B		D		B	D	A	B	B	A
Contractor	EOS	GCA	GCA	Zimney	CCA	GCA	Zimney	EOS	GCA	GCA	EOS
AME/DME frequency (RCVR/XMTR-Mc)	None	310/285	None	310/282	None	310/279	310/338	None	310/273	310/279	None
C-band frequency (RCVR/XMTR-Mc)	5700/5775	None	None		None	None	None	5700/5775	None	None	5750/5825
GMD beacon frequency (Mc)	1660	1670	1680	None	1680	1670	1660	1680	1670	1680	1660
Three-frequency beacon (Mc)	36.94 147.76 886.56	None	None	36.44 145.76 874.56	None	None	36.94 147.76 886.56	None	36.44 145.76 874.56	36.44 145.76 874.56	36.94 147.76 886.56
VHF telemetry frequency (Mc)	234.0	253.8	None	245.3	None	234.0	253.8	245.3	234.0	234.0	245.3

^a Legend:

C-22: Honest John-Nike-Nike (Aeroleb)

B-1: Nike-Cajun (Aeroleb)

D-4: Argo D-4 (Aeroleb)

^b Postflight prediction based upon best wind data at launch and other pertinent data^c Postflight computer simulation^d Based upon duration of VHF telemetry reception (except as noted)^e See Figure A.5

TABLE A.2 ROCKET PAYLOAD COMPOSITION

Instrumentation	Payload Number									
	I	IA	II	III	IIIA	IIIB	IIIC	IV	IVA	V
1. Three-frequency propagation beacon	X			X	X			X	X	X
2. RF impedance probe				X	X	X	X			
3. Mass spectrometer			X					X		
4. Gamma ray scanner	X	X								
5. Beta detector	X	X								
6. Gamma ray detector	X	X								
7. Auroral photometer	X	X								
8. X-ray, gamma-ray, beta, flux meters				X	X	X	X	X	X	X
9. Prompt X-ray, gamma-ray, flux meters				X	X	X	X	X	X	
10. Ion trap				X	X	X	X			
11. Langmuir probe								X	X	X
12. Retarding potential probe										X
13. Magnetic aspect	X	X	X		X	X		X	X	X
14. AHE/DME beacon				X	X	X	X	X	X	X
15. GMD telemeter/beacon	X	X	X	X	X	X	X	X	X	X
16. Telemeter	X	X	X	X	X	X	X	X	X	X
17. C-band beacon	X	X								

TABLE A.3 FIRE CONTROL PANEL OPERATION

Sequence of Operation	Results
1. All switches off, including BRL and battery charger	None
2. All connectors installed	None
3. Select rocket and check payload and battery umbilical squib circuits	Squib resistance
4. Main power switch on	Light on, power supplied to master switch
5. Master key switch on	Light on, power to battery charger, section switch, transformer switch, and first-motion switch
6. Battery chargers on	Charge batteries ($\frac{1}{2}$ ampere for 30 minutes)
7. Battery chargers off	Test & monitor battery voltage
8. First-motion switch on	All first-motion lights on
9. Reset first-motion relay with selector switch and reset switch	All first-motion lights off, relays set in no-fire position
10. Umbilical transformer switch on	Umbilical transformer light on, power to umbilical relay
11. All section switches on	Ready lights on, power to firing relay
12. BRL, lock-out switch on	Supplies power to EG&G relay
13. EG&G relay closes	a. Closes umbilical release relay b. Starts firing timer (BRL)
14. Umbilical block ejects	Ejects umbilicals and turns umbilical lights on
15. Timer switch closes	Firing light on, closes firing junction box relay
16. Firing junction box relay closes	Fires first-stage igniter, supplies power to first-motion box
17. Rocket flight initiated	Separates clip lead, closes first-motion relay
18. First-motion relay closes	Initiates second stage and unlatch squibs, closes first-motion relay in control panel
19. Control panel first-motion relay closes	First-motion light on, gives signal to BRL-EOS-CRL & GCA

TABLE A.4 VELOCITY INCREMENTS FOR ARGO C-22 ROCKETS

Source: BRL doppler velocity corrected to estimated flight path conditions.

Rocket No.	Stage 1		Stage 2		Stage 3	
	Predicted ft/sec	Actual ft/sec	Predicted ft/sec	Actual ft/sec	Predicted ft/sec	Actual ft/sec
19	1800	1740	1700	1580	4200	3800
20	1780	N/A	1600	N/A	3980	N/A
24	1800	N/A	1650	N/A	4030	N/A
26	1800	N/A	1700	N/A	4200	N/A
27	1840	1790	1630	1660	3880	3860
28	1840	1790	1630	1590	3880	3920
29	1800	1760	1700	N/A	4200	4250

No second-stage ignition

TABLE A.5 VELOCITY INCREMENTS FOR ARGO D-4 ROCKETS

Source: BRL doppler velocity corrected to estimated flight path conditions.

Rocket No.	Stage 1		Stage 2		Stage 3		Stage 4	
	Predicted ft/sec	Actual ft/sec						
1	16.50	16.25	1220	983	2520	2428	7200	7150
5	16.72	16.20	1230	1222	2580	2362	7520	7410
7	16.70	16.50	1240	1090	2570	2490	7430	7740
8	17.04	17.30	1319	1230	2651	2613	7800	7640
9	17.04	16.63	1319	1038	2651	2380	7735	7440
22	16.50	16.48	1230	N/A	2530	2700	7250	4380
25	16.50	16.55	1220	1420	2510	2365	7250	7340

No second-stage ignition

TABLE A.6 LAUNCHING PROJECT CARD, ROCKET 8

1. PROGRAM: Fishbowl, Program A
2. PROJECT: 6.2; Rocket-Borne Gamma Ray Scanner
3. EVENT: Star Fish Prime
4. LOCATION OF PROJECT ACTIVITY: Johnston Island
5. VEHICLE DESCRIPTION:
 - a. Type of Rocket and Round Number: Argo D-4 Rd. No. 8
Aerolab No. 29
 - b. Detail Vehicle Description: Four-stage solid propellant rocket;
Honest John, Nike, Nike booster and X-248.
 - c. Rocket and Igniter Serial Number and Time Delay:

	Rocket	Igniter	Time Delay
1st Stage	3031	61	0
2nd Stage	10359	Unknown	9.7 sec
3rd Stage	11551	Unknown	25 sec
4th Stage	195	Unknown	65 sec
 - d. Total Rocket Weight (Incl. Payload): 7487 lb
 - e. Total Rocket Length (Incl. Payload): 592.24 inches
 - f. Rocket Center of Gravity: 342.1 in. from 1st-stage nozzle
 - g. Rocket Fins (Descriptive):

Stage	1st	2nd	3rd	4th
Size	7.5 ft ²	2.73 ft ²	2 ft ²	None
Angle	30' cw	6.9' cw	50.4' cw	
 - h. Rocket Spin Rate: 3rd-stage b.o. Estimated 6.75 rps Actual 5.5 rps
4th-stage ignition Estimated 6.2 rps 5.5 rps
 - i. Agency Responsible for Vehicle: Electro-Optical Systems
Aerolab Development Company
 - j. Number to be Launched: Two

TABLE A.5 CONTINUED

6. PAYLOAD:

- a. Gross Payload Weight (Incl. nose shield and extension tube): 159 lb
- b. Net Payload Weight and Length (Incl. extension tube): 133 lb 53" long
CG 20.7" fwd of motor face.
- c. Payload Balanced: Static and Dynamic₂
1"oz. 8" oz.
- d. Payload Environment Tests: Spin, Vibration, and Thermal
- e. Payload Integrators: Electro-Optical Systems
- f. Payload Instrumentors:
 - 1. Electro-Optical Systems
 - 2. Ballistic Research Laboratories
 - 3. ARFA (Radio Corporation of America)
- g. Payload Description:
 - 1. Gamma Ray Scanner: Consists of four gamma ray flux tubes attached to two gamma shields, mounted at approximately 90° to each other. Scanning will be accomplished by rocket rotation. Will map vertical distribution of gamma ray sources.
 - 2. Beta Ray Detector: Designed to vertical beta ray distribution of debris. Will consist of scintillation crystal and photomultiplier tube looking out side of rocket.
 - 3. Gamma Ray Detector: Similar to beta ray detector. Contained entirely within payload, consequently is not sensitive to beta rays.
 - 4. Photometer: Consists of photomultiplier tube (1 response). Will measure intensity and distribution of N₂ emission line (3914Å) of induced aurora.
 - 5. Three-frequency phase coherent transmitter.
 - 6. 10-watt FM/FM telemeter.
 - 7. G&D-1 transmitter (1W) for telemetry and for rocket azimuth and elevation angular data.
 - 8. Three axis aspect magnetometers.

TABLE A.6 CONTINUED

9. ARPA (RCA) C-band radar beacon for trajectory and measurements of induced refractive effects.

Model AGA C/T 505 Type Transponder

h. Instrument Serial Numbers:

X Aspect Sensor: No. 637

Y Aspect Sensor: No. 638

Z Aspect Sensor: No. 635

Temp Sensor: A No. 19

B No. 11

C No. 57

D No. 27

Duracom: No. 10881

T/M PWR Converter: No. 501

Gamma Scanner Electronics: No. 4

Horiz. Scanner: No. 34 and 32

Vertical Scanner: No. 17 and 42

Beta Detector No. 3

Gamma Omni Detector: No. 4

"C" Band Beacon: No. 23

GMD-1: No. 11

T/M XMTR: No. 1588

PWR AMP: No. 885

i. Nose Cone Structure (Descriptive):

Standard D-4 Fiberglass nosecone. Nosecone will not be ejected during flight. Internal structure consists of full-length metal conic frustum from instrumentation base plate to nose of rocket. Three-frequency beacon, telemetry, and GMD-1 antennas are mounted on this conic frustum.

j. Transmitters:

1. Three-Freq. beacon: 36.44, 145.76, and 874.56 Mc 150, 100 and 500 milliwatts, respectively.

2. Telemetry 234 Mc (10 watt)

3. GMD-1 1670 Mc (1 watt)

4. RCA Beacon. Trans 5700 Mc Rec. 5775 Mc

TABLE A.6 CONTINUED

k. Antennas (Descriptive):

1. 36.44: Loop, consisting of one BRL shroud antenna mounted on metal conic frustum.
2. 145.76: Loop, two BRL shroud antennas mounted 180° apart on upper section of metal conic frustum.
3. 874.56: Stubs; two each 180° apart. They protrude from special raised section conic frustum stubs contained within heat shield.
4. 234.0: Quadraloop. Two each used. Mounted 180° apart on lower section of metal conic frustum.
5. 1670: Slots; 4 each slot, 90° apart mounted on special raised section near upper section of conic frustum.
6. RCA Beacon: Slot; 4 each slot antenna mounted 90° apart on rocket extension section.

l. Other:

The standard short rocket extension section is used. Heat shield around X-248 motor and extension section will be separated from nosecone. Rocket will not be despun.

7. GROUND INSTRUMENTATION:

1. Timing BRL and EG&G
2. GMD-1
3. Telemetry Station
4. BRL ionosphere Station (6 ant)
5. ARPA DAMP Ship coordinates

8. PROBE PATH:

- a. Launch Location: Johnston Island
- b. Launcher Number: H (5)
- c. Launcher Elevation 80° Final 81.5°
- d. Launcher Azimuth: 15° true Final 8°

TABLE A.6 CONTINUED

-
- e. Launch Day and Hour: 8 July 1962 2320:12.5 HST
 - f. Launch time (Relative to Burst): Nominal H + 20 Min; Actual H + 20 Min
3.5 sec.
 - g. Predicted and Actual Peak Attitude: Predicted 640 km
Actual 625 km
 - h. Predicted and Actual Impact Range: Predicted 1160 km
Actual 1130 km

9. METEOROLOGICAL DATA:

Azimuth based on winds 1 hr. before actual launch was 38° true

10. SUMMARY OF OPERATIONS, RESULTS OBTAINED AND COMMENTS:

Predicted velocity increments were achieved. Launcher azimuth tie bar was bent during launch and the setting changed from 8° to 10° .

TABLE A.7 LAUNCHING PROJECT CARD, ROCKET 9

1. PROGRAM: Fishbowl, Program A
2. PROJECT: 6.2; Rocket-Borne Gamma Ray Scanner
3. EVENT: Star Fish Prime
4. LOCATION OF PROJECT ACTIVITY: Johnston Island
5. VEHICLE DESCRIPTION:
 - a. Type of Rocket and Round Number: Argo D-4 Round No. 9
Aerolab No. 30
 - b. Detail Vehicle Description: Four-stage solid propellant rocket;
Honest John, Nike, Nike Booster, and X-248
 - c. Rocket and Igniter Serial Number and Time Delay:

	<u>Rocket</u>	<u>Igniter</u>	<u>Time Delay</u>
1st Stage	2998	273	0
2nd Stage	10346	Unknown	9.7 sec
3rd Stage	10336	Unknown	25 sec
4th Stage	199	Unknown	65 sec
 - d. Total Rocket Weight (Incl. Payload): 7487 lb
 - e. Total Rocket Length (Incl. Payload): 592.24 inches
 - f. Rocket Center of Gravity: 324.1 in. from first-stage nozzle
 - g. Rocket Fins (Descriptive):

Stage	1st	2nd	3rd	4th
Size	7-1/2 ft ²	2.75 ft ²	2 ft ²	None
Angle	30' cw	6.9' cw	50.4' cw	
 - h. Rocket Spin Rate:

3rd-Stage b.o.	Predicted	Measured
4th-Stage ignition	<u>6.75 rps</u>	<u>5.5 rps</u>
	<u>6.1 rps</u>	<u>5.75 rps</u>
 - i. Agency Responsible for Vehicle: Electro-Optical Systems
Aerolab Development Company
 - j. Number to be Launched: Two

TABLE A.7 CONTINUED

6. PAYLOAD:

- a. Gross Payload Weight (Incl. nose shield and extension tube): 159 lb
- b. Net Payload Weight and Length (Incl. extension tube): 133 lb 53" long
CG 20.7" fwd of motor face
- c. Payload Balanced: Static and Dynamic
1" oz. 8" oz.²
- d. Payload Environmental Tests: Spin, Vibration, Thermal
- e. Payload Integrators: Electro-Optical Systems
- f. Payload Instrumentors:
 - 1. Electro-Optical Systems
 - 2. Ballistic Research Laboratories
 - 3. ARPA (Radio Corporation of America)
- g. Payload Description:
 - 1. Gamma Ray Scanner: Consists of four gamma ray flux tubes attached to two gamma shields; mounted at approximately 90° to each other. Scanning will be accomplished by rocket rotation. Will map vertical distribution of gamma ray sources.
 - 2. Beta Ray Detector: Designed to map vertical beta ray distribution of debris. Will consist of scintillation crystal and photomultiplier tube looking out side of rocket.
 - 3. Gamma Ray Detector: Similar to beta ray detector. Contained entirely within payload, consequently is not sensitive to beta rays.
 - 4. Photometer: Consists of photomultiplier tube (S-11 response) will measure intensity and distribution of N₂ and emission line(3914A) of induced aurora.
 - 5. Three-frequency phase coherent transmitter.
 - 6. 10-watt FM/FM telemeter
 - 7. GND-1 transmitter (1W) for telemetry and for rocket azimuth and elevation angular data.

TABLE A.7 CONTINUED

-
8. Three axis aspect magnetometers.
9. ARPA (RCA) C-band radar beacon for trajectory and measurements of Induced Refractive Effects.
Model AGA C/T 505 Type Transponder
- h. Instrument Serial Numbers:
- X Aspect Sensor: No. 642
Y Aspect Sensor: No. 636
Z Aspect Sensor: No. 639
Temp Sensor: A no number
 B No. 20
 C no number
 D No. 41
- Duracom: No. 10882
T/M Power Converter: No. 503
Gamma Scanner Electronics: No. 5
Horizontal Scanner: No. 24 and 44
Vertical Scanner: No. 38 and 47
Beta Detector: No. 5
Gamma Detector: No. 3
Photometer: No. 5
"C" Band Beacon: No. 5
GMD-1: No. 20
T/M XMTR: No. 1557
Power Amplifier: No. 884
- i. Nose Cone Structure (Descriptive)
- Standard D-4 fiberglass nose cone. Nose cone will not be ejected during flight. Internal structure consists of full-length metal conic frustum from instrumentation base plate to nose of rocket. Three-frequency beacon, telemetry, and GMD-1 antennas are mounted on this conic frustum.
- j. Transmitters:
1. Three-frequency beacon: 36.44, 147.76 and 886.56 Mc
150, 100 and 500 milliwatts, respectively.
 2. 234 Mc (10 watt)

TABLE A.7 CONTINUED

-
3. GMD-1 1690 Mc(1 watt)
 4. RCA Beacon Trans 5770 Mc Rec. 5775 Mc

k. Antennas (Descriptive):

1. 36.44: Loop, consisting of one BRL shroud antenna mounted on metal conic frustum.
2. 147.76: Loop, two BRL shroud antennas mounted 180° apart on upper section of metal conic frustum.
3. 886.56: Stubs; two each 180° apart. They protrude from special raised section conic frustum stubs contained within heat shield.
4. 234: Quadraloop. Two each used. Mounted 180° apart on lower section of metal conic frustum.
5. 1690: Slots; 4 each slot, 90° apart mounted on special raised section near upper section of conic frustum.
6. RCA Beacon: Slot; 4 each slot antenna mounted 90° apart on rocket extension section.

l. Other:

The standard short rocket extension section is used. Heat shield around X-248 motor and extension section will be separated from nosecone. Rocket will not be despun.

7. GROUND INSTRUMENTATION:

1. Timing BRL and EG&G
2. GMD-1
3. Telemetry Station
4. BRL Ionosphere Station (6 Ant)
5. ARPA DAMP ship coordinates

8. PROBE PATH:

- a. Launch Location: Johnston Island
- b. Launcher Number: J (4)
- c. Launcher Elevation: 80° Final 82.7°
- d. Launcher Azimuth: 15° true Final 0°

TABLE A.7 CONTINUED

-
- e. Launch Day and Hour: 8 July 1962 2340:09 HST
 - f. Launch Time (Relative to Burst): H + 40 Min nominal and actual
 - g. Predicted and Actual Peak Altitude: Predicted 640 km
Actual 685 km
 - h. Predicted and Actual Impact Range: Predicted 1160 km
Actual 790 km

9. METEOROLOGICAL DATA:

Azimuth based on winds 1 hour before actual launch was 32° T.

10. SUMMARY OF OPERATIONS, RESULTS OBTAINED AND COMMENTS:

Predicted velocity increments were achieved.
Measured total flight time 892 sec.
Launcher azimuth tie bar was bent during launch and
setting changed from 0° to 2° .

TABLE A.8 LAUNCHING PROJECT CARD, ROCKET 15

1. PROGRAM: Fishbowl, Program A
2. PROJECT: 6.2; Rocket-Borne Gamma Ray Scanner
3. EVENT: Blue Gill Prime
4. LOCATION OF PROJECT ACTIVITY: Johnston Island
5. VEHICLE DESCRIPTION:
 - a. Type of Rocket and Round No: Honest John, Nike, Nike Booster, Round No. 15
 - b. Detail Vehicle Description: Three-stage solid propellant rocket. Honest John, Nike Booster, Nike Booster
 - c. Rocket and Igniter Serial Number and Time Delay

	<u>Rocket</u>	<u>Igniter</u>	<u>Time Delay from Launch</u>
1st Stage	3000	40	0
2nd Stage	11305	ARC #9	10 seconds
3rd Stage	UNK	ARC #10	0
4th Stage			
 - d. Total Rocket Weight (Inc. payload):
 - e. Total Rocket Length (Inc. payload):
 - f. Rocket Center of Gravity:
 - g. Rocket Fins (Descriptive):

Stage	1	2	3	Single Wedge
Type	H-J Std	Nike Std	Nike Std	Nike Std/w
Size	6 ft ²	2.5 ft ²	2.5 ft ²	
Angle	30 ft cw	26 ft ccw	21 ft cw	
 - h. Rocket Spin Rate: Estimated 3.65 rps Actual 1.7 rps
 - i. Agency Responsible for Vehicle: Electro-Optical Systems, Inc. Atlantic Research Corp.
 - j. Number to be Launched: 2

TABLE A.8 CONTINUED

6. PAYLOAD

- | | | |
|----|--|---|
| a. | Gross Payload Weight | 167 lb, CG 16.5 fwd of motor face |
| b. | Net Payload Weight and Length
(Includes extension tube) | 141 lb, 49 inches long |
| c. | Payload Balanced: | Static and dynamic |
| d. | Payload Environmental Tests: | Spin, vibration, thermal |
| e. | Payload Integrator: | Electro-Optical Systems, Inc. |
| f. | Payload Instrumentors: | <ol style="list-style-type: none"> 1. Electro-Optical Systems, Inc. 2. Ballistic Research Laboratories 3. ARPA (Radio Corp. of America) |
| g. | Payload Description: | |
| 1. | Gamma Ray Scanner: Consists of four gamma ray flux tubes mounted on two gamma shields at angles of approximately 70 degrees to each other. Scanning will be accomplished by rocket rotation. Will map vertical distribution of gamma ray sources | <ol style="list-style-type: none"> 5. Three-frequency phase coherent transmitter 6. 2.5-watt FM/FM telemeter. 7. GMD-1 transmitter for telemetry and for rocket azimuth and elevation angular data. 8. Three axis aspect magnetometer |
| 2. | Beta Ray Detector: Designed to map vertical beta ray distribution of debris. Will consist of scintillation crystal and photomultiplier will look out side of rocket. | <ol style="list-style-type: none"> 9. ARPA (RCA) C-band radar beacon for trajectory and measurements of Induced Refractive Effects. Model 505A |
| 3. | Gamma Ray Detector: Similar to beta ray detector. Contained entirely within payload consequently is not sensitive to beta rays. | |
| 4. | Photometer: Consists of photomultiplier tube (S-11 response) will measure intensity and distribution of N_2 + emission line (3914Å) of induced aurora. | |

TABLE A.8 CONTINUED

- | | |
|--|--|
| h. Nose Cone Structure
(Descriptive): | Standard D-4 fiberglass nose cone. Nose cone will not be ejected during flight. Internal structure consists of full-length metal conic frustum from instrumentation base plate to nose of rocket. Three-frequency beacon, telemetry, and GMD-1 antennas are mounted on the conic frustum. A mating section from rocket (smaller dia.) to D-4 nose cone and instrumentation plate is utilized. RCA beacon antennas are mounted on this mating section as well as the pullaway receptacle. |
| i. Transmitters: | <ol style="list-style-type: none"> 1. Three-frequency beacon. 36.44, 145.76, and 874.56 Mc (150,100, and 500 milliwatts, respectively) 2. Telemetry 234 Mc (5 watt) 3. GMD-1 1690 (1 watt) 4. RCA Beacon Trans
Rec |
| j. Antennas (Descriptive): | <ol style="list-style-type: none"> 1. 36.44: Loop, consisting of one BRL shroud antenna mounted on metal conic frustum. 2. 145.76: Loop, two BRL shroud antennas mounted 180 degrees apart on upper section of metal conic frustum. 3. 874.56: Stubs; two each 180 degrees apart. They protrude from a special raised section on conic frustum. Stubs contained within heat shield. 4. 234: Quadraloop. Two each used. Mounted 180 degrees apart on lower section of conic frustum. 5. 1680: Slots; 4 each 90 degrees apart mounted on special raised section near upper section of conic frustum. 6. RCA Beacon: Bent valentine; two each mounted 180 degrees apart on nose cone rocket mating section. |
| k. Other: | |

TABLE A.8 CONTINUED

7.	GROUND INSTRUMENTATION	1. Timing BRL and EG&G 2. GMD-1 3. Telemetry Station 4. BRL ionosphere Station (6 ant) 5. ARPA DAMP Ship coordinates
8.	PROBE PATH:	
	a. Launch Location:	Johnston Island
	b. Launcher Number:	H (5)
	c. Launcher Elevation:	85 degrees Final 83 degrees
	d. Launcher Azimuth:	18 degrees true Final 0 degrees
	e. Launch Day and Hour:	26 00 ^h 14 ^m 49 ^s
	f. Launch Time (Relative to Burst):	H +15 minutes
	g. Predicted and Actual Peak Altitude:	Predicted 129 km Actual 137 km
	h. Predicted and Actual Impact Range:	Predicted 100 km Actual 170 km
9.	METEOROLOGICAL DATA:	
10.	SUMMARY OF OPERATIONS, RESULTS OBTAINED, AND COMMENTS	Severe coning

TABLE A.9 LAUNCHING PROJECT CARD, ROCKET 18

-
1. PROGRAM: Fishbowl, Program A
2. PROJECT: 6.2; Rocket-Borne Gamma Ray Scanner
3. EVENT: Blue Gill Prime
4. LOCATION OF PROJECT ACTIVITY: Johnston Island
5. VEHICLE DESCRIPTION:
- a. Type of Rocket and Round No: Honest John, Nike, Nike, Round No. 18
- b. Detail Vehicle Description: Three-stage solid propellant rocket; Honest John, Nike Booster, and Nike Booster
- c. Rocket and Igniter Serial
- | Number and Time Delay | Rocket | Igniter | Time Delay from Launch |
|-----------------------|--------|------------|------------------------|
| 1st Stage | 4078 | 25 | 0 |
| 2nd Stage | 10207 | Arc No. 8 | 10 sec |
| 3rd Stage | 11618 | ARC No. 11 | 0 |
| 4th Stage | | | |
- d. Total Rocket Weight (Inc. payload):
- e. Total Rocket Length (Inc. payload):
- f. Rocket Center of Gravity:
- g. Rocket Fins (Descriptive):
- | | Stage 1 | 2 | 3 |
|-------|-------------------|---------------------|---------------------|
| Type | H-J Std | Nike Std | Single wedge |
| Size | 6 ft ² | 2.5 ft ² | 2.5 ft ² |
| Angle | 30 ft cw | 26 ft cw | 21 ft cw |
- h. Rocket Spin Rate: Estimated 3.65 rps Actual 1.5
- i. Agency Responsible for Vehicle: Electro-Optical Systems, Inc.
Atlantic Research Corporation
- j. Number to be Launched: 2

TABLE A.9 CONTINUED

6. PAYLOAD

- a. Gross Payload Weight 167 lb, CG 16.5 inches fwd of motor face
- b. Net Payload Weight and Length (Includes extension tube) 141 lb, 49 inches overall length
- c. Payload Balanced: Static and dynamic
- d. Payload Environmental Tests: Spin, vibration and thermal
- e. Payload Integrator: Electro-Optical Systems, Inc.
- f. Payload Instrumentors: Electro-Optical Systems, Inc.
Ballistic Research Laboratories
ARPA (RCA)

g. Payload Description:

- 1. Gamma Ray Scanner: Consists of four gamma ray flux tubes mounted on two gamma shields at angles of approximately 90 degrees to each other. Scanning will be accomplished by rocket rotation. Will map vertical distribution of gamma ray sources.
- 2. Beta Ray Detector: Designed to map vertical beta ray distribution of debris. Will consist of scintillation crystal and photo-multiplier will look out side of rocket.
- 3. Gamma Ray Detector: Similar to beta ray detector. Contained entirely within payload consequently is not sensitive to beta rays.
- 4. Photometer: Consists of photo multiplier tube (S-11 response) will measure intensity and distribution of N_2 + emission line (3914Å) of induced aurora.
- 5. Three-frequency phase coherent transmitter.
- 6. 2.5-watt FM/FM telemeter.
- 7. GMD-1 transmitter for telemetry and for rocket azimuth and elevation angular data.
- 8. Three axis aspect magnetometer.
- 9. ARPA (RCA) C band radar beacon for trajectory and measurements of Induced Refractive Effects. Model 505A

TABLE A.9 CONTINUED

- | | |
|--|--|
| h. Nose Cone Structure
(Descriptive): | Standard D-4 fiberglass nose cone. Nose cone will not be ejected during flight. Internal structure consists of full length metal conic frustum from instrumentation base plate to nose of rocket. Three-frequency beacon, telemetry, and GMD-1 antennas are mounted on the conic frustum. A mating section from rocket (smaller div.) to D-4 nose cone and instrumentation plate is utilized. RCA beacon antennas are mounted on this mating section as well as the pullaway receptacle. |
| i. Transmitters: | <ol style="list-style-type: none"> 1. Three-frequency phase-coherent transmitters. 36.44; 145.76 and 874.56 Mc (150, 100, and 500 milliwatts, respectively) 2. Telemetry 234 Mc (2.5 watt) 3. GMD-1 1670 Mc (1 watt) 4. RCA Beacon Rec |
| j. Antennas (Descriptive): | <ol style="list-style-type: none"> 1. 36.44: Loop, consisting of one BRL shroud antenna mounted on metal conic frustum. 2. 145.76: Loop; two BRL shroud antennas mounted 180 degrees apart on upper section of metal conic frustum. 3. 874.56: Stubs; two each 180 degrees apart. They protrude from a special raised section on conic frustum. Stubs contained within heat shield. 4. 234: Quadraloop. Two each used, mounted 180 degrees apart on lower section of conic frustum. 5. 1670: Slots; four each 90 degrees apart, mounted on special raised section near upper section of conic frustum. 6. RCA Beacon: Bent valentine; two each mounted 180 degrees apart on nose cone—rocket mating section. |
| k. Other: | |

TABLE A.9 CONTINUED

7.	GROUND INSTRUMENTATION	1. Timing BRL and EG&G 2. GMD-1 3. Telemetry Station 4. ARPA (DAMP ship) coordinates 5. BRL ionosphere station (6 ant.)
8.	PROBE PATH:	
	a. Launch Location:	Johnston Island
	b. Launcher Number:	J (4)
	c. Launcher Elevation:	85 degrees Final 83 degrees
	d. Launcher Azimuth:	18 degrees true Final 0 degree
	e. Launch Day and Hour:	26 00 ^h 30 ^m 49 ^s
	f. Launch Time (Relative to Burst):	H +1860 seconds
	g. Predicted and Actual Peak Altitude:	Predicted 129 km Actual 51.4 km
	h. Predicted and Actual Impact Range:	Predicted 100 km Actual ~42 km
9.	METEOROLOGICAL DATA:	
10.	SUMMARY OF OPERATIONS, RESULTS OBTAINED, AND COMMENTS	Severe coning, third stage tumbled

TABLE A.10 LAUNCHING PROJECT CARD, ROCKET 19

-
1. PROGRAM: Fishbowl, Program A
2. PROJECT: 6.2; Rocket-borne Gamma Ray Scanner
3. EVENT: King Fish
4. LOCATION OF PROJECT ACTIVITY: Johnston Island
5. VEHICLE DESCRIPTION:
- a. Type of Rocket and Round No: Honest John, Nike-Nike Booster
Round No. 19
- b. Detail Vehicle Description: Three-stage solid propellant rocket.
Honest John and two Nike boosters.
- c. Rocket and Igniter Serial
- | Number and Time Delay | Rocket | Igniter | Time Delay from Launch |
|-----------------------|--------|-----------|------------------------|
| 1st Stage | 1847 | 21 | 0 |
| 2nd Stage | 10363 | ADC No. 5 | 9.5 seconds |
| 3rd Stage | 10441 | ADC No. 2 | 26.5 seconds |
| 4th Stage | | | |
- d. Total Rocket Weight
(Inc. payload): 6,965 lb
- e. Total Rocket Length
(Inc. payload): 523 inches
- f. Rocket Center of Gravity: 205 inches from first stage nozzle
- g. Rocket Fins (Descriptive):
First stage: Double wedge type, 31 minutes clockwise (average) incidence
Second stage: 3½ ft², Double wedge type, 2 ft ccw incidence
Third stage: 2-¾ ft², Double swept, single wedge type, 17 ft cw incidence
- h. Rocket Spin Rate: Estimated 5.5 rps Actual 2.0 rps nominal
- i. Agency Responsible for Vehicle: Electro-Optical Systems, Inc.
Aerolab
- j. Number to be Launched: 7

TABLE A.10 CONTINUED

6. PAYLOAD

- a. Gross Payload Weight 210 lb
- b. Net Payload Weight and Length (Includes extension tube) 140 lb, 49 inches overall length
- c. Payload Balanced: 1 inch/ounce
- d. Payload Environmental Tests: Shock, vibration, thermal per specifications
- e. Payload Integrator: Electro-Optical Systems, Inc.
- f. Payload Instrumentors:
 - 1. Electro-Optical Systems, Inc.
 - 2. Ballistic Research Laboratories
 - 3. ARPA (Radio Corp. of America)
- g. Payload Description:
 - 1. Gamma Ray Scanner: Consists of four gamma ray flux tubes attached to two gamma shields mounted at approximately 90 degrees to each other. Scanning will be accomplished by rocket rotation. Will map vertical distribution of gamma ray sources.
 - 2. Beta Ray Detector: Designed to map vertical beta ray distribution of debris. Will consist of scintillation crystal and photomultiplier tube looking outside of rocket.
 - 3. Gamma Ray Detector: Similar to beta ray detector. Contained entirely within payload, consequently is not sensitive to beta rays.
 - 4. Photometer: Consists of photomultiplier tube (S-11 response) will measure intensity and distribution of N_2 and emission line (3914Å) of induced aurora.
 - 5. Three-frequency phase coherent transmitter.
 - 6. 10-watt FM/FM telemeter
 - 7. GMD-1 transmitter (1 watt) for telemetry and for rocket azimuth and elevation angular data.
 - 8. Three axis aspect magnetometers.
 - 9. ARPA (RCA) C-band radar beacon for trajectory and measurements of Induced Refractive Effects. Model 505A

TABLE A.10 CONTINUED

<p>h. Nose Cone Structure (Descriptive):</p>	<p>Standard D-4 fiberglass nose cone. Nose cone will not be ejected during flight. Internal structure consists of full-length metal conic frustum instrumentation base plate to nose of rocket. Three-frequency beacon, telemetry, and GMD-1 antennas are mounted on this conic frustum.</p>
<p>i. Transmitters:</p>	<ol style="list-style-type: none"> 1. Three-frequency beacon: 36.94, 147.76, and 886.56 Mc; 150, 100, and 500 milliwatts, respectively. 2. 234 Mc (10 watt) 3. GMD-1 1660 Mc (1 watt) 4. RCA Beacon Trans. 5750 Mc Rec. 5825 Mc
<p>j. Antennas (Descriptive):</p>	<ol style="list-style-type: none"> 1. 36.94: Loop, consisting of one BRL shroud antenna mounted on metal conic frustum. 2. 147.76: Loop, two BRL shroud antennas mounted 180 degrees apart on upper section of metal conic frustum. 3. 886.56: Stubs, two each 180 degrees apart. They protrude from special raised section conic frustum stubs contained within heat shield. 4. 234: Turnstiles, four each used. Mounted 90 degrees apart on mid-section of metal extension tube. 5. 1660 Mc : Slots, four each slot, 90 degrees apart mounted on special raised section near upper section of conic frustum. 6. RCA Beacon: two each bent valentine antenna mounted 180 degrees apart on rocket extension section.
<p>k. Other:</p>	

TABLE A.10 CONTINUED

7.	GROUND INSTRUMENTATION	1. Timing BRL and EG&G 2. GMD-1 3. Telemetry Station 4. BRL Ionosphere Station (6 ant) 5. ARPA DAMP ship coordinates				
8.	PROBE PATH:					
	a. Launch Location:	Johnston Island				
	b. Launcher Number:	1				
	c. Launcher Elevation:	85 degrees Final 86.1 degree				
	d. Launcher Azimuth:	120 degrees true Final 155 degrees				
	e. Launch Day and Hour:	1 November 1962, 0208:6.5				
	f. Launch Time (Relative to Burst):	H-2 minutes				
	g. Predicted and Actual Peak Altitude:	<table border="0" style="margin-left: 20px;"> <tr> <td style="padding-right: 10px;">Predicted</td> <td>190 km</td> </tr> <tr> <td>Actual</td> <td>185 km</td> </tr> </table>	Predicted	190 km	Actual	185 km
Predicted	190 km					
Actual	185 km					
	h. Predicted and Actual Impact Range:	<table border="0" style="margin-left: 20px;"> <tr> <td style="padding-right: 10px;">Predicted</td> <td>110 km</td> </tr> <tr> <td>Actual</td> <td>95 km</td> </tr> </table>	Predicted	110 km	Actual	95 km
Predicted	110 km					
Actual	95 km					
9.	METEOROLOGICAL DATA:					
10.	SUMMARY OF OPERATIONS, RESULTS OBTAINED, AND COMMENTS					

TABLE A.11 LAUNCHING PROJECT CARD, ROCKET 26

1. PROGRAM: Operation Fishbowl, Program A
2. PROJECT: 6.2; Rocket-borne Gamma Ray Scanner
3. EVENT: King Fish
4. LOCATION OF PROJECT ACTIVITY: Johnston Island
5. VEHICLE DESCRIPTION:
- a. Type of Rocket and Round No: Honest John, Nike-Nike Booster No. 26
- b. Detail Vehicle Description: Three-stage solid propellant rocket. Honest John and two Nike Boosters.
- c. Rocket and Igniter Serial
- | Number and Time Delay | Rocket | Igniter | Time Delay from Launch |
|-----------------------|--------|-----------|------------------------|
| 1st Stage | 1729 | 56 | 0 |
| 2nd Stage | 10406 | ADC No. 9 | 9.5 sec. |
| 3rd Stage | 10425 | ADC No. 7 | 26.5 sec. |
| 4th Stage | | | |
- d. Total Rocket Weight (Inc. payload): 6.965 pounds
- e. Total Rocket Length (Inc. payload): 523 inches
- f. Rocket Center of Gravity: 205 inches from first stage nozzle
- g. Rocket Fins (Descriptive):
- 1st Stage: Avg. incidence = 33.3 ft cw; Double wedge type
- 2nd Stage: 3 1/2 ft², Double wedge type, 2 ft ccw incidence
- 3rd Stage: 2 3/4 ft², Double swept, single wedge, 17 ft cw incidence per fin
- h. Rocket Spin Rate: Estimated 5.5 rps Actual 3.2 rps nom.
- i. Agency Responsible for Vehicle: Aerolabs
Electro-Optical Systems
- j. Number to be Launched: 7

TABLE A.11 CONTINUED

6. PAYLOAD

a.	Gross Payload Weight (Inc. nose shield and extension tube)	210 pounds	
b.	Net Payload Weight and Length (Inc. extension tube)	140 pounds	42 inches
c.	Payload Balanced:	1 in. oz static	
d.	Payload Environmental Tests:	Shock, vibration, thermal per specification	
e.	Payload Integrator:	Electro-Optical Systems	
f.	Payload Instrumentors:	<ol style="list-style-type: none"> 1. Electro-Optical Systems 2. Ballistic Research Laboratories 3. AKPA (Radio Corp. of America) 	
g.	Payload Description:	<p>(1) Gamma Ray Scanner: Consists of four gamma ray flux tubes attached to two gamma shields mounted at approx. 90° to each other. Scanning will be accomplished by rocket rotation. Will map vertical distribution of gamma ray sources.</p> <p>(2) Beta Ray Detector: Designed to measure vertical beta ray distribution of debris. Will consist of scintillation crystal and photo-multiplier tube looking outside of rocket.</p> <p>(3) Gamma Ray Detector: Similar to beta ray detector. Contained entirely within payload, consequently is not sensitive to beta rays.</p> <p>(4) Photometer: Consists of photo-multiplier tube (S-11 response). Will measure intensity and distribution of N₂ and emission line (3194Å) of induced aurora.</p> <p>(5) 10-watt FM/FM telemeter.</p> <p>(6) GMD-1 transmitter (1W) for telemetry and for rocket azimuth and elevation angular data.</p> <p>(7) Three axis aspect magnetometers.</p> <p>(8) ARPA (RCA) C-band radar beacon for trajectory and measurements of induced refractive effects.</p> <p>Model 505A Type</p>	

TABLE A.11 CONTINUED

h. Nose Cone Structure (Descriptive):	Standard D-4 Fiberglas nosecone. Nose cone will not be ejected during flight. Internal structure consists of full-length metal conic frustum from instrumentation base plate to nose of rocket. GMD-1 antennas are mounted on this conic frustum.
i. Transmitters:	(1) Telemetry 245.3 Mc (10 watt) (2) GMD-1 1680 Mc (1 watt) (3) RCA Beacon Trans. 5700 Mc Rec. 5775 Mc
j. Antennas (Descriptive):	(1) 245.3; Turnstile. Four each used. Mounted 90° apart on mid-section of metal extension tube. (2) 1680: Slots; four each slot, 90° apart mounted on special raised section near upper section of conic frustum. (3) RCA Beacon: Two bent valentine antenna mounted 180° apart on rocket extension section.
k. Other:	

TABLE A.11 CONTINUED

7.	GROUND INSTRUMENTATION	(1) Timing BRL and EG&G (2) GMD-1 (3) Telemetry Station (4) ARPA DAMP Ship Coordinates
8.	PROBE PATH:	
	a. Launch Location:	Johnston Island
	b. Launcher Number:	2
	c. Launcher Elevation:	85° Final 86.1°
	d. Launcher Azimuth:	120° true Final 155°
	e. Launch Day and Hour:	1 November 1962 0223 hours 06.5 seconds
	f. Launch Time (Relative to Burst):	H + 13 minutes
	g. Predicted and Actual Peak Altitude:	Predicted 190 km Actual 172
	h. Predicted and Actual Impact Range:	Predicted 110 km Actual 110
9.	METEOROLOGICAL DATA:	
10.	SUMMARY OF OPERATIONS, RESULTS OBTAINED, AND COMMENTS	

TABLE A.12 LAUNCHING PROJECT CARD, ROCKET 29

-
1. PROGRAM: Operation Fishbowl, Program A
2. PROJECT: 6.2; Rocket-borne Gamma Ray Scanner
3. EVENT: King Fish
4. LOCATION OF PROJECT ACTIVITY: Johnston Island
5. VEHICLE DESCRIPTION:
- a. Type of Rocket and Round No: Honest John, Nike-Nike Booster No. 29
- b. Detail Vehicle Description: Three-stage solid propellant rocket. Honest John and two Nike Boosters.
- c. Rocket and Igniter Serial Number and Time Delay
- | | <u>Rocket</u> | <u>Igniter</u> | <u>Time Delay from Launch</u> |
|-----------|---------------|----------------|-------------------------------|
| 1st Stage | 4079 | 18 | |
| 2nd Stage | 10430 | ADC No. 7 | 9.5 seconds |
| 3rd Stage | 10377 | ADC No. 8 | 26.5 seconds |
| 4th Stage | | | |
- d. Total Rocket Weight (Inc. payload): 6,965 pounds
- e. Total Rocket Length (Inc. payload): 523 inches
- f. Rocket Center of Gravity: 205 inches from first stage nozzle
- g. Rocket Fins (Descriptive):
- 1st Stage: Dble wedge type, 30 ft cw incidence (average)
 - 2nd Stage: 3 1/2 ft², dble wedge type, 2 ft cw incidence per fin
 - 3rd Stage: 2 3/4 ft², dble swept, single wedge type, 17 ft cw incidence per fin.
- h. Rocket Spin Rate:
- | | Estimated | Actual |
|--|-----------|--------------|
| | 5.5 rps | 2.5 rps NOM. |
- i. Agency Responsible for Vehicle: Electro Optical Systems
Aerolabs
- j. Number to be Launched: 7

TABLE A.12 CONTINUED

6. PAYLOAD

- a. Gross Payload Weight (Inc. nose shield and extension tube) 210 pounds
- b. Net Payload Weight and Length (Inc. extension tube) 140 pounds 42 inches
- c. Payload Balanced: 1 in oz static
- d. Payload Environmental Tests: Shock, Vibration, thermal per specification

- e. Payload Integrator: Electro-Optical Systems

- f. Payload Instrumentors:
 - 1. Electro-Optical Systems
 - 2. Ballistic Research Laboratories
 - 3. ARPA (Radio Corp. of America)

- g. Payload Description:
 - (1) Gamma Ray Scanner: Consists of four gamma ray flux tubes attached to two gamma shields mounted at approximately 90° to each other. Scanning will be accomplished by rocket rotation. Will map vertical distribution of gamma ray sources.
 - (2) Beta Ray Detector: Designed to map vertical beta ray distribution of debris. Will consist of scintillation crystal and photo-multiplier tube looking outside of rocket.
 - (3) Gamma Ray Detector: Similar to beta ray detector. Contained entirely within payload, consequently is not sensitive to beta rays.
 - (4) Photometer: Consist of photo-multiplier tube (S-11 response) will measure intensity and distribution of N₂ and emission line (3914Å) of induced aurora.
 - (5) Three-frequency phase coherent transmitter
 - (6) 10-watt FM/FM telemeter.
 - (7) GMD-1 transmitter (1W) for telemetry and for rocket azimuth and elevation angular data.
 - (8) Three axis aspect magnetometers.
 - (9) ARPA (RCA) C band radar beacon for trajectory and measurements of Induced Refractive Effects.

Model 505A
Type

TABLE A.12 CONTINUED

h. Nose Cone Structure
(Descriptive):

Standard D-4 fiberglass nose cone. Nose cone will not be ejected during flight. Internal structure consists of full-length metal conic frustum instrumentation base plate to nose of rocket. Three frequency beacon, and GMD-1 antennas are mounted on this conic frustum.

i. Transmitters:

- (1) Three-frequency beacon: 36.94, 147.76, and 886.56 Mc; 150, 100, and 500 milliwatts, respectively.
- (2) 245.3 Mc (10 watt)
- (3) GMD-1 1660 Mc (1 watt)
- (4) RCA Beacon Trans. 5700 Mc
Rec. 5775 Mc

j. Antennas (Descriptive):

- (1) 36.94: Loop, consisting on one BRL shroud antenna mounted on metal conic frustum
- (2) 147.76: Loop, two BRL shroud antennas mounted 180° apart on rocket extension section.
- (3) 886.56: Stubs; two each 180° apart. They protrude from special raised section conic frustum stubs contained with heat shield.
- (4) 245.3: Turnstiles. 4 each used. Mounted 90° apart on midsection of metal extension tube.
- (5) 1660 Mc: Slots; 4 each slot, 90° apart mounted on special raised section near upper section of conic frustum.
- (6) RCA Beacon: 2 each bent valentine antenna mounted 180° apart on rocket extension section.

k. Other:

TABLE A.12 CONTINUED

7.	GROUND INSTRUMENTATION	(1) Timing BRL and EG&G (2) GMD-1 (3) Telemetry Station (4) BRL Ionosphere Station (6 Ant) (5) ARPA DAMP ship coordinates				
8.	PROBE PATH:					
	a. Launch Location:	Johnston Island				
	b. Launcher Number:	4				
	c. Launcher Elevation:	85° Final 86.1°				
	d. Launcher Azimuth:	120° true Final 155°				
	e. Launch Day and Hour:	1 November 1962 0235 hours 6.5 seconds				
	f. Launch Time (Relative to Burst):	H + 25 minutes				
	g. Predicted and Actual Peak Altitude:	<table border="0" style="margin-left: 20px;"> <tr> <td>Predicted</td> <td>194 km</td> </tr> <tr> <td>Actual</td> <td>67</td> </tr> </table>	Predicted	194 km	Actual	67
Predicted	194 km					
Actual	67					
	h. Predicted and Actual Impact Range:	<table border="0" style="margin-left: 20px;"> <tr> <td>Predicted</td> <td>100 km</td> </tr> <tr> <td>Actual</td> <td>41</td> </tr> </table>	Predicted	100 km	Actual	41
Predicted	100 km					
Actual	41					
9.	METECROLOGICAL DATA:					
10.	SUMMARY OF OPERATIONS, RESULTS OBTAINED, AND COMMENTS	Second stage failure				

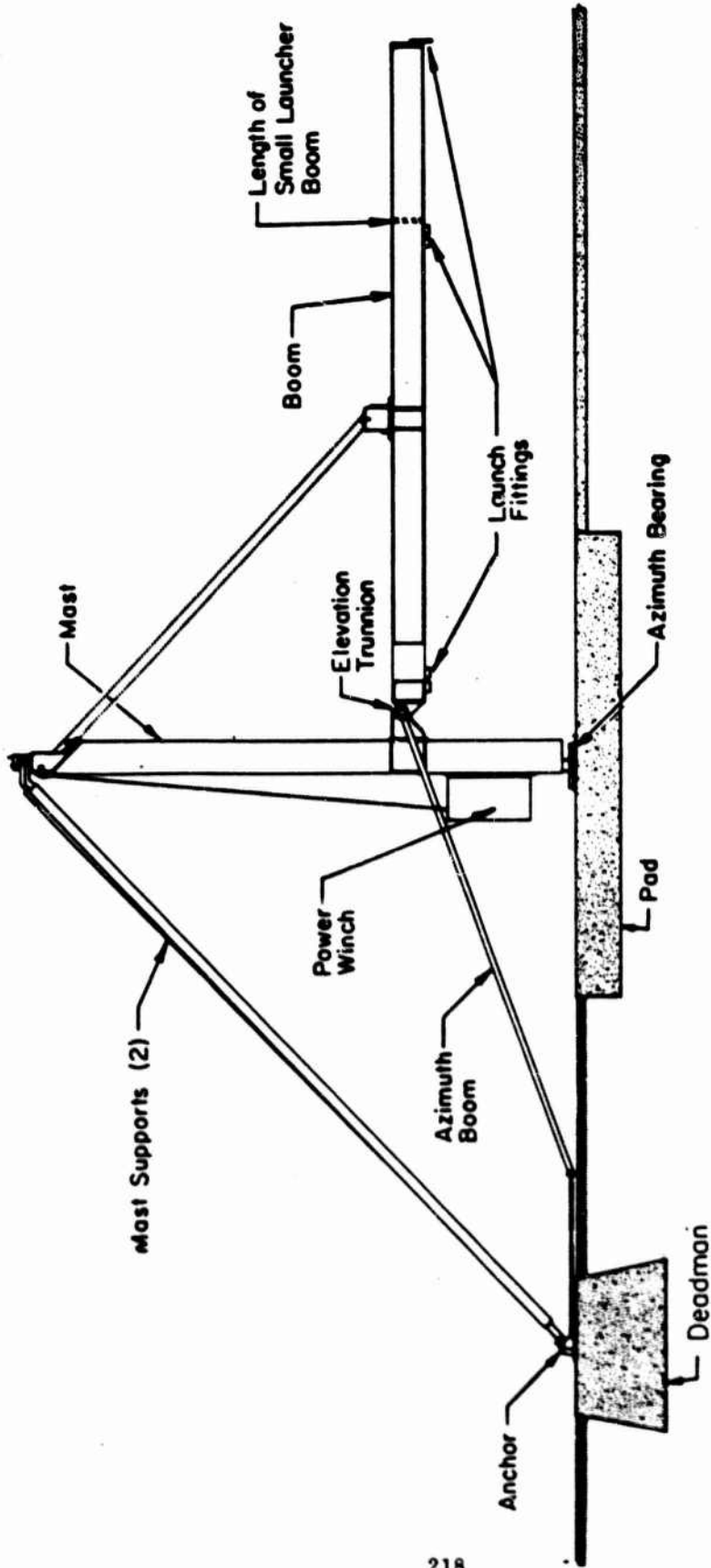


Figure A.1 Large launcher (elevation view).

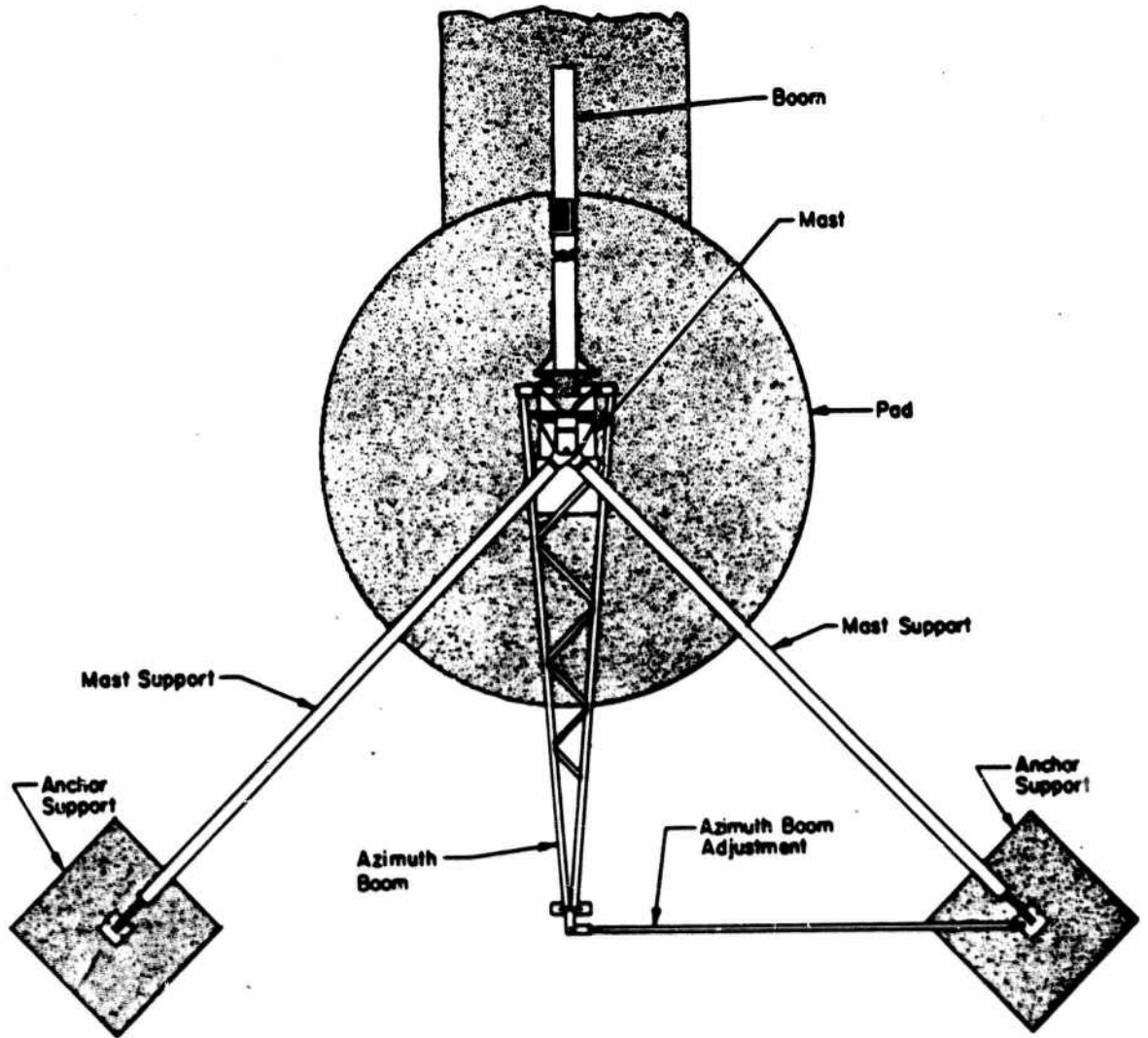


Figure A.2 Large launcher (plan view).

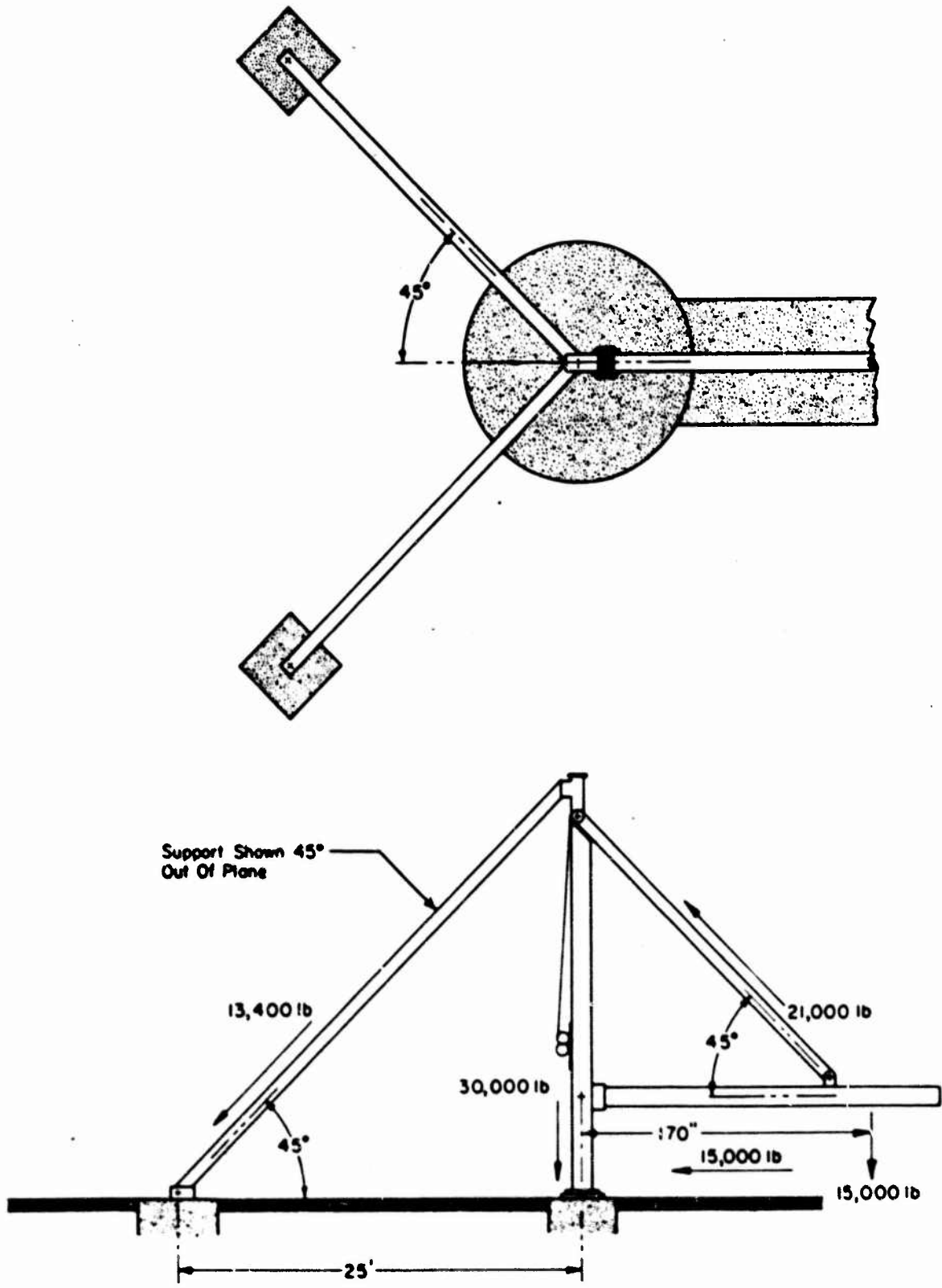


Figure A.3 Large launcher (loading diagram).

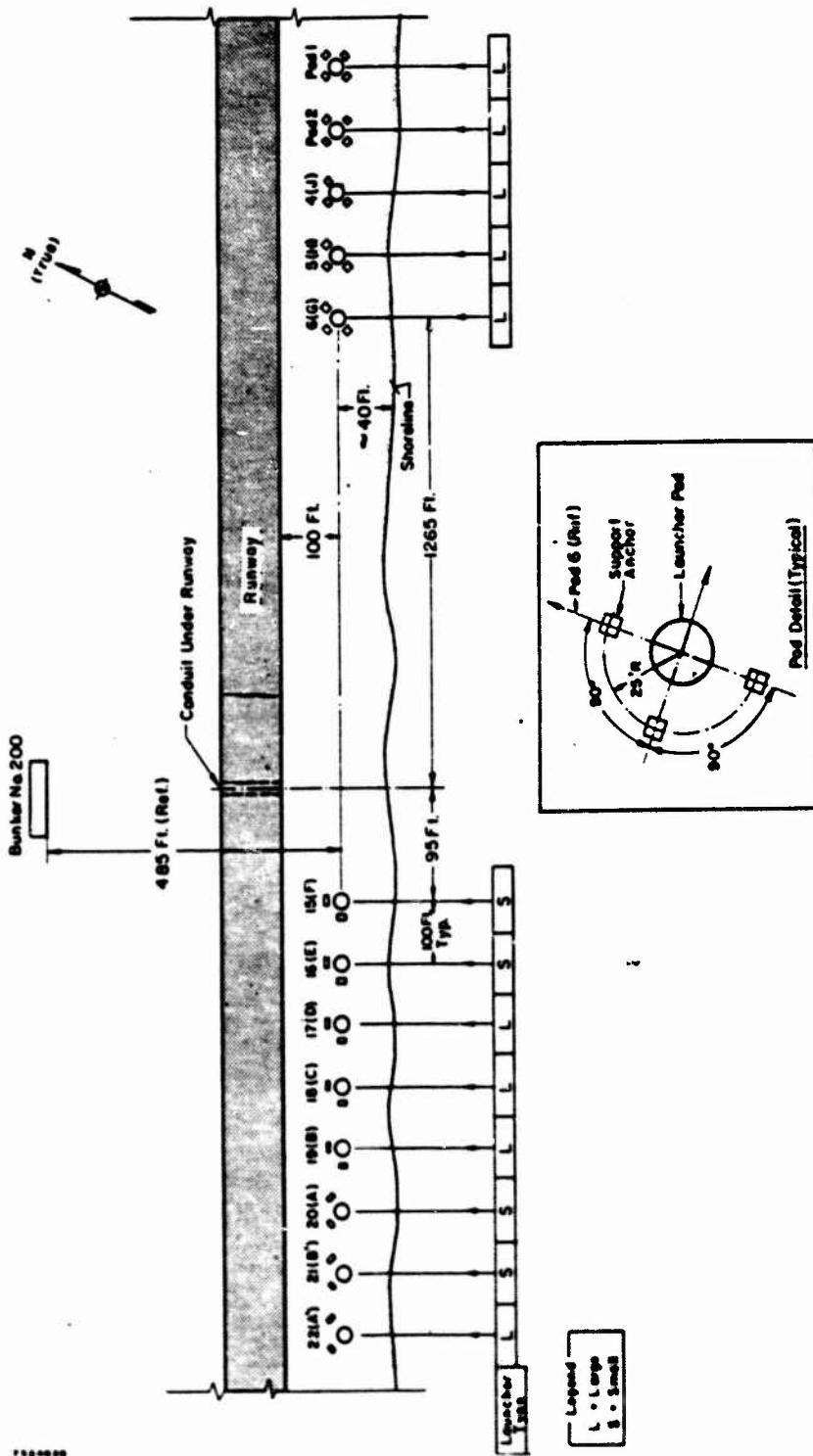
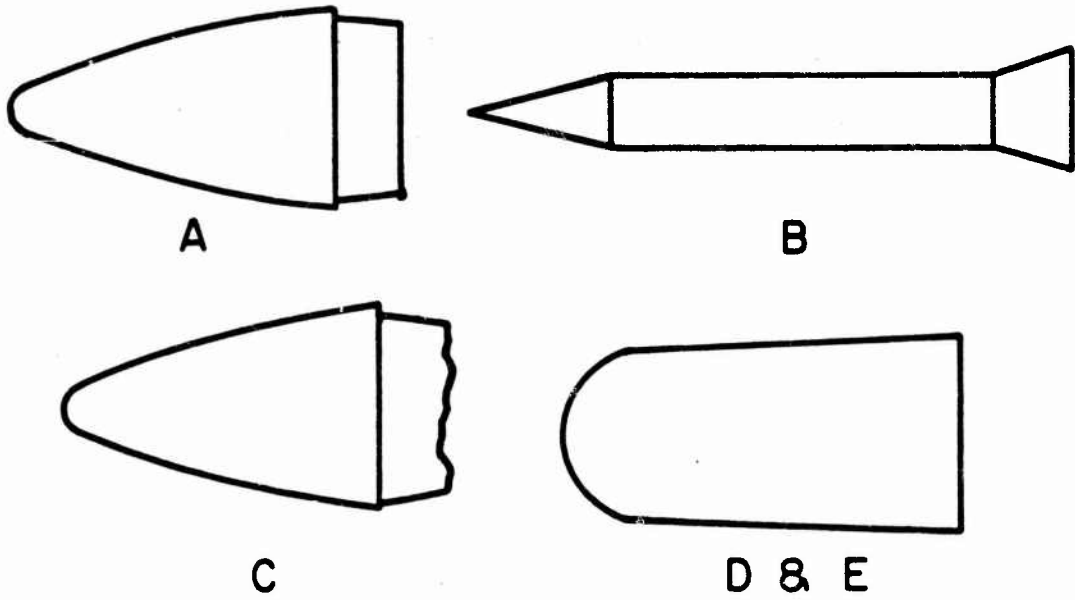


Figure A.4 Launcher locations, Projects 6.2, 6.3, and 6.4.



<u>Payload</u>	<u>Net (lb)</u>	<u>Ballast (lb)</u>	<u>Gross (lb)</u> *	<u>Rocket No.</u>
A	125	—	167	15, 18
A'	125	45	212	19, 26 & 29
B			290	11, 12, 14, 17, 20, 24, 27 & 28
C	125		161	8 & 9
D	132		189.5	1, 22 & 25
E	123		180.5	5 & 7

* Includes Nose Cone

Figure A.5 Payload designation and nose cone outlines.

APPENDIX B
ROCKET VEHICLE PERFORMANCE

B.1 INTRODUCTION

In the determination of a missile's flight path, ground-based instrumentation dispersed over several sites generally allows more flexibility and greater accuracy in data reduction than measuring systems concentrated at a single location. In addition to providing less accuracy, single-site systems frequently fail to yield sufficient data for position determination without the introduction of constraints such as parabolic or elliptical motion. To arrive at a trajectory under single-site conditions, it becomes necessary to assume that the motion of the missile may be characterized by a set of parameters that are functionally related to the measured quantities. A solution is possible if there are at least as many observations as parameters, and if the resulting system of condition equations is sufficiently independent.

The reduction and analysis of a large portion of the observed rocket trajectory data for Projects 6.2, 6.3, and 6.4 were based upon the flight paths of the missiles as a function of time. For many rockets, the various missile-tracking systems operating at or near Johnston Island failed to provide adequate coverage to meet all trajectory requirements. Therefore, it became necessary to develop methods of position determination from a combination of various measurements or observations. Frequently, these observations were neither of sufficient quantity nor quality to permit a high order of accuracy. Fortunately, most of the rocket measurements of atmospheric and event parameters could tolerate moderate errors in position determination, provided that the differential in position varied smoothly. In view of the relatively lax requirements for accuracy and the limited precision of the observations, it was considered reasonable to characterize the drag-free portion of the trajectory by simple parabolic motion.

B.2 TRAJECTORY PARAMETERS

With the assumption of parabolic motion within a plane, the reduction problem became two-dimensional. If ρ is defined as the horizontal coordinate and y as the vertical, the equations of motion are,

$$\rho = \rho_0 + \dot{\rho}_0(t-t_0) \quad (\text{B.1})$$

$$y = y_0 + \dot{y}_0(t-t_0) - 1/2 g(t-t_0)^2 \quad (\text{B.2})$$

where ρ_0 and y_0 are the position coordinates, and $\dot{\rho}_0$ and \dot{y}_0 are the velocity components for the initial time t_0 . The time variable is t , and $-g$ is the vertical component of acceleration resulting from the force of gravity which is assumed constant for each trajectory determination, but variable from rocket to rocket. For convenience, let $T \equiv (t-t_0)$ so that the above equations become

$$\rho = \rho_0 + \dot{\rho}_0 T \quad (\text{B.3})$$

$$y = y_0 + \dot{y}_0 T - 1/2 g T^2 \quad (\text{B.4})$$

The velocity components are obtained by differentiating the last two equations.

$$\dot{\rho} = \dot{\rho}_0 \quad (\text{B.5})$$

$$\dot{y} = \dot{y}_0 - g T \quad (\text{B.6})$$

Hence, if the parameters ρ_0 , y_0 , $\dot{\rho}_0$, and \dot{y}_0 can be evaluated from the observed data, position and velocity are determined as a function of time by the last four equations.

B.3 TRAJECTORY SOLUTIONS

A complete solution, for the problem as formulated, consisted of using the measured data to evaluate ρ_0 , y_0 , $\dot{\rho}_0$, and \dot{y}_0 , the trajectory parameters. This required the derivation of a system of equations of condition which related the trajectory parameters to the observed data.

Since Equations B.3 through B.6 relate the position and velocity components of the missile to the trajectory parameters and time, it is necessary to initially establish a functional relationship between the measured quantities and the missile's position and velocity. It was sufficient for the rocket flights here discussed to express the slant range r , and elevation angle ϵ , in terms of the position coordinates, while developing \dot{r} in terms of both the position coordinates and the velocity components. The equations follow:

$$r = \sqrt{\rho^2 + y^2} \quad (\text{B.7})$$

$$\epsilon = \tan^{-1}(y/\rho) \quad (\text{B.8})$$

$$\dot{r} = (\rho\dot{\rho} + y\dot{y})/r \quad (\text{B.9})$$

Combining the above equations with Equations B.3 through B.6, there result:

$$r = \sqrt{(\rho_0 + \dot{\rho}_0 T)^2 + (y_0 + \dot{y}_0 T - 1/2gT^2)^2} \quad (\text{B.10})$$

$$\epsilon = \tan^{-1}[(y_0 + \dot{y}_0 T - 1/2gT^2)/(\rho_0 + \dot{\rho}_0 T)] \quad (\text{B.11})$$

$$\begin{aligned} \dot{r} = & [(\rho_0 + \dot{\rho}_0 T)(\dot{\rho}_0) + (y_0 + \dot{y}_0 T - 1/2gT^2)(\dot{y}_0 - gT)] \\ & \times \left[\sqrt{(\rho_0 + \dot{\rho}_0 T)^2 + (y_0 + \dot{y}_0 T - 1/2gT^2)^2} \right]^{-1} \end{aligned} \quad (\text{B.12})$$

In particular, when $t = t_0$ so that $T = 0$, Equations B.10, B.11, and B.12 reduce to:

$$r_0 = \sqrt{\rho_0^2 + y_0^2} \quad (\text{B.13})$$

$$\epsilon_0 = \tan^{-1}(y_0/\rho_0) \quad (\text{B.14})$$

$$\dot{r}_0 = (\rho_0\dot{\rho}_0 + y_0\dot{y}_0)/r_0 \quad (\text{B.15})$$

Where r_0 , ϵ_0 , and \dot{r}_0 are respectively the slant range, the elevation angle, and the component of velocity in the direction of the radius vector at time $t = t_0$. The equations of condition were obtained by substituting measured data in one or more of Equations B.10 through B.15 or in equations derived from various combinations of these. If more than four observations were available, the system would be overdetermined, and in general, would require rather extensive computation. In selecting a set of equations of condition, caution was required to avoid a system in which the equations were so nearly dependent that they failed to yield a reliable solution. For example, observations of slant range for four times at the same site generally provided a very weak solution. Likewise, poor results were experienced from a set of observations consisting of elevation angle measurements for four times at a single location. However, several combinations of single-site observations provided useful results. Computational methods for three of these will be considered in detail below.

If measurements of either slant range or its first time derivative are available for the major portion of a missile's trajectory, together with the elevation angle for at least the initial portion of the flight above the effective atmosphere, its trajectory may be determined from measurements of r_0 , \dot{r}_0 , and ϵ_0 for time t_0 and a slant range, r , for any time, t , other than t_0 . If only the slant range is measured, \dot{r} may be obtained by either numerical or graphical differentiation. On the other hand, if \dot{r} is the measured quantity, integration may be used to derive the necessary values for r . The latter process requires a continuous record of \dot{r} from launch. Preferably, t_0 should occur on the upward leg of the trajectory and t on the downward leg. Both times are, of course, restricted to that portion of the trajectory where the missile is in free flight and above the effective atmosphere.

With ϵ_0 and r_0 as input, initial position for time t_0 may be readily obtained from the equations,

$$\rho_0 = r_0 \cos \epsilon_0 \quad (\text{B.16})$$

$$y_0 = r_0 \sin \epsilon_0 \quad (\text{B.17})$$

Solutions for the remaining trajectory parameters require Equation B.15 which may be written in the form

$$\dot{\rho}_0 = (r_0 \dot{r}_0 - y_0 \dot{y}_0) / \rho_0 \quad (\text{B.18})$$

Substituting for $\dot{\rho}_0$ in Equation B.10, yields,

$$r = \sqrt{[\rho_0 + \{(r_0 \dot{r}_0 - y_0 \dot{y}_0) / \rho_0\} T]^2 + [y_0 + \dot{y}_0 T - (1/2)gT^2]^2} \quad (\text{B.19})$$

After squaring and simplifying, this reduces to

$$A\dot{y}_0^2 + B\dot{y}_0 + C = 0 \quad (\text{B.20})$$

Where: $A = 1 + (y_0 / \rho_0)^2$

$$B = -[(gT + (2r_0 \dot{r}_0 y_0) / \rho_0^2)]$$

$$C = \{[r_0 \dot{r}_0 / \rho_0]^2 + [(r_0^2 - r^2) / T^2] + [2r_0 \dot{r}_0 / T] - g[y_0 - (gT^2) / 4]\}$$

One of the solutions for Equation B.20 yields a false result and may be neglected. The valid solution for \dot{y}_0 is obtained from

$$\dot{y}_0 = [-B - \sqrt{B^2 - 4AC}] / 2A \quad (\text{B.21})$$

$\dot{\rho}_0$ may now be evaluated with Equation B.18 to complete the solution.

If a reliable estimate of \dot{r}_0 is available, the method can be altered slightly to accept as input ϵ_0 , r_0 , and measurements of slant range, r_1 and r_2 , for two times, t_1 and t_2 , such that $t_0 < t_1 < t_2$. If $T_1 \equiv (t_1 - t_0)$ and $T_2 \equiv (t_2 - t_0)$, the equations of condition may be written as

$$[\rho_0 + \rho_0 T_1]^2 + [y_0 + \dot{y}_0 T_1 - (1/2)gT_1^2]^2 = r_1^2 \quad (\text{B.22})$$

$$[\rho_0 + \dot{\rho}_0 T_2]^2 + [y_0 + \dot{y}_0 T_2 - (1/2)gT_2^2]^2 = r_2^2 \quad (\text{B.23})$$

Since ρ_0 and y_0 may be determined by Equations B.16 and B.17, the above system contains the unknowns $\dot{\rho}_0$ and \dot{y}_0 . The solution of Equations B.22 and B.23 may be obtained rather quickly by employing an iterative type of computation in which an initial approximation to the result is improved by a series of corrections until the desired number of significant figures is obtained.

A reduction problem, which occurred frequently in the trajectory determinations here discussed, required a trajectory determination from a series of elevation angle measurements recorded as a function of time. However, a system of equations derived from observations of elevation angle alone is weak and the results unreliable. Fortunately, these reductions were required for rockets that were highly consistent in performance throughout the powered portion of flight. Hence, slant range could be rather accurately related to flight time near burnout. When such an estimate of slant range was combined with three observations of elevation angle, the resulting set of equations provided relatively reliable results.

When elevation angles alone were available, the input for the computation consisted of r_0 , the slant range for time t_0 , and three elevation angles, ϵ_0 , ϵ_1 , and ϵ_2 , corresponding to times t_0 , t_1 , and t_2 . The times were related so that $t_0 < t_1 < t_2$ with t_0 occurring on the upward leg of the trajectory and t_2 on the downward leg if possible. All three times were, of course, selected for a drag-free portion of the trajectory.

Proceeding with the derivations, the assumed value for r_0 and the observed ϵ_0 may be substituted directly into Equations B.16 and B.17 to determine the position of the rocket at the initial time t_0 . With ρ_0 and y_0 known, Equations B.22 and B.23 may be solved for the unknowns, $\dot{\rho}_0$ and \dot{y}_0 . The resulting solution consists of

$$\dot{\rho}_0 = [D(y_0 + 1/2 g T_1 T_2) + E \rho_0] / F \quad (\text{B. 24})$$

$$\dot{y}_0 = [(\tan \epsilon_2 (\rho_0 + \dot{\rho}_0 T_2) - y_0) / T_2] + g T_2 / 2 \quad (\text{B. 25})$$

where,

$$D = (T_2 - T)$$

$$E = (T_1 \tan \epsilon_2 - T_2 \tan \epsilon_1)$$

$$F = T_1 T_2 (\tan \epsilon_1 - \tan \epsilon_2)$$

B.4 RESULTS

The trajectories, which are presented in graphical form in Figures B.1 through B.14, were determined from the best observations available for the particular rocket. Where possible, the computed trajectories were derived from flight paths obtained by missile tracking systems such as radar or the Cubic system. For these flight paths, parabolic trajectories were fitted to the tracking results. In the absence of data from radar or the Cubic system, flight paths were computed by one of the methods previously described. In general, elevation angle measurements were preferred to observations of slant range for input data; the latter, in turn, were given preference over rate of change in slant range. This order of priority was dictated by the methods of measurement which resulted in better accuracy in the angle measurements than in the observations of slant range.

The parameters which characterized the motion of each rocket are presented in Table B.1. In addition, the source of the input data for the trajectory determination of each rocket is indicated. Elevation angle input is represented by ϵ and slant range by r . The value for

g is an average value based on the apogee of the flight path. In practice, initial estimates were adjusted by an iterative procedure until the values for g were consistent with the computed trajectory. It should be observed that trajectories for Rockets 8 and 9 were well determined by radar. These trajectories were of sufficient duration that, to obtain a better fit to the observations, ρ was redefined by the equation

$$\rho = \rho_0 + \dot{\rho}_0 T + (1/2) \ddot{\rho}_0 T^2 \quad (\text{B.26})$$

For Rocket 8, $\ddot{\rho}_0 = -0.000546 \text{ km/sec}^2$, and for Rocket 9, $\ddot{\rho}_0 = -0.000478 \text{ km/sec}^2$.

A three-dimensional trajectory may be obtained from the parameters of Table B.1 by adding the following equations to the previous development:

$$x = \rho \cos \alpha \quad (\text{B.27})$$

$$z = \rho \sin \alpha \quad (\text{B.28})$$

where α is the azimuth angle measured clockwise from north. A right-hand coordinate system is formed by x , y , and z , in which y is the vertical, x is positive north, and z is positive to the east. The origin of the system is located at Point John. The unit of length in the table is the kilometer, and the unit of time is the second. t_0 is the time after launch.

B.5 DISCUSSION

The accuracy of the computed trajectories is primarily a function of the type of input data used to determine the trajectory parameters. The most accurate reductions consist of the results derived from radar and cubic tracking measurement; of moderate accuracy are those based on elevation angle measurements. Finally, the reductions of uncertain quality are those derived solely from measurements of slant range.

The predominant error, in the parabolic flight paths fitted to the reductions of radar and Cubic tracking data, entered as a result of assuming parabolic motion. The tracking error of either system is negligible in comparison to the error introduced by the curve-fitting procedure. Hence, the error in the computed trajectory is essentially equivalent to the error in fitting. Generally, the uncertainty in position for such trajectories varies from 0.5 km on the upward leg of the trajectory to 1.5 km on the downward leg.

In considering the quality of the trajectory determination for other types of input data, direct evaluation of the errors is impossible, since there exists no well-defined trajectory for comparison. However, Table B.2 offers a method for indirectly evaluating the accuracy of those trajectories that were derived from measurements of elevation angles. Presented in Table B.2 are estimates of altitudes at which the rockets began to nose over upon reentry into the effective atmosphere on the downward leg of the trajectory. This reentry phase is primarily a function of the aerodynamic characteristics of the rocket. The entries in Table B.2 were obtained by estimating nose-over times from the occurrence of discontinuities in magnetometer records and also in GMD and AGC field strength measurements. For many rockets, these times could be determined from all three sources with an accuracy of from 1 to 5 seconds. Missile altitudes corresponding to nose-over times were extracted from the computed trajectories for entry in Table B.2. When more than one measurement of nose-over time was available for a rocket, an average value was used. It is observed that the values are quite well clustered for each rocket type. Since, for every rocket, the reentering vehicle consists of the payload and last stage, it is reasonable to include the Honest John-Nike and Honest John-Nike-Nike missiles together for comparison. Excellent agreement in nose-over altitude is apparent for both types of rockets regardless of the source of the reduction data. This strongly suggests that the accuracy of the trajectories based solely on elevation angle

data is equivalent to that of trajectories derived from radar or Cubic tracking data. However, other error evaluations indicate that the latter may be slightly more accurate. Hence, reasonable estimates of positional error for trajectories determined from observations of elevation angles would vary from 1 to 2 km over the initial portion of the trajectory, to 2 to 3 km near reentry.

Only two nose-over altitudes were available for rockets of the D-4 type. These altitudes were 84.7 km for Rocket 22, and 59.7 km for Rocket 25. These values are not necessarily in poor agreement if it is considered that Rocket 25 was well behaved, whereas the poor performance of Rocket 22 resulted in such erratic motion that the missile very probably did not reenter tail first. The low nose-over altitude for Rocket 25 is quite reasonable, since the reentry vehicle for this rocket had no tail fins.

It is difficult to estimate errors for reductions derived from range-only measurements. Huge errors could result from a shift in the frequency of the transmitter. If such a shift were abrupt, it could be observed and corrected. However, no satisfactory method was available for the detection of gradual shifts in the transmitter frequency. A reasonable estimate of positional error in such reductions would be 1 to 5 km on the upward leg of the trajectory, growing to 5 to 15 km near reentry.

Rocket 19 required special attention. The only observation available consisted of a recording of Doppler frequency as a function of time. This record was known to be of poor quality as a result of frequency drift. In measuring nose-over altitudes, it was observed that Rocket 19 turned over at 345 seconds after launch, whereas Rocket 26 nosed over at 346 seconds. These rockets were identical and were programmed to fly identical trajectories. The flight path Rocket 26 was well determined by radar tracking. Therefore, it was concluded that the best estimate for the trajectory of Rocket 19 could be obtained by using the results for Rocket 26 shifted to the appropriate azimuth for Rocket 19.

In conclusion, positional errors probably vary from 0.5 to 1.5 km for Rockets 8, 9, 11, 15, 17, 19, 20, 24, 26, 27, 28, and 29; from 1 to 3 km for Rockets 2, 4, 6, 7, 10, 12, 13, 14, 18, 21, 23, and 25; and from 1 to 15 km for Rockets 1, 5, and 22.

TABLE B.1 SOURCE OF INPUT DATA FOR DETERMINING ROCKET TRAJECTORIES, PROJECTS 6.2, 6.3, 6.4

Rocket Number	t_o	ρ_o	y_o	$\dot{\rho}_o$	\dot{y}_o	δ	α	Input Data
1	110	29.00	84.30	0.7990	2.6544	0.00867	130.0	r
2	30	4.64	30.44	0.1964	1.1540	0.00953	114.0	e
4	40	5.35	33.78	0.1811	0.9910	0.00958	111.5	e and r
5	110	43.20	98.00	1.3156	2.7125	0.00860	148.0	r
6	30	2.55	30.70	0.1750	1.1582	0.00953	103.0	e
7	110	30.18	82.34	1.4491	2.6854	0.00868	120.0	e
8	110	58.31	137.74	1.6350	2.7767	0.008213	26.2	Radar
9	110	40.71	140.62	1.1686	2.9372	0.008113	23.5	Radar
10	40	9.10	39.72	0.3000	1.0523	0.00962	101.8	e
11	40	8.68	32.52	0.2993	0.9450	0.00949	86.5	Cubic
12	35	7.20	27.10	0.3053	1.0187	0.00954	19.7	e
13	35	6.52	33.93	0.2370	1.0986	0.00957	87.5	e
14	40	4.70	34.10	0.1715	1.0710	0.00960	100.8	e
15	40	9.03	30.52	0.4964	1.4186	0.00945	21.0	Radar
17	35	7.39	23.15	0.3457	1.0576	0.00951	116.0	Radar
18	40	6.80	29.30	0.1594	0.6402	0.00966	35.6	e
19	35	5.73	29.83	0.2937	1.5786	0.00940	135.0	a
20	35	3.80	28.03	0.2347	1.5936	0.00950	109.2	Cubic
21	30	3.09	28.93	0.1480	1.2081	0.00953	79.0	e
22	110	35.66	49.00	0.9771	1.3201	0.00945	100.0	r
23	30	6.22	28.77	0.3210	1.2687	0.00949	100.5	e
24	35	7.69	27.38	0.4602	1.5483	0.00951	19.4	Cubic
25	110	31.19	107.56	0.7931	2.7864	0.00855	165.0	e
26	35	5.73	29.83	0.2937	1.5786	0.00940	113.5	Radar
27	35	6.54	27.93	0.2528	1.5715	0.00951	109.7	Cubic
28	40	9.51	33.06	0.4599	1.4914	0.00939	17.5	Radar
29	50	5.90	30.55	0.1695	0.8434	0.00960	91.0	Radar

^a Based on results for Rocket 26

TABLE B.2 ESTIMATED NOSE-OVER ALTITUDES FOR SELECTED ROCKETS OF PROJECTS 6.2, 6.3, AND 6.4

Rocket Number	Input Data	Rocket Type	Nose-over Altitude	Apogee
2	e	NC ^a	83.6 km	100.3 km.
6	e	NC	79.9	101.1
10	e	NC	84.0	97.4
13	e	NC	78.8	97.1
21	e	NC	80.0	105.5
			average 81.3	
4	e and r	HJN ^b	63.5	85.0
11	Cubic	HJN	66.2	79.7
12	e	HJN	67.4	81.6
14	e	HJN	68.1	93.9
17	Radar	HJN	65.2	82.1
			average 66.1	
19	d	HJN ^{2c}	66.9	162.6
20	Cubic	HJN ²	64.9	161.8
24	Cubic	HJN ²	63.4	154.0
26	Radar	HJN ²	66.9	162.6
27	Cubic	HJN ²	63.7	158.0
28	Radar	HJN ²	69.2	152.0
			average 65.8	

^a Nike-Cajun

^b Honest John-Nike

^c Honest John-Nike-Nike

^d Based on results of Rocket 26

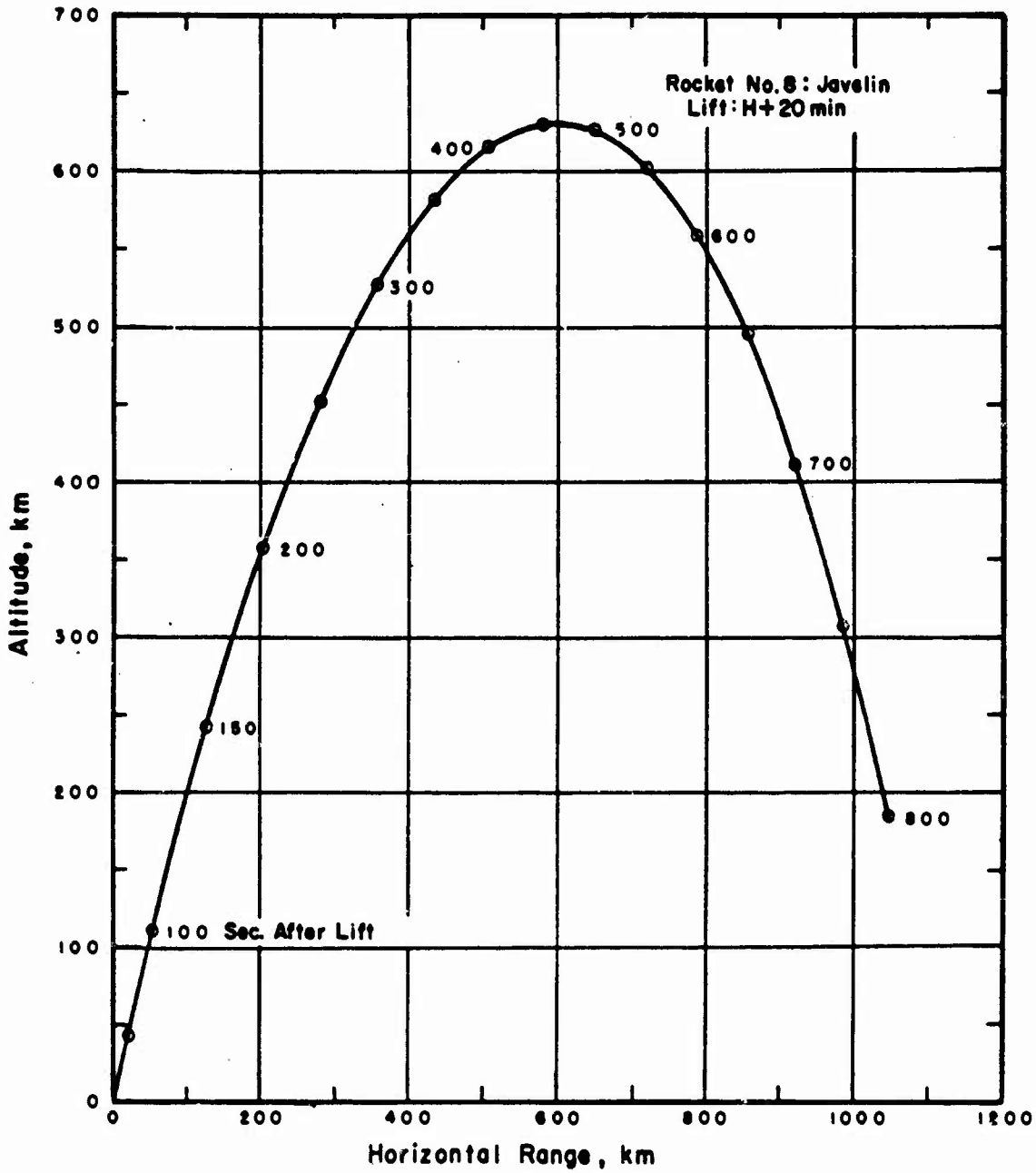


Figure B.1 Trajectory for Rocket 8, Star Fish event.

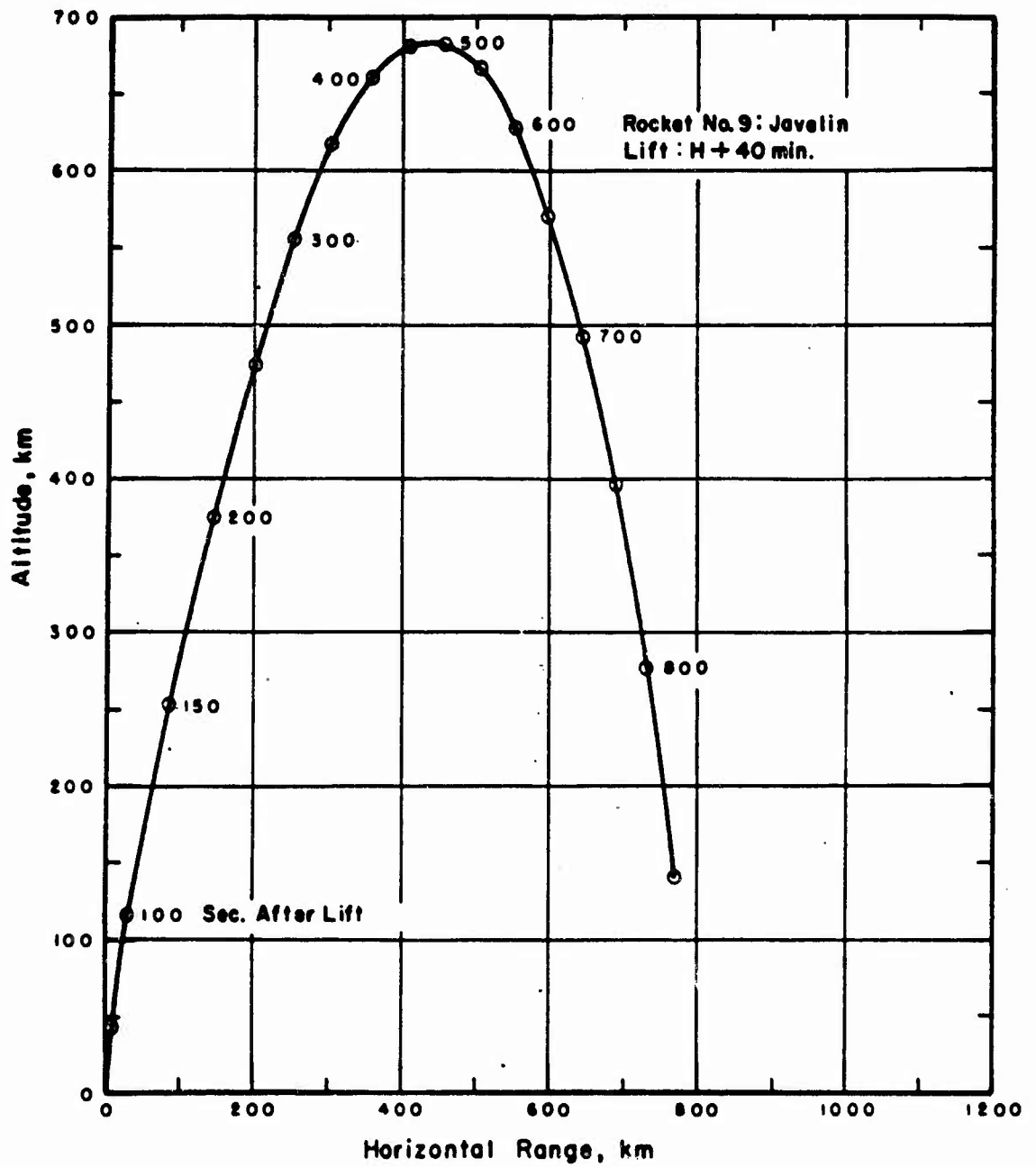


Figure B.2 Trajectory for Rocket 9, Star Fish event.

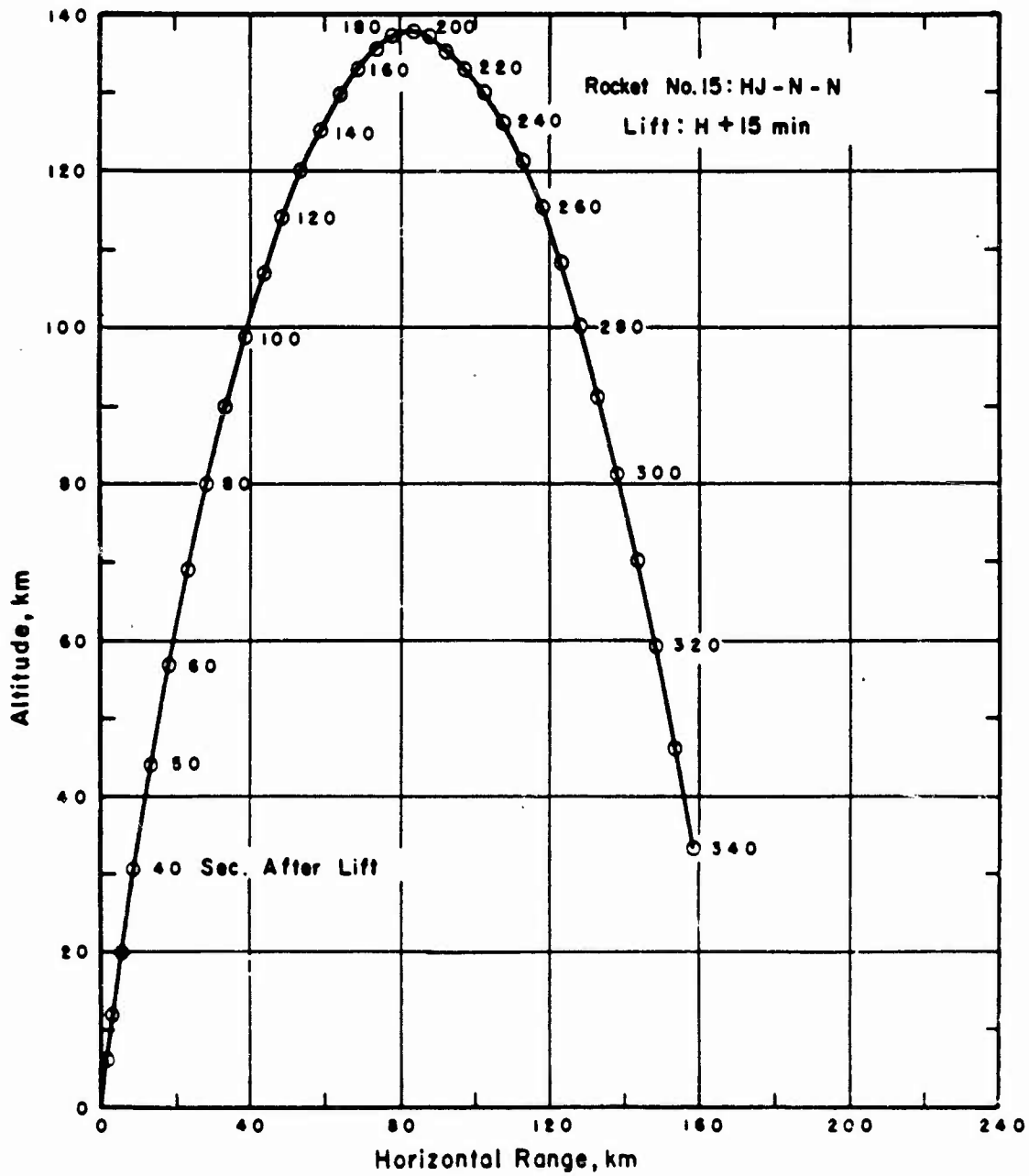


Figure B.3 Trajectory for Rocket 15, Blue Gill event.

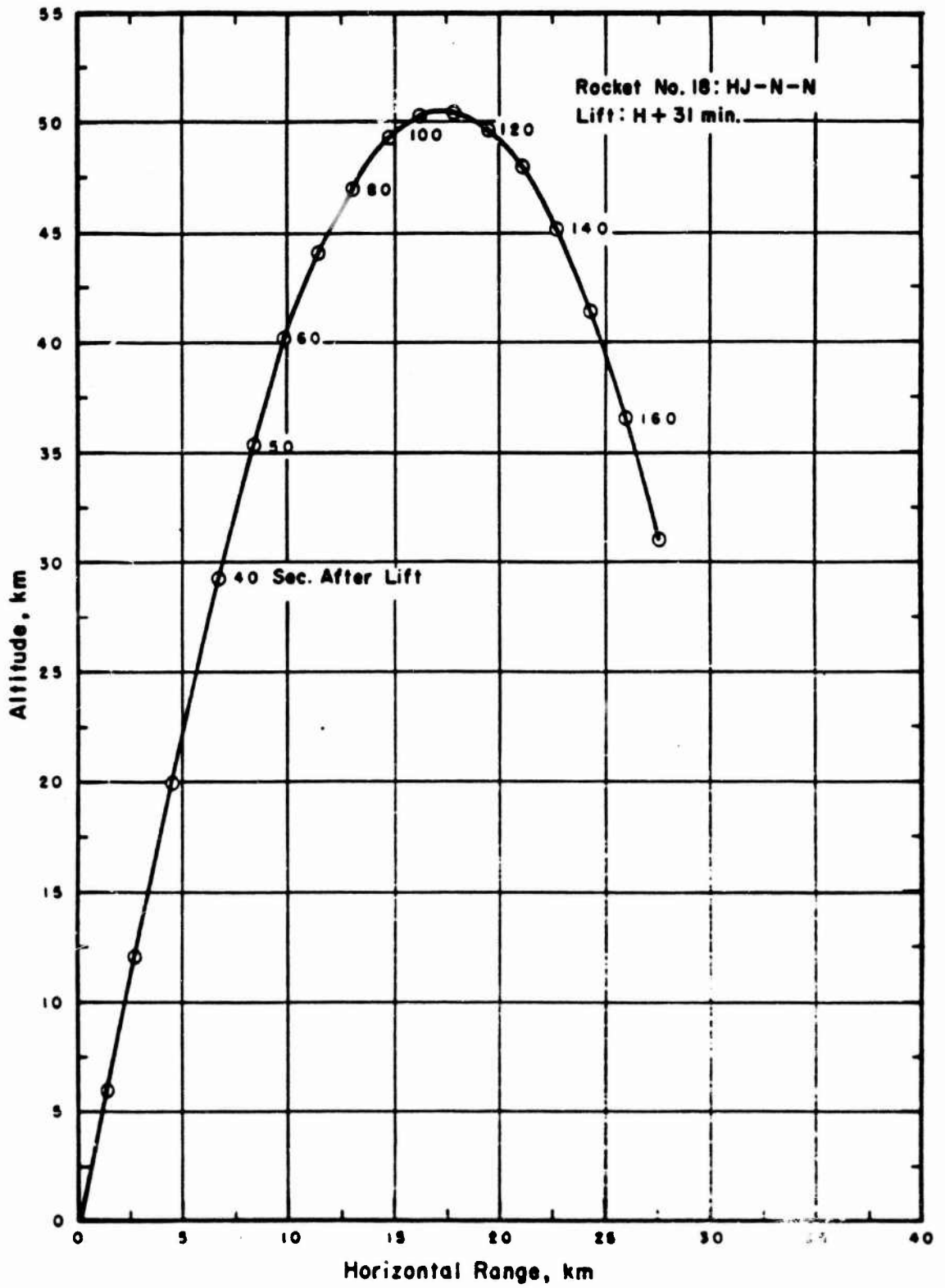


Figure B.4 Trajectory for Rocket 18, Blue Gill event.

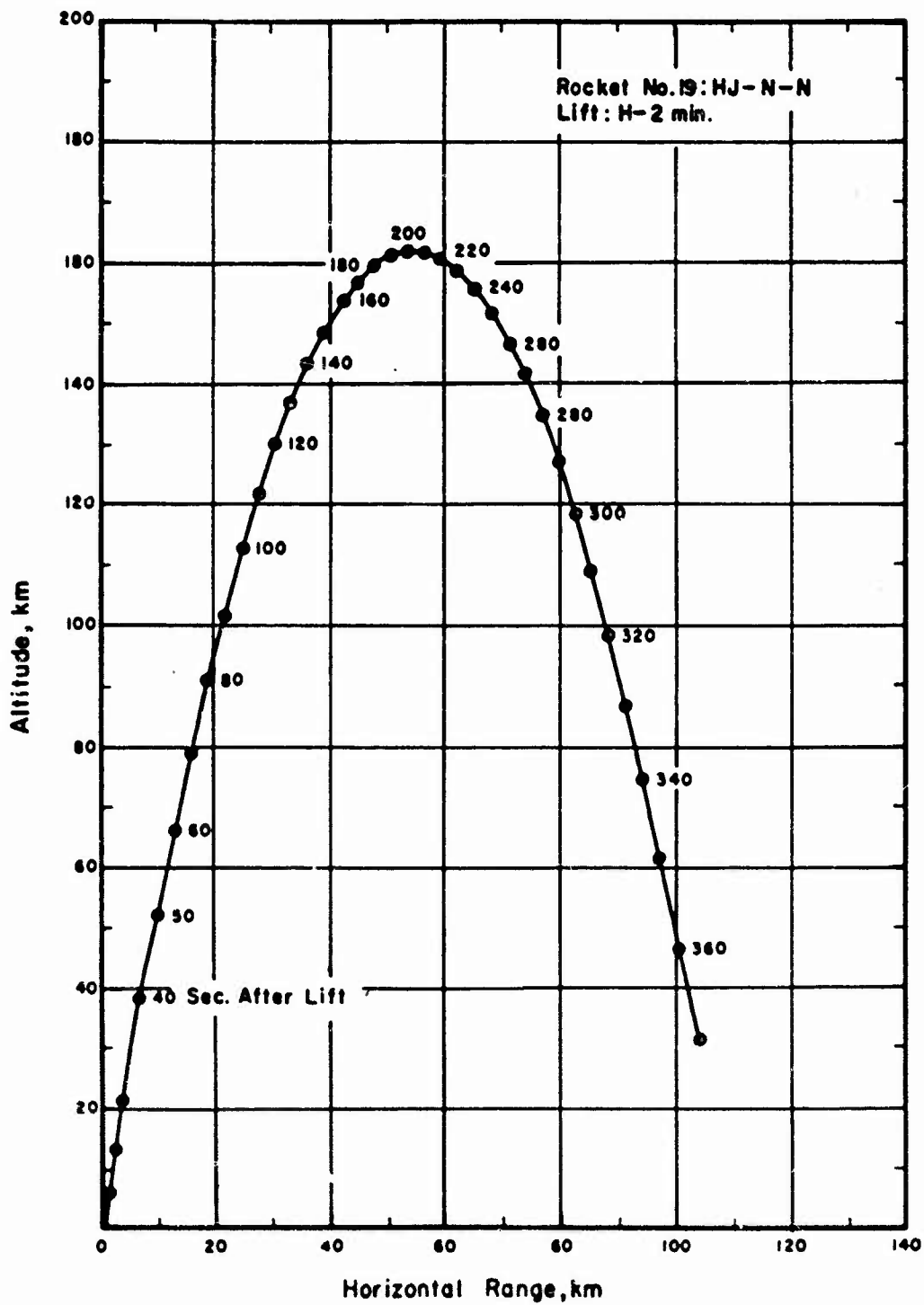


Figure B.5 Trajectory for Rocket 19, King Fish event.

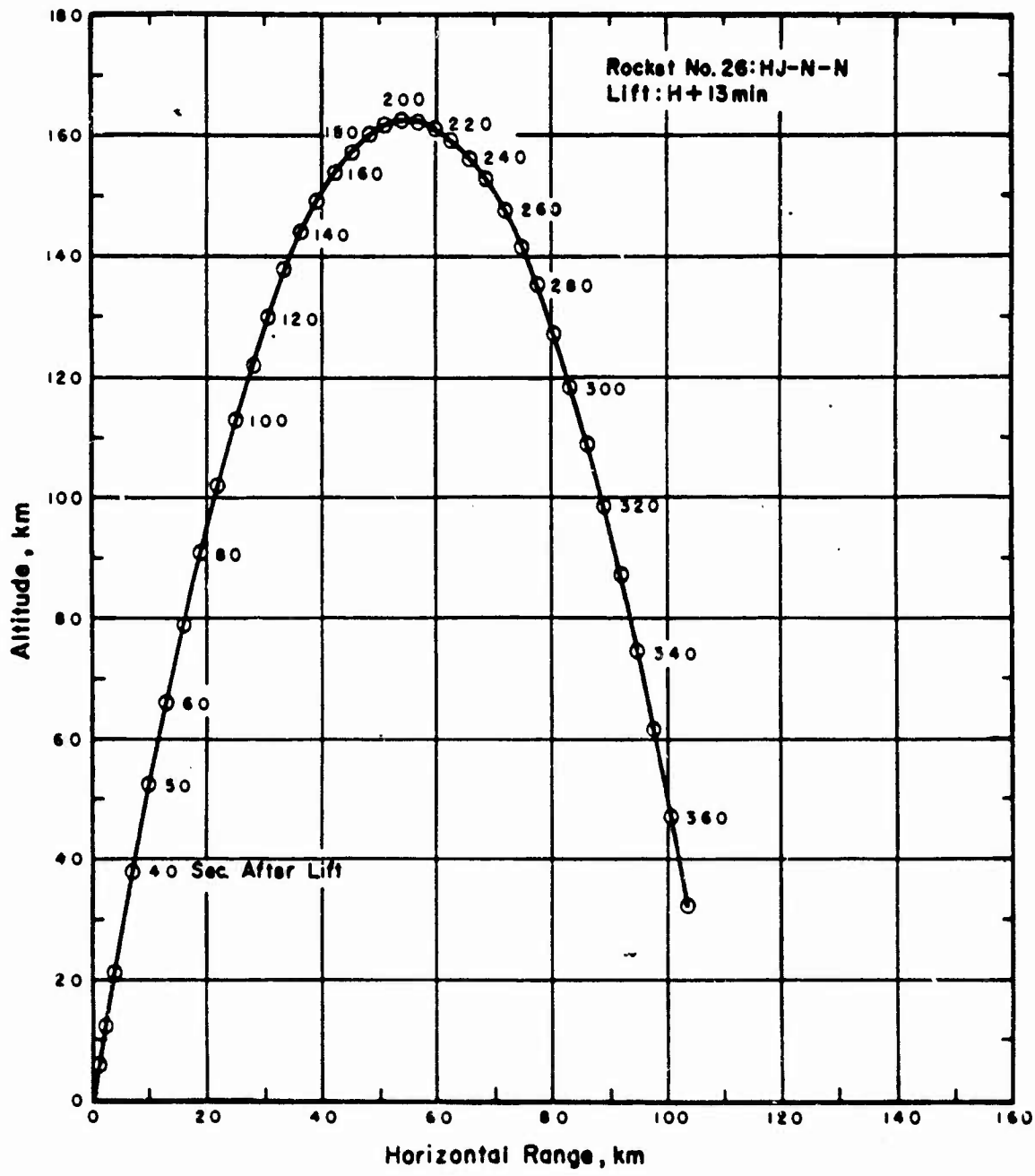


Figure B.6 Trajectory for Rocket 26, King Fish event.

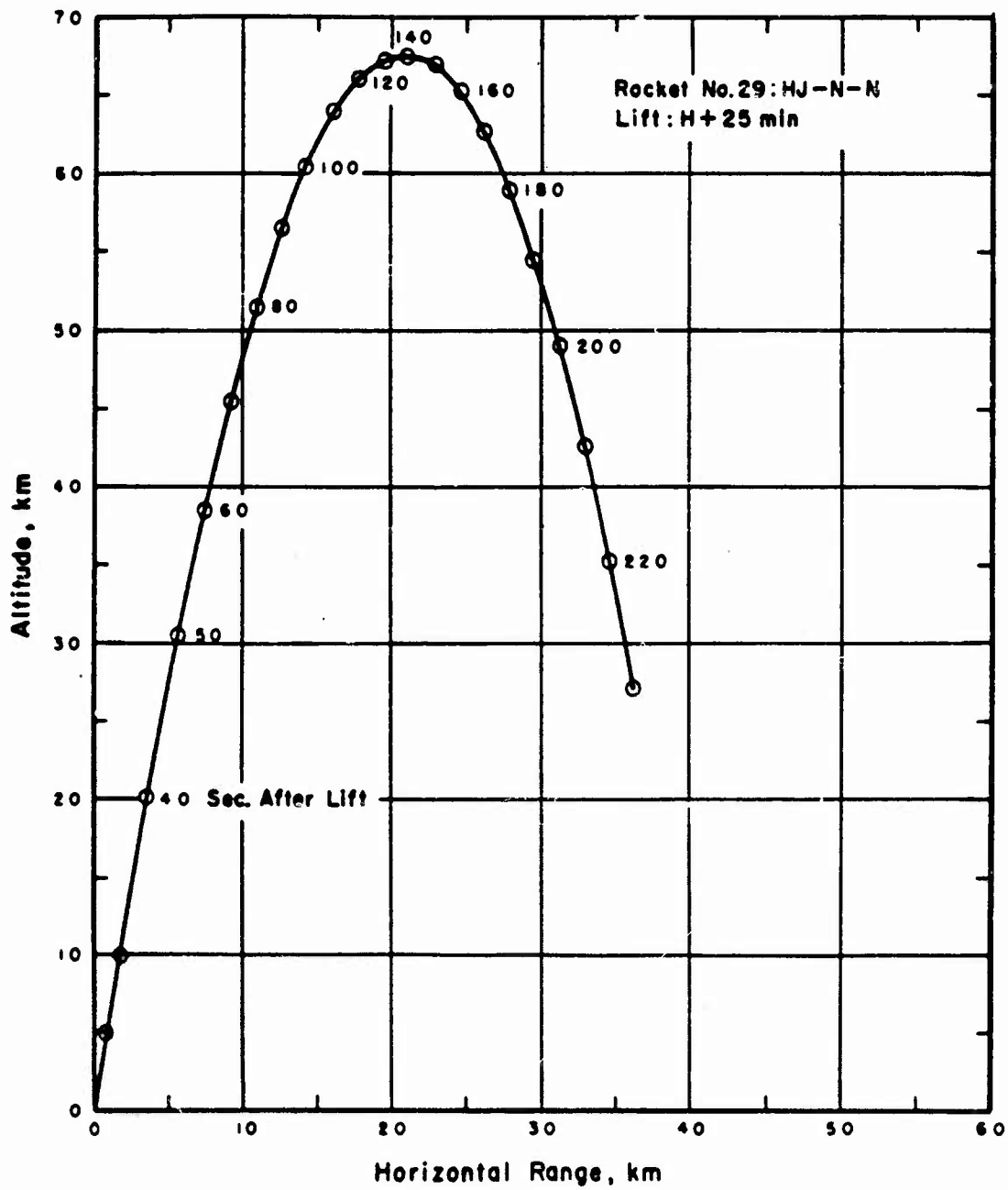


Figure B.7 Trajectory for Rocket 29, King Fish event.

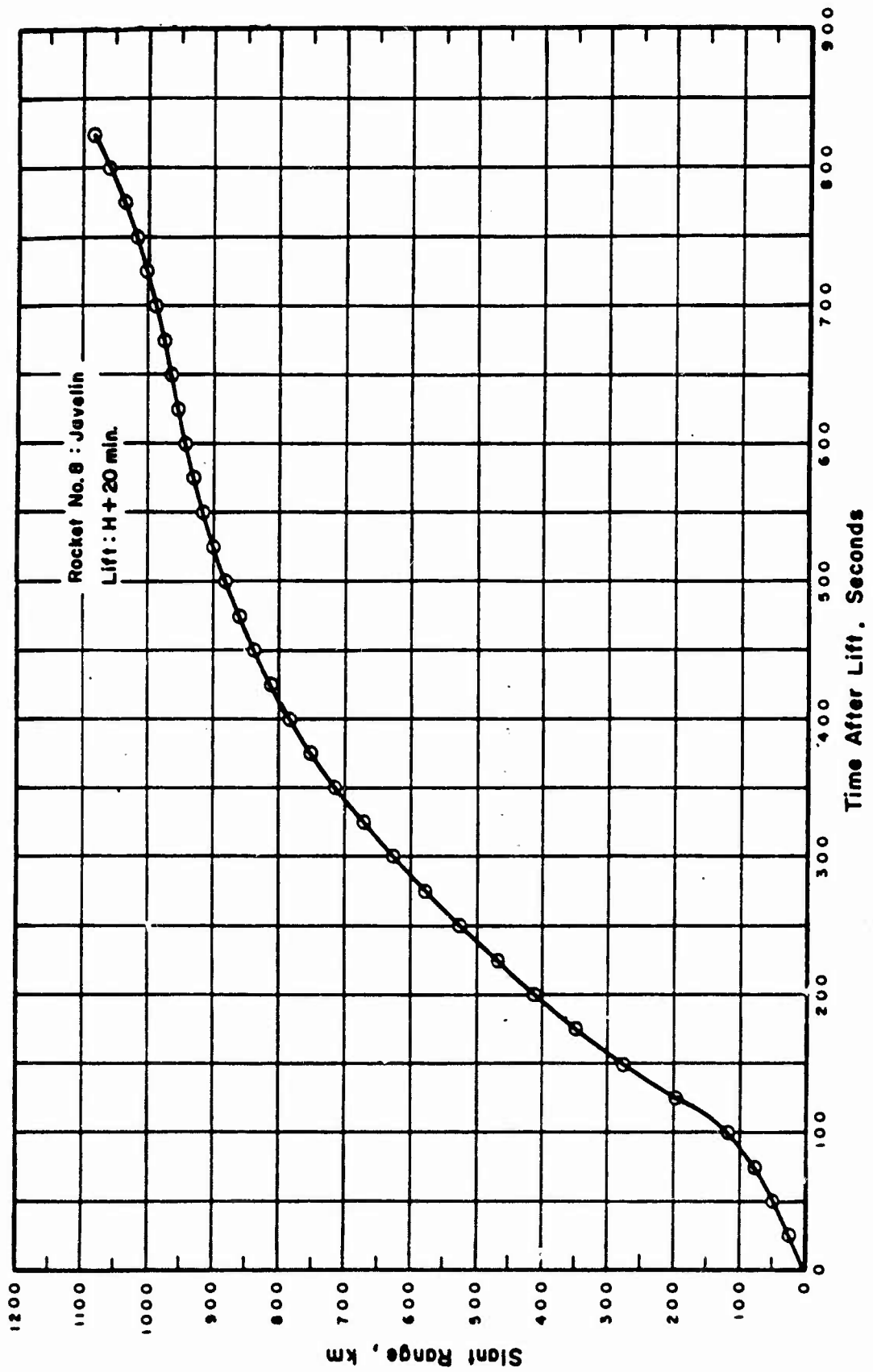


Figure B.8 Slant range versus time for Rocket 8, Star Fish event.

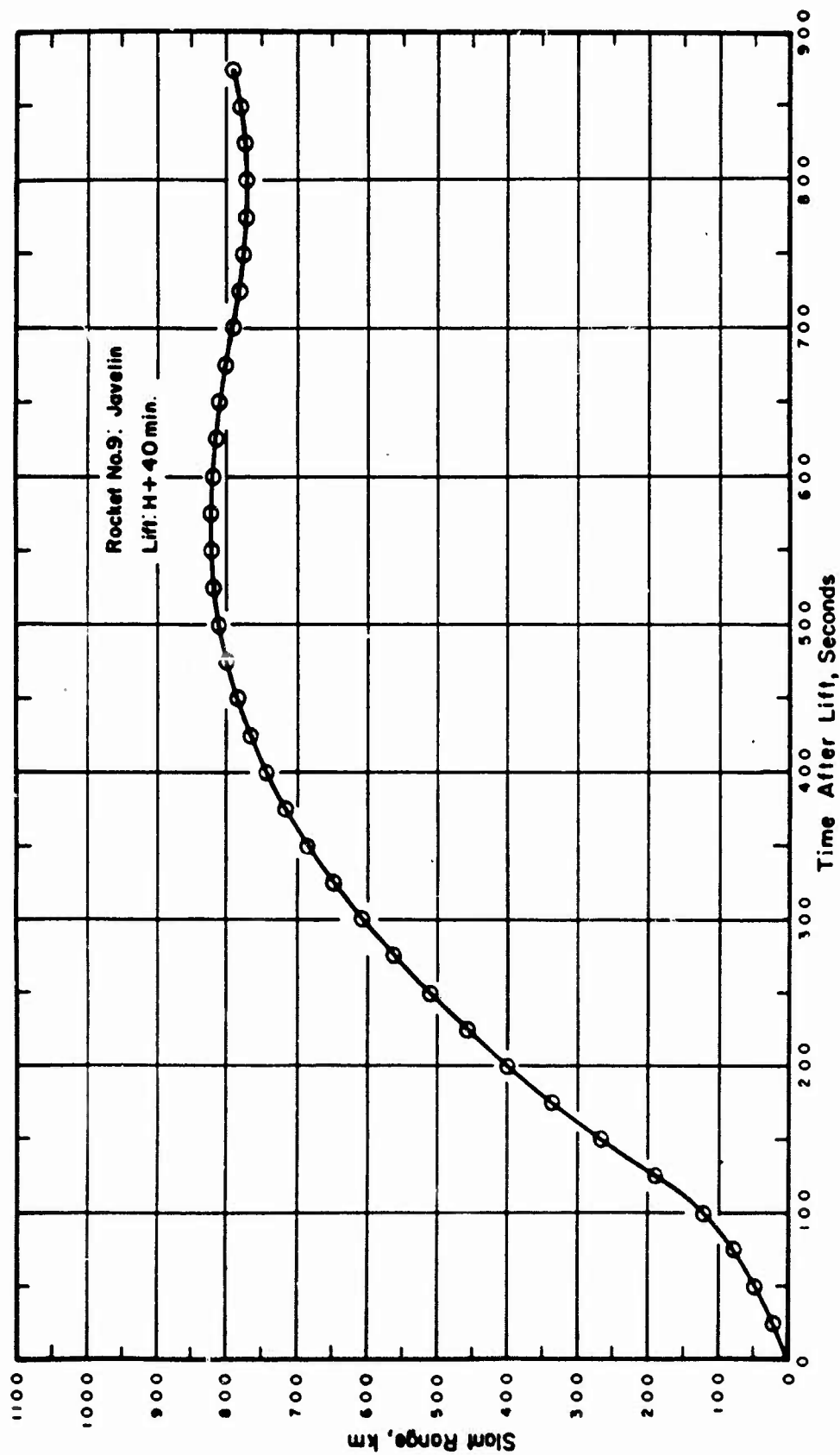


Figure B.9 Slant range versus time for Rocket 9, Star Fish event.

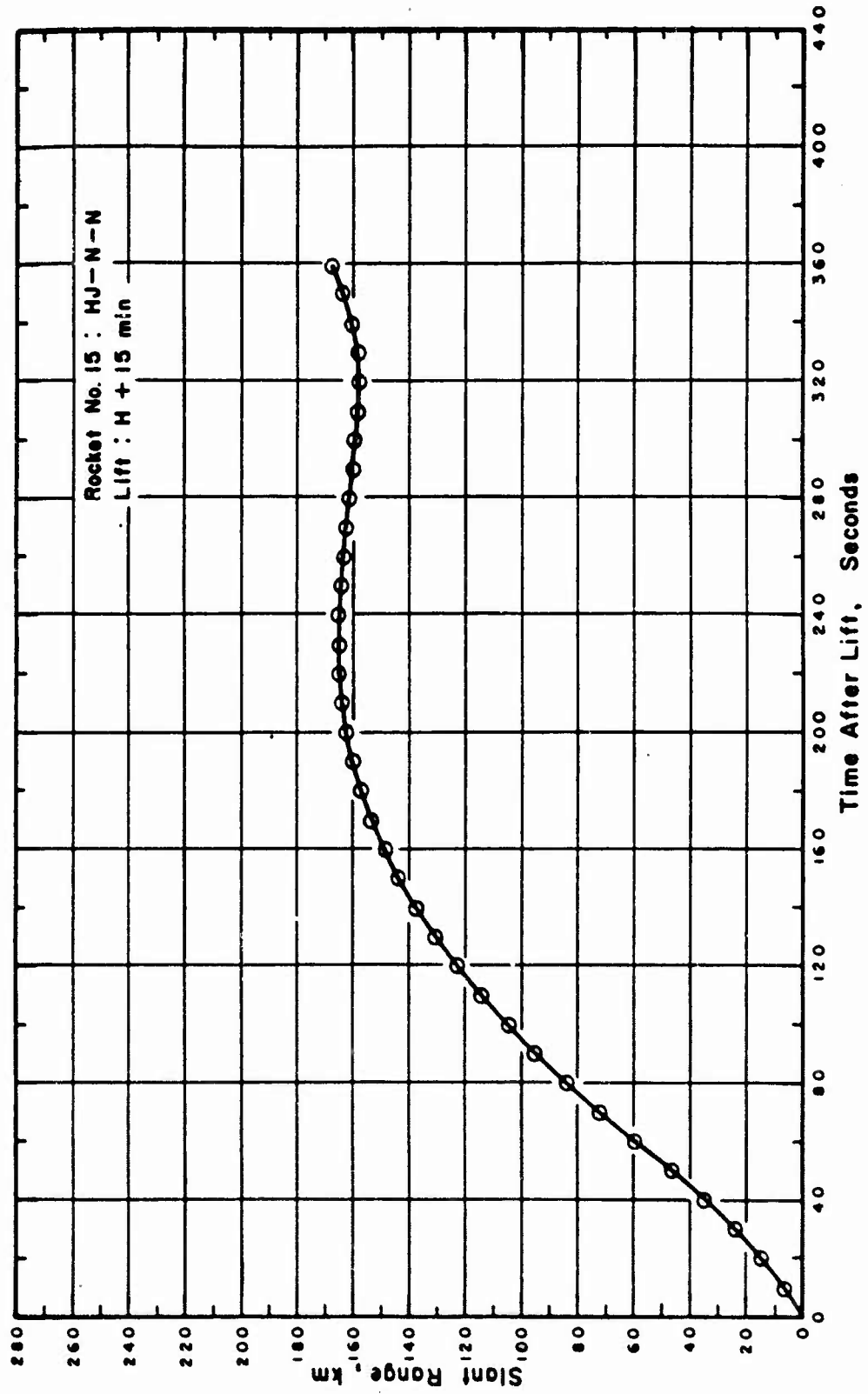


Figure B.10 Slant range versus time for Rocket 15, Blue Gill event.

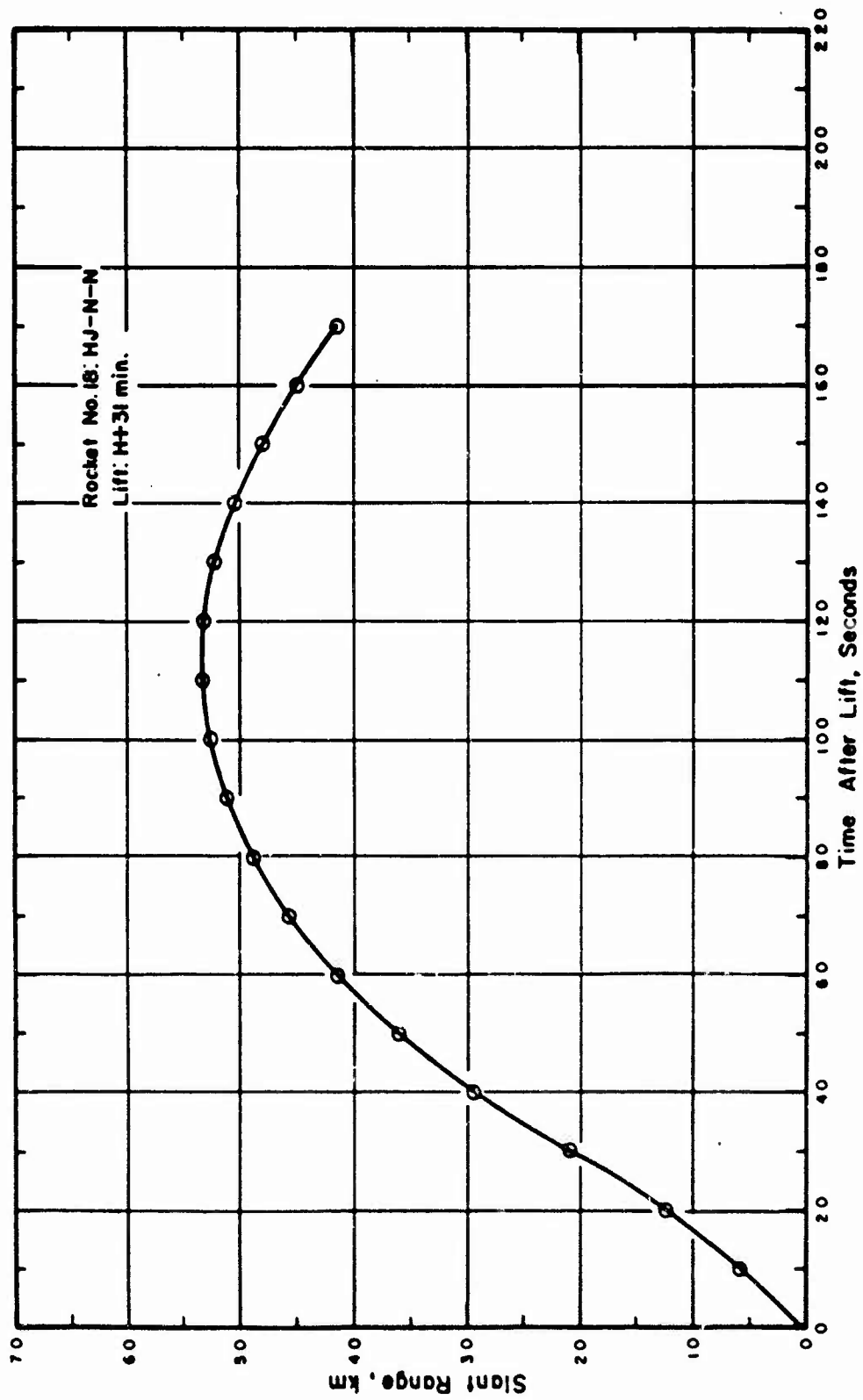


Figure B.11 Slant range versus time for Rocket 18, Blue Gill event.

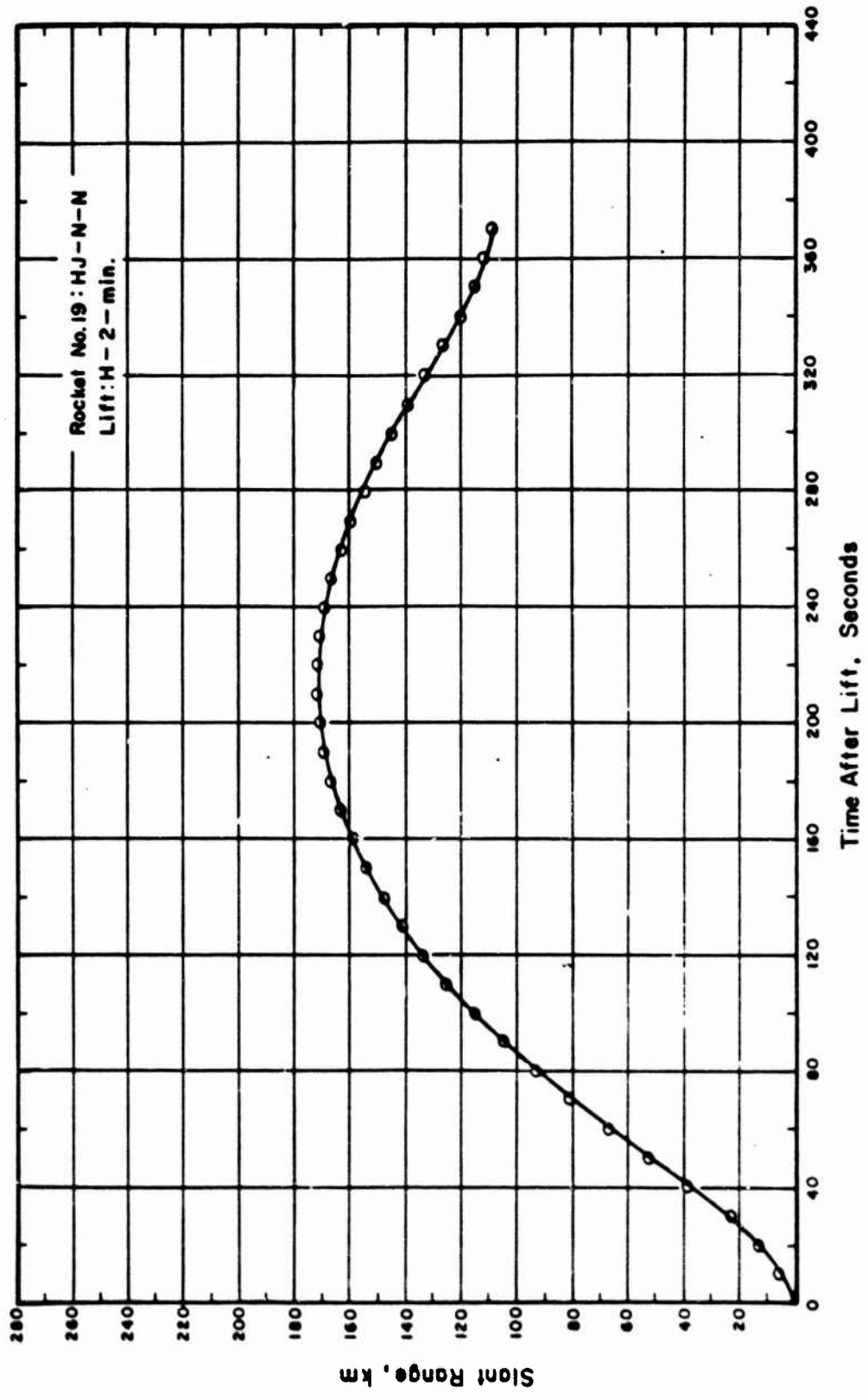


Figure B.12 Slant range versus time for Rocket 19, King Fish event.

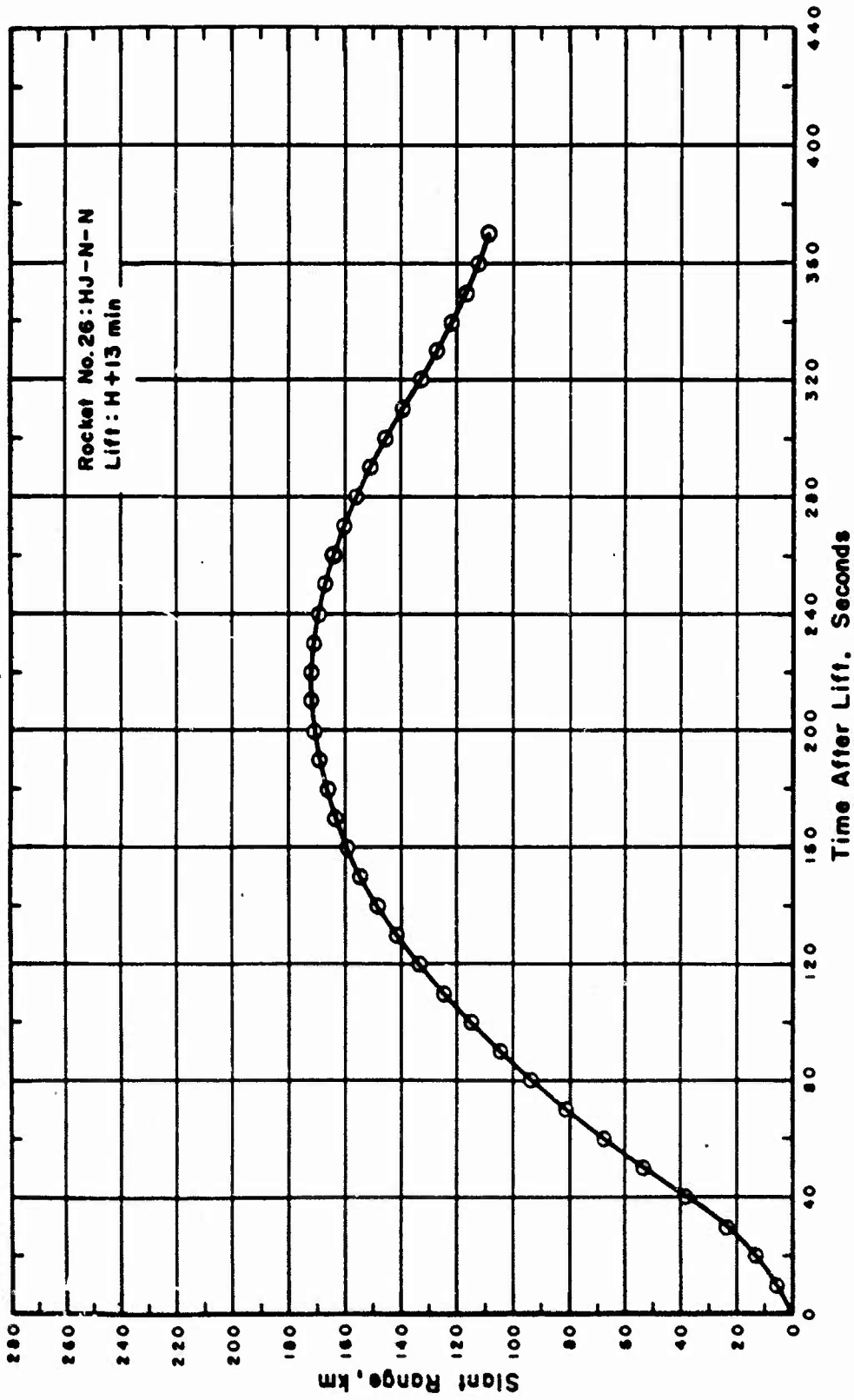


Figure B.13 Slant range versus time for Rocket 26, King Fish event.

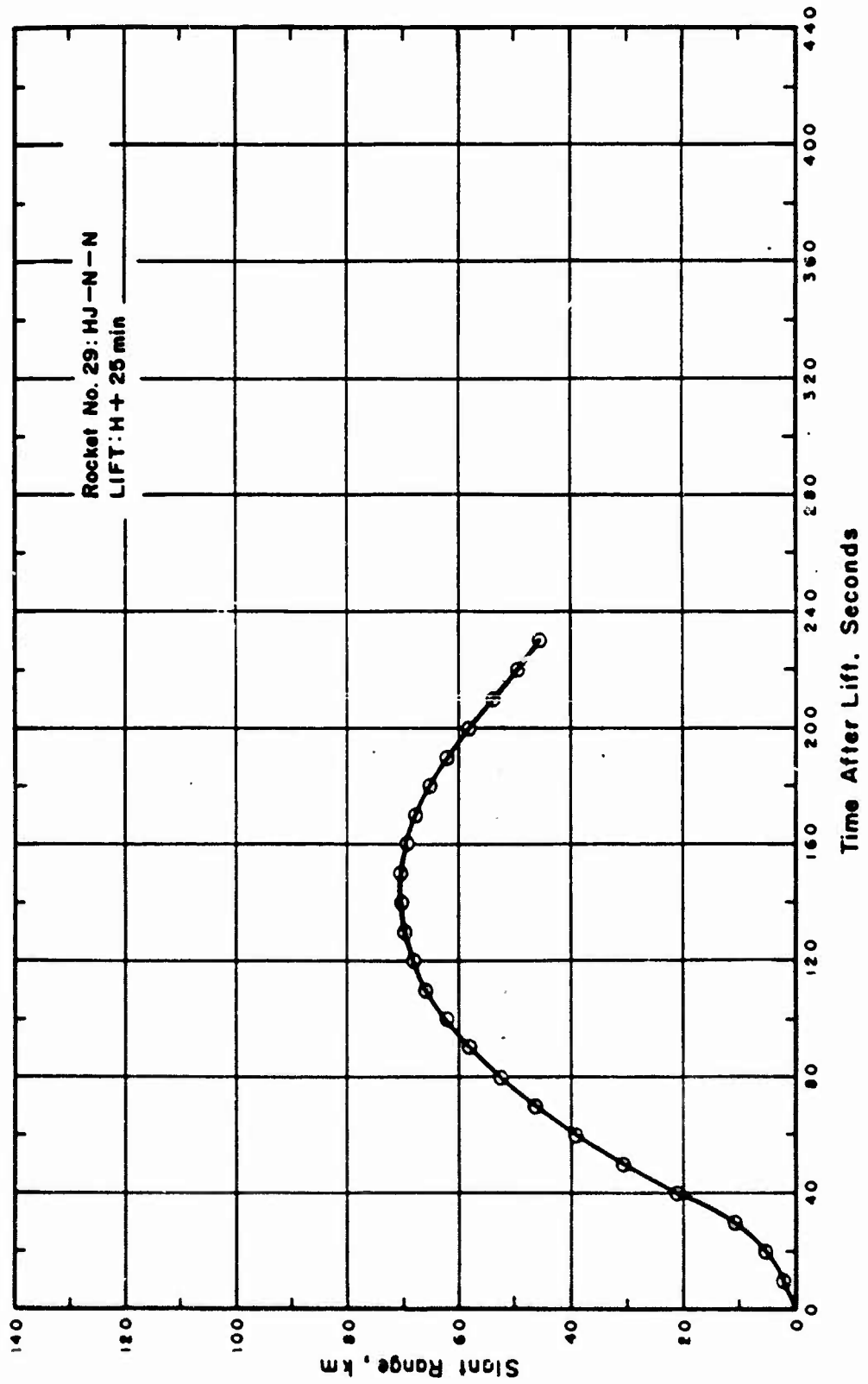


Figure B.14 Slant range versus time for Rocket 29, King Fish event.

APPENDIX C

REPORTS AND SPECIFICATIONS

Reports and specifications of general interest prepared during Project 6.2 are listed below. This list includes the principal documents delivered to EOS by the Aerolab Development Company, Pasadena, California, and the Atlantic Research Corporation, El Monte, California.

C.1 ELECTRO-OPTICAL SYSTEMS, INC., REPORTS

Pretest Report (S)	2190-IR-1
Sounding Rocket Trajectories and Performance (U)	2190-IR-2
Operation Fish Bowl (U)	2190-IR-3 Rev
Sounding Rocket Trajectories (U)	2190-IR-4
Preliminary Report on Gamma Ray Scanning Data on the Location of the Debris Cloud (S)	2190-DASA
Data Reduction Instructions and Background Information (U)	2190
Payload Spatial Calibration (U)	2190-51A
Payload Calibration Report (U)	2190-52.
Rocket Safety Information (U)	2190-1-76
Rocket Probe Measurements of Beta and Gamma Radiation (S)	2190-TR-1
Operating Characteristics of the Beta and Gamma Detectors (U)	2190-M-262

C.2 ELECTRO-OPTICAL SYSTEMS, INC., SPECIFICATIONS

Environmental Tests (U)	2190-45
Overseas Packaging (U)	2190-46
Payload Instruments (U)	2190-50
Magnetometer (U)	2192-1
Batteries (U)	2192-2
Beta Detector (U)	2192-3
Gamma Detector (U)	2192-4
Gamma Scanner (U)	2192-5
Experiment Electronics (U)	2192-6
Photometer (U)	2192-8
Ground Telemetry Van (U)	2202-41

C.3 SUBCONTRACTOR REPORTS

Trajectory and Dispersion Analysis (U)	ARC 7906-01
Basic Data Summary (U)	ARC 7906-02, 03, and 04
Basic Data Summary (U)	ARC 7906-05
Dispersion Data Argo D-4 (U)	Aerolab 26-2
Final Performance Data Argo D-4 Vehicle (U)	Aerolab 27-2
Traject and Dispersion Data Argo C-22 (U)	Aerolab 33-2
Final Performance Data Argo D-4 (U)	Aerolab 33-3
Final Post Flight and Field Service Report of Pacific Launch (U)	Aerolab 33-5
Radiation Dosimetry for EOS (U)	Edgerton, Germeshausen and Grier

APPENDIX D

CALIBRATION DATA FOR GAMMA SCANNER IN PAYLOAD

Five samples of computer-reduced calibration data for the vertical 20-degree gamma scanner (VGS-20) are given in this appendix. Count rates were normalized by the computer and represent a relative magnitude. Refer to Section 2.2 for a description of the calibration procedure.

A contour plot of the payload shielding effects (in percent) is shown in Figure D.1. The most significant shielding variation from the ideal pattern (when the instrument was calibrated independently of the payload) was caused by the horizontal scanner. This variation is shown in Figure D.1 between 140 and 170 degrees azimuth and between 10 and 60 degrees declination. Other variations shown in the left-hand side of the figure were caused by lead balance weights and the payload structure.

DECLINATION = 66.5 DEGREES

AZIMUTH (DEGREES)	NORMALIZED COUNT-RATE	AZIMUTH (DEGREES)	NORMALIZED COUNT-RATE	AZIMUTH (DEGREES)	NORMALIZED COUNT-RATE
0	.96115934	120	.80938191	240	.48131827
5	.86655834	125	.80406488	245	.36567226
10	.90478486	130	.75439667	250	.36685015
15	.95374162	135	.80406488	255	.46417385
20	1.00000000	140	.63230826	260	.45514125
25	.98410242	145	.56120533	265	.54828464
30	.95374162	150	.55596781	270	.72302579
35	.96869028	155	.46052039	275	.83702350
40	.94643466	160	.61928446	280	.80938191
45	.92515375	165	.60371251	285	.80406488
50	.96115934	170	.33434373	290	.80938191
55	.91147680	175	.16252101	295	.85450494
60	.92515375	180	.14528112	300	.87894655
65	.88527061	185	.13903165	305	.93214305
70	.91147680	190	.14847130	310	.96115934
75	.91147680	195	.19836046	315	.97633707
80	.98410242	200	.22218221	320	.98410242
85	.95374162	205	.29145533	325	.97633707
90	.95374162	210	.34881593	330	.97633707
95	.91826572	215	.43804036	335	.96869028
100	.94643466	220	.43314494	340	.96115934
105	.98410242	225	.43969549	345	.96869028
110	.93214305	230	.48329763	350	.93923592
115	.86655834	235	.493433089	355	.94643466

DECLINATION = 84.5 DEGREES

AZIMUTH (DEGREES)	NORMALIZED COUNT-RATE	AZIMUTH (DEGREES)	NORMALIZED COUNT-RATE	AZIMUTH (DEGREES)	NORMALIZED COUNT-RATE
0	.87558737	120	.92296430	240	.32843019
5	.83272253	125	.81001268	245	.36558856
10	.88863321	130	.73919923	250	.42231442
15	.93014264	135	.83272253	255	.53552624
20	.95997756	140	.76802086	260	.57840475
25	.96772991	145	.70388022	265	.57268931
30	.95234535	150	.49191185	270	.73919923
35	.93743057	155	.48358143	275	.84454730
40	.93743057	160	.57553345	280	.85670285
45	.93743057	165	.57553345	285	.86290905
50	.93743057	170	.37549747	290	.81557658
55	.91589314	175	.15317262	295	.88206336
60	.86920326	180	.13081726	300	.86290905
65	.90206272	185	.12911174	305	.89529896
70	.89529896	190	.15494502	310	.91589314
75	.95997756	195	.22797598	315	.92296430
80	.99173729	200	.22848312	320	.93743057
85	.95997756	205	.22899228	325	.94483059
90	.95997756	210	.23156918	330	.95997756
95	.97560535	215	.23314062	335	.98360681
100	.95234535	220	.31419615	340	1.00000000
105	.90892670	225	.34499347	345	.95997756
110	.94483059	230	.30881884	350	.97560535
115	.91589314	235	.33243024	355	.92296430

(VGS-20)

DECLINATION = 90.0 DEGREES

AZIMUTH (DEGREES)	NORMALIZED COUNT-RATE	AZIMUTH (DEGREES)	NORMALIZED COUNT-RATE	AZIMUTH (DEGREES)	NORMALIZED COUNT-RATE
0	•90206272	120	•93743057	240	•36318758
5	•84454730	125	•78326308	245	•37172322
10	•90892670	130	•72556040	250	•44742052
15	•99173729	135	•81001268	255	•51862666
20	•99173729	140	•80452197	260	•59622681
25	•96772991	145	•64934350	265	•60553885
30	•98360681	150	•42390476	270	•76802086
35	•93743057	155	•53059144	275	•86920326
40	•90892670	160	•63523004	280	•82693000
45	•93014264	165	•52574282	285	•88863321
50	•93014264	170	•42390476	290	•83859443
55	•91589314	175	•15168103	295	•90892670
60	•90892670	180	•13474625	300	•90206272
65	•90892670	185	•13120141	305	•90892670
70	•95234535	190	•14782319	310	•94483059
75	•94483059	195	•19690651	315	•93014264
80	1.00000000	200	•24528136	320	•95234535
85	•96772991	205	•30275714	325	•99173729
90	•96772991	210	•27619563	330	•99173729
95	•98360681	215	•26987103	335	•94483059
100	•96772991	220	•34283855	340	•98360681
105	•92296430	225	•41606420	345	•99173729
110	•95997756	230	•35615867	350	•95234535
115	•95997756	235	•38064310	355	•90206272

DECLINATION = 95.5 DEGREES

AZIMUTH (DEGREES)	NORMALIZED COUNT-RATE	AZIMUTH (DEGREES)	NORMALIZED COUNT-RATE	AZIMUTH (DEGREES)	NORMALIZED COUNT-RATE
0	•93115778	120	1.00000000	240	•34855243
5	•87098100	125	•97597693	245	•39371860
10	•88368975	130	•78592104	250	•46217568
15	•98385848	135	•62538654	255	•49796700
20	•95305416	140	•53943449	260	•57653241
25	•97597693	145	•52727030	265	•62870477
30	•95305416	150	•41530121	270	•73765288
35	•94564477	155	•53695896	275	•87729064
40	•96057751	160	•54955858	280	•89676418
45	•95305416	165	•42935288	285	•85862286
50	•92407524	170	•38046851	290	•86475903
55	•94564477	175	•15370917	295	•88368975
60	•93115778	180	•13885616	300	•90344352
65	•91709686	185	•13088340	305	•92407524
70	•91022037	190	•14359890	310	•91022037
75	•93115778	195	•19783861	315	•96821752
80	1.00000000	200	•22428254	320	•96057751
85	•97597693	205	•25354426	325	•97597693
90	•97597693	210	•24588916	330	•96057751
95	•99186518	215	•24361768	335	1.00000000
100	•96821752	220	•25660501	340	•96821752
105	•93834679	225	•30438104	345	•97597693
110	•96821752	230	•29136909	350	•96821752
115	•96821752	235	•32036101	355	•93834679

(VGS-20)

DECLINATION = 113.5 DEGREES

AZIMUTH (DEGREES)	NORMALIZED COUNT-RATE	AZIMUTH (DEGREES)	NORMALIZED COUNT-RATE	AZIMUTH (DEGREES)	NORMALIZED COUNT-RATE
0	.94441402	120	.75671218	240	.42843135
5	.86829530	125	.56235844	245	.43678561
10	.89455015	130	.52617257	250	.41723132
15	.95198267	135	.49419085	255	.48572455
20	.96748030	140	.42037439	260	.53354589
25	.97541513	145	.40956462	265	.60680756
30	.97541513	150	.40509109	270	.72848029
35	.96748030	155	.35433663	275	.83161044
40	.95198267	160	.33269626	280	.87471736
45	.94441402	165	.39926790	285	.83161044
50	.93696184	170	.29855817	290	.82004315
55	.90826539	175	.19643079	295	.86196435
60	.91527766	180	.17243828	300	.88123249
65	.90826539	185	.17212884	305	.90135697
70	.88784272	190	.17719977	310	.94441402
75	.92239622	195	.25583901	315	.92962345
80	.95198267	200	.34104868	320	1.00000000
85	.96748030	205	.34980120	325	.94441402
90	.95967045	210	.34980120	330	.97541513
95	.95967045	215	.34104868	335	.95967045
100	.95967045	220	.33269626	340	.95967045
105	.88123249	225	.45262683	345	.95967045
110	.88784272	230	.50517730	350	.95967045
115	.84349904	235	.44194781	355	.94441402

(VGS-20)

Notes:

- 1. Numbers in Plot Represent Percent Shielding.**
- 2. Payload Viewed from Outside.**

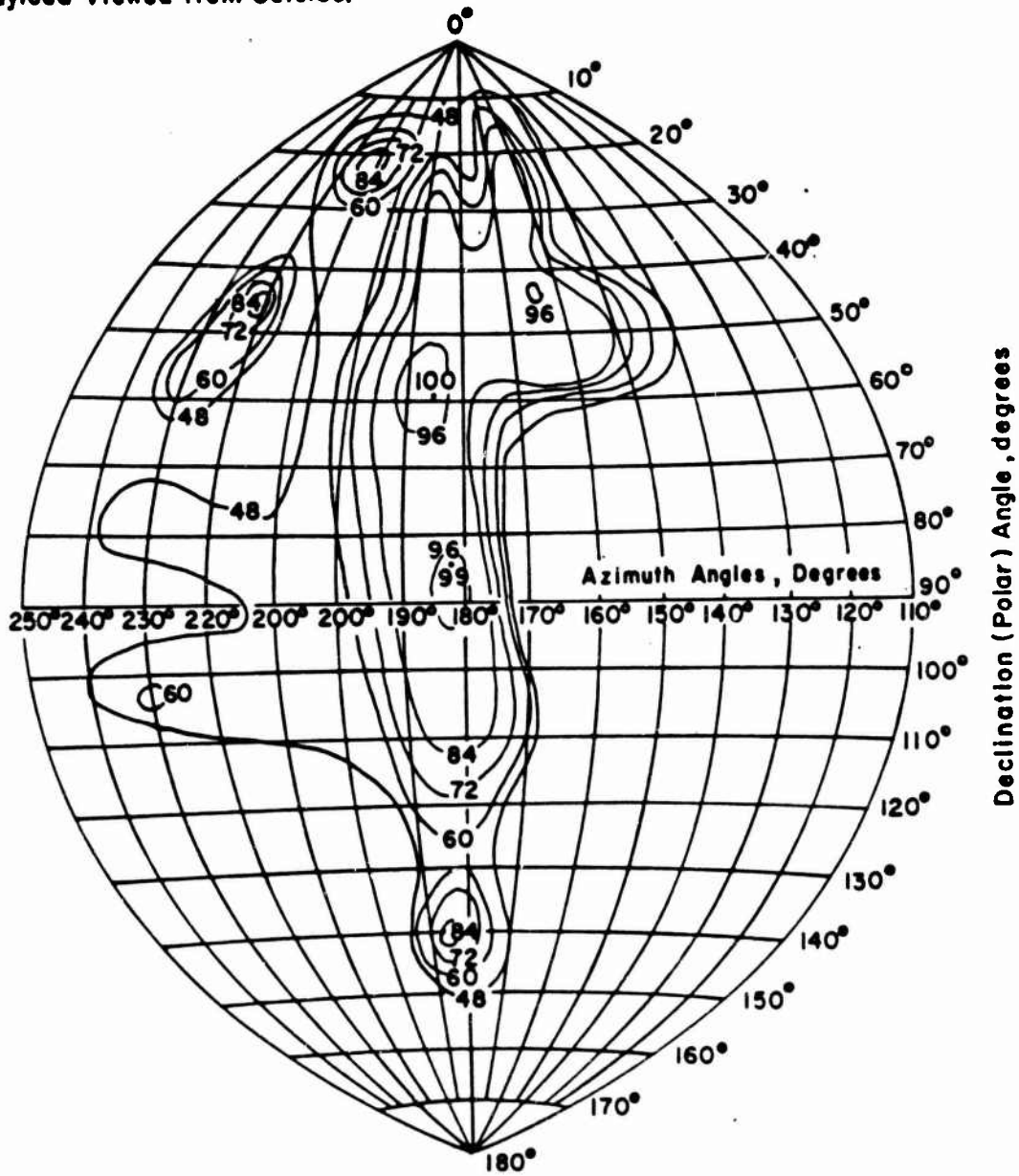


Figure D.1 Contour plot of equal shielding for vertical 20-degree gamma scanner (in payload) calibration data.

APPENDIX E

INSTRUMENT CALIBRATION DATA

This appendix includes typical calibration data for gamma scanners, an omnidirectional gamma detector, and a beta detector (Figures E.1 through E.7). Only a few data samples are given, but a complete set of curves is on file at EOS. Calibration data for each of the photometers is given in Table E.1.

TABLE E.1 PHOTOMETER CALIBRATIONS

Photometer Serial No.	Rocket	Calibration in Watt/cm ² Steradian for Each Volt Out
4	8	8.4×10^{-8}
5	9	51.7×10^{-8}
3	15	0.353×10^{-8}
6	18	0.46×10^{-8}
9	19	3.55×10^{-8}
8	26	1.8×10^{-8}
10	29	35.8×10^{-8}

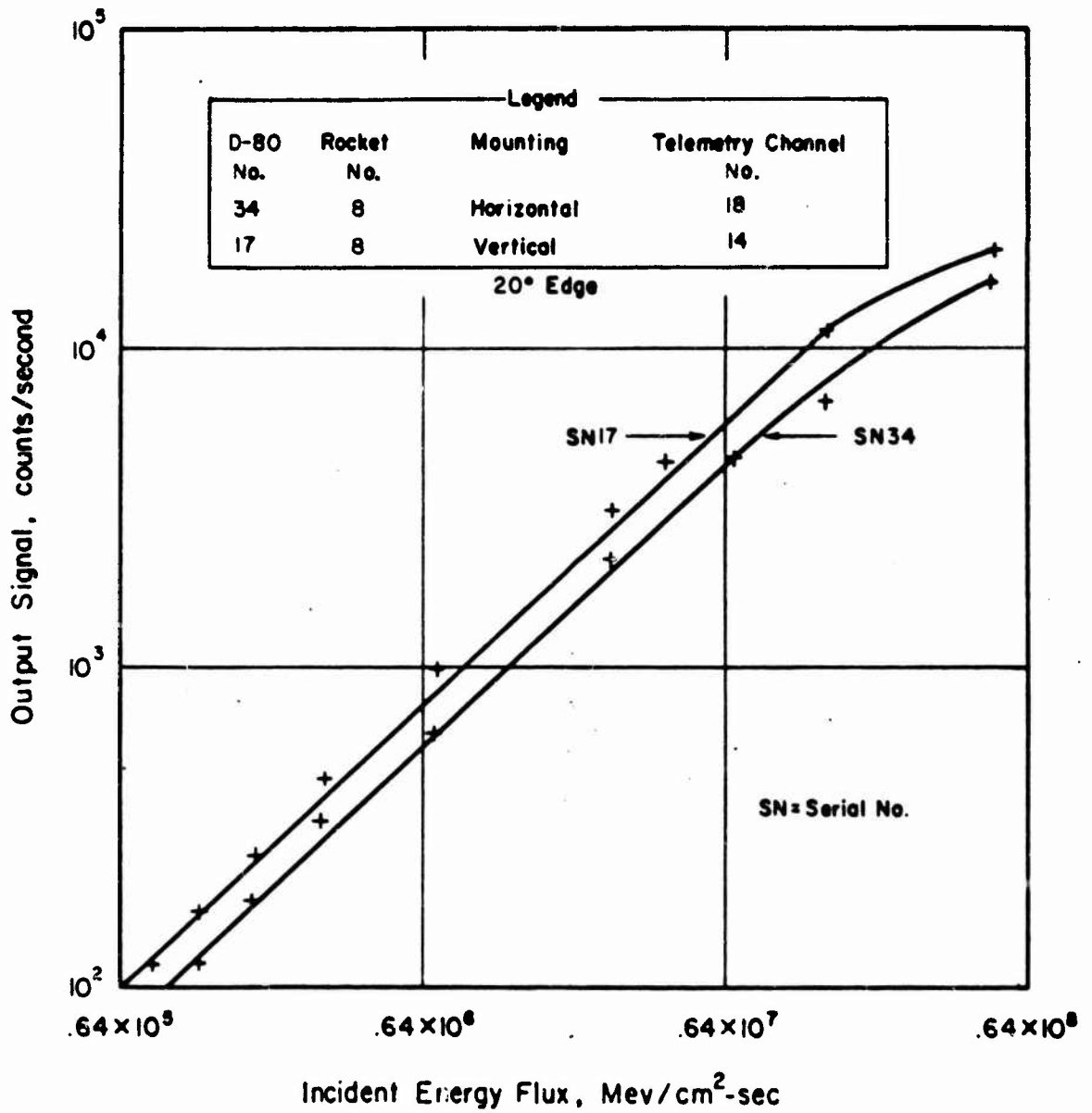


Figure E.1 Gamma scanner D-80 detector calibration curves for Rocket 8, SN 17 and 34.

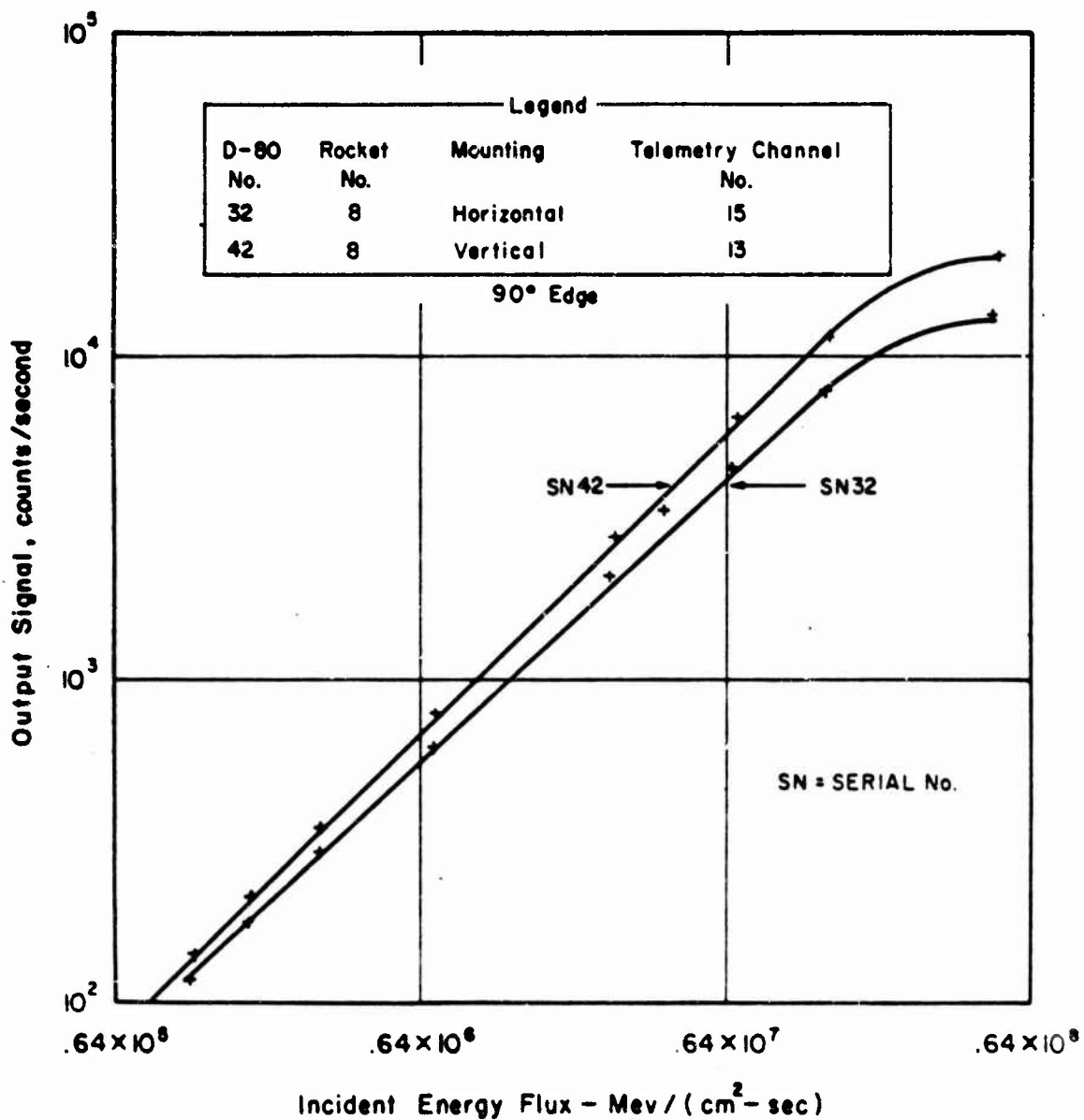


Figure E.2 Gamma scanner D-80 detector calibration curves for Rocket 8, SN 32 and 42.

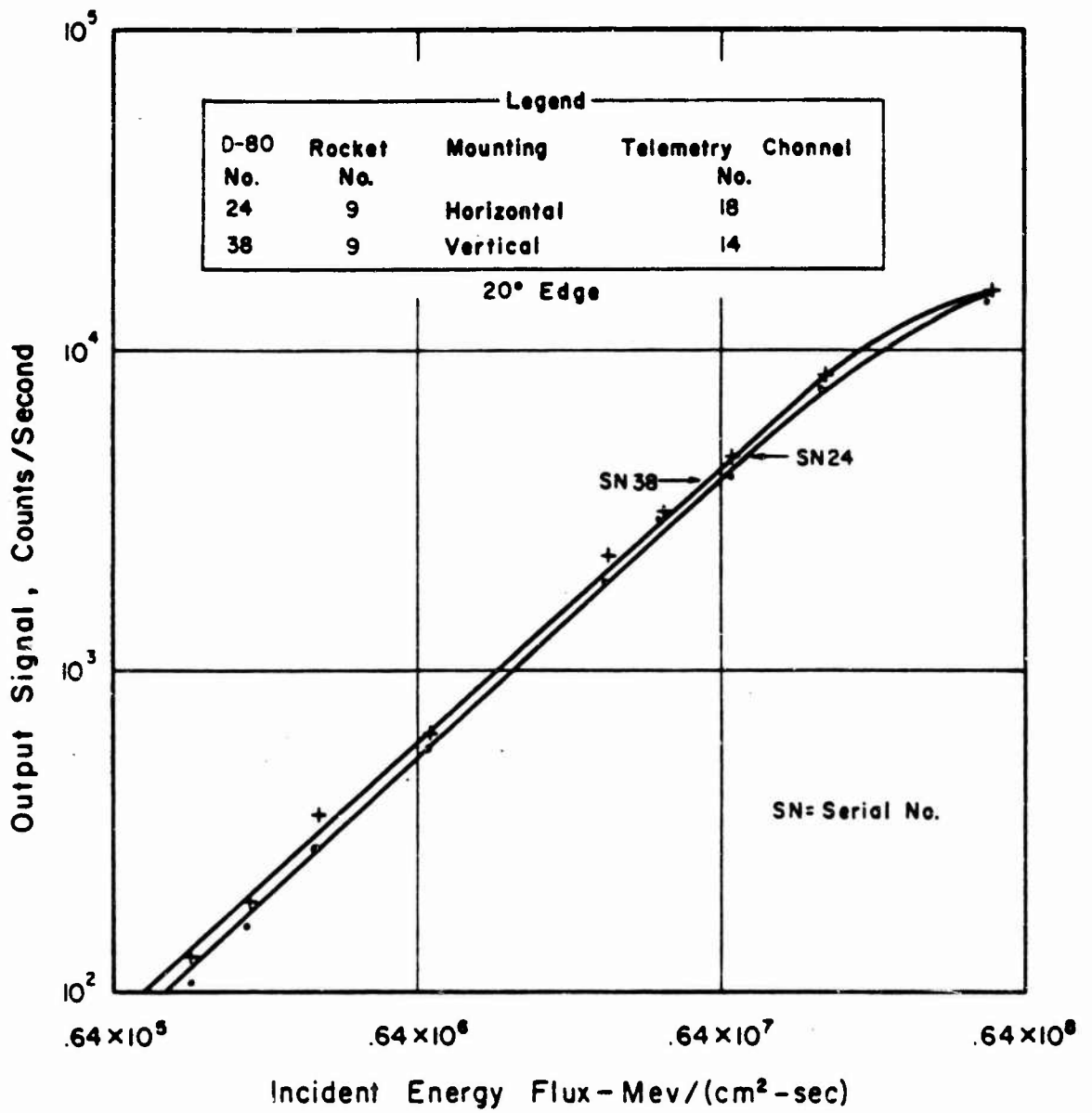


Figure E.3 Gamma scanner D-80 detector calibration curves for Rocket 9, SN 24 and 38.

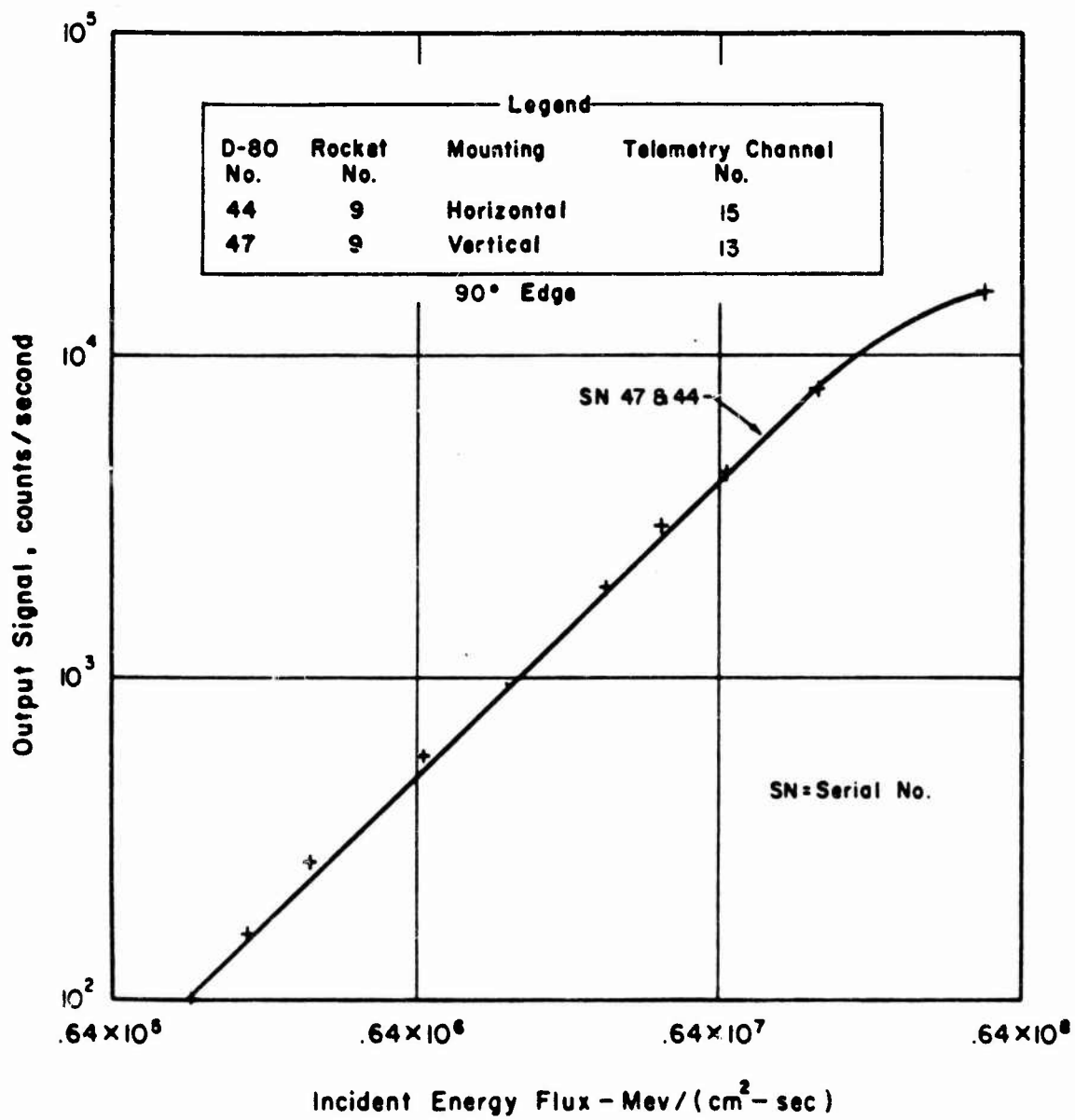


Figure E.4 Gamma scanner D-80 detector calibration curves for Rocket 9, SN 44 and 47.

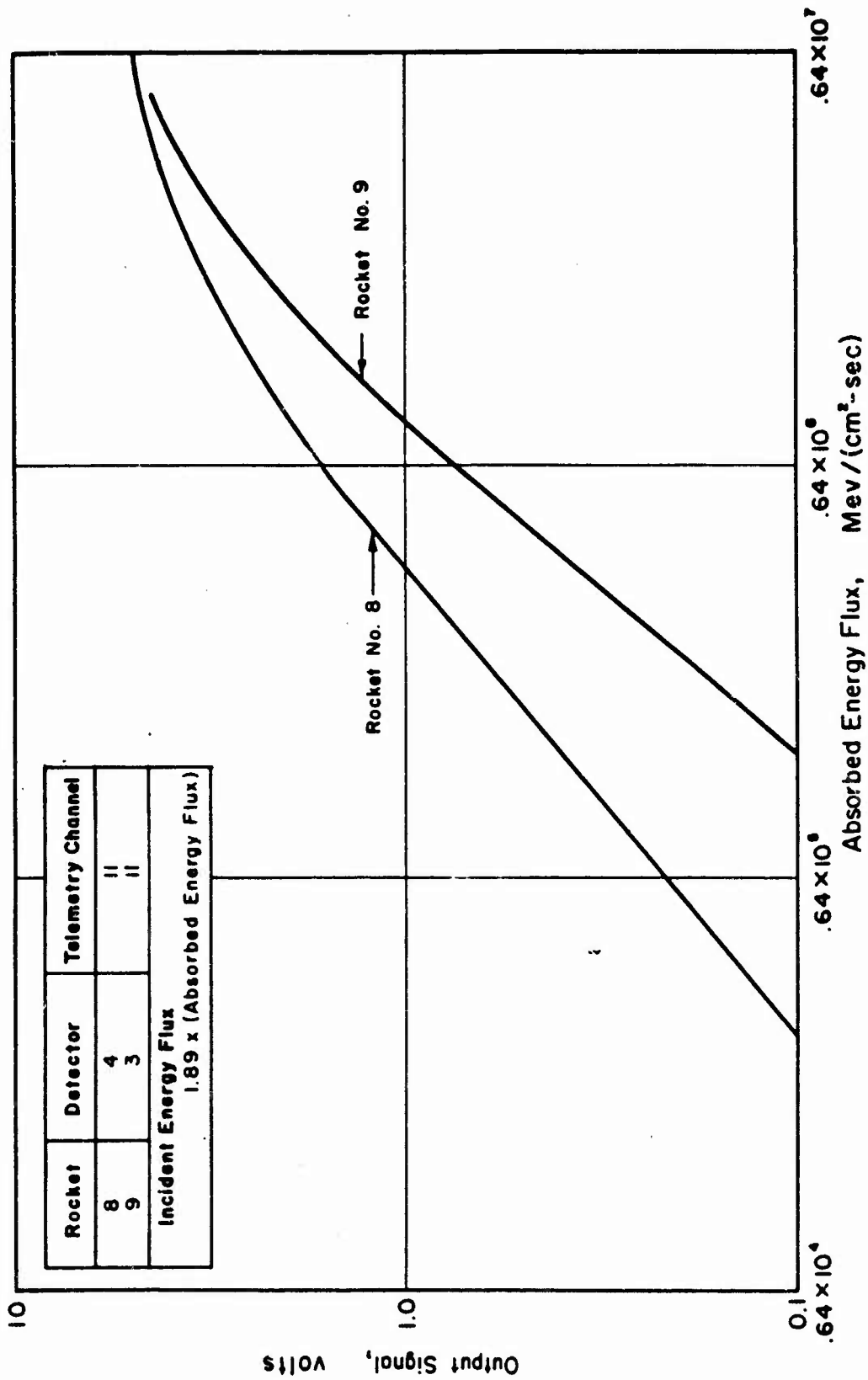


Figure E.5 Omnidirectional gamma detector calibration curves for Rockets 8 and 9.

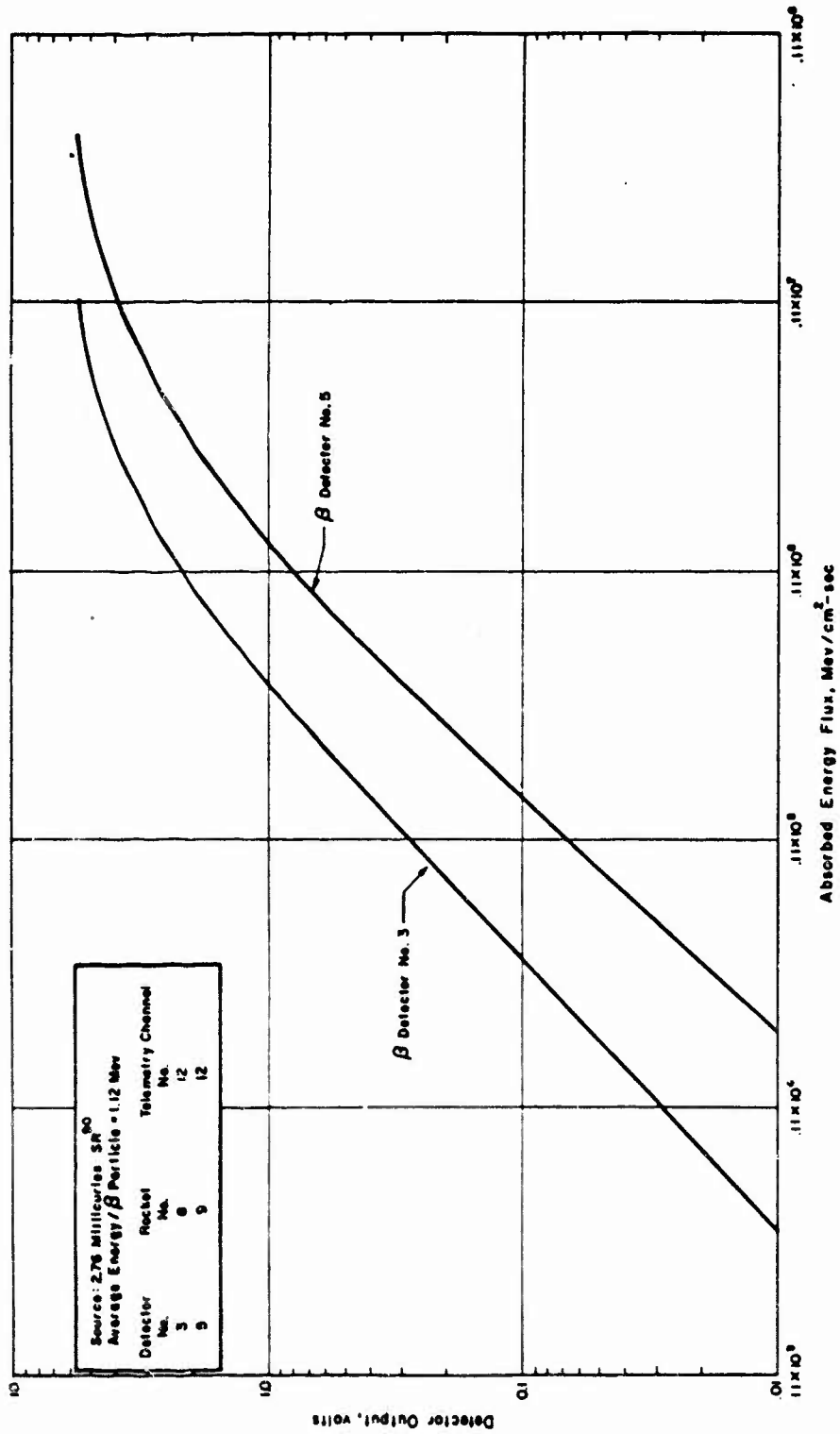


Figure E.6 Beta detector calibration curves for Rockets 8 and 9, absorbed energy flux.

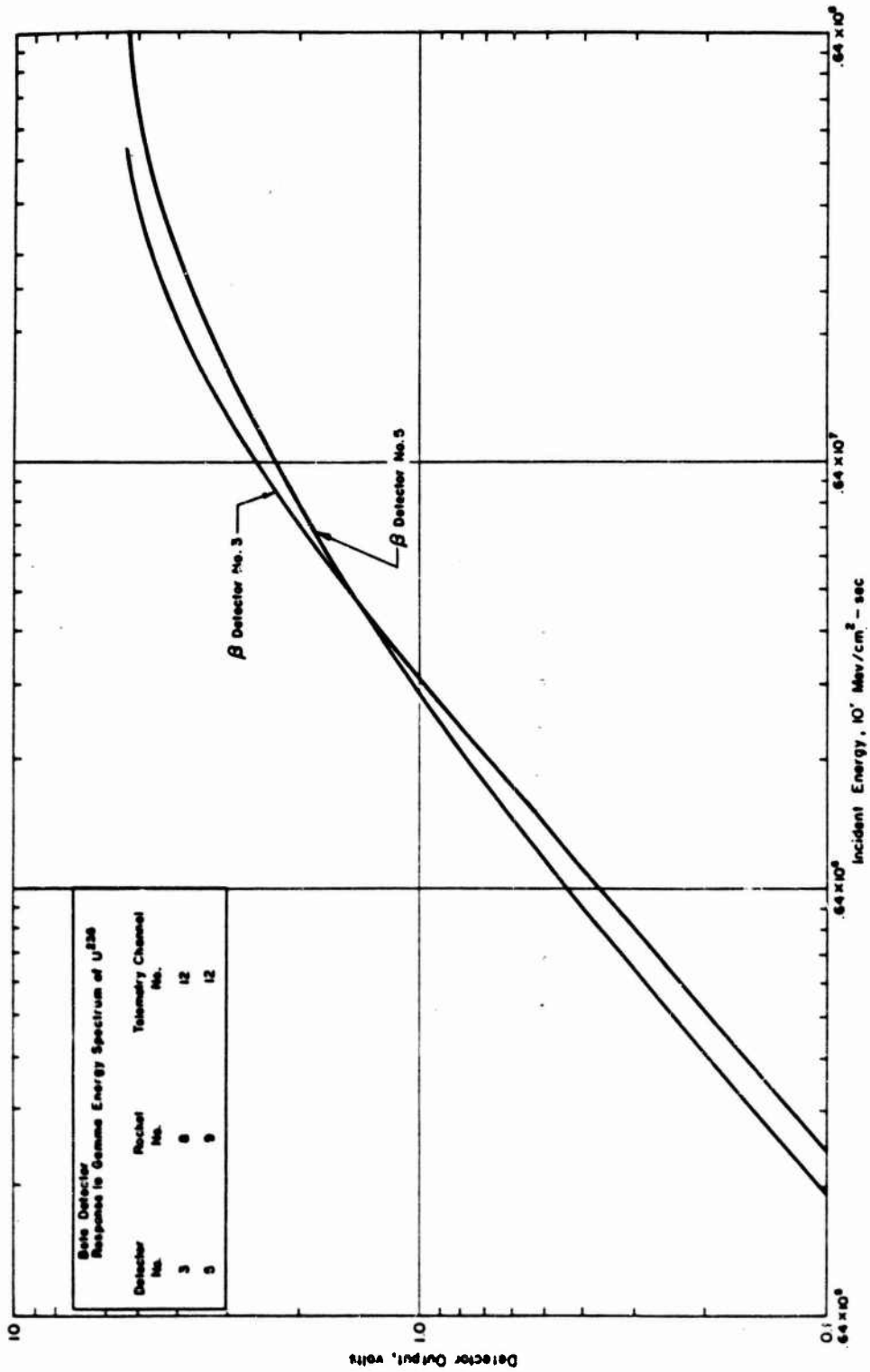


Figure E.7 Beta detector calibration curves for Rockets 8 and 9, incident energy.

APPENDIX F

MAGNETOMETER RESULTS AND ASPECT DETERMINATION

F.1 MAGNETOMETER RESULTS

The magnetometers provided useful data on all flights whenever the telemetry signal was above the noise level. Due to telemetry system drifts, the Z'-magnetometer (longitudinal) data is valid only on a relative basis. The outputs of the X'- and Y'-magnetometers are self-calibrating with respect to bias errors, as described below, and are useful for calculating the absolute payload aspect. Preliminary analysis of magnetometer results revealed that the instruments were not sufficiently sensitive to detect shifts in the magnetic field caused by the nuclear detonations. Data reduction of the magnetometer data is in progress.

F.2 ASPECT DETERMINATIONS

The magnetometers used on the Electro-Optical Systems, Inc. (EOS) payloads were designed to detect variations in the earth's magnetic field due to motion of the payload. The payload aspect will be computed from these magnetic field variations.

The magnetometers formed a right-handed coordinate system with the Z-axis lying along the longitudinal or spin axis of the payload. (This coordinate system is denoted as X', Y', and Z'.) The output of each magnetometer was proportional to the magnetic field intensity times the cosine of the angle between the magnetic field vector and the alignment direction of the magnetometer. Therefore, data was obtained which allowed the calculation of the direction cosines of each of the three payload axes with respect to the local magnetic

field vector of the earth. This is known as magnetic aspect. Theoretically, the three mutually perpendicular magnetometers provided sufficient data to calculate the absolute magnitude of the local magnetic field; therefore, the accuracy of the measured data can be checked by comparing the magnitude of the measured magnetic field vector with the theoretical magnetic field at that point in space.

As noted above, the output voltage of the magnetometers was proportional to the magnitude of the magnetic field times the cosine of the angle between the sensitive axis of the detector and the magnetic field vector. As this angle became greater than 90 degrees, the output voltage became negative. Since negative output was incompatible with the telemetry subcarrier oscillators, the magnetometer output voltage was biased at 2.4 volts. This bias voltage was controlled by a Zener diode in each magnetometer output circuit and remained stable to within ± 1 percent when the input voltage was between 5.7 and 7 volts. Drifts in output signal bias were noted on all magnetometer channels, but, with the exception of one payload, the input voltage remained between the above limits. It was assumed that bias errors were caused by telemetry VCO drift. Unfortunately, EOS was unable to obtain in-flight calibrators for five of the seven payloads, and drifts inherent in FM/FM telemetry systems due to temperature and humidity changes caused, in some cases, very large percentage errors in the measured magnetic field component. This error occurred when the sensitive axis of the magnetometer was nearly at right angles to the magnetic field vector, thus producing a magnetic field reading of nearly zero gauss, which corresponded to a magnetometer output of 2.4 volts. Thus, a telemetry bias drift of only 2 percent of full scale (0.1 volts) changed the actual magnetic field reading by a very large percentage. (For readings near zero, errors exceeded 50 percent.) Although this caused the Z'-axis magnetometer data to be valid only on a relative basis, it did not, as demonstrated below, invalidate the X'- and the Y'-magnetometer data because of an inherent self-calibrating feature of the instrument.

In the absence of coning (i.e., rotation around axes which were perpendicular to the longitudinal axis) the payload rolled about the longitudinal axis only, and the outputs of the X'- and Y'-(transverse) magnetometers were symmetrical about zero gauss. These outputs varied between maximum positive and maximum negative readings (gauss) when the magnetometers were oriented so that the angles between the magnetometers and the magnetic field vector F were minimum, and maximum, respectively. This type of output provided a self-calibration on the telemetry signal, because zero gauss could always be found. On all flights, except Rocket 18, the spin frequency (the rotation of the payload around its longitudinal or Z'-axis) was much greater than the coning frequency. Therefore, it was assumed that for short periods (a few spin cycles) the payload did not cone. In addition to employing the no-coning assumption, the X'- and Y'-magnetometer outputs must be 90 degrees out of phase with each other. The maximum positive and maximum negative readings (gauss) on any one channel can be averaged, thus eliminating bias errors. In addition, the four extrema ($\pm X'$ and $\pm Y'$) can be averaged over a short time period (one cycle) to reduce gain errors.

The angle of closest approach of either the X'- or Y'-magnetometer to the F-vector defines the orientation of the X'-Y' plane of the payload (and therefore the Z'-axis of the payload) with respect to the F-vector. This can be determined from the above data and the theoretical absolute value of F. Note that the Z'-axis magnetometer data will not be used. Since the Z'-axis magnetometer data cannot be calibrated in the above manner, the data output from this channel can only be trusted on a relative basis. Relative measurements can be used to determine the coning frequency, and to note where to take the readings on X'- and Y'-channels to find the extrema; i.e., the maximum and minimum excursions of the cone upon which the Z'-axis of the vehicle is moving. The same information, coning frequency and extremes of the cone, can be determined from the pattern of X' or Y' readings.

The instantaneous magnetic aspect can be obtained by use of a computer in finding the maximum positive and negative readings (gauss) of the X'-magnetometer closest to the point in time where information is desired; in the same time period, the maximum positive and maximum negative readings of the Y'-axis magnetometer can be determined. These four data inputs can then be averaged and divided by the absolute value for the total magnetic field vector F to provide the cosine of the angle between the X'-Y' plane and the F-vector. The aspect of the Z', or longitudinal axis is then the complement of the X-Y plane. The actual readings of the X'- and Y'-channel at the desired time will then, when processed with theoretical magnetic field data, give the cosine of the angle between the X'- and Y'-axes and the F vector at the desired point in space and time. Determination of the payload attitude is discussed in Appendix G.

F.3 STATIC MAGNETOMETER CALIBRATION

A static calibration of the magnetometer package was performed to determine if the components of the payload distorted the earth's magnetic field detected by the magnetometers. This calibration was performed in an open field where the earth's magnetic field was unperturbed by surrounding objects or power lines.

The magnetometer package consisted of a phenolic block and three sensors. These sensors were mounted in three mutually perpendicular holes which were drilled out of the block. The calibration procedure consisted of two steps: (1) orienting the magnetometer package in about 25 directions and reading the outputs of the magnetometers on a digital voltmeter, and (2) placing the magnetometer package in the payload and repeating step (1) for the same 25 positions.

The orientation of the magnetometer package and the payload was known to only ± 3 degrees accuracy. In most orientations this was a greater error than the expected 1-percent accuracy of the magnetometers.

Figure F.1 shows histograms of the errors calculated from differences between the magnetometer package output readings and the

actual field (calculated from information supplied by U. S. Coast and Geodetic Survey). Histograms of errors calculated from differences between the payload-mounted magnetometer package readings and the actual field are shown in Figure F.2 . Inspection of the histograms reveals a bias error in the Y¹-axis, but it was generally below 3 percent. This error was acceptable, since it was smaller than telemetry errors.

F.4 DYNAMIC MAGNETOMETER CALIBRATION

The magnetometer package was mounted in the top of the payload and surrounded by a truncated conical aluminum shell. As the payload rotated (spun about the roll or longitudinal axis) in the presence of the earth's magnetic field, eddy currents flowed in the ground plane which produced the effect of rotating the direction of the earth's magnetic field vector internal to the aluminum shell. This field rotation was represented by two vector components within the shell as shown in Figure F.3 . Two vectors were sufficient for this calibration, because the vector rotation was only in the plane perpendicular to the angular velocity vector of the shell.

To determine whether these eddy currents caused a noticeable change in the direction of the magnetic field, a theoretical calculation was performed. A solution for a truncated cone or cylinder proved to be too time-consuming for the limited results expected, so an infinite cylinder approximation to the aluminum shell was used. Figure F.4 shows the configuration employed. B_o was the component of the earth's magnetic field perpendicular to the angular velocity vector ω of the payload and located far from the payload.

B_{11} was parallel to B_o and inside the cylinder, and B_{\perp} was perpendicular to B_o . Both B_{11} and B_{\perp} were in the plane perpendicular to ω . The cylinder had a radius $r = 0.1$ meter, a wall thickness $t = 1.5 \times 10^{-3}$ meter, and a resistivity $\rho = 4.3 \times 10^{-8}$ ohm-meter. Then,

$$|B_{11}| = B_o [1 / 1 + \Lambda^2] \quad (F.1)$$

and

$$|B_{\perp}| = B_0[\Lambda / 1 + \Lambda^2] \quad (\text{F.2})$$

The angle of rotation of the field vector is

$$B_{\perp} / B_{11} = \tan \phi = \Lambda$$

where

$$\Lambda = \omega \mu_0 \text{tr} / 2 \quad (\text{F.3})$$

$$\mu_0 = \text{permeability of free space} = 4 \pi \times 10^{-7}$$

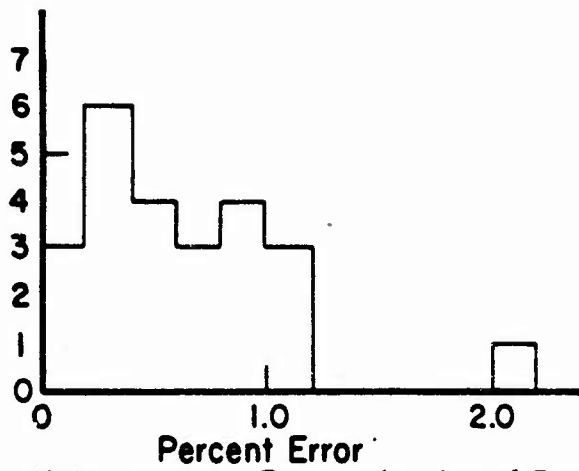
Inserting the numbers given above in Equation F.3

$$\Lambda = (2.2 \times 10^{-3})\omega$$

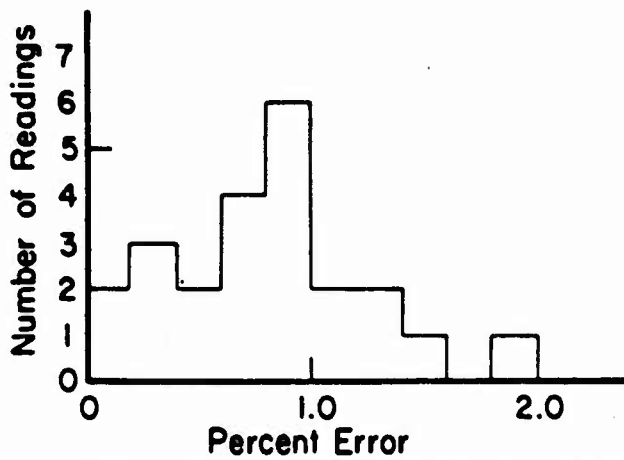
Rockets 8 and 9 (Star Fish event) rotated at approximately 5 to 6 rps, and the remainder of Project 6.2 rockets rotated at 1 to 2.5 rps. For $\omega = 38$ (6 rps), $\Lambda = 0.084$ radian or 5 degrees.

This could cause some trouble for the magnetometer readings in some of the faster rotating payloads, but errors of less than two degrees on the other payloads were of little consequence. Since this calculation provided only coarse data on the effects of eddy currents on the direction of the magnetic field, a dynamic experiment was desirable to provide more accurate and reliable calibration data. However, scheduling difficulties prevented this experiment from being performed prior to the submission of this report.

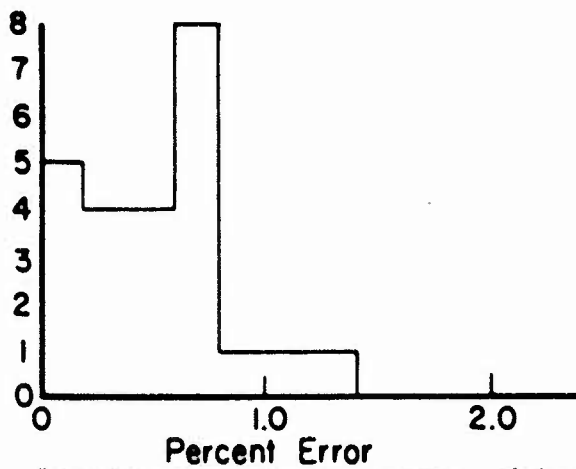
Note: All Errors Are Compared to Predicted Readings, Which Are Accurate Only to 3°



X-Magnetometer Error vs. Number of Readings



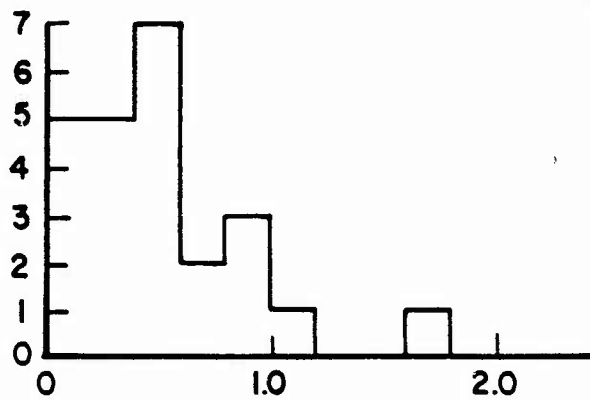
Y-Magnetometer Error vs. Number of Readings



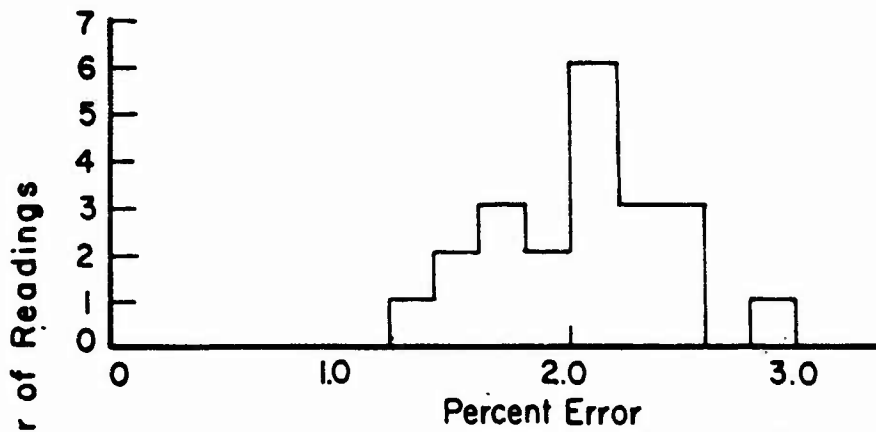
Z-Magnetometer Error vs. Number of Readings

Figure F.1 Error histograms of X-, Y-, and Z-magnetometers in phenolic packages.

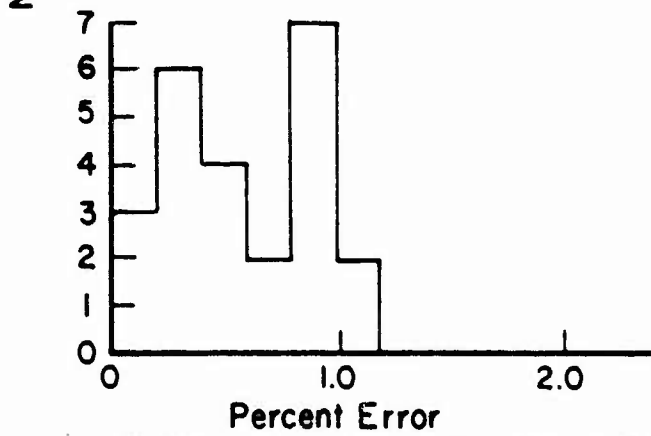
Note: All Errors Are Compared to Predicted Readings, Which Are Accurate Only to 3°



X-Magnetometer Error vs. Number of Readings

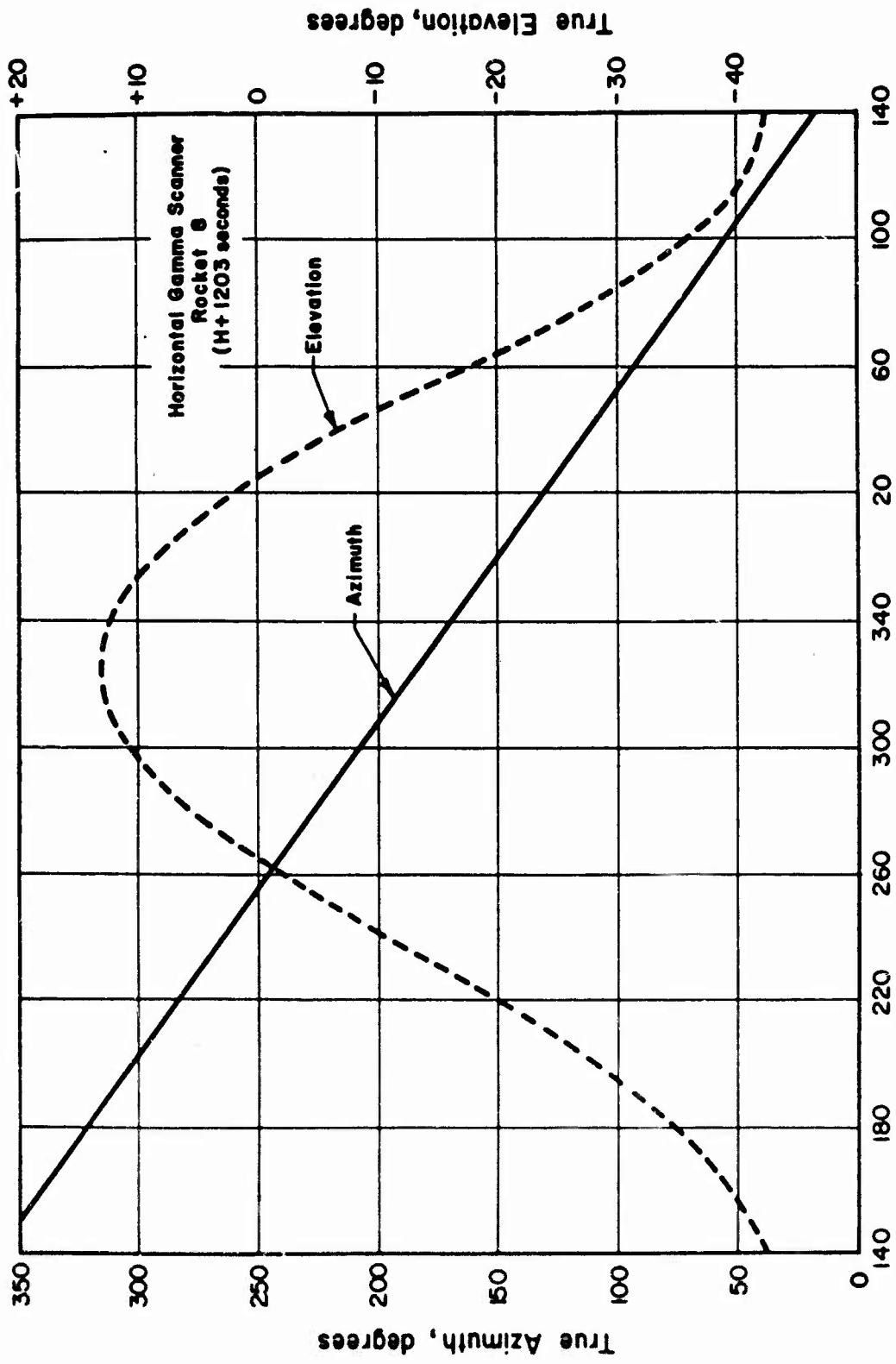


Y-Magnetometer Error vs. Number of Readings



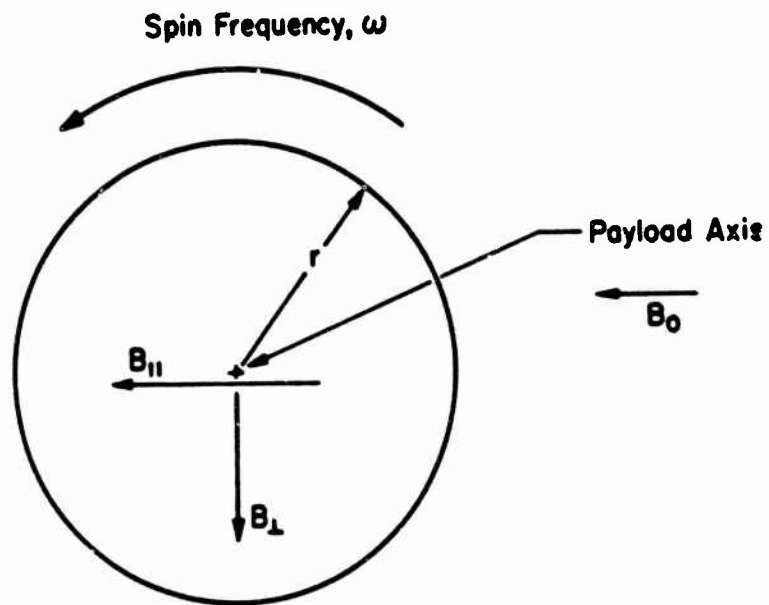
Z-Magnetometer vs. Number of Reading

Figure F.2 Error histograms of X-, Y-, and Z-magnetometers in payload.



Y-Axis Magnetometer - Position From Magnetic East, degrees

Figure P.3 True azimuth and elevation look angles with respect to the Y-axis magnetometer position.



Note: B = Magnetic Field Components
 r = Radius of Theoretical Cylinder

Figure F.4 Assumed configuration for calculation of dynamic effects of payload on the earth's magnetic field.

APPENDIX G

INSTRUMENT ATTITUDE DETERMINATION

To adequately describe the debris cloud resulting from the nuclear explosion, it is essential to know the direction, at any time, of each detector on the payload relative to an inertial coordinate system. Since the payload flight time is small relative to the earth's period of rotation, the coordinate system can, for most practical purposes, be fixed in the earth without resulting in a significant error. Thus, during an interval of 400 seconds, which is the average flight time, the earth will rotate through an angle of 1.67 degrees. This error is probably less than the accuracy with which one can determine the payload attitude by means of the magnetometer data. A convenient coordinate system for determining the payload attitude is the $X; Y; Z$ -system shown in Figure G.1(a) which has its origin at Johnston Island. The Z -axis points along the local vertical (out of the earth), the Y -axis points to true north, and the X -axis points due east. Here, D denotes the sensitive axis of a detector (e.g., a gamma scanner); θ and ϕ are the polar coordinates of this axis. Figure G.1(b) defines the fixed polar angles θ' , ϕ' of the detector axis relative to the X' , Y' , and Z' -magnetometer axes. Although the origin of the X' , Y' , and Z' -system moves through space with the payload, it can be considered to coincide with Johnston Island if only rotation between the $X'; Y'; Z'$ and $X; Y; Z$ -systems is to be measured. Alternatively, a third coordinate system can be assumed that translates with the payload, but maintains an orientation fixed with respect to the $X; Y; Z$ -system. The angles θ and ϕ remain the same as shown in Figure G.1. Since the separation of this third coordinate system from that shown in Figure G.1(a) is not of interest, the latter will

suffice for attitude determination. Refer to Figure G.1(c). Here, F denotes the magnetic field vector at the origin of the X^L, Y^L, Z^L system, i.e., at the payload.

Direction of Instruments. The instantaneous polar angles θ and ϕ , of a detector are of primary interest in determining its attitude. These are given by

$$\phi = \tan^{-1} [\cos (D,X) / \cos (D,Y)] \quad (G.1)$$

$$\theta = \cos^{-1} [\cos (D,Z)] \quad (G.2)$$

where:

$$\begin{aligned} \cos (D,X) &= a_{11} \sin \theta' \sin \phi' + a_{21} \sin \theta' \cos \phi' + a_{31} \cos \theta' \\ \cos (D,Y) &= a_{12} \sin \theta' \sin \phi' + a_{22} \sin \theta' \cos \phi' + a_{32} \cos \theta' \\ \cos (D,Z) &= a_{13} \sin \theta' \sin \phi' + a_{23} \sin \theta' \cos \phi' + a_{33} \cos \theta' \end{aligned} \quad (G.3)$$

Here, a_{ij} are the transformation (rotation) coefficients, i.e., direction cosines, between the X - and X' -systems. Thus,

$$\begin{aligned} X' &= a_{11}X + a_{12}Y + a_{13}Z \\ Y' &= a_{21}X + a_{22}Y + a_{23}Z \\ Z' &= a_{31}X + a_{32}Y + a_{33}Z \end{aligned} \quad (G.4)$$

Of course, the values of θ' and ϕ' are already known (see Table G.1). Of the nine coefficients a_{ij} , three can be determined experimentally. These are a_{31} , a_{32} , a_{33} , which define the direction of the Z' -axis in the $X; Y; Z$ -system. Since the Z' -axis points along the longitudinal (symmetry) axis of the payload, a knowledge of this direction will yield the values of a_{31} , a_{32} , a_{33} . The task of determining this direction becomes difficult if the payload is coning, i.e., if Z' describes the surface of a cone in space. This problem is discussed

below. If the payload does not cone, then, since final burnout occurs relatively low in the atmosphere (at an average altitude of 30 statute miles), the Z'-axis will nearly coincide with the payload velocity vector at the instant of burnout. It will maintain this zero angle of attack as long as the atmosphere exerts a significant influence on the fins of the last stage. After the payload leaves the atmosphere, the Z'-axis will maintain the same orientation as it had just before leaving until re-entry. The altitude at which the payload leaves the atmosphere is assumed to be the same as the re-entry altitude and is determined for each payload by examining the Z' axis magnetometer data for evident changes in attitude. These altitudes are shown in Table G.2. The direction of the velocity vector at burnout can readily be determined from a space plot of the payload trajectory.

The remaining six coefficients a_{11} , a_{12} , a_{13} , a_{21} , a_{22} , a_{23} are determined from the following six simultaneous equations:

$$\begin{aligned}
 a_{11} \cos(F, X') + a_{21} \cos(F, Y') + a_{31} \cos(F, Z') &= \cos(F, X) \\
 a_{12} \cos(F, X') + a_{22} \cos(F, Y') + a_{32} \cos(F, Z') &= \cos(F, Y) \\
 a_{13} \cos(F, X') + a_{23} \cos(F, Y') + a_{33} \cos(F, Z') &= \cos(F, Z) \\
 a_{11} &= a_{22}a_{33} - a_{32}a_{23} \\
 a_{12} &= a_{31}a_{23} - a_{33}a_{21} \\
 a_{13} &= a_{21}a_{32} - a_{22}a_{31}
 \end{aligned} \tag{G.5}$$

The values of $\cos(F, X')$, $\cos(F, Y')$, $\cos(F, Z')$ are readily determined from the magnetometer data. Thus, for example,

$$\cos(F, X') = F_{X'} / (F_{X'}^2 + F_{Y'}^2 + F_{Z'}^2)^{1/2}$$

To determine the values of $\cos(F, X)$, $\cos(F, Y)$, $\cos(F, Z)$, a knowledge of the earth's magnetic field is required.

Recall that the four direction-sensitive detectors on the payload were the photometer, beta detector, horizontal gamma scanner, and vertical gamma scanner. Table G.1 lists the polar angles θ' and ϕ' of each detector axis. (Refer to Figure G.1(b)). The pointing direction of the horizontal and vertical gamma scanners is defined as the direction away from the shield along a line from the 90-degree edge to the 20-degree edge, along the axis of the detector.

Coning Motion. If the payload cones (rotates about axes perpendicular to the Z' or longitudinal axis so that the Z' -axis traces out the surface of a cone), then the coefficients a_{31} , a_{32} , a_{33} will be some periodic function of time. Figure G.2 illustrates a simple coning motion of the payload. Here, μ and χ are the polar angles of the Z' -axis, μ' and χ' are the polar angles of the axis of the cone, and γ is the half angle of the cone. The coefficients are then given by

$$\begin{aligned} a_{31} &= \sin \mu \sin \chi \\ a_{32} &= \sin \mu \sin \chi \\ a_{33} &= \cos \mu \end{aligned} \tag{G.6}$$

where,

$$\begin{aligned} \mu &= \mu' + \gamma \sin (\omega t + \delta) \\ \chi &= \chi' + \gamma \cos (\omega t + \delta) \end{aligned} \tag{G.7}$$

Here, ω is the angular frequency of the coning motion, and δ is a constant to be evaluated. The coning angle γ and the angular frequency ω can readily be determined from the magnetometer data. A possible way of determining μ' and χ' is as follows: Assume the Z' -axis at burnout lies in the center of the cone. Then, let a_{310} , a_{320} , a_{330} denote the direction cosines of the axis on the cone (which are known from the trajectory and magnetometer data). Hence,

$$\begin{aligned} \chi' &= \tan^{-1} (a_{310} / a_{320}) \\ \mu' &= \cos^{-1} a_{330} \end{aligned} \tag{G.8}$$

There should be no ambiguity in the values assigned to χ' and μ' , since the direction of the payload velocity vector, relative to the X, Y, Z coordinate system, is known at all times from the trajectory data.

In order to determine the coefficients a_{31} , a_{32} , a_{33} we must evaluate the constant δ . In order to evaluate δ , we shall first obtain a unique solution of the following set of equations:

$$\begin{aligned} a_{31} a_{310} + a_{32} a_{320} + a_{33} a_{330} &= \cos \gamma \\ a_{31} \cos (F,X) + a_{32} \cos (F,Y) + a_{33} \cos (F,Z) &= \cos (F,Z') \quad (G.9) \\ a_{31}^2 + a_{32}^2 + a_{33}^2 &= 1 \end{aligned}$$

The quantities a_{310} , a_{320} , a_{330} , $\cos \gamma$, $\cos (F,X)$, $\cos (F,Y)$, $\cos (F,Z)$, $\cos (F,Z')$ are all known. The first equation represents a plane in the a_{31} , a_{32} , a_{33} coordinate system that passes a distance $|\cos \gamma|$ from the origin, and the second equation represents a plane that passes a distance $|\cos(F,Z')|$ from the origin. The third equation represents a unit sphere about the origin. Refer to Figure G.3. Here, α is the inclination angle between the two planes, given by

$$\cos \alpha = a_{310} \cos(F,X) + a_{320} \cos(F,Y) + a_{330} \cos(F,Z)$$

and L is the line (perpendicular to the page) formed at the intersection of the planes. Thus, α is the angle between the axis of the cone and the magnetic field vector F. From the figure we see that L is at a distance less than unity from the origin, so that L passes through the sphere at two points, thereby giving rise to two solutions: a_{31} , a_{32} , a_{33} and a_{31}' , a_{32}' , a_{33}' . Now, if the second plane in Equation G.9 were displaced parallel to itself so that it occupied either position C or D in Figure G.3, then L would be tangent to the sphere, and only one solution would be obtained from Equation G.9. The position C corresponds to the maximum permissible value of $|\cos(F,Z')|$, or the maximum angle between F and Z'. The foregoing can also be demonstrated in Figure G.4. Here, the coning circle is the circular path described

by the nose of the payload (the Z' -axis), which we assume to lie on the surface of a sphere whose center coincides with the center of mass of the vehicle. F denotes the intersection of the magnetic field vector (which passes through the vehicle center of mass) with this sphere. Positions A and B on the coning circle denote the two solutions that result when L is at a distance less than unity from the origin of the unit sphere, and positions C and D correspond to C and D in Figure G.3, which denote the unique solutions that are obtained when L is tangent to the unit sphere.

In view of the above, we see that in order to obtain a unique solution of Equation G.9, we must employ either a maximum or minimum value of $|\cos(F, Z')|$, i.e., a maximum or minimum absolute reading of the Z' -magnetometer. Let a_{311} , a_{321} , a_{331} denote the unique solution so obtained from Equation G.9. Then the corresponding values of χ and μ are given by

$$\begin{aligned}\chi_1 &= \tan^{-1} (a_{311} / a_{321}) \\ \mu_1 &= \cos^{-1} a_{331}\end{aligned}\tag{G.10}$$

If we let t_1 denote the time at which the above maximum or minimum Z' -magnetometer reading was taken, then, employing the first equation in Equation G.7, we finally obtain

$$\delta = \sin^{-1} (\mu_1 - \mu' / \gamma) - \omega t_1\tag{G.11}$$

Since the arc sine function is double valued, the above equation will yield two values for δ . The correct δ is that which, when substituted in the second equation of Equation G.7 (at $t = t_1$), yields the same χ as that computed in Equation G.10.

The angular frequency, ω , of the coning motion, appearing in Equations G.7 and G.11, will either be positive or negative, depending on the direction of coning. If the vehicle cones in a clockwise

direction (viewed from the vehicle center of mass) about the axis of the cone, then $\omega > 0$; if the vehicle cones in a counterclockwise direction, then $\omega < 0$. Refer to Figure G.5.

Conclusions. At the time of this writing a method for determining attitude similar to the method described above was unsuccessfully attempted. A number of assumptions were made in Appendix F (Aspect Determination) and in this appendix. Although these assumptions are entirely compatible with the accuracy expected in payload attitude (5 degrees to 10 degrees), there is a possibility that the assumptions are incompatible with each other, so the computer cannot solve the equations. Unfortunately, the data reduction contract was terminated almost immediately after it became apparent that the computer solution was not correct. Thus, even very simple checks on the compatibility of assumptions were not possible. It is anticipated that a new data reduction contract will be funded in the near future and that the difficulties will be resolved.

A brief review of the assumptions made in both aspect and attitude determination follows:

Aspect Determination Assumptions.

1. The X' - and Y' -magnetometer bias levels were self-calibrating, and the amplitudes of the output signals were sufficiently accurate for aspect determination.
2. The Z' -axis magnetometer signal can be reconstructed from X' - and Y' -magnetometer data and the theoretical magnetic field.
3. The earth's magnetic field was not perturbed by the events.
4. Instantaneous payload aspect can be calculated from magnetometer data; i.e., the orientation of the Z' -axis of the payload in the X , Y , Z -system can be determined to within a cone of uncertainty around the earth's magnetic field vector. This cone of uncertainty results because the magnetometer output only indicates the angular separation between the sensor axis and the magnetic field vector. Thus, the sensor location can be anywhere along the circumference of

a cone made by rotating the sensor axis about the magnetic field vector.

Attitude Determination Assumptions.

Nonconing.

1. Orientation of the Z'-axis of the payload in the atmosphere (dependent on the location of the payload in the trajectory) was coincident with the payload velocity vector and remained unchanged outside the atmosphere.

Coning.

2. That the Z'-axis coned about the payload velocity vector as a center.

3. The direction of coning motion (e.g., clockwise, etc.) was known.

The assumptions that are most likely to be in error are Aspect 1. and Attitude 1. In addition, the assumption Attitude 1 may not lie on the cone of uncertainty of Aspect 4.

At this writing, it is still believed that all these assumptions and the above suggested incompatibilities are within the accuracy limits that were originally anticipated.

Attitude Determination Results.

Star Fish.

Rockets 8 and 9 (H + 1203 and H + 2400 seconds). An inspection of the Z-axis magnetometer data on both Rockets 8 and 9 indicated that, after burnout, the output signal did not vary appreciably during flight. This was interpreted as evidence that the payload did not cone or precess about the spin axis to any significant extent (probably less than 2 degrees). Consequently, the temporal variation of the true azimuth and elevation field of view of the various directional instruments could be calculated by simple coordinate transformations.

The payload rate of spin for Rocket 8 was calculated from the magnetometer data to be 6.38 cps at 198 seconds after launch.

Blue Gill.

Rocket 15 (H + 901 Seconds). The spin frequency about the longitudinal axis was roughly 1.5 cps. High-frequency coning (2 cps) occurred about 30 seconds after burnout but decreased to zero in 5 to 7 seconds. The period of small amplitude coning gradually increased from 15 to 25 seconds until about 60 seconds after launch and stabilized to a period of 24 to 26 seconds until re-entry.

Output readings of the Z-axis magnetometer were too close to zero (2.4 volts) to be of much value without an in-flight calibrator. Therefore, the steady-state, total-included coning angle can only be estimated at between 5 degrees and 12 degrees.

The vehicle coned around an attitude estimated from trajectory data to be:

elevation = 71 degrees

azimuth = 25 degrees (from true north)

Rocket 18 (H + 1861 Seconds). Rocket 18 became unstable around the time of third stage burnout—nominally 30 seconds, and the coning angle increased from the time of burnout to about 60 seconds after launch. At this time the coning angle became maximum, and the vehicle spun about the maximum moment of inertia axis with a period of 4 seconds per cycle.

King Fish.

Rocket 19 (H - 120 Seconds). The spin rate about the longitudinal axis of Rocket 19 was 2.06 cps (28 seconds after liftoff). High-frequency coning occurred just after third-stage burnout and lasted

about 43 seconds. The coning period stabilized between 25 and 27 seconds until re-entry. The total included coning angle was approximately 13 degrees. The orientation of this payload with respect to the magnetic field made computation of the coning angle easier than for Rocket 15.

The vehicle coned around an attitude estimated from the trajectory to be

elevation = 78 degrees

azimuth = 155 degrees (from true north)

Rocket 26 (H + 780 Seconds). The spin frequency about the longitudinal axis was 2.5 cps. There was no perceptible high-frequency coning after burnout as in the previously discussed payloads. Considerable noise on the telemetry channels during this period obscured the precise motion. Coning at about a 20-second period was observed 70 seconds after launch, but its amplitude was too small to measure.

Attitude estimated from trajectory data was

elevation = 81 degrees

azimuth = 115 degrees (from true north)

Rocket 29 (H + 1500 Seconds). The spin frequency about the longitudinal axis decreased continually throughout the flight, starting about 1.9 cps shortly after burnout and decreasing to about 1.4 cps near re-entry. The payload spin rate decreased after first-stage firing and increased after third-stage ignition. Very little coning was noticed until late in the flight. The attitude of the longitudinal axis changed continually throughout the flight. This latter event was more noticeable in the decreasing amplitude of the transverse magnetometers than in the longitudinal magnetometer. At 200 seconds after launch (50 km and falling) the X-Y-plane became perpendicular to the magnetic field, and the output of these magnetometers decreased to zero.

As noted above, the attitude of this payload continually changed during the flight, but from trajectory data it is estimated that elevation was 80 degrees and azimuth was 90 degrees (from true north).

TABLE G.1 POLAR ANGLES OF EACH DETECTOR IN THE PAYLOAD-CENTERED COORDINATE SYSTEM

DETECTOR	θ'	ϕ'
Photometer	90°	90°
3 Detector	90°	90°
Horizontal Gamma Scanner	105°	45°
Vertical Gamma Scanner	90°	0°
Total Gamma Scanner	90°	0°

TABLE G.2 ALTITUDES WHERE PAYLOADS LEFT THE ATMOSPHERE

ROCKET	ALTITUDE
	km
8	60
9	60
15	69
18	Did not leave atmosphere. Flat spin. Started to recover from flat spin at 22 km.
19	107
26	76
29	Did not leave atmosphere. Zero angle of attack through- out flight.

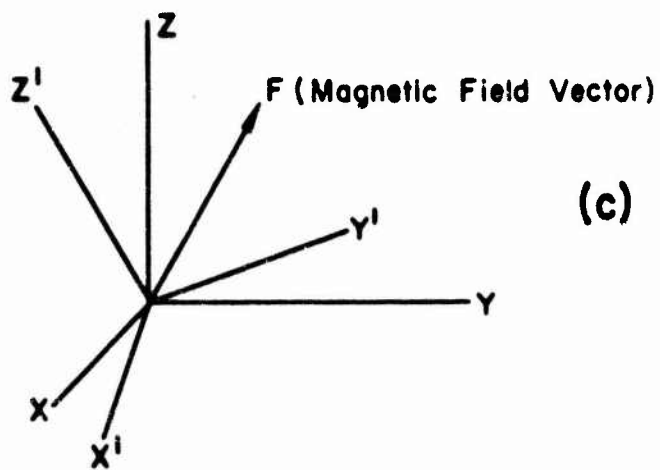
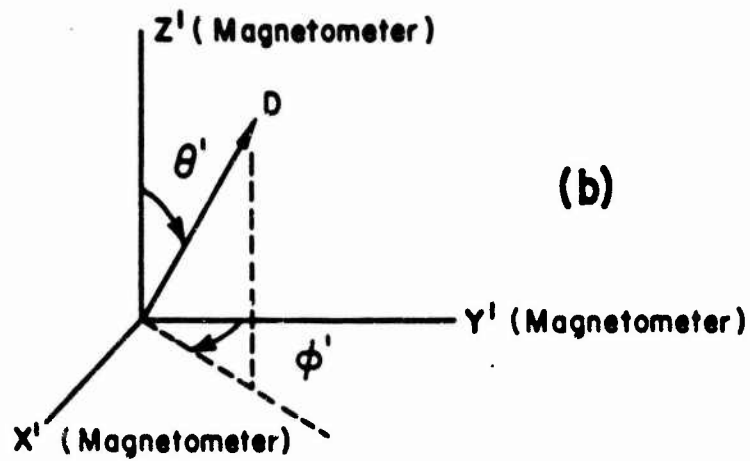
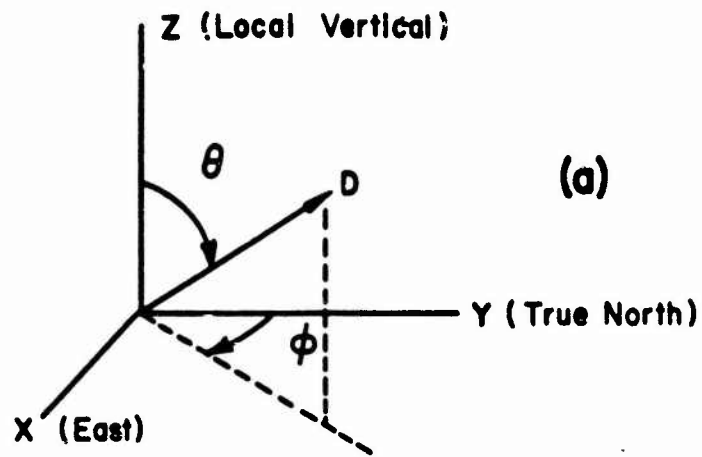


Figure G.1 Coordinate systems for determining instrument attitude.

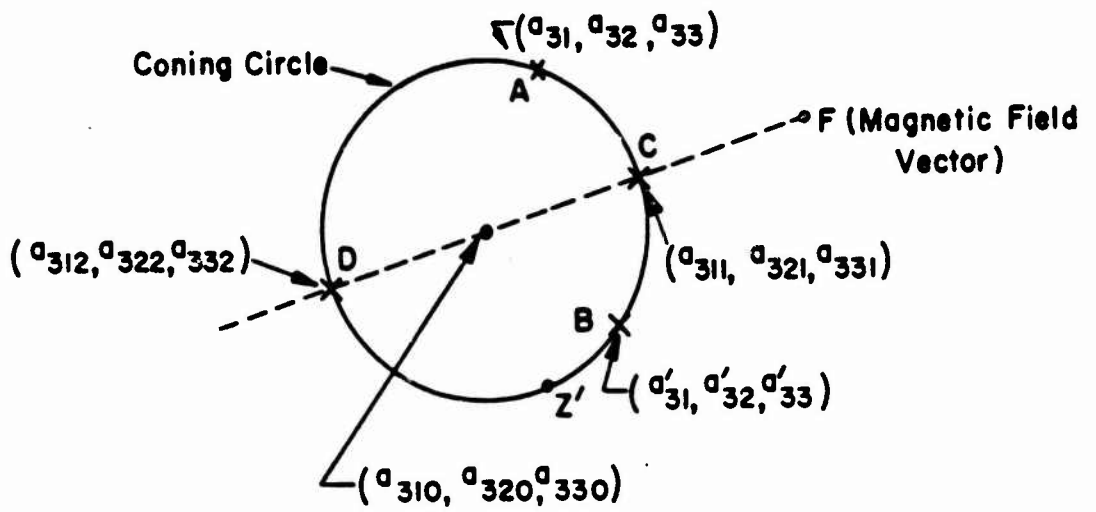


Figure G.4 Solution of Equation G.9 on coning circle.

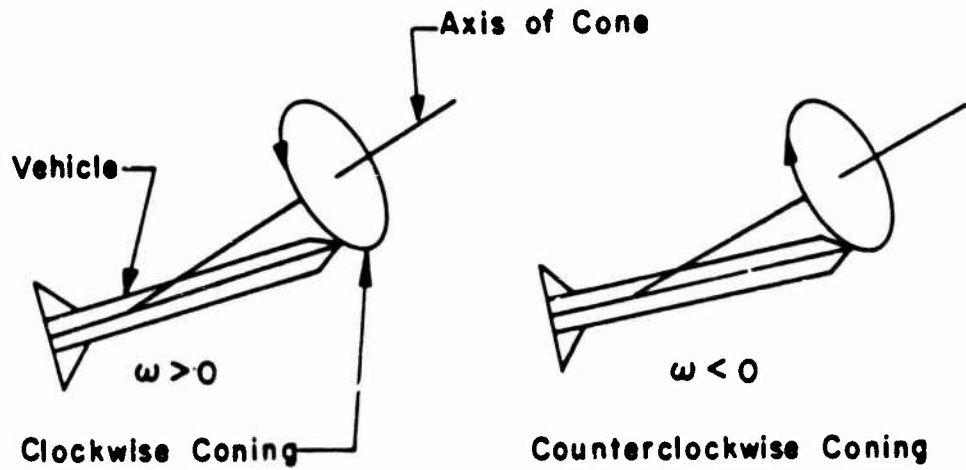


Figure G.5 Vehicle coning directions.

APPENDIX H

VHF TELEMETRY SYSTEM DATA

This appendix contains telemetry channel summaries, data allocations on taped records, and summaries of data included on tapes from the Brush and CEC recorders in the telemetry ground station. This information is given for all rockets flown by Projects 6.2, 6.3, and 6.4.

TABLE H.1 TELEMETRY CHANNEL SUMMARY, ROCKET NUMBER 1

Project Number	6.4	Date of Record	9 July 1962
Event	Ster Fish	Rocket Type	Argo (D-4)
Experiment Title	Unknown	Time Launched	2251:09W
Date Launched	8 July 1962	Where Recorded	EOS TM Ven
Where Launched	Johnston Island Pad 22	Recorder Number	1
Recorded Data Source	VHF TM 253.8 Mc	Track Number	5 end 6
Tape Reel Number	30	Paper Records Copy	
Date Location on Tape	2248 - 2252:17	Distribution	Zimney Corporation

GND-1 Data: Generally poor except for 39 seconds to 72 seconds; low signal level.

IRIG Channel Number	Channel Frequency	Description of Data	Comments
2	560 cps	Aspect X	Quality good from launch to 72 seconds end from 136 to 137 seconds. No useable signals after 137 seconds due to poor RF signal levels.
3	730 cps	Aspect Y	
4	960 cps	Aspect Z	
5	1.3 kc	Mass Spectrometer Sweep	
11	7.35 kc	Monitor Commutator	
12	10.5 kc	Beta end Gamma	2.5 rps, 30 segment
14	22.0 kc	Mass Spectrometer	--
15	30.0 kc	Langmuir Probe	--

TABLE H.2 TELEMETRY CHANNEL SUMMARY, ROCKET NUMBER 2

Project Number	6.3	Date of Record	9 July 1962
Event	Ster Fish	Rocket Type	Nike-Cajun (N-C)
Experiment Title	D-Region Physical Chem.	Time Launched	2259:09W
Date Launched	8 July 1962	Where Recorded	EOS TM Ven
Where Launched	Johnston Island Pad 16	Recorder Number	1
Recorded Data Source	VHF TM 234.0 Mc	Track Number	1 end 2
Tape Reel Number	30	Paper Records Copy	
Date Location on Tape	2254.5 - 2304:08	Distribution	Geophysical Corp. of America (GCA)

IRIG Channel Number	Channel Frequency	Description of Data	Comments
13	14.5 kc	Sweep Signal	Record length 5:08, Record quality excellent.
14	22.0 kc	Mass Number	Record length 5:08, Record quality excellent.
18	70.0 kc	Aspect Monitor	10 rps 60 segment, Record length 5:08, Record quality excellent.

TABLE H.3 TELEMETRY CHANNEL SUMMARY, ROCKET NUMBER 3

Project Number	6.3	Date of Record	9 July 1962
Event	Star Fish	Rocket Type	Honest John-Nike (HJ-N)
Experiment Title	D Region Physical Chem.	Time Launched	2258:40.5W
Date Launched	9 July 1962	Where Recorded	EOS TM Van
Where Launched	Johnston Island Pad 6	Recorder Number	1
Recorded Data Source	VHF TM 245.3 Mc	Track Number	3 and 4
Tape Reel Number	30	Paper Records Copy	
Data Location on Tape	2254 - 2300:18	Distribution	GCA

IRIG Channel Number	Channel Frequency	Description of Data	Comments
10	5.4 kc	Ion Trap	Record length 1:47.5, Record quality excellent.
11	7.35 kc	Ion Trap	Record length 1:47.5, Record quality excellent.
12	10.5 kc	Monitor Commitator	2.5 rps, 30 segment, Record length 1:47.5, Record quality excellent.
13	14.5 kc	Prompt X ray	2.5 rps, 60 segment, Record length 1:47.5, Record quality excellent.
14	22.0 kc	Beta and Gamma Experiment	2.5 rps, 60 segment, Record length 1:47.5, Record quality excellent.
15	30.0 kc	General Devices, Inc. Commutator	2.5 rps, 30 segment, Record length 1:47.5, Record quality excellent.
16	40.0 kc	RF Probe	10.0 rps, 60 segment, Record length 1:47.5, Record quality excellent.
18	70.0 kc	Aspect and Monitor	10.0 rps, 60 segment, Record length 1:47.5, Record quality excellent.

TABLE H.4 TELEMETRY CHANNEL SUMMARY, ROCKET NUMBER 4

Project Number	6.3	Date of Record	9 July 1962
Event	Star Fish	Rocket Type	HJ-N
Experiment Title	D-Region Physical Chem.	Time Launched	2307:09W
Date Launched	9 July 1962	Where Recorded	EOS TM Van
Where Launched	Johnston Island Pad 18	Recorder Number	1
Recorded Data Source	VHF TM 234.0 Mc	Track Number	1 and 2
Tape Reel Number	31	Paper Records Copy	
Data Location on Tape	2306 - 2310:58	Distribution	GCA

GMD-1 Data usable through 4:41 seconds; quality fair to good.

IRIG Channel Number	Channel Frequency	Description of Data	Comments
10	5.4 kc	Ion Trap	Record length 3:58, Record quality good.
11	7.35 kc	Ion Trap	Record length 3:58, Record quality good.
12	10.5 kc	Monitor Commutator ^a	2.5 rps, 30 segment, Record length 3:58, Record quality good.
14	22.0 kc	Beta and Gamma Experiment	2.5 rps, 60 segment, Record length 3:58, Record quality good.
15	30.0 kc	General Devices, Inc. Commutator ^b	2.5 rps, 60 segment, Record length 3:58, Record quality good to fair.
16	40.0 kc	RF Probe ^c	10.0 rps, 60 segment, Record length 3:58, Record quality good.
18	70.0 kc	Aspect and Monitor ^d	10.0 rps, 60 segment, Record length 3:58, Record quality good.

^a See Table H.41 for commutated channel summary.

^b See Table H.39 for commutated channel summary.

^c See Table H.40 for commutated channel summary.

^d See Table H.35 for commutated channel summary.

TABLE H.5 TELEMETRY CHANNEL SUMMARY, ROCKET NUMBER 5

Project Number	6.4	Date of Record	10 July 1962
Event	Star Fish	Rocket Type	D-4
Experiment Title	E-F Region Physical Chemistry	Time Launched	2307:09W
Date Launched	8 July 1962	Where Recorded	EOS TM Van
Where Launched	Johnston Island Pad 19	Recorder Number	1 and 2
Recorded Data Source	VHF TM 245.3 Mc	Track Number	3 and 4
Tape Reel Number	31 and 34	Paper Records Copy	
Date Location on Tape	From 2306 to 2309:20(1) 2314 to 2309:20(2)	Distribution	Zimney Corporation

GND-1 Date: Poor quality data from launch to 19 seconds, good from 19 to 76 seconds, end poor or none after 79 seconds.

IRIG Channel Number	Channel Frequency	Description of Data	Comments
2	560 cps	Aspect X	} Quality good from 0-53 seconds, poor or none thereafter.
3	730 cps	Aspect Y	
4	960 cps	Aspect Z	
11	7.35 kc	Monitor Commutator	2.5 rps, 30 segments
12	10.5 kc	Beta end Gamma	2.5 rps, 30 segments
14	22.0 kc	Retarding Potential	4 rps, 18 segments
15	30.0 kc	Langmuir Probe	--

* See Table H.34 for commutated channel summary.

TABLE H.6 TELEMETRY CHANNEL SUMMARY, ROCKET NUMBER 6

Project Number	6.3	Date of Record	9 July 1962
Event	Star Fish	Rocket Type	N-C
Experiment Title	D-Region Physical Chem.	Time Launched	2308:09W
Date Launched	8 July 1962	Where Recorded	EOS TM Van
Where Launched	Johnston Island Pad 15	Recorder Number	1
Recorded Data Source	VHF TM 253.8 Mc	Track Number	5 and 6
Tape Reel Number	31	Paper Records Copy	
Date Location on Tape	2306 - 2313:29	Distribution	GCA

IRIG Channel Number	Channel Frequency	Description of Data	Comments
13	14.5 kc	Sweep Signal	Record length 5:29, Record quality excellent.
14	22.0 kc	Mass Number	Record length 5:29, Record quality excellent.
18	70.0 kc	Aspect Monitor	10 rps, 60 segment, Record length 5:29, Record quality excellent.

TABLE H.7 TELEMETRY CHANNEL SUMMARY, ROCKET NUMBER 7

Project Number	6.4	Date of Record	10 July 1962
Event	Star Fish	Rocket Type	D-4
Experiment Title	E-F Region Physical Chemistry	Time Launched	2316:09W
Date Launched	8 July 1962	Where Recorded	EOS TM Van
Where Launched	Johnston Island Pad 17	Recorder Number	1 and 2
Recorded Data Source	VHF TM 253.8 Mc	Track Number	5 and 6
Tape Reel Number	31 and 34	Paper Records Copy	Zimney Corporation
Data Location on Tape	2314 - 2316:17 (1) 2314 - 2316:17 (2)	Distribution	

CHD-1 Data: Data poor to good from launch to 70 seconds, poor to 103 seconds, no data thereafter.

IRIG Channel Number	Channel Frequency	Description of Data	Comments
2	560 cps	Aspect X	Data good from 0-17 seconds,
3	730 cps	Aspect Y	no data after 17 seconds.
4	960 cps	Aspect Z	
11	7.35 kc	Monitor Commutator Subcommutated ^a	2.5 rps, 30 segment
12	10.5 kc	Beta and Gamma Subcommutated ^b	2.5 rps, 30 segment
14	22.0 kc	Retarding Potential Subcommutated ^a	4 rps, 18 segment
15	30.0 kc	Langmuir Probe	--

^a See Table H.43 for commutated channel summary.

^b See Table H.34 for commutated channel summary.

TABLE H.8 TELEMETRY CHANNEL SUMMARY, ROCKET NUMBER 8

Project Number	6.2	Date of Record	10 July 1962
Event	Star Fish	Rocket Type	D-4
Experiment Title	Gamma Ray Scanner Beta and Gamma Detector, Photometer	Time Launched	2320:14W
Date Launched	8 July 1962	Where Recorded	EOS TM Van
Where Launched	Johnston Island Pad 5	Recorder Number	1 and 2
Recorded Data Source	VHF TM-234 Mc	Track Number	1 and 2
Tape Reel Number	34	Paper Records Copy	
Data Location on Tape	2315:45 to 2335	Distribution	EOS

GMD-1 Data: Obtained 2 minutes 20 seconds of usable but only fair quality data.
Nothing but noise after that time.

IRIG Channel Number	Channel Frequency	Description of Data	Comments
4	960 cps	Z-Axis Magnetometer	Good data for 12 min 8 seconds out of approximately 13-min flight for all channels. Good data-output noted from 1-min 14 seconds to 2 minutes. Output noted from 1-1/2 to 5 minutes from launch, good data. Usable output from 1-1/2 to 2 minutes 20 seconds, good quality. Vertical D-80 No. 42 good quality data. Vertical D-80 No. 17 good quality data. Horizontal D-80 No. 32 good quality data. Good quality data. Horizontal D-80 No. 34 good quality data.
5	1.3 kc	X-Axis Magnetometer	
9	3.9 kc	Y-Axis Magnetometer	
10	5.4 kc	Photometer	
11	7.35 kc	Total Gamma Detector	
12	10.5 kc	Beta Detector	
13	14.5 kc	Gamma Scanner No. 1 Output 1. Vertical 90° Detector (inboard)	
14	22.0 kc	Gamma Scanner No. 1 Output 2. Vertical 20° Detector (outboard)	
15	30.0 kc	Gamma Scanner No. 2 Output 3. Horizontal 90° Detector (inboard)	
16	40.0 kc	Commuted Channel	
18	70.0 kc	Gamma Scanner No. 2 Output 4. Horizontal 20° Outboard.	

^a See Table H.45 for commutated channel summary.

TABLE H.9 TELEMETRY CHANNEL SUMMARY, ROCKET NUMBER 9

Project Number	6.2	Date of Record	8 July 1962
Event	Star Fish	Rocket Type	D-4
Experiment Title	Gamma Ray Scanner Beta and Gamma Detector, Photometer	Time Launched	2340:09W
Date Launched	8 July 1962	Where Recorded	EOS TM Van
Where Launched	Johnston Island Pad 6	Recorder Number	1 and 2
Recorded Data Source	VHF TM-234 Mc	Track Number	1 and 2
Tape Reel Number	32 and 35	Paper Records Copy	
Data Location on Tape	Reel 32 (2336:30 to 2355) Reel 35 (2338 to 2355)	Distribution	EOS

CMD-1 Data: Obtained only 1 minute 20 seconds of poor quality.
Noisy data remainder of flight (shows noise only).

IRIG Channel Number	Channel Frequency	Description of Data	Comments
4	960 cps	Z-Axis Magnetometer	All channels noisy 30 percent of time, have data for 13 minutes 52-1/2 sec of 14+ minute flight. General quality fair. No variations observed. No variations observed. Slight variation observed from 2 minutes to 4 minutes. Vertical D-80 No. 47 small output from 2 min to approximately 4 min. Vertical D-80 No. 38 larger output from 2 to 4 min. Scanning action observed. Horizontal D-80 No. 44 small output from 2 to 4 minutes. Bad VCO, no data. Horizontal D-80 No. 24 significant output 2-to 4-min cloud scan observed.
5	1.3 kc	X-Axis Magnetometer	
9	3.9 kc	Y-Axis Magnetometer	
10	5.4 kc	Photometer	
11	7.35 kc	Total Gamma Detector	
12	10.5 kc	Beta Detector	
13	14.5 kc	Gamma Scanner No. 1 Output 1. Vertical 90° Detector (inboard)	
14	22.0 kc	Gamma Scanner No. 1 Output 2. Vertical 20° Detector (outboard)	
15	30.0 kc	Gamma Scanner No. 2 Output 3. Horizontal 90° Detector (inboard)	
16	40.0 kc	Commuted Channel ^a	
18	70.0 kc	Gamma Scanner No. 2 Output 4. Horizontal 20° Outboard.	

^a See Table H.45 for commuted channel summary.

TABLE H.10 TELEMETRY CHANNEL SUMMARY, ROCKET NUMBER 10

Project No. 6.3	Date of Record 25 Oct 1962
Event Blue Gill Triple Prime	Rocket Type N-C
Experiment Title D-Region Physical Chemistry	Time Launched 2358:49.2W
Date Launched 25 Oct 1962	Where Recorded EOS TM Van
Where Launched Johnston Island Pad 16	Recorder No. 1
Recorded Data Source VHF-TM 253.8	Track Number VHF 5 and 6, GMD 8
Tape Reel Number 74	Paper Records Copy
Data Location on Tape Lift-off thru 0005:22.8	Distribution GCA

IRIG			
Channel Number	Channel Frequency	Description	Comments
13	14.5 kc	Sweep signal	AGC recording indicates that all SCO's would have high S/N ratio throughout flight for good data. A tape recorder failure at H-0 and lasting 1 min., 40 sec. caused loss of all data for this period from the EOS TM van.
14	22.0 kc	Mass number	
16	70.0 kc	Aspect and monitor	

TABLE H.11 TELEMETRY CHANNEL SUMMARY, ROCKET NUMBER 11

Project No. 6.3	Date of Record 25 Oct 1962
Event Blue Gill Triple Prime	Rocket Type HJ-N
Experiment Title D-Region Physical Chemistry	Time Launched 2357:49.3W
Date Launched 25 Oct 1962	Where Recorded EOS TM Van
Where Launched Johnston Island Pad 19	Recorder No. 1
Recorded Data Source VHF-TM-245.3 Mc	Track Number VHF 3 and 4, GMD 9
Tape Reel Number 74	Paper Records Copy
Data Location on Tape Lift-off thru 0004:42.3	Distribution Geophysical Corp. of America

IRIG			
Channel Number	Channel Frequency	Description	Comments
10	5.4 kc	Ion trap	A tape recorder failure at H-0 and lasting 1 min., 40 sec. caused loss of all data during this period. AGC recording indicates that all SCO's would have high S/N ratio throughout flight for good data.
11	7.35 kc	Ion trap	
12	10.5 kc	Monitor commutator	
13	14.5 kc	Prompt X ray	
14	22.0 kc	Beta and gamma experiment	
15	30.0 kc	GRD commutator	
16	40.0 kc	RF probe	
18	70.0 kc	Aspect and monitor	

TABLE H.12 TELEMETRY CHANNEL SUMMARY, ROCKET NUMBER 12

Project No.	6.3	Date of Record	26 Oct 1962
Event	Blue Gill Triple Prime	Rocket Type	H J-N
Experiment Title	D-Region Physical Chemistry	Time Launched	0004:49.5W
Date Launched	26 Oct 1962	Where Recorded	BOS TM Van
Where Launched	Johnston Island Pad 6	Recorder No.	1
Recorded Data Source	VHF-TM-234.0 Mc	Track Number	VHF 1 and 2, GMD 10
Tape Reel Number	74	Paper Records	Copy
Data Location on Tape	Lift-off thru 0004:44.1	Distribution	GCA

IRIG			
Channel Number	Channel Frequency	Description	Comments
10	5.4 kc	Ion trap	AGC recording indicates that all SCO's would have high S/N ratio throughout flight for good data.
11	7.35 kc	Ion trap	
12	10.5 kc	Monitor commutator	
13	14.5 kc	Prompt X ray	
14	22.0 kc	Beta and Gamma experiment	
15	30.0 kc	GRD commutator	
16	40.0 kc	RF probe	
18	70.0 kc	Aspect and monitor	

TABLE H.13 TELEMETRY CHANNEL SUMMARY, ROCKET NUMBER 13

Project No.	6.3	Date of Record	26 Oct 1962
Event	Blue Gill Triple Prime	Rocket Type	N-C
Experiment Title	D-Region Physical Chemistry	Time Launched	0005:49.4W
Date Launched	26 Oct 1962	Where Recorded	EOS TM Van
Where Launched	Johnston Island Pad 15	Recorder No.	1
Recorded Data Source	VHF-TM 253.8	Track Number	VHF 5 and 6, GMD 8
Tape Reel Number	74	Paper Records	Copy
Data Location on Tape	Lift-off thru 0005:25.6	Distribution	GCA

IRIG			
Channel Number	Channel Frequency	Description	Comments
13	14.5 kc	Sweep signal	AGC recording indicates that all SCO's would have high S/N ratio throughout flight for good data.
14	22.0 kc	Mass number	
18	70.0 kc	Aspect and monitor	

TABLE H.14 TELEMETRY CHANNEL SUMMARY, ROCKET NUMBER 14

Project No. 6.3	Date of Record 26 Oct 1962
Event Blue Gill Triple Prime	Rocket Type H-J-N
Experiment Title D-Region Physical Chemistry	Time Launched 0010:58.9W
Date Launched 26 Oct 1962	Where Recorded EOS TM Van
Where Launched Johnston Island Pad 18	Recorder No. 1
Recorded Data Source VHF-TM-245.3	Track Number VHF 3 and 4, CMD 9
Tape Reel Number 74	Paper Records Copy
Data Location on Tape Lift-off thru 0004:18.1	Distribution GCA

IRIG			Comments
Channel Number	Channel Frequency	Description	
10	5.4 kc	Ion trap	AGC recording indicates that all SCO's would have high S/N ratio throughout flight for good data.
11	7.35 kc	Ion trap	
12	10.5 kc	Monitor commutator	
14	22.0 kc	Beta and gamma experiment	
15	30.0 kc	GRD commutator	
16	40.0 kc	RF probe	
18	70.0 kc	Aspect and monitor	

TABLE H.15 TELEMETRY CHANNEL SUMMARY, ROCKET NUMBER 15

Project No.	6.2	Date of Record	26 Oct 1962
Event	Blue Gill Triple Prime	Rocket Type	HJ-N-N
Experiment Title	Gamma Ray Scanner, Beta and Gamma Detector, Photometer	Time Launched	0014:49.3W
Date Launched	26 Oct 1962	Where Recorded	EOS TM Van
Where Launched	Johnston Island Pad 5	Recorder No.	2
Recorded Data Source	VHF TM 234 Mc	Track Number	1 and 2 (VHF), GMD 10
Tape Reel Number	81	Paper Records Copy	
Data Location on Tape	Launch thru 0021:01	Distribution	EOS

IRIG Channel Number	Channel Frequency	Description	Comments
4	960 cps	Z-axis magnetometer	All SCO's received with excellent quality from lift-off 0014:49.3 through 0019:56, with the following exceptions: Occasional losses of data for less than 1/10 sec. each, from 0016:11 through 0018:06. From 0019:56 data drop-outs occur more often and for longer durations until all data was lost at 0021:01.
5	1.3 kc	X-axis magnetometer	
9	3.9 kc	Y-axis magnetometer	
10	5.4 kc	Photometer	
11	7.35 kc	Total gamma detector	
12	10.5 kc	Beta detector	
13	14.5 kc	Gamma scanner No. 1 Output 1. Vert. 90 ^o det (inboard)	
14	22.0 kc	Gamma scanner No. 1 Output 2. Vert. 20 ^o det (outboard)	
15	30.0 kc	Gamma scanner No. 2 Output 3. Horiz. 90 ^o det (inboard)	
16	40.0 kc	Commuted channel	
18	70.0 kc	Gamma scanner No. 2 Output 4. Horiz. 20 ^o outboard	

TABLE H.16 TELEMETRY CHANNEL SUMMARY, ROCKET NUMBER 17

Project No.	6.3	Date of Record	26 Oct 1962
Event	Blue Gill Triple Prime	Rocket Type	HJ-N
Experiment Title	D-Region Physical Chemistry	Time Launched	0021:49.3W
Date Launched	26 Oct 1962	Where Recorded	EOS TM Van
Where Launched	Johnston Island Pad 17	Recorder No.	1
Recorded Data Source	VHF-TM 245.3 Mc	Track Number	VHF 3 and 4, GMD 8
Tape Reel Number	81	Paper Records Copy	
Data Location on Tape	Lift-off thru 0004:48.7	Distribution	GCA

IRIG Channel Number	Channel Frequency	Description	Comments
10	5.4 kc	Ion trap	AGC recording indicates that all SCO's would have high S/N ratio throughout flight for good data.
11	7.35 kc	Ion trap	
12	10.5 kc	Monitor commutator	
14	22.0 kc	Beta and gamma experiment	
15	30.0 kc	GRD commutator	
16	40.0 kc	RF probe	
18	70.0 kc	Aspect and monitor	

TABLE H.17 TELEMETRY CHANNEL SUMMARY, ROCKET NUMBER 18

Project No.	6.2	Date of Record	26 Oct 1962
Event	Blue Hill Triple Prime	Rocket Type	HJ-N-N
Experiment Title	Gamma Ray Scanner, Beta and Gamma Detector, Photometer	Time Launched	0030:49.7W
Date Launched	26 Oct 1962	Where Recorded	EOS TM Van
Where Launched	Johnston Island Pad 4	Recorder No.	2
Recorded Data Source	VHF TM 234 Mc	Track Number	1 and 2 (VHF), GMD 9
Tape Reel Number	81	Paper Records Copy	
Data Location on Tape	Launch thru 0034:52.7	Distribution	EOS

IRIG Channel Number	Channel Frequency	Description	Comments
4	960 cps	Z-axis magnetometer	All SCO's received with excellent quality from lift-off 0030:49.7 through 0034:52 with the following exceptions: A 1/4-sec. loss at 0032:40. An occasional loss for less than 1/10 second each from 0033:04 through 0034:20, where losses become longer and occur more often until end of data.
5	1.3 kc	X-axis magnetometer	
9	3.9 kc	Y-axis magnetometer	
10	5.4 kc	Photometer	
11	7.35 kc	Total gamma detector	
12	10.5 kc	Beta detector	
13	14.5 kc	Gamma scanner No. 1	
14	22.0 kc	Output 1. Vert. 90 ^o det (inboard)	
15	30.0 kc	Gamma scanner No. 1 Output 2. Vert. 20 ^o det Gamma scanner No. 2 Output 3. Horiz. 90 ^o det (inboard)	
16	40.0 kc	Commutated channel	
18	70.0 kc	Gamma scanner No. 2 Output 4. Horiz. 20 ^o outboard	

TABLE H.18 TELEMETRY CHANNEL SUMMARY, ROCKET NUMBER 19

Project No.	6.2	Date of Record	2 Nov 1962
Event	King Fish	Rocket Type	HJ-N-N
Experiment Title	Gamma Ray Scanner, Beta and Gamma Detector, Photometer	Time Launched	0208:06.4W
Date Launched	2 Nov 1962	Where Recorded	EOS TM Van
Where Launched	Johnston Island Pad 1	Recorder No.	1
Recorded Data Source	VHF TM 234 Mc	Track Number	1 and 2 (VHF), GMD 8
Tape Reel Number	98	Paper Records Copy	
Data Location on Tape	Launch thru 0214:51.7	Distribution	EOS

Channel Number	Channel Frequency	Description	Comments
4	960 cps	Z-axis magnetometer	AGC recordings indicate an electrical loss of two of the turnstile antenna elements which caused: <ol style="list-style-type: none"> 1. deep nulls in the antenna pattern 2. an additional loss of signal strength due to corona breakdown in the antenna or feed system. This loss existed until the rocket had reached an altitude where the corona could not be supported. Approximate loss due to corona was 15 db.
5	1.3 kc	X-axis magnetometer	
9	3.9 kc	Y-axis magnetometer	
10	5.4 kc	Photometer	
11	7.35 kc	Total gamma detector	
12	10.5 kc	Beta detector	
13	14.5 kc	Gamma scanner No. 1	
14	22.0 kc	Output 1. Vert. 90° det (inboard)	
		Gamma scanner No. 1	
		Output 2. Vert. 20° det (outboard)	
15	30.0 kc	Gamma scanner No. 2	
		Output 3. Horiz. 90° det (inboard)	
16	40.0 kc	Commuted channel	
18	70.0 kc	Gamma scanner No. 2	
		Output 4. Horiz. 20° outboard	

Telemetry Quality

ALL SCO's received with excellent quality from lift-off 0208:06.4 through 0214:50 except for a radio blackout at H-0 0210:06 lasting 3 seconds. A few short losses occurred during a 5-second period commencing at 0213:37, due to R.F.I.

TABLE H.19 TELEMETRY CHANNEL SUMMARY, ROCKET NUMBER 20

Project No.	6.3	Date of Record	2 Nov 1962
Event	King Fish	Rocket Type	HJ-N
Experiment Title	D-Region Physical Chemistry	Time Launched	0208:06.4W
Date Launched	2 Nov 1962	Where Recorded	EOS TM Van
Where Launched	Johnston Island Pad 17	Recorder No.	1
Recorded Data Source	VHF TM 253.8 Mc	Track Number	5 and 6 (VHF), GMD 10
Tape Reel Number	98	Paper Record Copy	
Data Location on Tape	Lift-off thru 0214:43	Distribution	GCA

IRIG			
Channel Number	Channel Frequency	Description	Comments
10	5.4 kc	Ion trap	AGC recording indicates that all SCO's would have high S/N ratio throughout flight for good data records except for a 3-second signal loss following H-0.
11	7.35 kc	Ion trap	
12	10.5 kc	Monitor commutator	
13	14.5 kc	Prompt X-ray	
14	22.0 kc	Beta and gamma experiment	
15	30.0 kc	GRD commutator	
16	40.0 kc	RF probe	
18	70.0 kc	Aspect and monitor	

TABLE H.20 TELEMETRY CHANNEL SUMMARY, ROCKET NUMBER 21

Project No.	6.3	Date of Record	2 Nov 1962
Event	King Fish	Rocket Type	N-C
Experiment Title	D-Region Physical Chemistry	Time Launched	0210:06.4W
Date Launched	2 Nov 1962	Where Recorded	EOS TM Van
Where Launched	Johnston Island Pad 15	Recorder No.	1
Recorded Data Source	GMD only	Track Number	GMD 9
Tape Reel Number	98	Paper Record Copy	
Data Location on Tape	Lift-off thru 0215:23	Distribution	GCA

IRIG			
Channel Number	Channel Frequency	Description	Comments
13	14.5 kc	Sweep Signal	AGC recording indicates that all SCO's would have high S/N ratio throughout flight for good data.
14	22.0 kc	Mass number	
18	70.0 kc	Aspect and monitor	

TABLE H.21 TELEMETRY CHANNEL SUMMARY, ROCKET NUMBER 22

Project No.	6.4	Date of Record	2 Nov 1962
Event	King Fish	Rocket Type	D-4
Experiment Title	E-F Region Physical Chemistry	Time Launched	0209:06.5W
Date Launched	2 Nov 1962	Where Recorded	EOS TM Van
Where Launched	Johnston Island Pad 19	Recorder No.	1
Recorded Data Source	VHF TM 245.3 Mc	Track Number	3 and 4 (VHF), GMD nona
Tape Reel Number	98	Paper Records Copy	
Data Location on Tape	Lift-off thru 0217:33.5	Distribution	Zimnat Corp.

IRIG			
Channel Number	Channel Frequency	Description	Comments
2	560 cps	Aspect X	AGC recording indicates that all SCO's would have high S/N ratio throughout flight for good data.
3	720 cps	Aspect Y	
4	960 cps	Aspect Z	
5	1.3 kc	Mass spectrometer sweep	
11	7.35 kc	Monitor comutator	2.5 rps, 30 segment
12	10.5 kc	Beta and gamma	2.5 rps, 30 segment
14	22.0 kc	Mass spectrometer	
15	30.0 kc	Langmuir probe	

TABLE H.22 TELEMETRY CHANNEL SUMMARY, ROCKET NUMBER 23

Project No.	6.3	Date of Record	2 Nov 1962
Event	King Fish	Rocket Type	N-C
Experiment Title	D-Region Physical Chemistry	Time Launched	0216:06W
Date Launched	2 Nov 1962	Where Recorded	EOS TM Van
Where Launched	Johnston Island Pad 16	Recorder No.	1
Recorded Data Source	GMD only	Track Number	GMD 9
Tape Reel Number	98	Paper Records Copy	
Data Location on Tape	Lift-off thru 0221:51	Distribution	GCA

IRIG			
Channel Number	Channel Frequency	Description	Comments
13	14.5 kc	Sweep signal	AGC recording indicates that all SCO's would have high S/N ratio throughout flight for good data.
14	22.0 kc	Mass number	
18	70.0 kc	Aspect and monitor	

TABLE H.23 TELEMETRY CHANNEL SUMMARY, ROCKET NUMBER 24

Project No.	6.3	Date of Record	2 Nov 1962
Event	King Fish	Rocket Type	HJ-N
Experiment Title	D-Region Physical Chemistry	Time Launched	0216:06.3W
Date Launched	2 Nov 1962	Where Recorded	EOS TM Van
Where Launched	Johnston Island Pad 5	Recorder No.	1
Recorded Data Source	VHF TM 234.0 Mc	Track Number	1 and 2 (VHF), GMD 10
Tape Reel Number	98	Paper Records Copy	
Data Location on Tape	Lift-off thru 0222:35	Distribution	GCA

IRIG			
Channel Number	Channel Frequency	Description	Comments
10	5.4 kc	Ion trap	AGC recording indicates that all SCO's would have high S/N ratio throughout flight for good data except for short periods during the last 60 seconds of flight.
11	7.35 kc	Ion trap	
12	10.5 kc	Monitor commutator	
13	14.5 kc	Prompt X ray	
14	22.0 kc	Beta and gamma experiment	
15	30.0 kc	GRD commutator	
16	40.0 kc	RF probe	
18	70.0 kc	Aspect and monitor	

TABLE H.24 TELEMETRY CHANNEL SUMMARY, ROCKET NUMBER 25

Project No.	6.4	Date of Record	2 Nov 1962
Event	King Fish	Rocket Type	D-4
Experiment Title	E-F Region Physical Chemistry	Time Launched	0219:00W
Date Launched	2 Nov 1962	Where Recorded	EOS TM Van
Where Launched	Johnston Island Pad 22	Recorder No.	1
Recorded Data Source	VHF TM 253.8 Mc	Track Number	5 and 6 (VHF), GMD 8
Tape Reel Number	98	Paper Records Copy	
Data Location on Tape	Lift-off thru _____	Distribution	Zbney Corp.

IRIG			
Channel Number	Channel Frequency	Description	Comments
2	560 cps	Aspect X	AGC recording indicates that all SCO's would have high S/N ratio throughout flight for good data.
3	730 cps	Aspect Y	
4	960 cps	Aspect Z	
11	7.35 kc	Monitor commutator	
12	10.5 kc	Beta and gamma	
14	22.0 kc	Retarding potential	
15	30.0 kc	Langmuir probe	
			2.5 rps, 30 segments
			4 rps, 18 segments

TABLE H.25 TELEMETRY CHANNEL SUMMARY, ROCKET NUMBER 26

Project No.	6.2	Date of Record	2 Nov 1962
Event	King Fish	Rocket Type	HJ-N-N
Experiment Title	Rocket-borne Gamma Ray Scanner	Time Launched	0223:06.5W
Date Launched	2 Nov 1962	Where Recorded	EOS TM Van
Where Launched	Johnston Island Pad 2	Recorder No.	1
Recorded Data Source	VHF TM 245.3	Track Number	3 and 4 (VHF), GMD 9
Tape Reel Number	98	Paper Records Copy	
Data Location on Tape	Launch thru 0230:25.8	Distribution	EOS

IRIG			
Channel Number	Channel Frequency	Description	Comments
4	960 cps	Z-axis magnetometer	All SCO's received with excellent quality from lift-off 0223:06.5 through 0230:18. Thereafter drop-outs occur, due to weak signals, increasing in duration and rate until all data is lost at 0230:25.
5	1.3 kc	X-axis magnetometer	
9	3.9 kc	Y-axis magnetometer	
10	5.4 kc	Photometer	
11	7.35 kc	Total Gamma Detector	
12	10.5 kc	Beta detector	
13	14.5 kc	Gamma scanner No. 1	
		Output 1. Vert. 90°det (inboard)	
14	22.0 kc	Gamma scanner No. 1	
		Output 2. Vert. 20°det (outboard)	
15	30.0 kc	Gamma scanner No. 2	
		Output 3. Horiz. 90°det (inboard)	
16	40.0 kc	Commuted channel	
18	70.0 kc	Gamma scanner No. 2	
		Output 4. Horiz. 20°outboard	

TABLE H.26 TELEMETRY CHANNEL SUMMARY, ROCKET NUMBER 27

Project No.	6.3	Date of Record	2 Nov 1962
Event	King Fish	Rocket Type	HJ-N
Experiment Title	D-Region Physical Chemistry	Time Launched	0223:36.2W
Date Launched	2 Nov 1962	Where Recorded	EOS TM Van
Where Launched	Johnston Island Pad 18	Recorder No.	1
Recorded Data Source	VHF TM 234.0 Mc	Track Number	1 and 2 (VHF), GMD 10
Tape Reel Number	98	Paper Records Copy	
Data Location on Tape	Lift-off thru 0230:08.7	Distribution	GCA

IRIG			
Channel Number	Channel Frequency	Description	Comments
10	5.4 kc	Ion trap	AGC recording indicates that all SCO's would have high S/N ratio throughout flight for good data.
11	7.35 kc	Ion trap	
12	10.5 kc	Monitor commutator	
17	22.0 kc	Beta and gamma experiment	
15	30.0 kc	GRD commutator	
16	40.0 kc	RF probe	
18	70.0 kc	Aspect and monitor	

TABLE H.27 TELEMETRY CHANNEL SUMMARY, ROCKET NUMBER 28

Project No.	6.3	Date of Record	HJ-N
Event	King Fish	Rocket Type	0250:06.5W
Experiment Title	D-Region Physical Chemistry	Time Launched	EOS TM Van
Date Launched	2 Nov 1962	Where Recorded	Recorder No. 1
Where Launched	Johnston Island Pad 6	Track Number	1 and 2 (VHF), GMD 9
Recorded Data Source	VHF TM 234 Mc	Paper Records Copy	
Tape Reel Number	99	Distribution	GCA
Data Location on Tape	Lift-off thru 0256:32.4		

IRIG Channel Number	Channel Frequency	Description	Comments
10	5.4 kc	Ion trap	AGC recording indicates that all SCO's would have high S/N ratio throughout flight for good data.
11	7.35 kc	Ion trap	
12	10.5 kc	Monitor commutator	
14	22.0 kc	Beta and gamma experiment	
15	30.0 kc	GRD commutator	
16	40.0 kc	RF probe	
18	70.0 kc	Aspect and monitor	

TABLE H.28 TELEMETRY CHANNEL SUMMARY, ROCKET NUMBER 29

Project No.	0.2	Date of Record	2 Nov 1962
Event	King Fish	Rocket Type	HJ-N-N
Experiment Title	Rocket-horne Gamma Ray Scanner	Time Launched	0235:06.7W
Date Launched	2 Nov 1962	Where Recorded	EOS TH Van
Where Launched	Johnston Island Pad 4	Recorder No.	1
Recorded Data Source	VHF TH 245.3	Track Number	3 and 4 (VHF), GMD 8
Tape Reel Number	99	Paper Records Copy	
Data Location on Tape	Launch thru 0239:41.7	Distribution	EOS

IRIG

Channel Number	Channel Frequency	Description	Comments
4	960 cps	2-axis magnetometer	All SCO's received with excellent quality from lift-off 0235:06.7 through splash 0239:4.5.
5	1.3 kc	X-axis magnetometer	
9	1.9 kc	Y-axis magnetometer	
10	5.4 kc	Photometer	
11	7.35 kc	Total gamma detector	
12	10.5 kc	Beta detector	
13	14.5 kc	Gamma scanner No. 1	
		Output 1. Vert. 90 ^o det (inboard)	
14	22.0 kc	Gamma scanner No. 1	
		Output 2. Vert. 20 ^o det (outboard)	
15	30.0 kc	Gamma scanner No. 2	
		Output 3. Horiz. 90 ^o det (inboard)	
16	40.0 kc	Communtated channel	
18	70.0 kc	Gamma scanner No. 2	
		Output 4. Horiz. 20 ^o outboard	

TABLE H.29 TELEMETRY DATA TAPE CHANNEL ALLOCATION

Recorder Location: EOS TM Van; type MINCOM C-100; tape speed 60 in/sec.

Tape Track	Description of Data	Rocket Number		
		Star Fish	Blue Gill	King Fish
1.	Receiver No. 1 Video (234 Mc)	2,4,8,9		
2.	Receiver No. 2 Video (234 Mc)	2,4,8,9		
3.	Receiver No. 3 Video (245.3 Mc)	3,5		
4.	Receiver No. 4 Video (245.3 Mc)	3,3		
5.	Receiver No. 5 Video (253.8 Mc)	1,6,7		
6.	Receiver No. 6 Video (253.8 Mc)	1,6,7		
7.	Cyclelock (17 kc mod. with 60 cps), 100 kc ref., and voice			
8.	GMD Video A (1.6 kMc)	1,2,3	10,13,17	19,25,29
9.	GMD Video B (1.6 kMc)	4,5,6	11,14,18	21,23,26,28
10.	GMD Video C (1.6 kMc)	7,8,9	12,15	20,24,27
11.	234Mc Receiver AGC (on 2300 cps SCO)	2,4,8,9		
12.	254.3-Mc Receiver AGC(on 2300 cps SCO)	3,5		
13.	253.8-Mc Receiver AGC(on 2300 cps SCO), and B-1 time code (on 5400 cps SCO)	1,6,7		
14.	Time Code (AMR D-5)			

TABLE H.30 RECORDED DATA SUMMARY, TAPE RECORD

RECORDING	PROJECT	ROCKET	EVENT	DESCRIPTION	DATE	T I M E	
						START	FINISH
1	6.2	15,18	Blue Gill	Cobalt 60. Calib.	5/29	1600	1630
4	6.2	8,9	Star Fish	Cobalt 60. Calib.	6/12	1030	1100
10	6.2	15	Blue Gill	Gamma-Beta Test	6/16	0930	0945
28	6.2,3,4	1-8	Star Fish Prime	M-8 hrs. Horiz test Reel 1 of 7/8 2	7/8	1500	1525
29	6.2	8,9	"	M-8 hrs. Horiz Test Reel 2 of 2	"	1525	1535
30	6.3,4	1,2,3	"	M-O Event II Shot Reel 1 of 6	"	2247	2305
31	6.2,3,4	4,5,6, 7,8	"	" reel 2 of 6	"	2306	2330
32	6.2	8,9	"	M-O Shot - Event II Reel 3 of 6	"	2331	2355
33	6.3,4	1,2,3, 4,5,6	"	" Reel 4 of 6	"	2249	2313
34	"	5,7,8	"	" Reel 5 of 6	"	2314	2337
35	6.2	9	"	" Reel 6 of 6	"	2338	2357

TABLE H.31 RECORDED DATA SUMMARY, BRUSH RECORDER RECORD

RECORDING	PROJECT	ROCKET	EVENT	SCO CHANNELS	DATE	T I M E	
						START	FINISH
101	6.4	1	Star Fish Vert. Test	2,3,4,5,15	6/16	H-90	H-86
102	"	5	"	2,3,4,15	"	H-70	H-66
103	"	7	"	" " "	"	H-60	H-56
104	6.3	6	"	13,14	"	H-65	H-64
105	"	2	"	" "	"	H-85	H-84
106	"	3	"	10,11,12	"	H-80	H-76
107	"	4	"	" " "	"	H-75	H-71
108	6.2	8	"	10,11,12,13, 14,15,18	"	H-55	H-51
109	"	9	"	" " " "	"	H-50	H-46
110	6.4	7	Star Fish Special Test.	11,12,14,15	6/17	0920	0930
111	"	7	"	"	"	1455	1500
112	"	1	Star Fish H-8 hr.	2,3,4,5,14,15	6/19	H-90	H-87 1/2
113	"	5	"	2,3,4,14,15	"	H-78	H-75 1/2
114	"	7	"	"	"	H-72	H-70 1/2
115	6.3	3	"	10,11	"	H-87	H-84 1/2
116	"	4	"	"	"	H-81	H-78 1/2
117	"	2	"	13,14	"	H-84	H-81 1/2
118	"	6	"	"	"	H-75	H-72 1/2
119	6.2	8	"	10,11,12,13 14, 15,18	"	H-70	H-67 1/2

TABLE H.31 CONTINUED

RECORDING	PROJECT	ROCKET	EVENT	SCO CHANNELS	DATE	T I M E	
						START	FINISH
120	6.2	9	Star Fish H-8 hr.	10,11,12,13, 14,15,18	6/19	H-67	H-63 1/2
121	"	8	"	4,5,9	"	H-70	H-67 1/2
122	"	9	"	"	"	H-67	H-63 1/2
123	6.3	4	Star Fish Prime.(full freq.full pr)	10,11,12	6/29	H+5	H+7
124	"	3	"	"	"	H-6	H-2
125	"	2	"	13,14	"	H-5 1/2	H-1
126	"	6	"	"	"	H+6	H+8
127	6.2	8	"	10,11,12,13, 14,15,18	"	H+15 3/4	H+20
128	"	9	"	"	"	H+36 1/2	H+40
129	6.4	1	"	2,3,4,5,15	"	H-12	H-10
130	"	5	"	2,3,4,15	"	H+5	H+7
131	6.2	8	Special Test	10,11,12,13 14,15,18	6/30	1350	1420
132	6.3	2	Star Fish Prime.H-90 Horiz.	13,14,18	7/2	H-85	H-84
133	"	6	"	"	"	H-65	H-64
134	"	3	"	10,11,12	"	H-80	H-76
135	"	4	"	"	"	H-75	H-71

TABLE H.31 CONTINUED

RECORDING	PROJECT	ROCKET	EVENT	SCO CHANNELS	DATE	T I M E	
						START	TIME
136	6.2	8	Star Fish	10,11,12,13	7/2	H-55	H-51
137	"	9	Prime.H-90	14,15,18	"	H-50	H-46
138	6.4	1	Horiz.	2,3,4,5,14, 15	"	H-90	H-86
139	"	5	"	2,3,4,15	"	H-70	H-66
140	"	7	"	2,3,4,15	"	Special 1800	
141	"	7	"	"	"	H-60	H-56
142	6.2	8	Spec.Test	10,11,12,13 14,15,18	7/3	0848	0907
143	6.2,3,4		GMD Sens. Dev.Test		"	1040	1104
144	6.2	8	Spec.Test	10,11,12,13, 14,15,18	"	1515	1518
145	"	8,9	Star Fish Prm. H-8 hr	"	7/5	H-70 H-67	H-67 1/2 H-63 1/2
146	6.3	3	"	10,11,12	"	H-87	H-84 1/2
147	"	4	"	"	"	H-81	H-78 1/2
148	"	2.6	"	13,14,18	"	H-82 1/2 H-73 1/2	H-81 1/2 H-72 1/2
149	"	1	"	"	"	H-90	H-87 1/2
150	6.4	5 7	" "	2,3,4,14,15 "	"	H-78 H-72	H-75 1/2 H-70 1/2

TABLE H.31 CONTINUED

RECORDING	PROJECT	ROCKET	EVENT	SCO CHANNELS	DATE	T I M E	
						START	TIME
151	6.2	{ 8 9	Star Fish Prm.H-90	10,11,12,13 "	7/5	H-70 H-67	H-67 1/2 H-63 1/2
152	"	{ 8 9	Star Fish Prm.H-8 hr.	10,11,12,13 14,15,18	7/8	H-55 H-50	H-51 H-46
153	6.3	3	H-90 Horiz. count.	10,11,12 "	"	H-80	H-76
154	"	4	"	"	"	H-75	H-71
155	"	{ 2 6	" "	13,4 "	"	H-85 H-65	H-84 H-64
156	6.4	{ 1 5 7	" " "	2,3,4,5,15 2,3,4,15 2,3,4,15	" " "	H-90 H-70 H-60	H-86 H-66 H-56
157	6.2	8	"	4,5	"	H-70	H-67 1/2
158	"	8	Star Fish Prm.Event 2	11,12,10,5,9 4,7	7/9	H+19 1/2	H+34
159	"	9	"	"	"	H+39 1/2	H+53
160	"	8 GMD	"	"	"	H+19 1/2	H+34
161	"	9 GMD	"	"	"	H+39 1/2	H+53
162	"	9	"	"	"	H+39 1/2	H+53
163	6.2	8	Star Fish Prime II	13,14,15,18 5,9,10,12	7/9	H-19 1/2	H+34
164	"	9	"	"	"	H-39 1/2	H+54
165	6.4	1	"	2,3,4,5,15 7,(AGC)	"	H-10 1/2	H-13 1/2

TABLE H.31 CONTINUED

RECORDING	PROJECT	ROCKET	EVENT	SCO CHANNELS	DATE	T I M E	
						START	TIME
166	6.4	1(GMD)	Star Fish Prima II	2,3,4,5,15, 7,(AGC)	7/9	H-10 1/2	H-13 1/2
167	"	1	"	2,3,4,5,11, 15	"	"	"
168	"	1	"	2,3,4,5,15, 7,(AGC)	"	"	"
169	"	5	"	2,3,4,11,15, 7,(AGC)	"	H+6 1/2	H+9
170	"	5(GMD)	"	"	"	"	"
171	"	5	"	"	"	"	"
172	"	7	"	"	"	H+15	H+15 1/2
173	"	7(GMD)	"	"	"	"	"
174	"	"	"	"	"	"	"
175	"	5	"	"	"	H+6 1/2	H+9
176	6.3	3	"	10,11,12,7	"	H-1	H+ 1/2
177	"	3(GMD)	"	"	"	"	"
178	"	4(GMD)	"	"	"	H+6	H+12
179	"	4	"	"	"	H+6	H+11
180	"	2	"	7(AGC),13,4	"	H-1 1/2	H+4
181	"	2(GMD)	"	"	"	"	"
182	"	6	"	"	"	H+7 1/2	H+13 1/2
183	"	6(GMD)	"	"	"	"	"
184	"	4(GMD)	"	10,11,12,7	7/10	H+10	H+12
185	6.2	8	"	1,12,10,5 9,4,7	"	H+20 1/2	H+25
186	"	9	"	"	"	H+40	H+42

TABLE H.32 RECORDED DATA SUMMARY. CEC RECORDING GALVANOMETER RECORD

RECORDING	PROJECT	ROCKET	EVENT	SCO CHANNELS	DATE	T I M E	
						START	FINISH
101	6.2	15	Blue Gill Beta and Gamma Test	11,12	6/16	0930	6 bursts at 1' each
102	6.4	1	Star Fish Vert. Test	2,3,4,5,11, 12,14,15	"	H-87	± 15 sec.
103	"	5	"	2,3,4,11,12, 14,15	"	H-67	"
104	"	7	"	"	"	H-57	"
105	6.3	3	"	10,11,12,13, 14,15,16,18	"	H-77	+ 15 sec. - 30 sec.
106	"	2	"	13,14,18	"	H-84 1/2	"
107	"	6	"	"	"	H-64 1/2	"
108	"	4	"	10,11,12,14, 15,16,18	"	H-72	"
109	6.2	8	"	"	"	H-52	10 sec.
110	"	9	"	"	"	H-47	+ 10 sec.
111	6.4	7	Star Fish Spec. Test	10,11,14,15	6/17	1500	2 ft.
112	"	1	Star Fish H-8 hr.	2,3,4,5,11, 12,14,15	6/19	H-88	15 sec.
113	"	5	"	2,3,4,11,12, 14,15	"	H-76	"
114	"	7	"	"	"	H-71	"
115	6.3	3	"	10,11,12,13, 14,15,16,18	"	H-85	"

TABLE H.32 CONTINUED

RECORDING	PROJECT	ROCKET	EVENT	SCO CHANNELS	DATE	T I M E	
						START	FINISH
116	6.3	4	Star Fish	10,11,12,14, 15,16,18	6/19	H-79	15 sec.
117	"	2	"	13,14,18	"	H-82	20 sec.
118	"	6	"	"	"	H-73	"
119	6.2	8	"	10,11,12,13, 14,15,16,18	"	H-68	± 5 sec.
120	"	9	"	"	"	H-64	"
121	"	8	Star Fish Prm.Full Pwr.Full Freq.	"	6/29	H+18	5 sec.
122	"	9	"	"	"	H+38	"
123	6.4	1	"	2,3,4,5,11, 12,14,15	"	H-11	± 15 sec.
124	"	5	"	2,3,4,11,12, 14,15	"	H-16	"
125	6.3	2	"	13,14,18	"	H-2	50 sec.at 1-IPS,10 sec.at 1-IPS
126	"	6	"	"	"	H+7	"
127	"	3	"	10,11,12,13, 14,15,16,18	"	H-2 1/2	"
128	"	4	"	10,11,12,14, 15,16,18	"	H+6	"
129	6.4	5	Re-Run FF,FP ^a	2,3,4,11,12, 14,15	6/30	1330	20 sec.

^a Full frequency. full power

TABLE H.32 CONTINUED

RECORDING	PROJECT	ROCKET	EVENT	SCO CHANNELS	DATE	T I M E	
						START	FINISH
130	6.4	7	Re-Run FF,FP	2,3,4,11,12, 14,15	6/30	1340	20 sec.
131	6.3	2	Star.Prm. H-90 Horiz	13,14,18	7/2	H-84 1/2	VHF and GMD 10-sec.Int.
132	"	6	"	"	"	H-64 1/2	± 30 sec. at 1-IPS 10 sec. at 1-IPS
133	"	3	"	10,11,12,13, 14,15,16,18	"	H-77	"
134	"	4	"	10,11,12,14, 15,16,18	"	H-72 1/2	"
135	6.2	8	"	10,11,12,13, 14,15,16,18	"	H-52	± 5 sec.
136	"	9	"	"	"	H-47	"
137	6.4	1	"	2,3,4,5,11,12, 14,15	"	H-87	30-sec.Int.
138	"	5	"	2,3,4,11,12, 14,15	"	H-67	"
139	"	7	"	"	"	H-57	"
140	6.3	6	"	13,14,18	"	H-64 1/2	VHF,GMD 10-sec.Int.
141	"	3	"	10,11,12,13, 14,15,16,18	"	H-77	"
142	"	4	"	10,11,12,14, 15,16,18	"	H-72 1/2	"

^a Full frequency. full power

TABLE H.32 CONTINUED

RECORDING	PROJECT	ROCKET	EVENT	SCO CHANNELS	DATE	T I M E	
						START	FINISH
143	6.2	9	Star.Prm. H-90 Horiz	10,11,12,13,14, 15,16,18	7/2	H-47	VHF,GMD 10-sec. Interval
144	6.4	1	"	2,3,4,5,11,12, 14,15	"	H-87	"
145	"	5	"	2,3,4,11,12,14, 15,	"	H-67	"
146	"	7	"	"	"	H-57	"
147	6.2	8	"	10,11,12,13,14, 15,16,18	"	H-52	"
148	"	8	Star Fish Prm.H-8 hr.	"	7/5	H-68	+ 5 sac. at 10 IPS Int.
149	"	9	"	"	"	H-64	"
150	6.3	3	"	"	"	H-85	last min. at 1-IPS 10 sac. at 10 IPS(Int)
151	"	4	"	10,11,12,14, 15,16,18	"	H-79	"
152	"	2	"	13,14,18	"	H-82	15-sac.Int. at 10 IPS
153	"	6	"	"	"	H-73	"
154	6.4	1	"	2,3,4,5,11, 12,14,15	7/5	H-88	20-sac. Int. at 4 IPS
155	"	5	"	2,3,4,11,12, 14	"	H-76	"

TABLE H.32 CONTINUED

RECORDING	PROJECT	ROCKET	EVENT	SCO CHANNELS	DATE	T I M E	
						START	FINISH
156	6.4	7	Star Fish Prm.H-8 hr.	2,3,4,11,12, 14	"	H-71	20-sec.Int. at 4 IPS
157	"	5	"	"	"	H-76	10 sec.
158	6.3	4	Spacial	11,12,13,4	"	2330	30 sac.
159	"	4	"	11,12,13,4,15	7/6	1130	"
160	6.2	8	Star Fish Prm.H-8 hr.	"	"	H-52	+ 5 sac. Int.
161	6.3	3	"	10,11,12, (13),14,15, 16,18	7/8	H-47	"
		4	"	"	"	H-77	1 min. at 1 IPS
162	"	2	"	13,14,18	"	H-72	1/2 10 sec.at 10 IPS
		6	"	"	"	H-84	1/2 1 min.at 1 IPS
						H-64	1/2 15 sec. et 10 IPS
163	6.4	1	Star Fish Prm.H-8 hr.	2,3,4,5,11, 12,14,15	"	H-87	20 sac. Int.
		5	"	2,3,4,11,12, 14,15	"	H-67	"
		7	"	"	"	H-57	"
164	"	1	Star Fish Prm.Evant II	2,3,4,5,11, 12,14,15	7/9	H-9	1/2 H+15 1/2
165	"	5	"	2,3,4,7(ACC) 11,12,14,15	"	H+6	1/2 H+9
166	"	7	"	"	"	H+14	1/2 H+15 1/2
167	"	5	"	"	"	H+6	1/2 H+9

TABLE H.32 CONTINUED

RECORDING	PROJECT	ROCKET	EVENT	SCO CHANNELS	DATE	T I M E	
						START	FINISH
168	6.4	1	Star Fish Prm.Event II	2,3,4,5,11, 14,15	7/9	H-9 1/2	H+13 1/2
169	6.2	8	"	11,12,10,5, 9,4,7,16	"	H+19 1/2	H+34
170	"	8	"	"	"	"	"
171	"	8	"	"	"	"	"
172	"	8	"	13,14,15,18, 5,9,10,12	"	"	"
173	"	8	"	"	"	"	"
174	"	8	"	"	"	"	"
175	"	9	"	"	"	H+39 1/2	H+54
176	"	9	"	"	"	"	"
177	"	9	"	"	"	"	"
178	"	9	"	11,12,10,5, 9,4,7,16	"	"	"
179	"	9	"	"	"	"	"
180	"	9	"	"	"	"	"
181	"	9	"	"	"	"	"
182	6.3	3	"	10,11,12,13, 14,15,16,18	7/9	H-2	H+ 1/2
183	"	4	"	10,11,12,7, 14,15,16,18	"	H+6 1/2	H+12
184	"	2	"	7(AGC),13,14, 18	"	H-1 1/2	H+7 1/2

TABLE H.32 CONTINUED

RECORDING	PROJECT	ROCKET	EVENT	SCO CHANNELS	DATE	T I M E	
						START	FINISH
185	6.3	2	Star Fish Prm.Event II	10,11,12,7, 14,15,16,18 7(AGC),13,14, 18	7/9	H-1/1/2	H+7 1/2
186	"	6	"	"	"	H+7 1/2	H+14
187	"	6	"	"	"	"	"
188	"	4	"	10,11,12,7, 14,15,16,18	7/10	H+10	H+12
189	"	4	"	16	"	2308:10	2308:30
190	"	6	"	14,13	"	2308:40	1 min.
191	"	2	"	"	"	2259:40	1 min.
192	6.2	9	"	13,14,15,18 5,9,10,12	"	H+40	2 min. ea. 30 sec. to H+54

TABLE H.33 COMMUTATED CHANNEL SUMMARY, CHANNEL 11

Frame sync voltage 5.155

Project 6.4
Rocket Number 1
Channel Number 11

<u>Segment</u>	<u>Function</u>
1	Aspect X Bias
2	Aspect Y Bias
3	Aspect Z Bias
4	Pirani Gage Output
5	Mass Spectrometer Sweep Power
6	37-Mc Signal Strength
7	880-Mc Signal Strength
8	3-Frequency Beacon Package Temperature
9	1680-Mc Signal Strength
10	Aspect Power
11	28-v Battery Voltage
12	Langmuir Power
13	Mass Spectrometer Power
14	AME/DME Power
15	Beta and Gamma Power
16	Langmuir Probe Extension
17	Nose Cone Ejection
18	Mass Spectrometer Dust Cover
19	Telemetry B+ Voltage
20	Power Amplifier B+
21 - 30	Spares

TABLE H.34 COMMUTATED CHANNEL SUMMARY. CHANNEL 12

All voltages notated "Approx" vary from package to package;
Precise values given with calibration information.

CR = Counting Rate, UL = Upper Level, LL = Lower Level,
PM = Photomultiplier, Disc = Pulse Height Discriminator

Rocket Numbers 1, 5 and 7
Channel Number 12 10.5 kc

<u>Segment</u>	<u>Function</u>	<u>Normal Operating Voltage</u> volts
30	Synchronization	+5.00
29	Synchronization	+5.00
28	Beta Logic Ground Reference	0.0
27	" " Calibration	+5.00
26	" " +6.75 v Monitor	Approx 1.5
25	" " +20.0 v Monitor	Approx 3.0
24	" " Log PM Current	Approx 0.1
23	" " Log CR, UL Disc	Approx 0.3
22	" " Log CR, LL Disc	Approx 0.3
21	Beta Logic PM Hi-Voltage Monitor	Approx 1.5
20	Gamma Logic Hi-Voltage Monitor	Approx 1.5
19	" " Log CR, LL Disc	Approx 0.3
18	" " Log CR, UL Disc	Approx 0.3
17	" " Log PM Current	Approx 0.5
16	" " +20.0 v Monitor	Approx 3.0
15	" " +6.75 v Monitor	Approx 1.5
14	" " Calibration	+5.00
13	" " Ground Reference	0.0
12	" " Spare (Open)	Approx 0.0
11	" " " "	Approx 0.0
10	" " " "	Approx 0.0
9	" " " "	Approx 0.0
8	" " " "	Approx 0.0
7	" " " "	Approx 0.0
6	" " " "	Approx 0.0
5	" " " "	Approx 0.0
4	" " " "	Approx 0.0
3	" " " "	Approx 0.0
2	" " " "	Approx 0.0
1	Gamma Logic Spare (Open)	Approx 0.0

TABLE H.35 COMMUTATED CHANNEL SUMMARY.
CHANNEL 18

Rocket Numbers 2, 3 and 6 (Star Fish)
10, 13, (Blue Gill)
21, 23 (King Fish)

Channel Number 18 70.0 kc

<u>Segment</u>	<u>Function</u>
1	Frame Sync +5 v
2	" " "
3	" " "
5	" " "
	" " "
even segments 4 thru 60	Channel Sync -1.5 v
7	Trans Aspect
11	" "
15	" "
19	" "
23	" "
27	" "
31	" "
35	" "
39	" "
43	" "
47	" "
51	" "
55	" "
59	" "
9	Zero Calibration
13	Zero Calibration
17	Long Center
21	Trans Center
25	Battery Monitor
29	Regulator Monitor
33	Long Aspect
37	Long Aspect
41	Long Aspect
45	Mass Spectrometer Battery
49	Timer Monitor
53	Nose and Squib Monitor
57	Pressure Monitor

TABLE H.36 COMMUTATED CHANNEL SUMMARY, CHANNELS 12 AND 18

Rocket Numbers 3 and 4 (Star Fish)
Channel Number 18

Rocket Numbers 11, 12, 14, 17 (Blue Gill)
20, 24, 27, 28 (King Fish)
Channel Number 12

10.5 kc

<u>Segment</u>	<u>Function</u>	<u>Segment</u>	<u>Function</u>
1	+5-v Calibration	35	Probe Position B
2	" "	36	Probe Position B
3	" "	37	Probe Position B
4	" "		
5	" "	38	Squib Door A
	" "	39	Squib Door A
6	+2.5-v Calibration		
7	" "	40	Gas Generator Door A
8	" "	41	Gas Generator Door A
9	" "		
		42	Squib Door B
10	Zero Calibration	43	Squib Door B
11	" "		
12	" "	44	Gas Generator Door B
13	" "	45	Gas Generator Door B
20	Squib 1, Door A	14	Potential Door A
21	Squib 1, Door A	15	" "
		16	" "
22	Squib 2, Door A	46	" "
23	Squib 2, Door A	47	" "
		48	" "
24	Door Release A		
25	Door Release A	17	Potential Door B
		18	" "
26	Squib 1, Door B	19	" "
27	Squib 1, Door B	49	" "
		50	" "
28	Squib 2, Door B	51	" "
29	Squib 2, Door B		
		52	37 Mc
30	Door Release B	53	37 Mc
31	Door Release B		
		54	888 Mc
32	Probe Position A	55	888 Mc
33	Probe Position A		
34	Probe Position A	56	Temperature
		57	Temperature
		58	1680 Mc
		59	1680 Mc
		60	1680 Mc

TABLE H.37 COMMUTATED CHANNEL SUMMARY, CHANNEL 13

All voltages notated "Approx" vary from package to package. Precise values given with calibration information.

Rocket Number 3 (Star Fish)
 11, 12 (Blue Gill)
 20, 24 (King Fish)

Channel Number 13 14.5 kc

<u>Segment</u>	<u>Function</u>	<u>Normal Operating Voltage</u> volts
1	FX-3 Ground Reference	0.00
2	FX-3 Log Energy Signal	Approx 0.20
3	FX-3 Calibration	Approx 4.8
4	FX-3 +20.0-v Monitor	Approx 3.0
5	FX-3 Log Energy Signal ^a	Approx 0.2
6	FX-3 Hi-Voltage Monitor	Approx 1.5
7	Py-1 Ground Reference	0.00
8	Py-1 Log Energy Signal	Approx 0.2
9	Py-1 Calibration	Approx 4.8
10	Py-1 +20.0-v Monitor	Approx 3.0
11	Py-1 Log Energy Signal ^a	Approx 0.2
12	Py-1 Hi-Voltage Monitor	Approx 1.5
13	FX-4 Ground Reference	0.00
14	FX-4 Log Energy Signal	Approx 0.2
15	FX-4 Calibration	Approx 4.8
16	FX-4 +20.0-v Monitor	Approx 3.0
17	FX-4 Log Energy Signal ^a	Approx 0.2
18	FX-4 Hi-Voltage Monitor	Approx 1.5
19	Py-2 Ground Reference	0.00
20	Py-2 Log Energy Signal	Approx 0.2
21	Py-2 Calibration	Approx 4.8
22	Py-2 +20.0-v Monitor	Approx 3.0
23	Py-2 Log Energy Signal ^a	Approx 0.2
24	Py-2 Hi-Voltage Monitor	Approx 1.5
25	Spare (Open)	Approx 0.0
26	Spare (Open)	Approx 0.0
27	Spare (Open)	Approx 0.0
28	Spare (Open)	Approx 0.0
29	Synchronization	+5.00
30	Synchronization	+5.00

^a On Rocket 12 only these points are tied to the appropriate ground reference instead.

TABLE H.38 COMMUTATED CHANNEL SUMMARY, CHANNEL 14

CR = Counting Rate, UL = Upper Level, LL = Lower Level,
 PM = Photomultiplier, Disc = Pulse Height Discriminator

All voltages notated "Approx" vary from package to package.
 Precise values given with calibration information.

Rocket Number 3 (Star Fish)
 11, 12 (Blue Gill)
 20, 24 (King Fish)

Channel Number 14 22.0 kc

<u>Segment</u>	<u>Function</u>	<u>Normal Operating Voltage</u>
		volts
1	Beta Logic Ground Reference	0.00
2	" " Calibration	+5.00
3	" " +6.75 v Monitor	Approx 1.5
4	" " +20.0 v Monitor	Approx 3.0
5	" " Log PM Current	Approx 0.1
6	" " Log CR, UL Disc	Approx 0.3
7	" " Log CR, LL Disc	Approx 0.3
8	Beta Logic PM Hi-Voltage Monitor	Approx 1.5
9	Gamma Logic PM Hi-Voltage Monitor	Approx 1.5
10	" " Log CR, LL Disc	Approx 0.3
11	" " Log CR, UL Disc	Approx 0.3
12	" " Log PM Current	Approx 0.1
13	" " +20.0 v Monitor	Approx 3.0
14	" " +6.75 v Monitor	Approx 1.5
15	" " Calibration	+5.00
16	Gamma Logic Ground Reference	0.00
17	PX-1 Ground Reference	0.00
18	" Log Energy Signal	Approx 0.2
19	" Calibration	Approx 4.8
20	" +20.0 v Monitor	Approx 3.0
21	" Log Energy Signal ^a	Approx 0.2
22	PX-1 Hi-Voltage Monitor	Approx 1.5
23	PX-2 Ground Reference	0.00
24	" Log Energy Signal	Approx 0.2
25	" Calibration	Approx 4.8
26	" +20.0 v Monitor	Approx 3.0
27	" Log Energy Signal ^a	Approx 0.2
28	PX-2 Hi-Voltage Monitor	Approx 1.5
29	Synchronization	+5.00
30	Synchronization	+5.00

^a On Rocket 12 only these points are tied to the appropriate ground reference instead.

TABLE H.39 COMMUTATED CHANNEL SUMMARY. CHANNEL 15

Rocket Numbers 3 and 4 (Star Fish)
 11, 12, 14, 17 (Blue Gill)
 20, 24, 27, 28 (King Fish)
 Channel Number 15 30.0 kc

<u>Segment</u>	<u>Function</u>
1	Frame Sync +5 v
2	" " "
3	" " "
23	" " "
even segments 4 thru 60	Channel Sync -1.5 v
5	Sweep Number 1
15	" "
25	" "
35	" "
45	" "
55	" "
7	Sweep Number 2
17	" "
27	" "
37	" "
47	" "
57	" "
9	Event Monitor
29	Event Monitor
49	Event Monitor
19	Zero Calibration
21	+2.5-v Calibration
11	Bias Box Number 1
31	" "
41	" "
51	" "
13	Bias Box Number 2
33	" "
43	" "
53	" "
39	Amplifier Number 1 Out
59	Amplifier Number 2 Out

TABLE H.40 COMMUTATED CHANNEL SUMMARY. CHANNEL 16

Rocket Numbers 3 and 4 (Star Fish)
 11, 12, 14, 17 (Blue Gill)
 20, 24, 27, 28 (King Fish)
 Channel Number 16 40.0 kc

<u>Segment</u>	<u>Function</u>
1	Frame Sync +5 v
2	Frame Sync +5 v
3	Frame Sync +5 v
even segments 4 thru 60	Channel Sync 0 volt
5	2.5-v Calibration
7	5.0-v Calibration
9	1.0-v Calibration
11	SWR 1, 2, 3, 4 etc. thru 24
13	"
15	"
17	"
etc.	"
thru	"
57	"
59	Mode Indicator

TABLE H.41 COMMUTATED CHANNEL SUMMARY, CHANNEL 12

Rocket Numbers 3 and 4 (Star Fish)
 Channel Number 12 10.5 kc

<u>Segment</u>	<u>Function</u>
1	Frame Sync +5 v
2	" " "
3	" " "
5	" " "
9	" " "
even segments 4 thru 60	Channel Sync -1.5 v
7	Trans Aspect
11	" "
15	" "
19	" "
23	" "
27	" "
31	" "
35	" "
39	" "
43	" "
47	" "
51	" "
55	" "
59	" "
13	Zero Calibration
17	Zero Calibration
21	Long Center
25	Long Center
29	Trans Center
33	Trans Center
37	Long Aspect
41	Long Aspect
45	Long Aspect
49	Battery Monitor
53	+26.5-v Monitor
57	Timer Monitor

TABLE H.42 COMMUTATED CHANNEL SUMMARY, CHANNEL 14

CR = Counting Rate, UL = Upper Level, LL = Lower Level,
 PM = Photomultiplier, Disc = Pulse Height Discriminator

Rocket Number 4 (Star Fish)
 14, 17 (Blue Gill)
 27, 28 (King Fish)

Channel Number 14 22.0 kc

<u>Segment</u>	<u>Function</u>	<u>Normal Operating Voltage</u> volts
1	Beta Logic Ground Reference	0.00
2	" " Calibration	+5.00
3	" " +6.75-v Monitor	Approx 1.5
4	" " +20.0-v Monitor	Approx 3.0
5	" " Log PM Current	Approx 0.1
6	" " Log CR, UL, Disc	Approx 0.3
7	" " Log CR, LL, Disc	Approx 0.3
8	Beta Logic PM Hi-Voltage Monitor	Approx 1.5
9	Gamma Logic Hi-Voltage Monitor	Approx 1.5
10	" " Log CR, LL, Disc	Approx 0.3
11	" " Log CR, UL, Disc	Approx 0.3
12	" " Log PM Current	Approx 0.5
13	" " +20.0-v Monitor	Approx 3.0
14	" " +6.75-v Monitor	Approx 1.5
15	" " Calibration	+5.00
16	Gamma Logic Ground Reference	0.0
17	Spare (Open)	Approx 0.0
18	" "	Approx 0.0
19	" "	Approx 0.0
20	" "	Approx 0.0
21	" "	Approx 0.0
22	" "	Approx 0.0
23	" "	Approx 0.0
24	" "	Approx 0.0
25	" "	Approx 0.0
26	" "	Approx 0.0
27	" "	Approx 0.0
28	Spare (Open)	Approx 0.0
29	Synchronization	+5.00
30	Synchronization	+5.00

All voltages notated "Approx" vary from package to package.
 Precise values given with calibration information.

TABLE H.43 COMMUTATED CHANNEL SUMMARY, CHANNEL 11

Frame sync voltage 5.166 and 5.090

Project 6.4

Rocket Numbers 5 and 7 (Star Fish)

Channel Number 11

<u>Segment</u>	<u>Function</u>
1	Aspect X Bias
2	Aspect Y Bias
3	Aspect Z Bias
4	Spare
5	Not Used
6	37-Mc Signal Strength
7	888-Mc Signal Strength
8	3 Frequency Package Temperature
9	1680-Mc Signal Strength
10	Aspect Power
11	28-v Battery Voltage
12	Langmuir Power
13	Retarding Potential Power
14	AME/DME Power
15	Beta and Gamma Power
16	Langmuir Probe Extension
17	Nose Cone Ejection
18	Not Used
19	Telemetry B+ Voltage
20	Power Amplifier B+
21 - 30	Spares

TABLE H.44 COMMUTATED CHANNEL SUMMARY, RETARDING POTENTIAL ANALYZER

Rocket Numbers 5 and 7 (Star Fish)
Channel Number 14

Frame I (Nose Detector)

<u>Segment</u>	<u>Function</u>	<u>Characteristic</u>
1 thru 11	E_{os} Amplifier Output	Analog Signal 0 to +5 v
12	E_{on} Mode	Quantized 4 Levels 0 to +2 v
13	V_{rn} Retardation Voltage	Quantized 16 Levels 0 to +5 v
14	E_{tn} Amplitude Sensor Range	Quantized 16 Levels 0 to +5 v
15	E_{on} Amplifier Output	Analog Signal 0 to +5 v
16	Calibration Voltage	Constant
17	Frame	+5 v
18	Frame	+5 v

Frame II (Side Detector)

<u>Segment</u>	<u>Function</u>	<u>Characteristic</u>
1 thru 11	E_{os} Amplifier Output	Analog Signal 0 to +5 v
12	E_{os} Mode	Quantized 3 Levels 3.5 to +5 v
13	V_{rs} Retardation Voltage	Quantized 16 Levels 0 to +5 v
14	E_{ts} Amplitude Sensor Range	Quantized 16 Levels 0 to +5 v
15	E_{on} Amplifier Output	Analog Signal 0 to +5 v
16	Frame	
17	Frame	
18	Not Used	

TABLE H.45 COMMUTATED CHANNEL SUMMARY, CHANNEL 16

10 rps x 60 segments (30 brought out)

Project 6.2

Rocket Numbers 8 and 9 (Star Fish)
 15 and 18 (Blue Gill)
 19, 26, 29 (King Fish)

Channel Number 16

<u>Segment</u>	<u>Function</u>
Sync	Frame Sync and Full Scale (5 v) Calibration
1 ^a	-12 volts
2	28-v RCA (11.2/1)
3 _b	+12 v (5.0/1)
4 _b	Temperature A
5 _b	Temperature D
6	5-v Reference Gamma Scanner
16	+6 v (2.5/1)
17	+28 v (11.2/1)
18 _b	GMD 1 RF Power BRL No. 4
19 _b	Temperature B
20 _b	Temperature C
21	3-Frequency Beacon
22	RF power 888 Mc BRL Number 1
23	Beacon Temperature BRL Number 3
24 - 30	Not Used

^a Except for Rockets 8 and 9.

^b Except for Rockets 15 and 18.

TABLE H.46 TELEMETRY CHANNEL SUMMARY, ROCKET 25

	<u>Monitor Commutator</u>
Position No.	
1	Nose Cone Ejection
2	Aspect X-Bias
3	Aspect Y-Bias
4	Nose Cone Ejection
5	Aspect Z-Bias
6	Nose Cone Ejection
7	Nose Cone Ejection
8	Nose Cone Ejection
9	37-Mc Signal Strength
10	Nose Cone Ejection
11	880-Mc Signal Strength
12	Package Temperature
13	Nose Cone Ejection
14	1680-Mc Signal Strength
15	Aspect Power
16	Nose Cone Ejection
17	28V Battery Volts
18	Langmuir Power
19	Nose Cone Ejection
20	Mass Spectrometer or RPA Power
21	AME-DME Power
22	Beta Gamma Power
23	Nose Cone Ejection
24	Langmuir Probe Extension
25	Nose Cone Ejection
26	TM B+
27	Nose Cone Ejection
28	Nose Cone Ejection
	Frame Sync Voltage <u>Unknown</u>

TABLE H.47 TELEMETRY CHANNEL SUMMARY, ROCKET 22

Monitor Commutator

Position No.

1	Nose Cone Ejection
2	Aspect X-Bias
3	Aspect Y-Bias
4	Nose Cone Ejection
5	Aspect Z-Bias
6	Pirani Gage Output
7	Nose Cone Ejection
8	Mass Spectrometer Sweep Power
9	37-Mc Signal Strength
10	Nose Cone Ejection
11	880-Mc Signal Strength
12	Package Temperature
13	Nose Cone Ejection
14	1680-Mc Signal Strength
15	Aspect Power
16	Nose Cone Ejection
17	28V Battery Volts
18	Langmuir Power
19	Nose Cone Ejection
20	Mass Spectrometer or RPA Power
21	AME-DME Power
22	Beta Gamma Power
23	Nose Cone Ejection
24	Langmuir Probe Extension
25	Mass Spectrometer Dust Cover
26	TM B+
27	Nose Cone Ejection
28	Nose Cone Ejection

Frame Sync Voltage Unknown

REFERENCES

1. "Electromagnetic Blackout Guide, Effects of High Altitude Nuclear Bursts on Electromagnetic Waves"; Vol. II; 1 May 1961; Report DASA 1229; General Electric TEMPO, Santa Barbara, California; Secret Restricted Data.
2. "High Altitude Nuclear Effects, Proceedings, Conference on Nuclear Interference Review 62-1"; 14 November 1961; General Electric TEMPO, Santa Barbara, California; Secret Restricted Data.
3. Stair, Johnson and Halbach; "Standard of Spectral Radiance for the Region of 0.25 to 2.6 Microns"; Vol. 64A; July-August 1960; Journal of Research, National Bureau of Standards, Washington, D.C.; Unclassified.
4. "Graphic Displays of Geomagnetic Geometry"; 1 April 1963; Report DASA 1372; General Electric TEMPO, Santa Barbara, California; Unclassified.
5. Warren W. Berning; "D-Region Physical Chemistry (U)"; Operation Dominic, Fish Bowl Series, POR-2018; Ballistic Research Laboratories, Aberdeen Proving Ground, Maryland; Secret Data.